

CONCENTRATION-TIME PROFILES OF AMLODIPINE, GLYBURIDE, AND
DIGOXIN IN RATS: PREDICTIONS USING A CONTINUOUS ABSORPTION
MODEL

A Dissertation
Submitted to the
Temple University Graduate Board

In Partial Fulfillment of the Requirements for the Degree of
DOCTOR OF PHILOSOPHY

By
Casey Radice
December 2021

Examining Committee Members:

Dr. Swati Nagar, Advisory Chair, Department of Pharmaceutical Science

Dr. Kenneth Korzekwa, Department of Pharmaceutical Science

Dr. Carlos Barrero, Department of Pharmaceutical Science

Dr. Reza Fassihi, Department of Pharmaceutical Science

Dr. Mehran Yazdanian, External Member, Teva Pharmaceutical, West Chester, PA

©

Copyright

2021

By

Casey Radice

All Rights Reserved

ABSTRACT

The most common route of administration is oral, despite absorption barriers leading to variable exposure and therapeutic effect. Preclinical species are used to study this variability, though they are expensive and time-consuming. Modeling and simulation provide an alternative to preclinical studies. In this study, a continuous rodent absorption model was developed and refined to predict drug absorption prior to entering animals.

The continuous absorption model describes the change in drug concentration over distance and time. The intestine is defined by a physiologically based pharmacokinetic (PBPK) model, which is attached to a simpler classical compartmental model to represent the rest of the body. Physiological factors and drug physicochemical properties were incorporated to predict the absorption profiles of amlodipine (AML), glyburide (GLY), and digoxin (DIG).

The anatomy of the gastrointestinal tract and therefore, the physiological factors inputted into the model, are species specific. The region lengths, such as the jejunum, and absorptive surface area amplifiers, such as the villi, of the small intestine differ in humans versus rats. In addition, the stomach composition and presence of the gallbladder is not consistent between the two species. Similarly, food alters the physiology of the intestines. Periods of fasting can induce changes in intestinal pH and gastrointestinal motility.

Chapter One details the background concerning this project, along with the hypothesis and goals. Chapter Two involves the development and validation for bioanalytical methods for the drugs of interest. Chapter Three discusses the collection of anatomical data, specifically the intestinal pH and gastrointestinal motility under fed and fasted conditions. Chapter Four includes in vitro ADME data collection and in vivo IV pharmacokinetic studies in male Sprague-Dawley rats to determine the systemic disposition functions in for amlodipine (AML), glyburide (GLY) and digoxin (DIG). Chapter Five includes the in vivo pharmacokinetic studies in male Sprague-Dawley rats to determine the effect of food on the absorption of amlodipine (AML), glyburide (GLY) and digoxin (DIG). Chapter Six details the in vivo rat studies involving the influence of particle size on GLY suspension absorption. Chapter Seven discusses the input of physiological factors and prediction of drug absorption using a continuous absorption model in rats. Chapter Eight details future directions and the summary of the project.

DEDICATION

TO

MY MOM, NANA, AND POPPOP

ACKNOWLEDGMENTS

I fell in love with science at a young age, but it wasn't until my Ph.D. journey that truly grew as a scientist. Over the past 5 years I went from a biologist to a pharmacokineticist. During this journey, I not only learned how to think critically, but that great achievements aren't the product of a single person. I want to thank the dedicated and supportive group of individuals who made this possible.

I would like to thank my Ph.D. advisor Dr. Swati Nagar. She has been an inspiration to me, not only as a scientist, but especially as a female scientist. During my 5 years at Temple, she was promoted to professor and director of graduate studies while maintaining her duties as an advisor and member of various scientific committees, highlighting how powerful an intelligent woman can be. Dr. Nagar was the ideal mentor, encouraging me to develop my critical thinking skills and grow as a scientist. She was always supportive of my extracurricular activities, such as participating in the AAPS committee and serving as the DVDMDG audio/visual technician. She facilitated the development of my leadership and interpersonal skills, whether it was encouraging me to attend conferences or networking. Her abilities as an advisor allowed for me to grow, while providing the necessary structure to continue to strengthen my abilities during my doctoral studies and after my graduation. I am forever grateful she was my mentor.

I would like to acknowledge Dr. Kenneth Korzekwa. He is always a wealth of knowledge and I learn something new every time we speak. He deepened my love for science by reminding me that it is a dynamic field and the horizons of today will be eclipsed by the discoveries of tomorrow. He was able to take very difficult concepts, such as net clearances, and make them easier to digest. Watching Dr. Korzekwa work and explain the human continuous intestinal absorption model was incredible. I aspire to achieve even a quarter of his abilities as a scientist. I am extremely lucky to have him as my co-mentor.

I would like to thank Dr. Reza Fassihi and Dr. Carlos Barrero for being part of my Ph.D. advising committee. They provided me with amazing insights into my project. Their knowledge about absorption manifested into excellent questions designed to make me think and grow. I also want to recognize Dr. Mehran Yazdanian for being my external committee member.

I want to acknowledge my current colleagues in the lab. Not only did they help me progress as a scientist, but they created a friendly atmosphere to strive in. Min Ye taught me everything I know about animal work and handling. Dr. Erickson Paragas helped me with the LC-MS/MS and microsomal protein binding assay, but also served as a sounding board, encouragement, and coffee buddy. Dr. Zeyuan Wang was with me from day one, and I am thankful for all his support through everything. I also want to thank Tirtha Nandi, Leonard Hridoy, and Yifan Gong. You all will do amazing in the future.

I am very thankful for my past lab mates Dr. Jaydeep Yadav and Dr. Kim Holt for all their assistance through the initial years of my Ph.D. I am not sure I could have started as strong as I did without them. They continue to be an inspiration to me, as both are now successful scientists in the industry. I would like to thank the Dean and School of Pharmacy for providing me with financial support and the opportunity to pursue my Ph.D. I am thankful for Almira Cutler for her administrative help.

I lastly want to thank my family and friends. My mom was always supportive through everything, encouraging me to be my best. She told me I could achieve anything I set my mind to. My mom has always been a driven and intelligent woman, which set an example for me moving forward in my life and career. Nana and Poppop have always been some of my biggest fans and never doubted me. I miss you every day, Poppop. I can't thank Ritesh Mehra enough for being my partner and pillar through all these years. He never failed to make me laugh or feed me when I was too focused on my project to remember to eat. He was the inspiration for my continued education. Ritesh reminded me that I am capable and was my light in the darkest days. I want to acknowledge the unconditional love and motivation created by my puppies Sasha, Vladimyr, and Nataliya. I am where I am today because of all these people, and I couldn't be more appreciative.

TABLE OF CONTENTS

ABSTRACT ii

ACKNOWLEDGMENTS v

LIST OF TABLES xiv

LIST OF FIGURES xviii

ABBREVIATIONS xxii

CHAPTER 1: INTRODUCTION 1

 1.1 Oral Administration and Pharmacokinetics 1

 1.2 Anatomy, Physiology, and Absorption 2

 1.3 Anatomy and Pharmacokinetics 7

 1.4 Human versus Rat Anatomy 13

 1.5 Influence of Food on Anatomy 16

 1.6 Influence of Particle Size on PK 18

 1.7 Absorption Modeling 19

 1.8 Drugs of Interest 22

 1.8.1 Glyburide (GLY) 23

 1.8.2 Digoxin (DIG) 25

 1.8.3 Amlodipine (AML) 27

 1.9 Hypothesis 29

 1.10 Goals 29

 1.11 Specific Aims 30

CHAPTER 2: BIOANALYTICAL METHODS 32

 2.1 Rationale 32

viii

2.2	Materials	32
2.3	Assay Development	33
2.3.1	Preparation of Stocks and Calibration Samples	33
2.3.2	Sample Preparation	34
2.3.3	LC- MS/MS conditions.....	35
2.4	Assay Validation	37
2.5	Results.....	38
2.5.1	Assay Development	38
2.5.2	Assay Validation.....	43
2.6	Discussion and Conclusion	51
CHAPTER 3: ANATOMICAL DATA COLLECTION		53
3.1	Rationale	53
3.2	Materials	59
3.3	Methods.....	59
3.3.1	pH Determination.....	60
3.3.2	Gastrointestinal Motility	62
3.3.3	Intestinal Dimension Collection	64
3.4	Data Analysis	65
3.5	Results.....	65
3.5.1	pH Determination.....	65

3.5.2	Gastrointestinal Motility	68
3.5.3	Intestinal Dimension Collection	73
3.6	Discussion and Conclusion	74
CHAPTER 4: IN VITRO ADME AND IN VIVO IV DATA		78
4.1	Rationale	78
4.2	Materials	80
4.3	Study Design.....	80
4.3.1	Microsomal Partitioning Assay.....	80
4.3.2	Animals.....	81
4.3.3	Glyburide Pilot Study	81
4.3.4	Glyburide and Amlodipine IV Study.....	82
4.3.5	Digoxin IV Study	83
4.4	Data Analysis.....	83
4.4.1	F_{um}	83
4.4.2	IV PK Studies	84
4.5	Results.....	87
4.5.1	F_{um}	87
4.5.2	GLY Pilot Study	88
4.5.3	AML + GLY Study.....	89

4.5.4	DIG Study	94
4.6	Discussion and Conclusion	97
CHAPTER 5: FOOD EFFECTS ON GLY AND DIG ORAL ABSORPTION		99
5.1	Rationale	99
5.2	Materials	102
5.3	Study Design.....	102
5.3.1	Animals.....	102
5.3.2	Glyburide Pilot Study	103
5.3.3	Glyburide and Amlodipine Food Effects Study.....	104
5.3.4	Digoxin Food Effects Study.....	104
5.4	Data Analysis	105
5.5	Results.....	107
5.5.1	AML + GLY Study.....	107
5.5.2	DIG Study	116
5.6	Discussion and Conclusion	120
CHAPTER 6: PARTICLE SIZE EFFECTS ON GLY ORAL DISPOSITION.....		122
6.1	Rationale	122
6.2	Materials	124
6.3	Study Design.....	124
6.3.1	Animals.....	124

6.3.2	Drug and Formulation Preparation	125
6.3.3	PK Study	127
6.4	Data Analysis	128
6.5	Results	128
6.5.1	Drug and Formulation Preparation	128
6.5.2	PK Study	129
6.6	Discussion and Conclusion	133
6.7	Acknowledgments	134
CHAPTER 7: RODENT CONTINUOUS INTESTINAL ABSORPTION MODEL ...		135
7.1	Rationale	135
7.2	Methods	140
7.3	Data Analysis	149
7.4	Results	150
7.4.1	AML Food Effects	153
7.4.2	GLY Food Effects	160
7.4.3	DIG Food Effects	167
7.5	Discussion and Conclusion	173
CHAPTER 8: FUTURE STUDIES		176
8.1	Anatomical Data Collection	176
8.2	Food Effects	179
8.3	Particle Size	180

8.4 Rat Continuous Intestinal Absorption Model	180
REFERENCES	182
APPENDIX A- INDIVIDUAL ANATOMIC DATA	201
APPENDIX B- PARTICLE SIZE CHARACTERIZATION.....	208
APPENDIX C- EXAMPLE SOLUTION NOTEBOOK.....	212
APPENDIX D- EXAMPLE SUSPENSTION NOTEBOOK.....	212

LIST OF TABLES

Table 2.1 Optimized operating parameters for AML and GLY combined method.....	39
Table 2.2 Optimized operating parameters for GLY and DIG	40
Table 2.3 Inter-day (n=3) validation for AML and GLY (combined method) in rat plasma	45
Table 2.4 Intra-day (n=3) validation for AML and GLY (combined method) in rat plasma	45
Table 2.5 Inter-day (n=3) validation for GLY and DIG in rat plasma	47
Table 2.6 Intra-day (n=3) validation for GLY and DIG in rat plasma	48
Table 2.7 Inter-day (n=3) validation for AML and GLY in rat liver microsomes	50
Table 2.8 Intra-day (n=3) validation for AML and GLY in rat liver microsomes	50
Table 2.9 LLOQ comparisons experimental versus literature	51
Table 3.1 Labels regarding the percentage of food present in the lumen	61
Table 3.2 Average segment pH by rat	66
Table 3.3 Average estimated percent of the lumen containing food contents	66
Table 3.4 Pilot charcoal study information.....	69
Table 3.5 Individual fed charcoal study information.....	69
Table 3.6 Individual fasted charcoal study information	70
Table 3.7 Average fed charcoal study information.....	71
Table 3.8 Average fasted charcoal study information	71
Table 3.9 Fed versus fasted velocity data	73

Table 3.10 Average rat intestinal length data	74
Table 3.11 Width information for individual rats and averages	74
Table 4.1 Microsomal binding assay results.....	87
Table 4.2 Non-compartmental PK parameters and metrics for GLY pilot study IV	88
Table 4.3 Goodness of fit metrics for 2C and 3C models for GLY IV (n=2).....	88
Table 4.4 GLY pilot study IV PK parameters and metrics for 2C	89
Table 4.5 Parameter estimates of GLY for 2C calculated for individual rats.....	89
Table 4.6 Non-compartmental PK parameters and metrics for AML and GLY IV (n=3)	90
Table 4.7 Goodness of fit metrics for mean 2C and 3C models for AML IV	91
Table 4.8 Goodness of fit metrics for mean 2C and 3C models for GLY IV	91
Table 4.9 PK parameters and metrics for AML and GLY IV for 2C (n=3)	92
Table 4.10 Parameter estimates of AML for 2C calculated for individual rats and the average of values (n=3).....	93
Table 4.11 Parameter estimates of GLY for 2C calculated for individual rats and the average of values (n=3).....	93
Table 4.12 Parameter estimates of AML and GLY for 2C calculated for naïve pooled average rat (n=3)	94
Table 4.13 Non-compartmental PK parameters and metrics for DIG (n=3)	95
Table 4.14 Goodness of Fit Metrics for 2C and 3C Models for DIG IV	95
Table 4.15 PK parameters and metrics for DIG for 2C (n=3)	96

Table 4.16 Parameter estimates of DIG for 2C calculated for naïve pooled average (n=3)	96
Table 4.17 Parameter estimates of DIG for 2C calculated for individual rats and the average of values (n=3)	97
Table 5.1 PK parameters and metrics for AML PO for 2-hours fasted rats using NCA	108
Table 5.2 PK parameters and metrics for AML PO for 1-hour fasted rats	109
Table 5.3 PK parameters and metrics for AML PO for fed rats using NCA	110
Table 5.4 Comparison of average AML PK parameters and metrics for 2-hours fasted, 1-hour fasted, and fed rats	111
Table 5.5 PK parameters and metrics for GLY PO 2-hours fasted rats using NCA	112
Table 5.6 PK parameters and metrics for GLY PO 1-hour fasted rats using NCA	113
Table 5.7 PK parameters and metrics for GLY PO fed rats using NCA	114
Table 5.8 Comparison of average GLY PK parameters and metrics for 2-hours fasted, 1-hour fasted, and fed rats using NCA	115
Table 5.9 PK parameters and metrics for DIG in 1-hour fasted rats using NCA	117
Table 5.10 PK parameters and metrics for DIG PO 30-min fasted rats using NCA	118
Table 5.11 PK parameters and metrics for DIG PO fed rats using NCA	119
Table 5.12 Comparison of average DIG PK parameters and metrics for 1-hour fasted, 30-min fasted, and fed rats using NCA	120
Table 6.1 Mean and distributions for particle sizes	127
Table 6.2 Dosing consistency measured using GLY to GLY-d4 peak area ratios	129

Table 6.3 Percent of GLY in solution.....	129
Table 6.4 Individual PK parameter and metrics for Sample A (4.1 μm) using NCA.....	130
Table 6.5 Individual PK parameter and metrics for Sample B (42.7 μm) using NCA...	131
Table 6.6 Average PK parameter and metrics for Sample A (4.1 μm) using NCA	133
Table 6.7 Average PK parameter and metrics for Sample B (42.7 μm).....	133
Table 7.1 Input parameters and their sources	140
Table 7.2 Caco-2 sf and PL_t combinations for AML fasted and fed rats.	154
Table 7.3 Top Caco-2 sf, PL_t , and lag combinations for AML (fasted 2 hours)	155
Table 7.4 Top Caco-2 sf, PL_t , and lag combinations for AML (fasted 1 hour).....	157
Table 7.5 Top Caco-2 sf, PL_t , and lag combinations for AML (fed).....	158
Table 7.6 EOC values for fasted and fed rat groups using different pH functions.....	159
Table 7.7 Caco-2 sf and PL_t combinations for GLY fasted and fed rats.	161
Table 7.8 Top Caco-2 sf, PL_t , and lag combinations for GLY (fasted 2 hours).....	163
Table 7.9 Top Caco-2 sf, PL_t , and lag combinations for GLY (fasted 1 hour)	164
Table 7.10 Top Caco-2 sf, PL_t , and lag combinations for GLY (fed)	166
Table 7.11 Caco-2 sf and PL_t combinations for DIG fasted and fed rats.	168
Table 7.12 Top Caco-2 sf, PL_t , and lag combinations for DIG (fasted 1 hour).....	169
Table 7.13 Top Caco-2 sf, PL_t , and lag combinations for DIG (fasted 30 min).....	171
Table 7.14 Top Caco-2 sf, PL_t , and lag combinations for DIG (fed)	172
Table 8.1 Peptide Sequence Criteria.....	179
Table 8.2 Mean and distribution data for Sample C	180

LIST OF FIGURES

Figure 1.1 Pathways of drug absorption through enterocytes.....	4
Figure 1.2 Example of an oral C-t profile.....	8
Figure 1.3 Example of an oral C-t profile and the therapeutic range	10
Figure 1.4 Biopharmaceutics Classification System (BCS)	11
Figure 1.5 Condensed representation of the ACAT Model (Lin and Wong, 2017)	20
Figure 1.6 Structure of GLY.....	23
Figure 1.7 Structure of DIG	25
Figure 1.8 Structure of AML	27
Figure 2.1 Representative chromatogram for AML and GLY in rat plasma.....	41
Figure 2.2 Representative chromatogram for AML and GLY in RLM.....	41
Figure 2.3 Representative chromatogram for GLY in rat plasma	42
Figure 2.4 Representative chromatogram for DIG in rat plasma.....	42
Figure 2.5 Representative standard curve for AML in rat plasma (AML/GLY combined).	44
Figure 2.6 Representative standard curve for GLY in rat plasma (AML/GLY combined).	44
Figure 2.7 Representative standard curve for GLY in rat plasma.	46
Figure 2.8 Representative standard curve for DIG in rat plasma.	47
Figure 2.9 Representative standard curve for AML in RLM.....	49
Figure 2.10 Representative standard curve for GLY in RLM.	49

Figure 3.1 Depiction of rat intestinal segment division.....	54
Figure 3.2 Average pH of contents along the intestine in rats.....	67
Figure 3.3 Fed versus fasted charcoal plug distance traveled over time	72
Figure 3.4 Fed versus fasted plug length over time	72
Figure 4.1 Schematic representation of compartmental models.....	85
Figure 4.2 <i>In vivo</i> C-t profiles of GLY in SD rats (n=2) after an IV dose.....	89
Figure 4.3 <i>In vivo</i> C-t profile of AML and GLY in SD rats (n=3) after an IV dose.....	92
Figure 4.4 <i>In vivo</i> C-t profile of DIG in SD rats (n=3) after an IV dose.	95
Figure 5.1 Schematic representation of compartmental models.....	106
Figure 5.2 AML PO individual and average (n=3) PK C-t profiles for 2-hours fasted rats.	107
Figure 5.3 AML PO individual and average (n=4) PK C-t profiles for 1-hour fasted rats.	108
Figure 5.4 AML PO individual and average (n=4) PK C-t profiles for fed rats.....	109
Figure 5.5 Comparison of average AML PK C-t profiles for fasted and fed rats.....	111
Figure 5.6 GLY PO individual and average (n=3) PK C-t profiles for 2-hours fasted rats.	112
Figure 5.7 GLY PO individual and average (n=4) PK C-t profiles for 1-hour fasted rats.	113
Figure 5.8 GLY PO individual and average (n=3) PK C-t profiles for fed rats.	114
Figure 5.9 Comparison of average GLY PK C-t profiles for fasted and fed rats.	115

Figure 5.10 DIG PO individual and average (n=5) PK C-t profiles for 1-hour fasted rats.	116
Figure 5.11 DIG PO individual and average (n=3) PK C-t profiles for 30-min fasted rats.	117
Figure 5.12 DIG PO individual and average (n=5) PK C-t profiles for fed rats.....	118
Figure 5.13 Comparison of average DIG PK C-t profiles for fasted and fed rats.	119
Figure 6.1 PO individual and average (n=5) PK C-t profiles for Sample A (4.1 μm)....	130
Figure 6.2 PO individual and average (n=5) PK C-t profiles for Sample B (42.7 μm)..	131
Figure 6.3 Comparison of average PK C-t profiles for Sample A and Sample B	132
Figure 7.1 Depiction of the rat intestine as a continuous cylinder.....	138
Figure 7.2 Depiction of the radical compartments comprising the concentric cylinders of the rat intestine	139
Figure 7.3 Function of velocity along the distance (x) of the rat intestine	151
Figure 7.4 Function of fasted pH along distance (x) of the rat intestine	152
Figure 7.5 Function of fed pH along distance (x) of the rat intestine	152
Figure 7.6 Function of cross-sectional area along distance (x) of the rat intestine	153
Figure 7.7 Predicted versus observed C-t profiles for 2-hours fasted rats dosed a 5 mg/kg AML solution for (A) initial and (B) best parameter value combination.	156
Figure 7.8 Predicted versus observed C-t profiles for 1-hour fasted rats dosed a 5 mg/kg AML solution for (A) initial and (B) best parameter value combination.	157

Figure 7.9 Predicted versus observed C-t profiles for fed rats dosed a 5 mg/kg AML solution for (A) initial and (B) best parameter value combination.....	159
Figure 7.10 Predicted versus observed C-t profiles for 2-hours fasted rats dosed a 5 mg/kg GLY solution for (A) initial and (B) best parameter value combination. ..	163
Figure 7.11 Predicted versus observed C-t profiles for 1-hour fasted rats dosed a 5 mg/kg GLY solution for (A) initial and (B) best parameter value combination.....	165
Figure 7.12 Predicted versus observed C-t profiles for fed rats dosed a 5 mg/kg GLY solution for (A) initial and (B) best parameter value combination.....	166
Figure 7.13 Predicted versus observed C-t profiles for 1-hour fasted rats dosed a 0.75 mg/kg DIG solution for (A) initial and (B) best parameter value combination.....	170
Figure 7.14 Predicted versus observed C-t profiles for 30-minute fasted rats dosed a 0.75 mg/kg DIG solution for (A) initial and (B) best parameter value combination.....	171
Figure 7.15 Predicted versus observed C-t profiles for fed rats dosed a 0.75 mg/kg DIG solution for (A) initial and (B) best parameter value combination.....	173

ABBREVIATIONS

°C	Degrees in Celsius
2C	2-compartment
3C	3-compartment
ACAT	Advanced Compartment Absorption and Transit
ACN	Acetonitrile
AML	Amlodipine
AML-d4	Amlodipine-d4
AUC	Area under the concentration-time curve
AUCM	Area under the first moment curve
BCS	Biopharmaceutics Classification System
CE	Collision energy
CL	Clearance
cm	Centimeter
C _{max}	Highest concentration on the concentration over time profile
C-t	Concentration of drug over time
CXP	Collision exit potential
D	Duodenum
DIG	Digoxin
DIG-d3	Digoxin-d3
DMSO	Dimethyl sulfoxide
Dose _{IV}	Intravenous dose
Dose _{PO}	Oral dose
DP	Declustering potential
F	Bioavailability
FA	Formic acid
f _{um}	Fraction unbound in microsomes
g	Gram
g	Gravitational force
GI	Gastrointestinal

GLY	Glyburide
GLY-d3	Glyburide-d3
HPLC	High-performance liquid chromatography
IS	Internal standard
ITO	Indium-tin oxide
IV	Intravenous
J#	Jejunum segment #
k	Elimination rate constant
ka	Rate of absorption
Kp	Membrane partition constant
LC-MS/MS	Liquid chromatography tandem mass spectrometry
LLOQ	Lower limit of quantification
m	Meter
MALDI	Matrix-assisted laser desorption/ionization
MC	Methylcellulose
MDR	Multiple drug resistant
mg	Miligram
min	Minute
mL	Mililiter
mm	Milimeter
MMC	Migrating motor complex
MRT	Mean residence time
msec	Milisecond
MTBE	Methyl tert-butyl ether
n	Sample size
NCA	Non-compartmental analysis
ng	Nanogram
nM	Nanomolar
OATPs	Organic anion transporter polypeptides
PBPK	Physiologically based pharmacokinetics
PDE	Partial differential equations

P-gp	P-glycoprotein
PK	Pharmacokinetics
PO	Oral
psi	Pounds per square inch
QC	Quality control
R ²	Coefficients of determination
RLM	Rat liver microsomes
SD	Sprague-Dawley
SEM	Scanning electron microscopy
SEM	Scanning electron microscopy
t _{1/2}	Elimination half-life
t _{max}	Time at which the C _{max} occurs
U	Unit of heparin
V	Volts
V _d	Volume of distribution
V _{ss}	Volume of distribution at steady state
WMC	Wireless motility capsules
XRD	X-ray diffraction
μL	Microliter
μm	Micrometer
μM	Micromolar

CHAPTER 1: INTRODUCTION

1.1 Oral Administration and Pharmacokinetics

Most drugs are administered orally due to cost-efficacy and increased patient compliance, which is especially beneficial for chronic conditions. However, orally administered drugs are subject to complex biological processes, and their absorption depends on the physicochemical properties of the dosed drug. When dosed intravenously, the complete dose is assumed to be introduced into the systemic circulation. However, orally dosed drugs must survive the acidic conditions of the stomach and be available for absorption in the small intestine before entering the systemic circulation. Therefore, drugs must have desirable pharmacokinetics (PK) that allow for proper absorption, metabolism, distribution, and elimination, culminating in a therapeutic effect.

The absorption of oral drugs dictates their availability. The systemic exposure of these drugs depends on biological parameters like gastrointestinal transit, presence and type of food, pH, and transporter expression. Drug properties like lipophilicity, pKa, permeability, and solubility, along with formulation vehicle and particle size can impact a drug's ability to be taken up in the intestines.

In drug discovery, preclinical species are used prior to human trials. Because animal studies are time-consuming and expensive in both lives and money, it is beneficial to predict a drug's PK profile before proceeding to *in vivo* studies. Physiologically-based

pharmacokinetic (PBPK) modeling is a relatively inexpensive and time-saving alternative, as many physiological parameters can be collected or found in the literature. In addition, simulations can be performed before ever entering animals.

1.2 Anatomy, Physiology, and Absorption

The human gastrointestinal tract includes the oral cavity, esophagus, stomach, small and large intestine, rectum, and anus. The oral cavity, esophagus, rectum, and anus do not serve any absorptive purpose. The mucosa in these regions comprises a stratified squamous epithelium, which is several layers thick and has poorly vascularized lamina propria (Lai et al., 2009). In addition, these areas are hindered by their relatively small surface area, compared to the absorbing sections, and drugs spend little time there (DeSesso and Jacobson, 2001). Thus, the thick barrier, poor blood supply, small absorptive surface, and short residence time are not favorable to absorption. Exceptions to this are medications designed for sublingual or buccal administration, but those formulations will not be considered in the context of this thesis.

In humans, the intestines are the primary absorption site for most drugs, with minor absorption occurring in the stomach. The stomach is capable of absorbing soluble acidic drugs ($pK_a < 3$), but physiologic barriers limit intake at this site (Tannergren et al., 2009; Rubbens et al., 2018). The mucosa, which serves as a protective barrier, is thinnest in the small intestine (Lai et al., 2009). Additionally, the surface area of the human small intestine (30 m^2) and colon (1.9 m^2) is much larger than that of the stomach (500 cm^2).

Most of this increase in surface area in the small intestine is due to three enlargement factors: plicae circulares, villi, and microvilli. The plicae circulares, also called Kerckring's folds, are valvular flaps that project into the intestinal lumen. Villi, finger-like protrusions, are lined with enterocytes that possess microvilli on their apical surface. The intestinal surface area enlargement due to the Kerckring's folds, villi, and microvilli are 3-, 6.5-, and 13- fold, respectively (Helander and Fandriks, 2014). While the colon has a smaller surface area and thicker mucosa than the small intestine, it presents the benefit of longer residence time (Rubbens et al., 2018).

As mentioned previously, the intestinal lumen is lined with enterocytes, a single layer of epithelial cells bound together by tight junctions. Both endogenous and xenobiotic molecules must travel from the lumen and pass this cell layer to enter the vasculature surrounding the intestine before reaching the liver and systemic circulation (DeSesso and Jacobson, 2001). As shown in Figure 1.1, drugs typically rely on passive transcellular transport through the cells (Pathway A) due to their lipophilic nature. Highly permeable and soluble drugs are not likely to have significant absorption via carrier-mediated diffusion (Pathway B), even if they are substrates, due to the larger surface area available for passive diffusion and the saturable nature of transporters. Smaller hydrophilic compounds with a molecular weight less than 250 Da may rely on paracellular transport around the cells (Pathway C). Paracellular transport is a minor route for most drugs due to their lipophilic nature and the small surface area available for paracellular transport (Lennernas, 2007). Drugs can be effluxed back into the lumen by transporters (Pathway

D) or be metabolized (Pathway E), where both parent (E) and metabolite (E*) can be taken up into the blood.

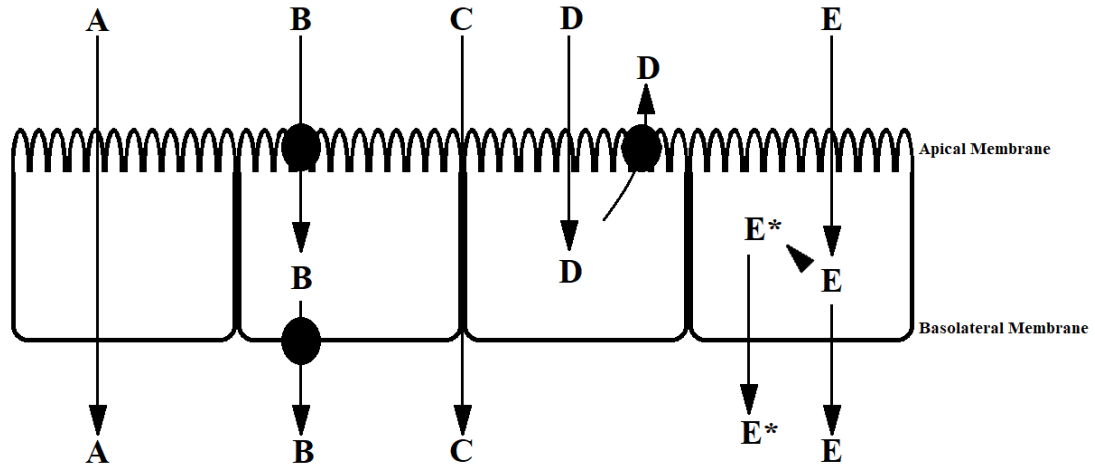


Figure 1.1 Pathways of drug absorption through enterocytes

Many physiological factors can influence the absorption of drug molecules, such as age, gender, gut bacteria, disease states, luminal water volume, and splanchnic perfusion.

Luminal pH and small intestinal transit time are essential because they can determine the passive diffusion of a drug and may be altered by age, gender, or disease state. As discussed below, transporters also play an essential role in the absorption of their substrates.

The pH of the lumen and drug pKa influence drug absorption. Charged drug compounds have two forms: ionized or unionized. The pKa is the pH at which 50% of the drug is ionized. According to the pH partition hypothesis, an unionized drug, which is more lipophilic, can interact and cross the phospholipid membrane (Shore et al., 1957).

Whether a drug is an acid or base will determine the ionized fraction at a given pH.

Acids, which donate protons to their environment, will dissociate into their ionized form as pH increases, preventing more of the compound from crossing membranes and being absorbed. Bases, which accept protons, become more unionized as pH increases, allowing for increased absorption. The human intestinal lumen is more basic, as the pH fluctuates between 6 – 8 (Evans et al., 1988). For acidic drugs with a $pK_a < 3$ and bases with a $pK_a > 8$, most of the compound is in its ionized form at physiological pH and is absorbed poorly (Manallack et al., 2013).

pH can also influence absorption by impacting a drug's solubility. For ionizable compounds, solubility values can vary depending on the pH of the medium (Shoghi et al., 2013). An inverse relationship exists between solubility and unionized form for weakly acid and basic ionizable drugs (Akula and Lakshmi, 2018). Weak acids dissociate into their ionized form as pH increases. Therefore, the solubility is expected to increase as pH increases. The opposite is assumed to occur for weakly basic compounds.

Intestinal motility, or velocity, is how quickly content moves along the intestines. The human intestine displays a three-phase migrating motor complex (MMC). MMC phase I is defined by no contractions. Phase II is the presence of irregular contractions. Phase III is initiated in the antral stomach or duodenum and consists of high-pressure peristalsis (Deloose and Tack, 2016).

The surface area and time spent in each intestinal segment should be considered simultaneously. The velocity of transit is faster in the proximal regions of the small intestine compared to the ileum and large intestine (DeSesso and Jacobson, 2001). Changes in intestinal transit will have the most effect on drugs with poor solubility and permeability. Drugs with good solubility and permeability will be quickly and adequately absorbed in the surface area-rich proximal regions of the small intestine (El-Kattan and Varma, 2011). For poorly soluble and permeable drugs, accelerated motility reduces contact time with the intestinal mucosa and can lead to insufficient absorption (Levine, 1970).

Poorly soluble and poorly permeable drugs do not efficiently diffuse through passive mechanisms and therefore are more likely to rely on transporters if they are substrates. Transporters are located on the apical side of the intestinal epithelium, which faces the lumen, and the basolateral side, which faces the blood. There are two types of transporters, uptake, which brings compounds into cells, and efflux, which removes compounds from cells back into the lumen. Apically located uptake transporters can aid in absorption by taking a substrate from the lumen into the enterocytes. Organic anion transporter polypeptides (OATPs) are a family of uptake transporters located throughout the body, but human OATP2B1 and OATP1A2 play an integral role in intestinal absorption of drugs (Estudante et al., 2013). On the other hand, apically located efflux transporters can hinder absorption by preventing drugs from entering the enterocytes. For example, P-glycoprotein (P-gp) is an ATP-dependent efflux pump with a broad substrate

specificity that removes compounds from the enterocyte membrane (Mouly and Paine, 2003; Suzuyama et al., 2007).

1.3 Anatomy and Pharmacokinetics

PK studies what the body does to the drug and can illuminate why only a fraction of a drug may reach its therapeutic target. Excessive metabolism, nonspecific binding or partitioning, drug-drug interactions, and poor absorption from the administration site can lead to insufficient therapy. Safe and efficacious dosing regimens can be designed with PK information. Prior to testing in humans, two preclinical species are typically investigated. *In vivo* PK is studied by dosing a drug, collecting samples at various time points, measuring the concentrations of the desired drug and/or its metabolite(s), and analyzing the data. Samples can be collected from various sources, such as urine, bile, and feces, but are typically collected as venous blood. The analyzed data is then plotted in a concentration of drug over time (C-t) profile.

The C-t profile of a drug can be used to determine a drug's three primary PK parameters: clearance (CL), volume of distribution (Vd), and bioavailability. For intravenously dosed drugs with no lung metabolism, F is equal to 1. Drugs given by extravascular administration have lower bioavailability due to incomplete absorption from the administration site to the systemic circulation.

Orally dosed drugs undergo two major phases, as shown in Figure 1.2. The first phase is absorption, where the drug is leaving its site of administration. The second, post-absorptive phase occurs as the drug is distributed throughout the body and eliminated. Typically, the rate of absorption is faster than the rate of elimination, resulting in an eventual elimination-only phase, where an elimination half-life can be determined. The elimination half-life ($t_{1/2}$) is how long it takes for 50% of the drug to be eliminated from the body. A rare exception to this is flip-flop kinetics, where the rate-limiting step is absorption, which is much slower than elimination. This results in a $t_{1/2}$ that is reflective of absorption, not elimination (Gibaldi and Perrier, 1982).

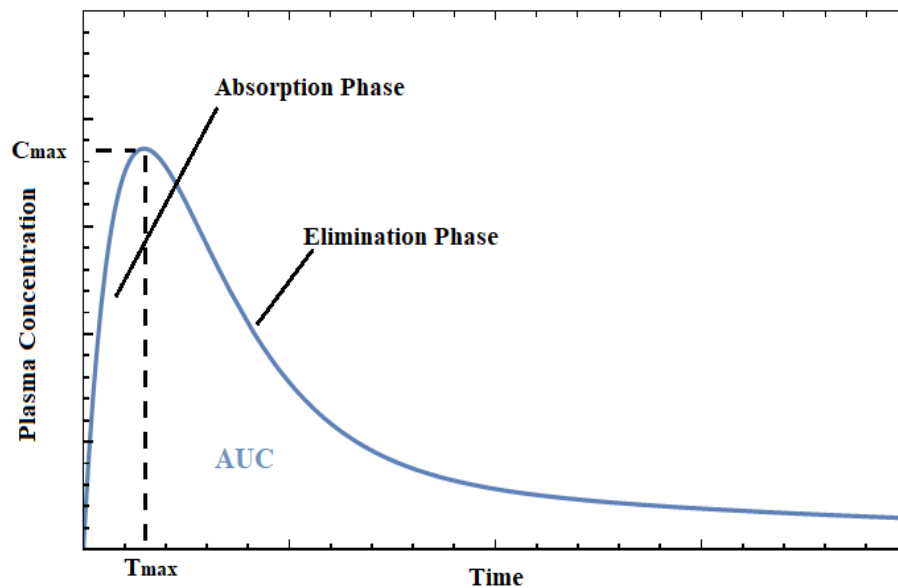


Figure 1.2 Example of an oral C-t profile

The rate and extent of absorption are essential in determining the overall bioavailability of a drug. The rate of absorption (k_a) is how fast the drug is being absorbed, while the

extent of absorption (F) is how much is being absorbed. C-t profiles can be used to determine other PK metrics. The area under the concentration-time curve (AUC) is the overall exposure of a drug. The highest concentration (C_{max}) and the time when this maximum concentration occurs (t_{max}) can also be estimated upon an oral dose. Each metric is vital when designing a therapeutic regimen.

Measuring drug concentrations is difficult at the therapeutic target so plasma concentrations are often associated with therapeutic or toxic levels of a drug in the body. The therapeutic range is the range of plasma concentrations where a drug exerted its desired effect with little or no adverse effects. As shown in Figure 1.3, the C_{max} should be in this range for the drug to be safe and effective (Schulz et al., 2012). A drug's t_{max} should match its therapeutic intent. For example, a shorter t_{max} is more beneficial if a drug's effect is needed quickly, like an analgesic, or to obtain a greater response by achieving a higher C_{max} . A longer t_{max} may be desired if there is a narrower therapeutic range or a prolonged duration of action is needed.

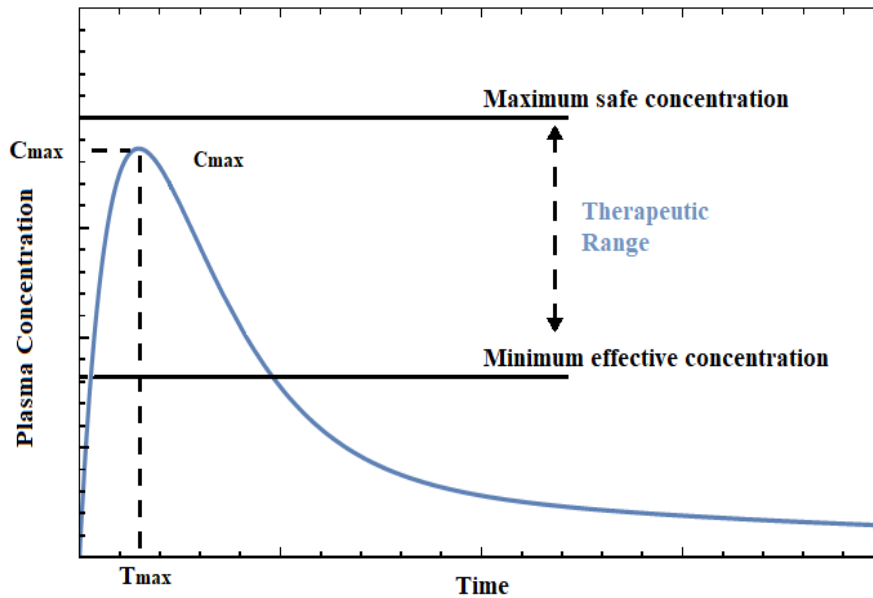


Figure 1.3 Example of an oral C-t profile and the therapeutic range

The FDA divides drugs into four Biopharmaceutics Classification System (BCS) classes based on their aqueous solubility and intestinal permeability, as shown in Figure 1.4. This aids in correlating *in vitro* dissolution to *in vivo* bioavailability (Khadka et al., 2014). Dissolution is the rate that a solute goes into a solution, while solubility is the inherent ability of a drug to stay in the solution. A compound is considered highly soluble when its highest dose is soluble in ≤ 250 mL of aqueous buffer (adjusted to a pH between 1.0 and 8.0) at 37°C (Yazdanian et al., 2004). This volume simulates an 8-ounce glass of water taken with a pill. While this volume may not be relevant as many people do not take their medications with exactly 250 mL of water, the BSC class system does provide important information about a drug. A highly permeable drug has $\geq 90\%$ systemic

bioavailability. The bioavailability can be determined by mass balance or by comparing the AUC of an oral and intravenous dose (Dahan et al., 2009).

Class I High Solubility High Permeability	Class II Low Solubility High Permeability
Class III High Solubility Low Permeability	Class IV Low Solubility Low Permeability

Figure 1.4 Biopharmaceutics Classification System (BCS)

Any alterations in pH, gastrointestinal (GI) motility, or transporter expression may alter the rate or extent of absorption depending on the BSC class. For example, BCS Class I drugs are dependent on gastric emptying. Because these drugs are highly permeable and soluble at intestinal pHs, they are readily absorbed when exposed to the increased surface area of the duodenum. If gastric emptying is delayed, so is the k_a (Fleisher et al., 1999). Delayed gastric emptying may aid in the absorption of certain BSC Class II drugs. Weak bases can benefit from increased dissolution time in the stomach, followed by dumping higher concentrations of a soluble drug into the intestine. For these drugs, a delayed gastric emptying can lead to an increase in F (Mitra and Kesisoglou, 2013; Tsume et al., 2014).

BCS Class II and Class III drugs are susceptible to transporters. Due to their highly permeable nature, BCS Class II drugs easily cross the membrane and do not depend on uptake transporters. Once in the enterocyte membrane or cytosol, they can be removed by efflux transporters. Saturation of efflux transporters is not likely as the solubility limits the concentration of drugs entering the cytosol. For BSC Class III drugs, low passive permeability combines with good lumen solubility to form a reliance on uptake transporters. For BSC Class II and III drugs, inhibition or induction of their prospective transporter expression can influence their F. Inhibition of efflux transporters can increase the F of BCS Class II drugs. In contrast, the inhibition of uptake transporters can decrease the F of BCS Class III drugs (Wu and Benet, 2005).

If F and/or k_a change, the AUC, C_{max} , or t_{max} may be altered. Changes in F proportionally influence the AUC, as shown in Equation 1.1. Similarly, the C_{max} is positively correlated to F, with a higher amount of drug entering the blood, increasing the C_{max} . The t_{max} is unaffected by changes in F because the time to reach C_{max} does not depend on the drug amount. If only k_a changes, the AUC will remain constant, as the same amount of drug enters the body. However, the t_{max} and C_{max} are affected by the k_a , as shown in Equations 1.2 and 1.3. As mentioned previously, the rate of absorption is typically faster than the rate of elimination, and both phases occur simultaneously. When the rate of drug input into the systemic circulation is slower, it takes more time for drug accumulation, which lengthens the t_{max} . Similarly, the decrease in drug accumulation results in a lower C_{max} (Duan, 2010). Equations 1.1 – 1.3 assume a one-compartment

model with first-order absorption and first-order elimination following a single oral dose. These assumptions were made for simplicity. The equation to calculate $AUC_{(0 \rightarrow \infty)}$ is:

$$AUC_0^\infty = \frac{Dose_{PO} \times F}{CL} \quad \text{Equation 1.1}$$

where $Dose_{PO}$ is the oral dose, F is the extent of absorption, and CL is the clearance. The equation for C_{max} is:

$$C_{max} = \frac{F \times Dose_{PO} \times ka}{Vd(ka - k)} \times (e^{-k \times tmax} - e^{-ka \times tmax}) \quad \text{Equation 1.2}$$

where ka is the rate of absorption, Vd is the volume of distribution, k is the elimination rate constant, and $tmax$ is given by the equation:

$$tmax = \frac{\ln \frac{ka}{k}}{(ka - k)} \quad \text{Equation 1.3}$$

1.4 Human versus Rat Anatomy

Preclinical species are used in drug discovery and development to look at efficacy and safety in a complex living system. This adds value by reducing the number of potential leads going into clinical trials, helping patients while saving time and money. However, preclinical species have limitations in their relevance to the human population due to species differences. Rodents are a commonly used preclinical species, as they are

relatively inexpensive, easy to handle, and provide pharmacokinetic, metabolic, and toxicity data (Dou et al., 2018). The dissimilarity in GI anatomy is a primary limitation. The most notable differences are the structure of the stomach and the composition of the intestine.

The human stomach is mainly gastric, with food entering from the esophagus at the top of the stomach and emptying into the duodenum at the bottom. The rodent stomach is both glandular, which contains glands that secrete gastric acid, and non-glandular. Food enters the middle of the stomach into the non-glandular region and exits into the duodenum through the gastric region, located on the side. The non-glandular portion, characterized by its thin walls, is primarily for storage. A limiting ridge, a thickened portion of lamina propria, separates this portion from the glandular region, whose function is digestion (Kararli, 1995; DeSesso and Jacobson, 2001). This limiting ridge and dual-portioned stomach may account for why food is present in the rat stomach after a 12 hour fast while the human stomach is over 90% empty after only 4 hours of fasting (Read et al., 1986; Jeffrey et al., 1987).

Similarly, intestinal anatomy is species-specific. The length of the human small intestine is about 83% of the entire intestinal tract, with the duodenum, jejunum, and ileum making up 4%, 38%, and 58% of the small intestine, respectively. The rodent duodenum, jejunum, and ileum are 8%, 90%, and 2% of the small intestine, respectively. In rats, the small intestine is 83% of the entire intestinal tract. The cecum is 26% of the length of the

large intestine in rats but is only 5% in humans (Kararli, 1995; Vdoviakova et al., 2016). As previously mentioned, humans have three enlargement factors that contribute to the increased absorptive surface area. Rats, however, lack Kerckring's folds. Segment distribution and surface area differences can lead to species-specific absorption profiles.

The overall trend of pH is similar in both humans and rodents. The pH starts low in the stomach, quickly rises in the duodenum, and gradually increases to the ileum. This alkalization is due to the continuous secretion of alkaline fluids into the intestine to neutralize the acidic chyme from the stomach (Lee et al., 2008). The pH drops in the cecum and proximal colon due to the acidic byproducts of bacteria present there, though the pH gradually climbs up in the transverse and distal colon (Kararli, 1995). Humans have a gastric pH around 1 – 2.5, while rats have a more alkaline gastric pH around 3 – 4. Both species have a similar pH range of 6 – 8 throughout the intestines (Ward and Coates, 1987; Evans et al., 1988).

Intestinal motility and transit time are similar for humans and rats. Both species have a small intestinal transit time of around 3 – 4 hours. Colon transit time is much longer, around 2 – 4 days for humans and 15 hours for rats. Both species have a faster transit velocity in the proximal versus distal regions (DeSesso and Jacobson, 2001).

Transporter expression is species-specific. Humans have two primary intestinal uptake transporters, OATP1A2 and OATP2B1, while rats only have one, Oatp1a5. Human OATP1A2 and rat Oatp1a5 share 72% amino acid identity and have some common

substrates, such as fexofenadine (Lan et al., 2009). Drug efflux can also occur along the intestine. There are two main groups of multiple drug resistant (MDR) genes. The first group, MDR1, encodes for proteins responsible for drug transport and can contribute to a reduction in absorption of xenobiotics. The second group, MDR2, has mostly endogenous substrates with little effect on drug transport. Rats have two *mdr1* genes, *mdr1a* and *mdr1b*, while humans only have one MDR1 gene. For both species, the protein expression of P-gp increases from the proximal to distal regions. For rats, the highest protein expression of P-gp is in the ileum and colon (Brady et al., 2002).

1.5 Influence of Food on Anatomy

Human biological functions depend heavily on the environmental conditions presented to them. Such examples include aging, disease, genetics but can also be influenced by day-to-day factors like circadian rhythm, stress, and food. This is especially true for gastrointestinal conditions. Food has been known to affect gastric emptying, small intestinal transit, pH, blood flow, transporter expression, and can even act as a mechanical barrier or binder.

In humans, the pH decreases in the fasted state, primarily due to the buffering capacity of food (Klein, 2010). The opposite is true for rodents. Overnight fasting led to significant (Lister hooded rats) and non-significant (Wistar rats) increases in pH along the intestine (Ward and Coates, 1987; McConnell et al., 2008).

In the fasted condition, humans experience MMC phases I through III. There are conflicting reports discussing food's influence on intestinal motility. Varum et al. states that following meal intake, MMC phases are replaced by continuous mixing and peristaltic contractions that propel food, leading to a shorter transit time (Varum et al., 2013). Conversely, it has been reported that food does not alter small intestinal transit time (Kararli, 1995). This controversy may stem from food's impact on gastric emptying and that ~70% of MMC contractions begin in the stomach.

In rats, the feeding state impacts the gastric emptying rate more than intestinal transit. Gastric emptying is significantly faster in fasted than fed rats. This is typically due to increased mixing and digestion of stomach contents when a meal is present (Poulakos and Kent, 1973; Kararli, 1995). Fasting has a minor impact on intestinal transit time. For example, 24-fasted and fed Sprague-Dawley (SD) rats were dosed Na²⁵¹CrO and ¹²⁵I-polyvinylpyrrolidone. In fasted rats, both isotopes traveled further than under fed conditions, though the difference was not significant after 60 minutes (Poulakos and Kent, 1973). Similarly, 12hr-fasted and fed Wistar rats were dosed with 10% charcoal in gum Arabic and sacrificed after 60 minutes. The charcoal solution traveled further in fasted rats, but the difference was not significant (Obembe et al., 2015).

Lastly, transporter expression can be altered with prolonged fasts. In humans, OATP2A1 mRNA expression was reported to increase by 1.4-fold after 24 hours of fasting (van den

Bosch et al., 2007). In male SD rats, P-gp gene and protein expression increased after a 12-hour fast (Dou et al., 2018).

1.6 Influence of Particle Size on PK

A drug's absorption is influenced by dissolution rate, solubility, and intestinal permeability. Particle size is a formulation property that can be manipulated to aid dissolution. The reduction of drug particle size can lead to improvements in a drug's pharmacokinetics. For example, decreasing the particle size of the contraceptive norethindrone led to an increase in AUC and C_{max} in humans. The t_{max} was shortened as the particle size decreased from 250 μm to 10 μm (Saperstein et al., 1989). This is per the modified Noyes-Whitney equation (Equation 1.4), which states:

$$\frac{dC}{dt} = \frac{DS}{Vh}(C_s - C_t) \quad \text{Equation 1.4}$$

where dC/dt is the dissolution rate, D is the diffusion coefficient of the drug in solution, S is the interfacial surface area of the drug particle, V is the volume of the solution, h is the thickness of the diffusion layer around each particle, C_s is the saturation solubility of drug in the diffusion layer, and C is the drug concentration in the GI fluid at time t.

When the particle size of a drug decreases, the specific surface area, which is the total surface area of a solid per unit mass, increases (Chu et al., 2012). In addition, the diffusion layer, the saturated stagnant layer surrounding the solid drug, decreases in

thickness with decreasing particle size (Niebergall et al., 1963). This combination of increasing surface area and reduction of the diffusion layer thickness leads to an increase in dissolution rate.

Formulation particle size has little effect on the solubility and no effect on drug permeability across the intestinal membrane. As mentioned previously, a reduction in particle size leads to an increase in surface area. The resulting increase allows for more interaction with the surrounding solvent, thus improving solubility. However, benefits of increased solubility are not typically seen until particles are in the submicron range, usually <100 nm (Junghanns and Muller, 2008; Sun et al., 2012).

1.7 Absorption Modeling

PK modeling divides the body into separate compartments. Classical compartmental modeling lumps kinetically homogenous organs and tissues together into a single mathematical compartment. For absorption models, the intestines are typically represented as separate mathematical compartments that link to the rest of the model by a single first-order absorption rate constant.

PBPK models attempt to be more mechanistic, as compartments represent specific organs or tissues that are connected by blood flows. PBPK models integrate drug physicochemical properties, typically collected from *in vitro* experiments or *in silico* predictions, and physiological parameters from animal or clinical data. Values can

also be obtained from the literature. Commonly incorporated drug-specific parameters include drug molecular weight, tissue to blood partition coefficient, pka, logP, and plasma protein binding. Blood flow, organ composition, and organ volume are physiological parameters integrated into PBPK models. In addition, the inclusion of transporters and metabolic enzymes are essential for better predictions of their drug substrates.

Many PBPK models have been created to capture the complex process of oral absorption. For humans, the Advanced Compartment Absorption and Transit (ACAT) model is a well-established, well-known example (Agoram et al., 2001). This model, shown in Figure 1.5, describes the gastrointestinal tract as a series of compartments, allocating one compartment to the stomach, seven to the small intestine, and one to the colon. The ACAT model uses ordinary differential equations to describe drug movement.

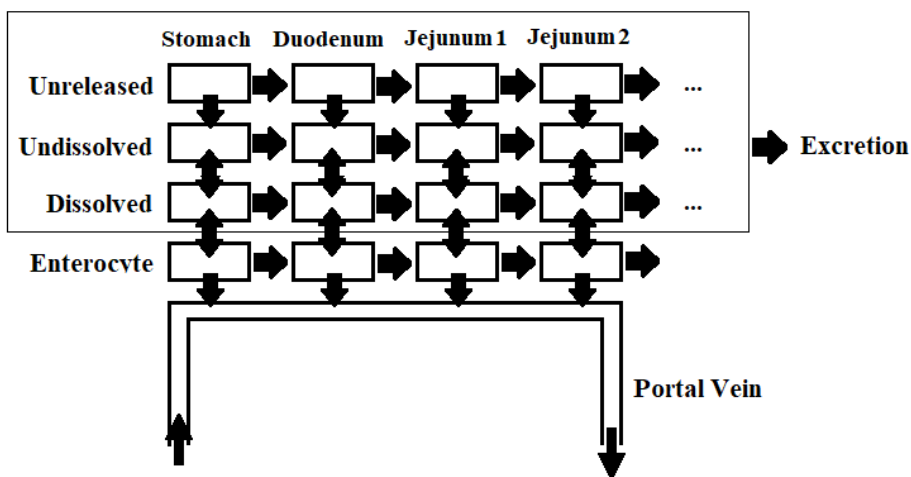


Figure 1.5 Condensed representation of the ACAT Model (Lin and Wong, 2017)

When considering a solid oral dose, the drug can exist as one of three forms: unreleased, released and undissolved, or released and dissolved. The drug moves from one compartment to the next in either a reversible manner, such as an undissolved to a dissolved drug, or irreversible manner, from the stomach to the duodenum, as indicated by double- or single-headed arrows, respectively. The drug moves along the compartments from the stomach to the colon and, if unabsorbed, is excreted in the feces. If the drug is released and dissolved, it can be taken up into the enterocytes and make its way into the portal vein. The portal vein leads to a first-pass liver compartment, a central compartment, an optional peripheral compartment, and clearance from the body (Huang et al., 2009).

The ACAT model was an extension of an earlier compartmental absorption and transit model (Yu et al., 1996). Unlike its predecessor, the ACAT model incorporated dissolution rate, pH-dependent solubility, first-pass metabolism (gut and liver), and absorption in the stomach and colon. The ACAT model also included physiological parameters such as the changes in surface area and transporter expression along the intestine (Agoram et al., 2001).

Another more recent approach to modeling intestinal absorption is the Continuous Intestinal Absorption Model (Nagar et al., 2017). Like the ACAT, this model considers many physiological factors and drug physicochemical properties. However, this model does not break the intestine into discrete compartments but assumes the intestine is a

single continuous compartment. Additionally, unlike the ACAT model, where each distinct compartment has its physiological parameters, this model describes pH, surface area, transporter expression, and gastrointestinal velocity as functions that fluctuate over the length of the intestine. The drug concentrations along the intestine change as a function of both distance and time, using partial differential equations.

This model includes dissolution as well as precipitation functions, which may occur if the concentration of the drug in the lumen exceeds the solubility of the drug. Explicit enterocyte apical membrane inclusion allows for more accurate modeling of efflux transporters, like P-gp, as drugs are transported directly out of the apical membrane. Also, the inclusion of explicit lipid compartments allows for partitioning into intracellular lipids.

Due to the widespread use of rats as a preclinical species, developing a continuous model to predict absorption in rodents would be valuable. Like the human model, it will incorporate physiological factors, such as pH and transporter expression along the intestine, surface area changes, and transit velocity. Areas of exploration include food intake and known particle size in suspensions.

1.8 **Drugs of Interest**

An ideal model should provide accurate predictions for a variety of compounds.

Glyburide (GLY) is an acidic BCS Class II compound that is expected to show pH- and

transit time-dependent absorption. Both GLY and digoxin (DIG), a neutral BSC Class IV compound, are transporter substrates. The incorporation of transporter expression along the intestine should improve predictions. Amlodipine (AML) is a basic BSC Class I drug, thus only gastric emptying is expected to influence its absorption profile. This drug can serve as a positive control when administered with GLY and may be used to refine the model before predicting exposure profiles for GLY.

1.8.1 Glyburide (GLY)

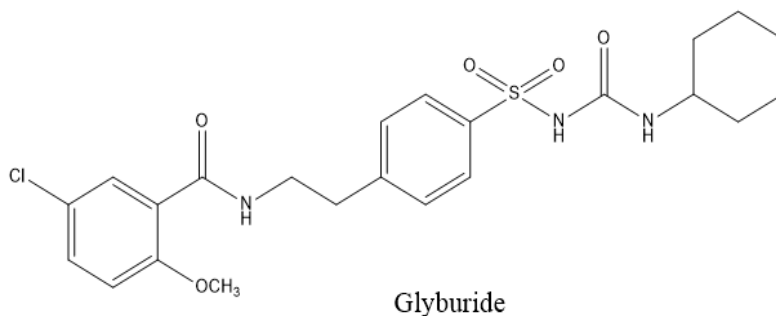


Figure 1.6 Structure of GLY

GLY (Figure 1.6), also called glibenclamide, is a potent second-generation sulfonylurea used to treat type II diabetes. GLY stimulates insulin secretion by blocking ATP-dependent potassium channels in pancreatic beta cells. GLY is an acid with a pKa and logP of 5.3 and 4.5, respectively (Wei et al., 2008). The blood to plasma ratio is 0.58 (Varma et al., 2014). GLY is >98% bound to plasma proteins (Olsen et al., 1995; Holt et al., 2019).

In humans, the oral bioavailability of GLY is formulation-dependent, but a micronized dose revealed a bioavailability of ~90% (Rydberg et al., 1995). GLY has a clearance and steady-state volume of distribution of ~4.5 L/h and ~5.4 L, respectively. The elimination half-life is 7 – 10 hours. GLY is metabolized into two primary pharmacologically active compounds, 4-trans-hydroxyglyburide and 3-cis-hydroxyglyburide, in the liver by CYP2C9 and CYP3A4 (Zuber et al., 2002). These metabolites leave the body through urinary (50%) and biliary excretion (50%) (Li et al., 2017). No significant enterohepatic recycling occurs (Pearson, 1985). GLY is reported to be a transporter substrate in humans. In the intestines, GLY is taken up by OATP2B1 and effluxed by BCRP and P-gp (El-Kattan and Varma, 2011; Estudante et al., 2013).

The clearance and volume of distribution in rats are ~5 L/hr/kg and ~250 ml, respectively. The elimination half-life is 1 – 3 hours (Neerati and Gade, 2011; Samala and Veeresham, 2016). The predominant metabolite produced in rat liver microsomes rats was ethyl-hydroxyl glyburide, primarily by CYP2C11 (Liu et al., 2012; Zhou et al., 2016). Jiang et al. performed inhibition studies in rats by co-administering GLY with the Oatp1a5 inhibitor naringin, indicating GLY is likely an Oatp1a5 substrate (Jiang et al., 2015). GLY is also a substrate for rodent Bcrp1 and P-gp (Berginc et al., 2010; Liu et al., 2012).

1.8.2 Digoxin (DIG)

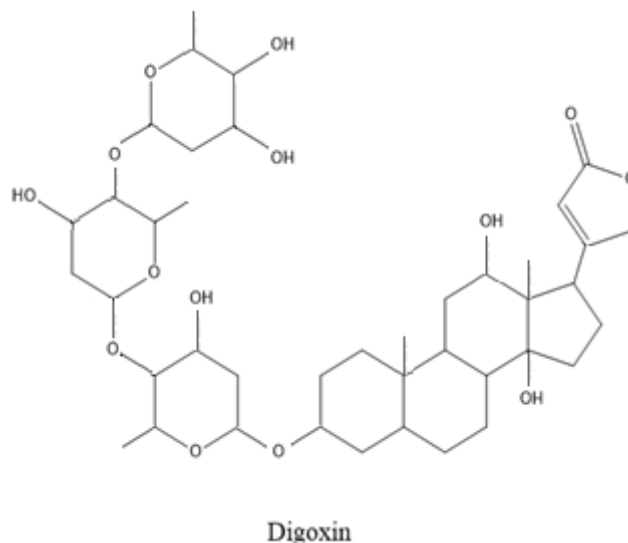


Figure 1.7 Structure of DIG

DIG (Figure 1.7) is a cardiac glycoside that inhibits the sodium-potassium ATPase pump in cardiac myocytes. This inhibition leads to a buildup in intracellular calcium and increased myocardial contractility. DIG is a neutral compound with a pKa of 7.15 (Hutchinson et al., 2018). The blood to plasma ratio and logP are 1.07 and 1.13, respectively (Scotcher et al., 2017). DIG is ~25% bound to plasma proteins (Koup et al., 1975; Scotcher et al., 2017).

Upon oral administration in humans, DIG has a bioavailability of 70 – 80% (Ochs et al., 1978). The clearance and volume of distribution of DIG are ~5 L/hr and ~6 L/kg, respectively. The elimination half-life is around 26 – 45 hours (Lisalo, 1977). In humans, ~ 75% of DIG is excreted unchanged in the urine (Koup et al., 1975). The remaining

~25% is eliminated through non-renal routes and non-CYP mediated metabolism to digoxigenin-bisdigitoxoside, digoxigenin monodigitoxoside, and dihydrodigoxin (Kramer et al., 1979; Dasgupta, 2012). Around 6.5 – 10% of the dose undergoes enterohepatic recycling (Doherty et al., 1970; Caldwell and Cline, 1976). DIG is a substrate of the efflux transporter P-gp in humans (El-Kattan and Varma, 2011). Studies in humans indicate DIG is not an intestinal OATP substrate (Taub et al., 2011).

The oral bioavailability in rats is around 70% (Salphati and Benet, 1998; Kato et al., 2008). DIG has a clearance and steady-state volume of distribution of 3 L/h/kg and 1.4 L/kg, respectively. The elimination half-life is 2 – 4 hours. In rats, > 60% of DIG is metabolized to digoxigenin bis-digitoxoside by CYP3A2, while the remaining drug is excreted unchanged through renal (30%) and biliary (10%) routes (Salphati and Benet, 1999). In rats, DIG is a substrate of Oatp1a4, which is highly expressed in the blood-brain barrier, but not the intestine. There is no current evidence of DIG being an Oatp1a5 substrate (Suzuki et al., 2014; Taskar et al., 2017). DIG is a substrate of the efflux transporter P-gp in rats (Suzuki et al., 2014)

1.8.3 Amlodipine (AML)

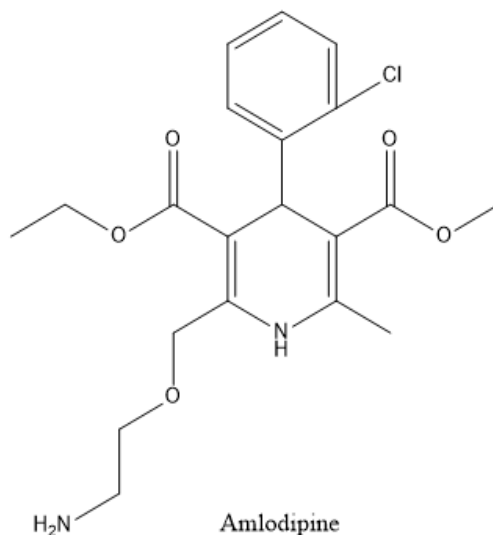


Figure 1.8 Structure of AML

AML (Figure 1.8) is an anti-hypertensive medication that blocks calcium channels in vascular smooth muscle and myocardial cells. This blockade of calcium influx inhibits the contraction of cardiac muscles, lowering blood pressure (Fares et al., 2016). AML is a base with a pKa and logP of 9.1 and 2.96, respectively (Caron et al., 2004). The blood to plasma ratio is 1.48 (Small et al., 2011). AML is ~98% bound to plasma proteins (Meredith and Elliott, 1992).

Upon oral administration in humans, AML has a bioavailability of ~64% (Meredith and Elliott, 1992). AML is considered a BCS Class I drug due to its high metabolite excretion in urine (~93%) (Shohin et al., 2010). In humans, AML has a clearance and apparent

volume of distribution of ~7 ml/min/kg and ~21 L/kg, respectively. The elimination half-life of AML is around 35 hours (Faulkner et al., 1986; Stopher et al., 1988). AML is >90% metabolized by CYP3A4 into multiple metabolites and is primarily (>60%) eliminated through urine (Stopher et al., 1988; Zhu et al., 2014). The major metabolite in humans, 2-([4-(2-chlorophenyl)-3-ethoxycarbonyl-5-methoxycarbonyl-6-methyl-2-pyridyl]methoxy) acetic acid, accounted for ~33% of metabolites in the urine (Beresford et al., 1988b). AML is not reported to be a substrate of P-gp (Vincent et al., 2000; Rausl et al., 2006). In vitro studies suggest AML is a weak P-gp inhibitor (Darvari and Boroujerdi, 2004) and a moderate BCRP inhibitor (Takara et al., 2012).

Upon oral administration in rats, AML has a bioavailability of ~100%. In rats, AML has a clearance and a steady-state volume of distribution of ~5 L/hr/kg and ~32 L/kg, respectively (Stopher et al., 1988; Wang et al., 2016; Zhang et al., 2019). The elimination half-life of AML is around 11 hours (Zhang et al., 2018). AML is ~90% metabolized into many metabolites, with the primary metabolite accounting for ~65% of metabolites found in the urine. AML is excreted through both renal (~40%) and fecal (60%) routes (Beresford et al., 1988a; Stopher et al., 1988). The AUC of AML significantly increased when administered with troleandomycin, a CYP3A1/2 inhibitor, indicating these enzymes may be responsible for AML metabolism (Lee et al., 2006).

1.9 Hypothesis

The broader hypothesis of this project is:

Physiological parameters and drug properties can be combined and incorporated into a new continuous rat intestinal absorption pharmacokinetic model to better predict a drug's absorption profile, and to characterize the effects of variables like food and particle size on drug absorption.

1.10 Goals

The broader goals of this project are:

1. To gather in-house anatomical data under fasted and fed conditions for use in a rodent absorption model
2. To determine the effect of presence and timing of food administration and particle size on the absorption of AML, GLY, and DIG
3. To develop and refine a continuous rodent absorption model from experimental data
4. To predict C-t profiles and compare against experimentally observed C-t profiles to test the goodness of predictions

1.11 Specific Aims

The goals of this thesis proposal were evaluated with the following specific aims. The thesis dissertation document is organized as a specific aim in each chapter.

1. Development and validation of bioanalytical methods for quantification of AML, GLY, and DIG in rat plasma and rat liver microsomes
 - Develop and validate methods for AML, GLY, and DIG using LC-MS/MS
2. Collection of data relating to pH over intestinal distance and gastrointestinal motility over time in the rat intestine under fed and fasted conditions
 - Collect pH along the intestine
 - Divide intestine into 10 parts (duodenum, jejunum 1 - jejunum 5, ileum, cecum, proximal colon and distal colon)
 - Collect luminal contents and measure pH in fed and 12-hour fasted rats
 - Collect motility data
 - Dose fed and fasted rats with 0.5 mL of 5% charcoal in 1.5% methylcellulose
 - Sacrifice rats after predetermined time points and measure plug length traveled
3. Collection of *in vitro* ADME and IV data for AML, GLY, and DIG
 - Perform equilibrium dialysis to determine the fraction unbound in microsomes
 - Run dialysis using 2 μ M AML in 0.1 mg/mL rat liver microsomes at 37°C and 5% CO₂ for 5 hours
 - Collect IV data
 - Intravenously dose male SD rats with (1) AML and GLY combination and (2) DIG
 - Collect blood samples over 24 hours and analyze data using LC-MS/MS

- Determine C-t profiles to evaluate the distribution and elimination information and obtain PK parameters
4. *In vivo* PK study to assess the effect of the presence and timing of feeding on the absorption profile of AML, GLY, and DIG
- Orally gavage fasted male SD rats with AML and GLY combination
 - Alter feeding schedule: (1) fed, (2) 12-hour fast followed by feeding 1 hour post-dose and (3) 12-hour fast followed by feeding 2 hours post-dose
 - Orally gavage male fasted male SD rats with DIG
 - Alter feeding schedule: (1) fed, (2) 12-hour fast followed by feeding 30 minutes post-dose, and (3) 12-hour fast followed by feeding 1 hour post-dose
 - Collect blood samples over 24 hours for all drugs and analyze data using LC-MS/MS
 - Determine C-t profiles, PK parameters, and effects of food presence/timing
5. *In vivo* PK study to assess the effect of particle size on the absorption profile of GLY
- Orally gavage fasted male SD rats with different particle sizes of GLY
 - Collect blood samples over 24 hours and analyze data using LC-MS/MS
 - Determine C-t profiles, PK parameters, and effects of particle size
6. Modeling the physiologic functions and *in vivo* data to predict the oral absorption profiles of AML, GLY, and DIG using the rat continuous intestinal absorption model
- Input analytical data collected from Specific Aim 2 and Specific Aim 3
 - Compare experimentally measured C-t profiles of AML, GLY, and DIG (from Specific Aim 4 and Specific Aim 5) to model profiles and check the correctness of the predictions versus experimental data

CHAPTER 2: BIOANALYTICAL METHODS

2.1 Rationale

To have confidence in plasma concentration measurements, a validated bioanalytical method is necessary. Numerous liquid chromatography-tandem mass spectrometric (LC-MS/MS) methods for glyburide (GLY) (Mistri et al., 2007; Narahariseti et al., 2007), digoxin (DIG) (Yao et al., 2003; Kirby et al., 2008), and amlodipine (AML) (Wang et al., 2016; Zhang et al., 2018) have been developed and validated. A robust bioanalytical method should be accurate, precise, linear, selective, and sensitive, with little carryover. This chapter aims to develop and validate an in-house LC-MS/MS method for AML, GLY, and DIG in rat plasma and rat liver microsomes (RLM).

2.2 Materials

Sprague-Dawley rat plasma was purchased from Equitech Biotech Inc (Kerrville, TX). Rat liver microsomes were purchased from SEKISUI XenoTech (Kansas City, KS). Glyburide was obtained from Frontier Scientific (Logan, Utah). Digoxin was obtained from Tocris (Ellisville, MO). Amlodipine was purchased from Alfa Aesar (Haverhill, MA). Glyburide-d3 and digoxin-d3 were ordered from Cayman Chemical (Ann Arbor, MI). Amlodipine-d4 was obtained from Toronto Research Chemicals (North York, Canada). Ammonium formate was purchased from Aldrich Chemical Company (Milwaukee, WI). Optima grade acetonitrile was ordered from Fisher Chemical (Fair

Lawn, NJ). Formic acid, an ACS Reagent, was purchased from Honeywell Fluka (Buches, Switzerland).

2.3 Assay Development

2.3.1 Preparation of Stocks and Calibration Samples

Stock solutions of AML, GLY, and DIG were prepared in dimethyl sulfoxide (DMSO). Internal standards (IS) glyburide-d3 (GLY-d3) and digoxin-d3 (DIG-d3) were prepared at 100 ng/ml and 390 ng/ml in acetonitrile (ACN), respectively. For the combined AML and GLY methods, a single IS solution was used. For this solution, amlodipine-d4 (AML-d4) and GLY-d3 were prepared at 25 ng/mL and 150 ng/mL in ACN, respectively. Working solutions of AML, GLY, and DIG were serially diluted in DMSO, then spiked 1:100 into matrix. Final standards included 1% DMSO. Calibration standards for GLY ranged from 12.5 – 500 ng/mL (0.0253 – 1.01 μ M) and DIG ranged from 0.75 – 96 ng/mL (0.960 – 122.9 nM) in rat plasma. Calibration standards for the combined AML and GLY plasma method ranged from 1.5 – 90 ng/mL (0.00367 – 0.221 μ M) and 25 – 1000 ng/mL (0.0506 – 2.03 μ M), for AML and GLY, respectively. In RLM, calibration standards for the combined AML and GLY method ranged from 15.6 – 1000 ng/mL (0.0382 – 2.45 μ M) and 15.6 – 1000 ng/mL (0.0316 – 2.03 μ M) for AML and GLY, respectively. Quality control (QC) samples were prepared from a separate stock and used for assay validation.

2.3.2 Sample Preparation

AML + GLY

Plasma samples analyzed for AML and GLY were mixed with two and a half times the volume of IS in ACN to precipitate proteins. Samples were vortexed and centrifuged at 15,000 g for 10 minutes at 4°C. Ten µL supernatant was injected into the LC-MS/MS system for analysis.

RLM samples for both AML and GLY were analyzed using the same method. RLM samples were mixed with an equal volume of 100 mM phosphate buffer containing 0.1 mM EDTA (pH 7.4). The mixture was combined with two times the volume of IS in ACN. Samples were vortexed and centrifuged at 15,000 g for 10 minutes at 4°C. Fifteen µL supernatant was injected into the LC-MS/MS system for analysis.

GLY

Plasma samples analyzed for GLY were mixed with two and a half times the volume of IS in ACN to precipitate proteins. Samples were vortexed and centrifuged at 15,000 g for 10 minutes at 4°C. Fifteen µL supernatant was injected into the LC-MS/MS system for analysis.

DIG

Method 1

DIG plasma samples were mixed with two times the volume of IS in ACN. Samples were vortexed and centrifuged at 15,000 g for 10 minutes at 4°C. Twenty µL supernatant was injected into the LC-MS/MS system for analysis.

Method 2

To 150 µL DIG plasma samples, 10 µL of IS in ACN was added and vortexed. The sample was combined with 1 mL methyl tert-butyl ether and vortexed for 10 minutes. The sample was then centrifuged at 15,000 g for 10 minutes at 4°C to separate the organic and aqueous phases. The organic phase was removed, placed into a separate tube, and then evaporated to dryness under a stream of nitrogen at 40 °C. The residue was reconstituted with 40 µL ACN and vortexed. Twenty µL supernatant was injected into the LC-MS/MS system for analysis.

2.3.3 LC- MS/MS conditions

Analysis was performed using an Agilent series 1100 high-performance liquid chromatography (HPLC) system coupled to an ABSciex API 4000 triple-quadrupole tandem mass spectrometer with an electrospray ionization source. The mass spectrometer was operated in positive ion mode. All LC-MS/MS data were acquired and processed using Analyst software version 1.6.

The mobile phase for AML and GLY consisted of water with 0.1% formic acid (FA) as the aqueous phase (A) and ACN with 0.1% FA as the organic phase (B). The gradient used for GLY elution started at 95% A and was maintained for 1.3 minutes. Mobile phase A was ramped down to 0% over 30 seconds and held for 5.7 minutes. Mobile phase A was then ramped back to 95% over 10 seconds and maintained until 9 minutes. The flow rate was 500 $\mu\text{L}/\text{min}$. Chromatographic separation for AML and GLY was performed on a Kinetex® C8 column (2.1 mm \times 50 mm, 5 μm) protected by a Phenomenex Security Guard C18 (2.0 \times 4 mm) guard column.

The mobile phase for GLY consisted of water with 0.1% FA as the aqueous phase (A) and ACN with 0.1% FA as the organic phase (B). The gradient used for GLY elution started at 70% A and was maintained for 1.3 minutes. Mobile phase A was ramped down to 0% over 30 seconds and held for 5.7 minutes. Mobile phase A was then ramped back to 70% over 10 seconds and maintained until 7.5 minutes. The flow rate was 500 $\mu\text{L}/\text{min}$. Chromatographic separation for GLY was performed on a Kinetex® C8 column (2.1 mm \times 50 mm, 5 μm) protected by a Phenomenex Security Guard C18 (2.0 \times 4 mm) guard column.

The mobile phase for DIG consisted of 10mM ammonium formate in water (pH to 4 with FA) as the aqueous phase (A) and ACN with 0.1% FA as the organic phase (B). The gradient used for DIG elution started at 70% A and was maintained for 1 minute. Mobile phase A was ramped down from 70% to 5% over 1.5 minutes and was maintained for 2.5

minutes before gradually increasing back to 70% over 0.1 minutes. Phase A then remained at 70% until 7 minutes. The flow rate was 600 $\mu\text{L}/\text{min}$. The analytical column used for HPLC was a Phenomenex® Gemini C18 column (100 mm \times 4.6 mm, 3 μm) protected by a Phenomenex Security Guard C18 (2.0 x 4 mm) guard column.

The columns remained at room temperature for analysis of all compounds. Declustering potential (DP), collision energy (CE), and collision exit potential (CXP) were optimized for AML, GLY, and DIG.

2.4 Assay Validation

To properly validate a method, the lower limit of quantification (LLOQ) must be established. The LLOQ serves as the lowest quantifiable concentration on the standard curve and must have a signal-to-noise ratio of at least 10. Tiwari et al. recommended measuring accuracy and precision with at least three concentration levels: low-QC, which should be within three times the LLOQ, mid-QC, and high-QC. Percent accuracy and precision should be within $\pm 15\%$ at all concentration levels (Tiwari and Tiwari, 2010).

Accuracy was calculated using the following equation:

$$\frac{(\text{Mean observed} - \text{Theoretical})}{\text{Theoretical}} \times 100$$

Precision was calculated using the following equation:

$$\frac{\text{Standard deviation}}{\text{Mean}} \times 100$$

The peak area ratio of analyte to IS and a weighting factor of 1/x for the combined AML and GLY method or 1/x² for GLY and DIG methods were used to build calibration curves with the linear least-squares regression method. Linearity was determined using at least six concentration standards. Selectivity was determined by preparing and analyzing blank plasma samples (Hartmann et al., 1994). Carryover was measured by running separately prepared highest standard (n=3), each followed by three blanks with IS. Subsequent blanks should be less than 20% of the LLOQ (Lowes et al., 2011).

2.5 Results

2.5.1 Assay Development

In rat plasma, the method for AML and GLY was satisfactory for quantification over the range of 1.5 – 90 ng/mL and 25 – 1500 ng/mL for AML and GLY, respectively. The method for GLY was suitable for quantification over the range of 12.5– 500 ng/mL. Method 2 for DIG was suitable for quantification from 0.75 – 96 ng/mL. In RLM, the method for AML and GLY was satisfactory for quantification over the range of 15.6 – 1000 ng/mL.

The retention time for AML and AML-d4 was ~3.00 minutes, while the retention time for GLY and GLY-d3 was ~3.27 minutes. The precursor → product ion transitions observed for AML, AML-d4, GLY, and GLY-d3 were 409.2 → 237.3, 413.2 → 237.3, 494.5 → 369.2, and 497.5 → 372.2, respectively. The dwell time for each ion transition was 200 msec. Table 2.1 summarizes the tandem mass spectrometer operating conditions for the combined AML and GLY method.

Table 2.1 Optimized operating parameters for AML and GLY combined method

Operating parameter	AML	GLY
Curtain gas (psi)	20	20
Ion source gas 1 (psi)	60	60
Ion source gas 2 (psi)	40	40
Ion spray voltage (V)	5000	5000
Temperature (°C)	500	500
DP (V)	71	96
CE (V)	17	21
CXP (V)	18	19

For GLY analyzed separately, the retention time for GLY and GLY-d3 was ~3.10 minutes. The precursor → product ion transitions observed for GLY and GLY-d3 were 494.5 → 369.2 and 497.5 → 372.2, respectively. The retention time for DIG and DIG-d3 was ~4.54 minutes. The precursor → product ion transitions analyzed for DIG and DIG-d3 were 798.5 → 651.5 and 801.5 → 654.5, respectively. The dwell time for each ion

transition was 200 msec. Table 2.2 summarizes conditions for GLY and DIG analyzed separately.

A representative chromatogram for AML and GLY using the combined method in rat plasma and RLM are shown in Figure 2.1 and Figure 2.2, respectively. A representative chromatogram for GLY and DIG in rat plasma is shown in Figure 2.3 and Figure 2.4, respectively.

Table 2.2 Optimized operating parameters for GLY and DIG

Operating parameter	GLY	DIG
Curtain gas (psi)	20	20
Ion source gas 1 (psi)	60	60
Ion source gas 2 (psi)	40	40
Ion spray voltage (V)	5000	5000
Temperature (°C)	500	350
DP (V)	55	70
CE (V)	30	20
CXP (V)	15	15

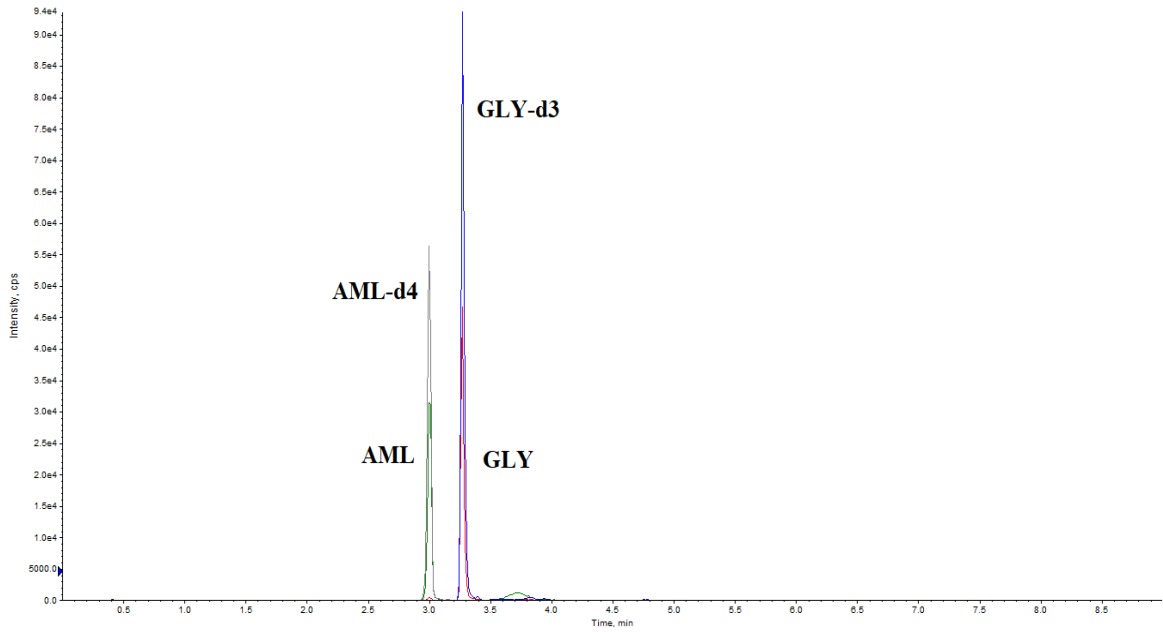


Figure 2.1 Representative chromatogram for AML and GLY in rat plasma

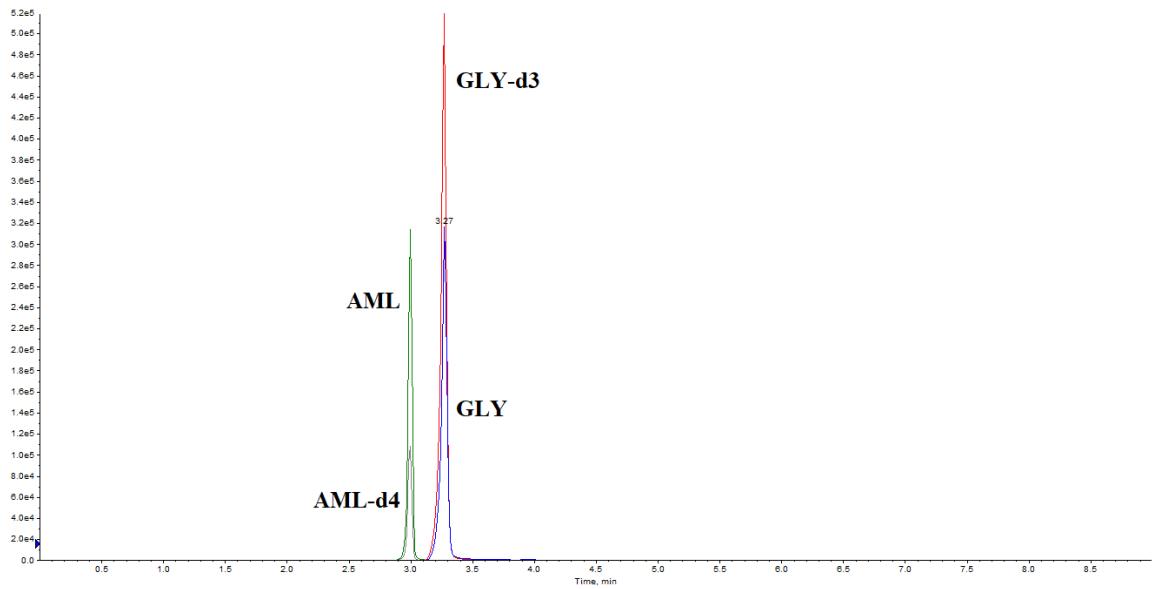


Figure 2.2 Representative chromatogram for AML and GLY in RLM

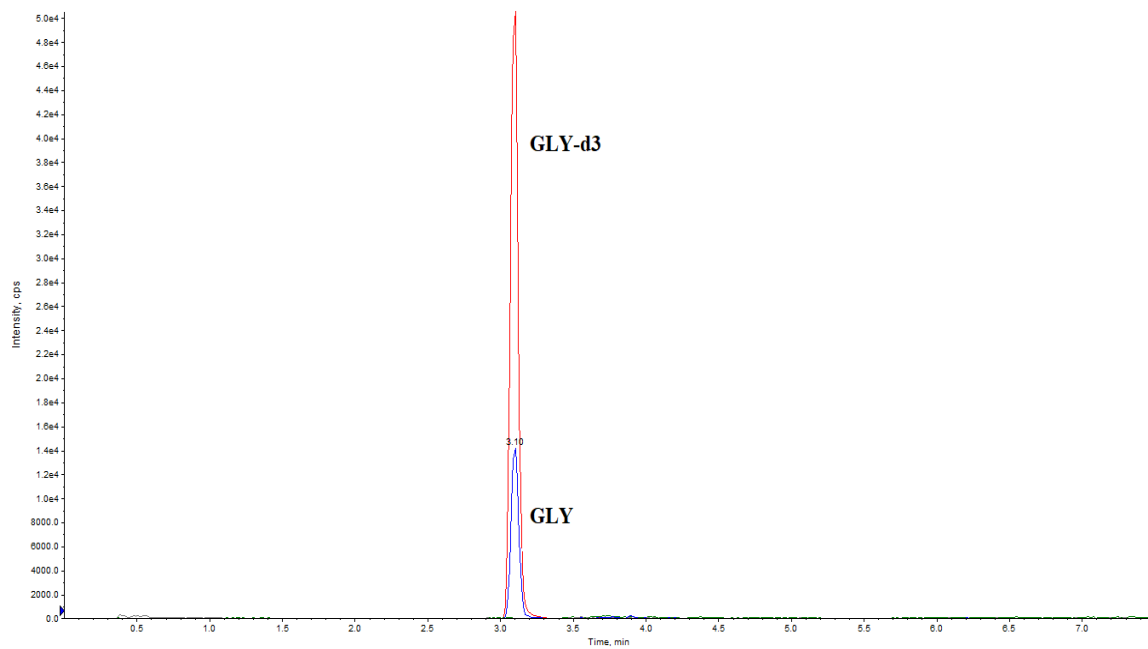


Figure 2.3 Representative chromatogram for GLY in rat plasma

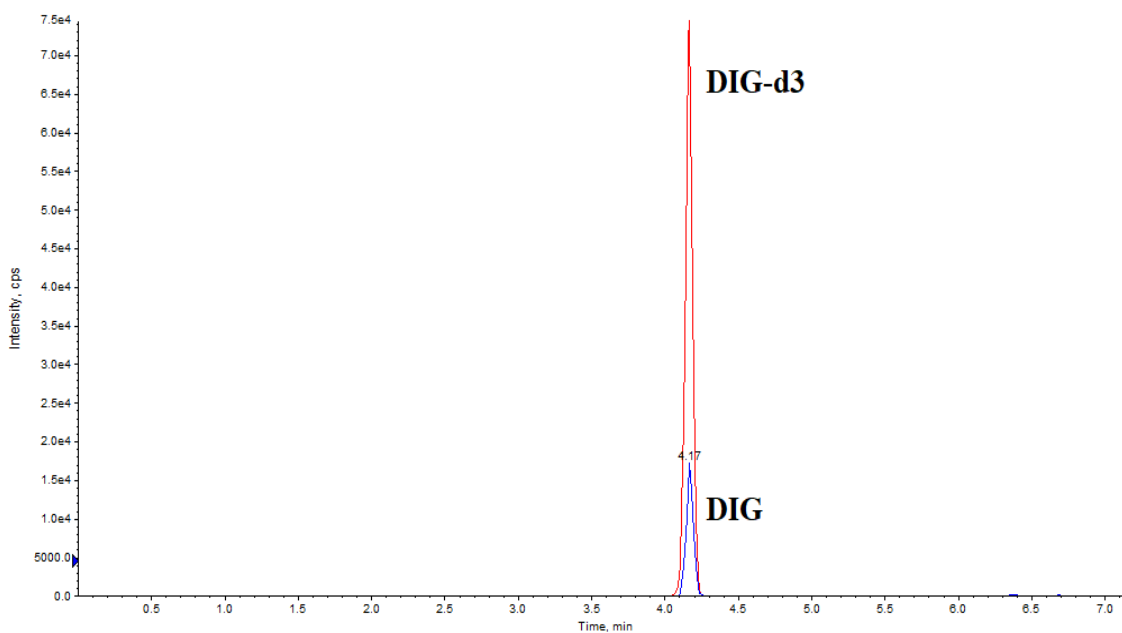


Figure 2.4 Representative chromatogram for DIG in rat plasma

2.5.2 Assay Validation

The relationship between the ratio of AML to AML-d4 and GLY to GLY-d3 peak area ratios and respective nominal concentrations were linear and well-represented by the equation $y = mx + c$. Representative standard curves for AML and GLY in rat plasma are shown in Figure 2.5 and Figure 2.6. The coefficient of determination (R^2) was > 0.99 when using a weighting factor of $1/x$, over the range 1.5 – 90 ng/mL and 25 – 1000 ng/mL for AML and GLY, respectively. The LLOQs, 1.5 ng/mL for AML and 25 ng/mL for GLY, can be measured with acceptable accuracy and precision. The inter- and intraday percent accuracy and percent precision were within $\pm 15\%$ for the tested QC samples for AML and GLY in rat plasma. Tables 2.3 and 2.4 summarize the results for inter- and intraday validation for AML and GLY in rat plasma.

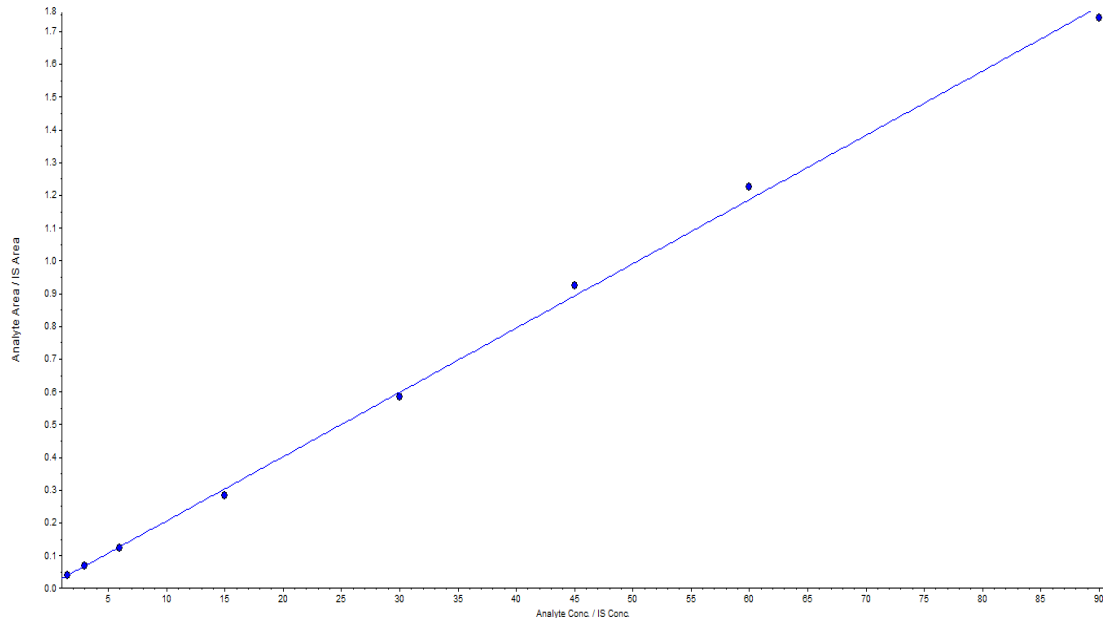


Figure 2.5 Representative standard curve for AML in rat plasma (AML/GLY combined). A single replicate for each standard concentration run on the same day is shown.

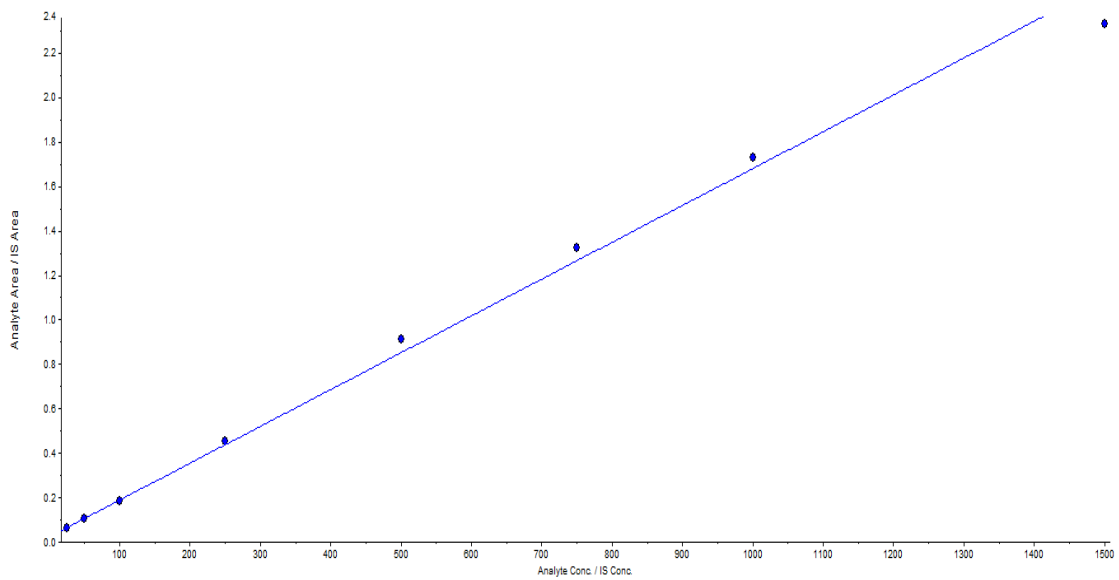


Figure 2.6 Representative standard curve for GLY in rat plasma (AML/GLY combined). A single replicate for each standard concentration run on the same day is shown.

Table 2.3 Inter-day (n=3) validation for AML and GLY (combined method) in rat plasma

Compound	Nominal Concentration (ng/mL)	% Accuracy	% Precision
GLY	1350	7.1	3.7
	450	-2.4	5.8
	150	-5.0	7.2
	50	5.0	7.4
AML	81	2.8	3.1
	27	2.7	5.7
	9	3.1	6.0
	3	0.04	7.2

Table 2.4 Intra-day (n=3) validation for AML and GLY (combined method) in rat plasma

Compound	Nominal Concentration (ng/mL)	% Accuracy	% Precision
GLY	1350	6.2	5.3
	450	-8.1	3.1
	150	-7.3	10.9
	50	5.3	6.7
AML	81	5.4	3.4
	27	0.1	2.7
	9	-0.9	5.7
	3	-2.1	2.0

The relationship between the ratio of GLY to GLY-d3 and DIG to DIG-d3 peak area ratios and respective nominal concentrations were linear and well-represented by the equation $y = mx + c$. Representative standard curves for GLY and DIG in rat plasma are shown in Figure 2.7 and Figure 2.8. The coefficient of determination (R^2) was > 0.99 when using a weighting factor of $1/x^2$, over the range 12.5 – 500 ng/mL for GLY and 0.75 – 96 ng/mL for DIG. The LLOQs, 12.5 ng/mL for GLY and 0.75 ng/mL for DIG, can be measured with acceptable accuracy and precision. The inter- and intraday percent accuracy and percent precision was within $\pm 15\%$ for the tested QC samples for GLY and DIG in rat plasma. Tables 2.5 and 2.6 summarize the results for inter- and intraday validation for GLY and DIG in rat plasma.

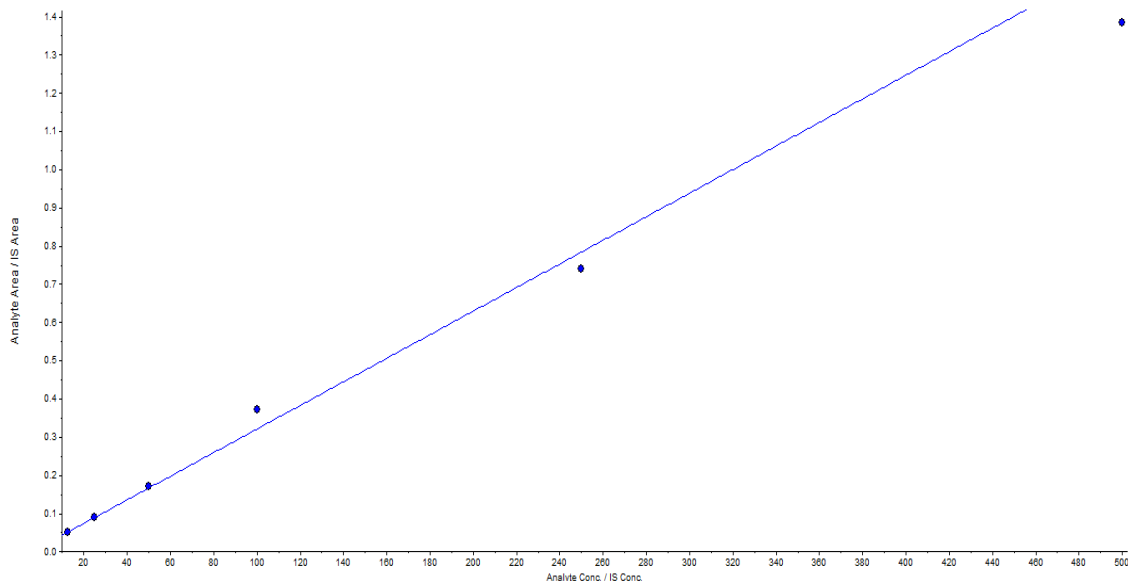


Figure 2.7 Representative standard curve for GLY in rat plasma. A single replicate for each standard concentration run on the same day is shown.

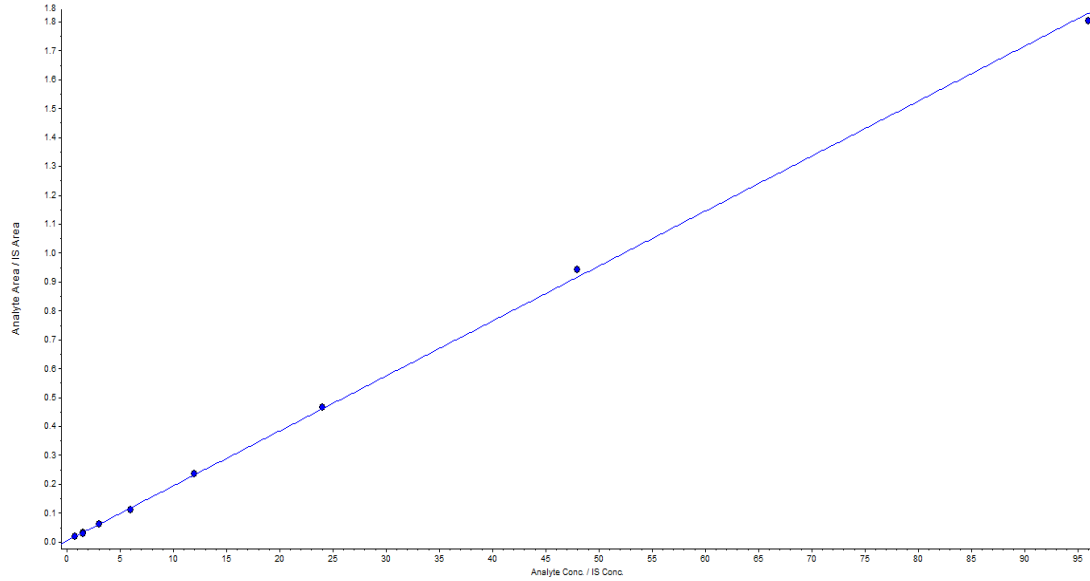


Figure 2.8 Representative standard curve for DIG in rat plasma. A single replicate for each standard concentration run on the same day is shown.

Table 2.5 Inter-day (n=3) validation for GLY and DIG in rat plasma

Drug	Nominal Concentration (ng/mL)	% Accuracy	% Precision
GLY	337.5	-5.0	2.3
	112.5	10.5	4.6
	37.5	5.5	12.2
	12.5	2.0	16.1
DIG (Method 2)	36	-2.1	4.6
	9	-1.1	5.6
	2.25	17.6	21.6

Table 2.6 Intra-day (n=3) validation for GLY and DIG in rat plasma

Drug	Nominal Concentration (ng/mL)	% Accuracy	% Precision
GLY	337.5	-2.8	3.7
	112.5	6.0	3.1
	37.5	7.7	8.5
	12.5	2.1	8.6
DIG (Method 2)	36	-2.1	9.3
	9	2.0	11.6
	2.25	1.8	29.6

The relationship between the ratio of AML to AML-d4 and GLY to GLY-d3 peak area ratios and respective nominal concentrations were linear and well-represented by the equation $y = mx + c$. Representative standard curves for AML and GLY in RLM are shown in Figure 2.9 and Figure 2.10, respectively. The coefficient of determination (R^2) was > 0.99 when using a weighting factor of $1/x^2$, over the range 15.6 – 1000 ng/mL for AML and GLY. The LLOQs, 15.6 ng/mL for AML and GLY, can be measured with acceptable accuracy and precision. The inter- and intraday percent accuracy and percent precision were within $\pm 15\%$ for the tested QC samples for AML and GLY in RLM. Tables 2.7 and 2.8 summarize the results for inter- and intraday validation for AML and GLY in RLM.

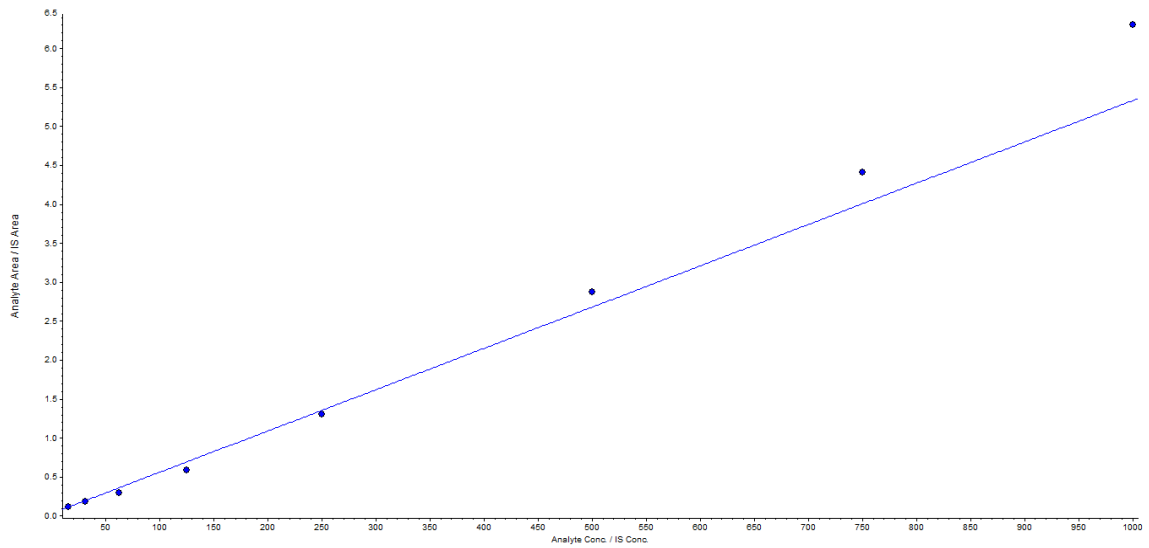


Figure 2.9 Representative standard curve for AML in RLM. A single replicate for each standard concentration run on the same day is shown here.

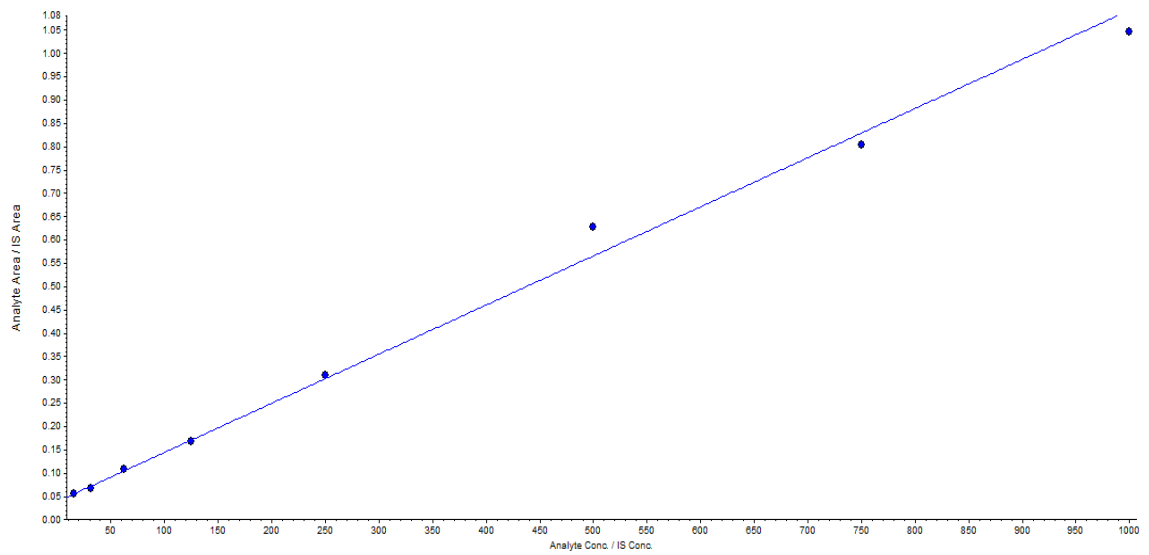


Figure 2.10 Representative standard curve for GLY in RLM. A single replicate for each standard concentration run on the same day is shown here.

Table 2.7 Inter-day (n=3) validation for AML and GLY in rat liver microsomes

Compound	Nominal Concentration (ng/mL)	% Accuracy	% Precision
AML	960	7.7	5.3
	240	-3.4	12.0
	60	-8.9	12.0
GLY	960	-8.8	0.8
	240	-4.2	2.3
	60	-1.9	18.4

Table 2.8 Intra-day (n=3) validation for AML and GLY in rat liver microsomes

Compound	Nominal Concentration (ng/mL)	% Accuracy	% Precision
AML	960	1.3	13.5
	240	5.2	7.6
	60	-3.2	8.2
GLY	960	-9.7	4.4
	240	-5.4	5.4
	60	-3.7	4.3

Blank plasma and microsomal samples showed no interfering peak at the analyte retention times for either AML, GLY, or DIG. Carry-over was less than 20% of LLOQ. For the combined AML and GLY rat plasma method, a wash was inserted between each sample to reduce carryover to an acceptable level.

2.6 Discussion and Conclusion

Accurate, precise, linear, selective, and sensitive LC-MS/MS methods for determining AML, GLY, and DIG concentrations in rat plasma and microsomes were developed and validated for analysis in *in vivo* PK studies and protein binding assays. Literature LLOQ's for AML, GLY, and DIG in rat plasma were around 1 ng/mL, 10 ng/mL, and 0.1 ng/mL, respectively (Yao et al., 2003; Mistri et al., 2007; Li et al., 2012; Wang et al., 2018). These values were similar to those achieved in-house (Table 2.9). The development of the RLM methods was adapted from previously validated LC-MS/MS methods in rat plasma.

Table 2.9 LLOQ comparisons experimental versus literature

Drug	Matrix	Experimental LLOQ (ng/mL)	Literature LLOQ (ng/mL)	Literature source
AML	Plasma	1.5	0.1 - 1.48	Wang et al. 2018
	RLM	15.6	n/a	Zhang et al. 2018
GLY	Plasma (combined method)	25	15 - 19.5	Mistri et al. 2007 Jiang et al. 2015
	Plasma (analyzed separately)	12.5		
	RLM	15.6	38.5	
DIG	Plasma	0.75	0.1	Yao, et al. 2003

A C8 column was necessary to prevent GLY from sticking to the column and to reduce carryover. A C8 column has less hydrophobicity, compared to a C18 column, due to its shorter carbon chain length, which reduces the retention of GLY, a hydrophobic compound. For DIG, the addition of 10 mM ammonium formate to the aqueous mobile phase supplies ammonium to form adducts. The ammonium adducts are less stable and fragment readily into daughter ions (Yao et al., 2003; Oiestad et al., 2009). The liquid-liquid extraction used in Method 2 was successful at concentrating samples for better detection.

CHAPTER 3: ANATOMICAL DATA COLLECTION

3.1 Rationale

Oral drug absorption is a complex process dependent on a variety of factors. The luminal environment plays a significant role and can be altered by age, gender, disease state, food intake, and other conditions (Abuhelwa et al., 2017). As mentioned in Chapter 1, important physiological factors contributing to a drug's absorption include luminal pH and gastrointestinal motility. To improve the representation of luminal conditions for the rodent absorption model in Chapter 7, in-house data was collected.

The rat intestine is divided into four major parts: the duodenum, jejunum, ileum, and colon (Figure 3.1). For data collection in this study, the duodenum was assumed to be the first 10 cm, starting immediately after the pylorus. The jejunum was the longest portion, ranging ~100 cm, and was thus divided into five portions. Five segments were chosen to minimize the number of segments, thus reducing handling time while reducing the length of each piece for ease of handling. The ileum was assumed to be the last 3 cm before the cecum. The short ileum length of the rat contrasts with human intestinal anatomy, where the ileum constitutes over half of the intestinal length. The rodent colon was divided into two equal parts, representing the proximal and distal regions. Anatomical observations supporting these divisions were reported in the literature (DeSesso and Jacobson, 2001; Vdoviakova et al., 2016).

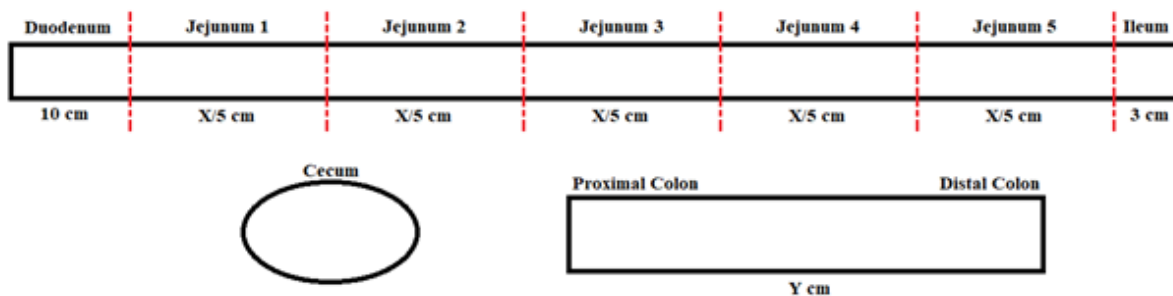


Figure 3.1 Depiction of rat intestinal segment division

SD rats are typically used in pharmacokinetic experiments, but there is little information regarding intestinal pH. Sparse small intestinal and colonic pH data is available but does not provide a detailed description (Knapp et al., 2013; Suksridechacin et al., 2020). The luminal pH can be affected by age, gender, rat strain, feeding conditions, and even food composition (Lin and Visek, 1991). For example, the current literature pH values for the rat proximal small intestine range from 5 - 7.5. Along with the variable reported values, the definition of each segment tends to be vague, with no clear description of portion length (Ward and Coates, 1987; McConnell et al., 2008; Christfort et al., 2019). More comprehensive measurements in the model animal, SD rats, at well-defined segments was collected for input into the absorption model detailed in Chapter 7. This is important because, as discussed below, pH variations may impact drug dissolution and transport.

For GLY (Figure 1.6, Chapter 1), which has a pKa of 5.3, changes in the luminal pH due to food consumption can severely impact its solubility. It has been reported that the dissolution of GLY is highly dependent on the pH of the surrounding media. For example, the percent of GLY powder dissolved in 30 minutes increased from 18% to

87% when the pH of the media was increased from 5.0 to 6.5 (Lobenberg et al., 2000). Additionally, in both humans and rats, the intraluminal pH becomes more alkaline along the intestine, increasing from the duodenum to the ileum (Fallingborg, 1999; McConnell et al., 2008). The solubility of GLY almost doubles as the pH of the surrounded media changes from pH 5.8 to pH 8.0, going from 2.59 $\mu\text{g/mL}$ to 4.57 $\mu\text{g/mL}$ (Singh et al., 2010). Due to the poorly soluble but highly permeable nature of GLY, this increase in solubility may aid in absorption at more alkaline portions of the intestine.

Contrarily, alterations in the intestinal pH range are not expected to change DIG (Figure 1.7, Chapter 1) dissolution because it is a neutral compound (Mudie et al., 2020). Additionally, the bidirectional transport of DIG across Caco-2 monolayers was shown to be pH-independent across the pH range 5 - 8 (Neuhoff et al., 2003). AML (Figure 1.8, Chapter 1) is a base with a pKa of 9.1, so it is ionized at physiological pH. As a BCS Class I compound, it has high solubility over the pH range 1.0 – 7.5, thus pH is not expected to influence its absorption (Tsume et al., 2014).

GI motility can greatly impact absorption by extending the time the drug is in contact with the absorptive surfaces of the small intestine. Due to the poor permeability and/or solubility of GLY and DIG, it is essential to capture the time at which drugs are exposed to each segment. Gastric emptying is delayed under fed conditions, leading to prolonged time in the acidic environment of the stomach. For weak acids, like GLY, with a pKa greater than the stomach pH, the drug is primarily unionized and permeable. While the

majority of GLY is absorbed in the proximal small intestine, a portion is taken up in the stomach, and prolonged stomach residence time may lead to increased absorption of GLY in humans (Brockmeier et al., 1985; Li et al., 2012).

In contrast, prolonged gastric emptying has been reported to degrade DIG and reduce exposure (Cohen et al., 1991). Exenatide-induced gastric delay increased the t_{max} and significantly decreased the C_{max} of DIG in humans (Kothare et al., 2005). Similarly, liraglutide-induced gastric delay resulted in a delayed t_{max} and a decrease in C_{max} . The authors mention that the changes in DIG's PK due to liraglutide are not clinically relevant enough to warrant a dose adjustment (Malm-Erfjelt et al., 2015). This may be less influential in rats, which have a stomach pH of 3 - 4, since degradation is minimal when the surrounding medium has a pH >3 (Gault et al., 1977; McConnell et al., 2008). In humans, delayed gastric emptying has no significant effect on AML exposure (Zimmermann et al., 1999; Rausl et al., 2006). However, a significant increase in AUC and shorter t_{max} was seen in vagotomized dogs. This was estimated to be due to a prolonged gastric emptying time and higher gastric pH (Kwak et al., 2006).

The most well-known methods for determining gastrointestinal transit time in preclinical species are scintigraphy, wireless motility capsules (WMC), and nonabsorbable marker tracking. Scintigraphy involves the ingestion of a radiolabeled meal or radiopharmaceutical, typically Technetium-99 or Indium-111. A collimator is used to focus the radiation, and a gamma camera takes images to create a 2D image. While this

method is accurate and nonterminal, this method is not feasible because it requires expensive equipment, upkeep, and training (Tougas et al., 2000; Maurer et al., 2013). WMC can capture multiple parameters in one use, including pH, temperature, and pressure along the intestine. Transit time is calculated by a change in one or more of those parameters. For example, an increase in pH and a sudden drop in pH indicate entrance into the duodenum and cecum, respectively. The time between these two events is the small intestinal transit time. Currently, the use of WMC has been validated in larger species, such as horses and dogs, while use in smaller animals, like rats, has not been well-studied (Stokes et al., 2012; Camilleri and Linden, 2016).

Nonabsorbable markers, such as phenol red and charcoal, are commonly used for determining intestinal transit time in rodents. A phenol red or charcoal test meal is dosed via oral gavage directly into the stomach. After a predetermined time has passed, the rodent is sacrificed, its intestines are removed, and the distance traveled by the meal is measured. This method requires terminal endpoints but is simple, well-studied, and inexpensive (Peddireddy, 2010). Both nonabsorbable markers are administered in a $\leq 10\%$ inert vehicle, such as methylcellulose or gum acacia. The most common doses are 0.05% phenol red (Souza et al., 2009; da Graca et al., 2015) or between 2 - 10% charcoal (Wang et al., 2001; Prior et al., 2012).

To reduce the number of animals sacrificed, rats from PK studies, Chapters 5 and 6, were used after at least a week of recovery. Blood loss is not reported to significantly impact

gastric emptying (Hatanaka et al., 1994). There is no literature evidence suggesting either GLY or DIG affect GI motility. Because both drugs are reported to have first-order elimination, 50% of the remaining drug is eliminated every $t_{1/2}$. Additionally, both drugs have a brief $t_{1/2}$ of <4 hours and a short t_{max} of <2 hours, most of either drug is expected to be eliminated by 36 hours post-dose in rats (Li et al., 2012; Suzuki et al., 2014). Therefore, after seven $t_{1/2}$ s have passed, less than 1% of the drug is expected to remain in the body (Gibaldi and Perrier, 1982).

Calcium channel blockers, like AML, are known to have gastrointestinal side effects such as constipation, which are brought upon by delayed gastric emptying and decreased intestinal contractility. Though the exact cellular mechanism is unclear, it is assumed that the calcium channel blockers reduce smooth muscle contractions in the intestinal tract (Brage et al., 1986; Koc, 2020). While there is little literature describing the effects of AML in rats, other calcium antagonists have been shown to produce dose-related gastric emptying delays in studies using phenol red. Verapamil was the most potent agent, with larger doses (20 - 40 mg/kg) significantly delaying gastric emptying of liquids (Brage et al., 1986). Conversely, lower doses of verapamil (1 - 4 mg/kg) do not show this effect (Ogle et al., 1985).

Furthermore, after a single administration in humans, the desired therapeutic effects subsided after 72 hours. Even after chronic dosing, pharmacodynamic effects subsided after 7 - 10 days (Abernethy, 1992). Lastly, AML is reported to have first-order

elimination. In rats, the $t_{1/2}$ is ~11 hours and the C_{max} is ~5 hours. Accounting for the $t_{1/2}$ and C_{max} , it is anticipated that less than 1% of the drug is expected to remain in the body after ~3.5 days. Rats that were administered AML were allowed to recover for at least ten days. The low dose (2 - 5 mg/kg), single administration, and prolonged recovery time should minimize any possible GI effects caused by AML administration.

3.2 Materials

Male Sprague-Dawley rats were ordered from Charles River (Wilmington, MA). Isotonic saline was obtained from Ricca Chemical (Arlington, TX). Activated charcoal (#05105-250G) and methylcellulose (viscosity 400cP) were purchased from Sigma-Aldrich (Allentown, PA). Isopropyl alcohol was obtained from LabChem (Zelienople, PA). Buffer solutions for pH calibration, the accupHast™ pH electrode (cat #13-620-297), and the accumet™ AE150 Benchtop pH meter were obtained from FisherScientific (Pittsburgh, PA). Phenol red was purchased from Alfa Aesar (Ward Hill, MA).

3.3 Methods

Male SD rats were singly housed under a 12-hr light/dark cycle. Rats were acclimated for at least four days in the Temple University Health Sciences Campus animal housing facility and 30 minutes in the procedure room prior to experimentation. Food and water were available ad libitum. All food was removed from the cages of fasted rat groups 12 hours prior to the beginning of the study.

3.3.1 pH Determination

Rats were euthanized by CO₂, followed by decapitation. Rats were placed on a platform, which was covered with a sterile cloth. The abdominal area was sprayed with 70% isopropyl alcohol to smooth down fur and maintain sterility. The abdomen was then cut open with sterilized scissors, avoiding the organs, to expose the viscera. The pyloric sphincter and the most distal portion of the colon that was accessible were clamped closed with forceps. The intestines were clamped to prevent bodily fluids from entering the lumen and influencing the pH. The intestines were then carefully removed, untangled, and rinsed once with saline. This rinse removed any fluids, such as blood from the mesentery, and kept the intestines from quickly drying out. Both intestines were laid out on a separate clean cloth.

The intestines were divided into a total of ten unequal segments (Figure 3.1), with the small intestine comprising seven of the segments. The first 10 cm, starting from the pylorus, was labeled the duodenum. The last 3 cm, ending at the cecum, was considered the ileum. The middle portion was divided into five equal parts, with jejunum 1 (J1) starting at the end of the duodenum and jejunum (J5) ending at the start of the ileum. The colon was divided into two sections: proximal and distal. The cecum was separately isolated.

Before handling, each segment was gently pat dry with a clean Kimwipe to remove excess saline. The next untouched portion was clamped prior to cutting to prevent

contamination. Once separated from the remaining intestines, a rough estimate of the percentage of the lumen that contained food contents was recorded. As shown in Table 3.1, there were six categories ranging from 0, where no food was seen in the segment, to 100, where food was present from the beginning to the end. These recordings were performed to aid in determining how the presence of food may affect the pH readings.

Table 3.1 Labels regarding the percentage of food present in the lumen

Label	Meaning
0	No food was seen in the lumen
0/25	Food present in the lumen but did not exceed 25%
25/50	Food contents made up between 25% and 50% of the lumen
50/75	Food contents made up between 50% and 75% of the lumen
75/100	Food contents made up between 75% and 100% of the lumen
100	Food was continuously present from the beginning to the end of the segment

The luminal contents were removed from each segment into a clean tube. A single, similarly-sized fecal pellet in the distal colon was mixed with 0.5 mL of water and vortexed to obtain a homogenous mixture for each rat. No water was added to any other segment. After initial pH measurements, an extra 0.5 mL of water was added to assess the influence of the water on the pH. This was done for one rat in each group.

The pH of the tube contents was measured using a pre-calibrated pH meter between one and three times, remixing between each reading. The order of the measurements was alternated to minimize post-mortem pH drift. The first rat was measured in the following order: duodenum, J1, J2, J3, J4, J5, ileum, cecum, proximal colon, and distal colon. The

next rat was measured from the distal colon to the duodenum in the opposite order. This alternation was followed for the entire study. The electrode was rinsed with distilled water between measurements, and the calibration was checked every five samples. The pH meter was recalibrated before a new set of rat samples or if the calibration was off by more than 0.05 pH units.

To determine the influence of food contents, the pH of the food pellets was measured. Three standard size rat pellets (~12 g) were placed in a tube containing 10 mL of water. The pellets were vortexed until fully disintegrated and no solid pieces could be seen. The pH meter was calibrated, and the pH of the pellet mixture was measured three times. The mixture was shaken between measurements. This procedure was done twice, using a total of six pellets divided into two tubes. The measurements were performed on two separate days.

3.3.2 Gastrointestinal Motility

Rats (n=36) were divided into one of two condition groups: fasted or fed. Rats were sacrificed at a predetermined time point of 10, 20, 30, 45, 60, 75, 100, or 120 minutes after dosing for each condition group.

Method 1

Phenol red solution was prepared by mixing phenol red powder in water until completely dissolved, then heating the solution to 90°C in a water bath. Methylcellulose (MC) was

added once the solution reached 90 °C. Once the MC was added, the solution was quickly and vigorously shaken for at least one minute. The solution was cooled by placing it on the benchtop and allowing the solution to come to room temperature prior to administration. This temperature transition is necessary as MC will only dissolve when in a hot solution (~90°C) and become viscous when cooled.

Male SD (n=3) rats were fasted for 12 hours, then given 0.5 mL of a 0.5 mg/mL phenol red in 1.5% MC solution by oral gavage. After a predetermined time passed, the rat was sacrificed. The rat's abdomen was opened in the same manner as described in 3.3.1. The intestines were cut along the length to lay flat. The position of phenol red along the intestine was visually evaluated and recorded.

Method 2

Two formulations were prepared to determine the most appropriate formulation for future studies. The goal was to minimize the percent charcoal and MC while not sacrificing color or viscosity. Formulation #1 consisted of 2.5% activated charcoal in 1% MC, while formulation #2 consisted of 5% activated charcoal in 1.5% MC.

A pilot study was composed of 12-hour fasted (n=2) and fed (n=3) male SD rats, which were administered 0.5 mL of a 2.5% activated charcoal in 1% MC (formulation #1) by oral gavage. A charcoal solution was made up at 1.5X the desired volume at room temperature. A MC solution was made up at 3X the desired volume at 90°C. The

solutions were mixed 2:4 MC:charcoal and vortexed for ~ 2 minutes. The mixture was allowed to cool to room temperature on the benchtop prior to administration. Formulation #1 was chosen for the pilot study due to the smaller amount of charcoal and MC.

The final study involved 12-hour fasted (n=18) and fed (n=17) male SD rats, which were administered 0.5 mL of a 5% activated charcoal in 1.5% MC (formulation #2) by oral gavage. The rats were sacrificed, and their intestines were inspected for charcoal visually, in the same manner to Method 1. The distance traveled by the charcoal plug was measured, along with the plug length. The furthest point of the charcoal plug was considered the distance traveled. Small dots of charcoal were noted but were not considered to be part of the plug.

3.3.3 Intestinal Dimension Collection

The length and width of each segment were collected during the other anatomical studies. Measurements were performed simultaneously with other terminal experiments to reduce the number of animals sacrificed and as a necessary part of previous studies. The intestines were cut along the length to lay flat, taking care not to overstretch the organs. The lengths of the small intestine (n=43) and colon (n=14) were measured with a tape measurer and recorded. Each segment's width (n=5) was also collected by measuring the distance from one side of the cut to another, perpendicular to the length.

3.4 Data Analysis

pH values and GI transit times were given as mean values (\pm standard deviation). Statistical analysis was performed using SPSS® Version 28 software (SPSS Inc., Chicago, IL, USA). Fasted versus fed pH data was analyzed using an Independent Samples t-test. Fasted versus fed GI motility data was analyzed using Welch's t-test to account for the unequal sample size between groups. A p-value < 0.05 was considered significant.

3.5 Results

3.5.1 pH Determination

The average pH of each intestinal segment for each rat is shown in Figure 3.2 and listed in Table 3.2. Table 3.3 lists the estimated average percent of the intestinal segment containing food contents. The complete list of pH measurements, rat weight, the exact length of each segment, total time fasted, and percentage estimate of food content is available in Appendix A.

Table 3.2 Average segment pH by rat

Segment Name	Fed group				Fasted group			
	Rat 25 [‡]	Rat 26 [‡]	Rat 33 ⁺	Rat 35 ⁺	Rat 34 ⁺	Rat 36 ⁺	Rat 37 ⁺	Rat 38 [‡]
Duodenum	6.1	6.0	5.9	6.2	6.6	6.4	6.4	6.3 [°]
Jejunum 1	6.0	6.0	5.7	6.1	6.5	6.4	6.3	6.5 [°]
Jejunum 2	6.3	6.3	6.1	6.2	6.8	6.5	6.5	6.6 [°]
Jejunum 3	6.5	6.7	6.5	6.5	6.5	6.5	6.5	6.6 [°]
Jejunum 4	6.7	7.0	6.9	6.9	6.7	6.6	6.7	6.7
Jejunum 5	7.0	7.1	6.7	7.0	7.1	7.8	7.3	7.4
Ileum	7.6	7.8	7.6	7.8	7.5	7.8	7.7	7.4
Cecum	5.8	5.6	5.5	5.8	6.9	6.9	6.6	6.3
Proximal Colon	5.6	5.5	5.4	5.8	6.7	6.5	6.4	6.1
Distal Colon	5.8	6.3	5.8	5.9	6.2	5.9	6.0	6.4

[°](n=1), [‡](n=2), and ⁺(n=3), where n is the number of pH readings taken per segment

Table 3.3 Average estimated percent of the lumen containing food contents

Segment Name	Duo	J1	J2	J3	J4	J5	Ileum	Cec	Prox colon	Dist colon
Fed (n=2)	12.5	25.0	50.0	75.0	81.3	87.5	100.0	100.0	100.0	100.0
Fasted (n=4)	6.3	12.5	31.3	37.5	53.1	50.0	81.3	100.0	100.0	65.6

Duo is the duodenum, J# is jejunum segment number #, Cec is the cecum, Prox colon is the proximal colon, and Dist Colon is the distal colon

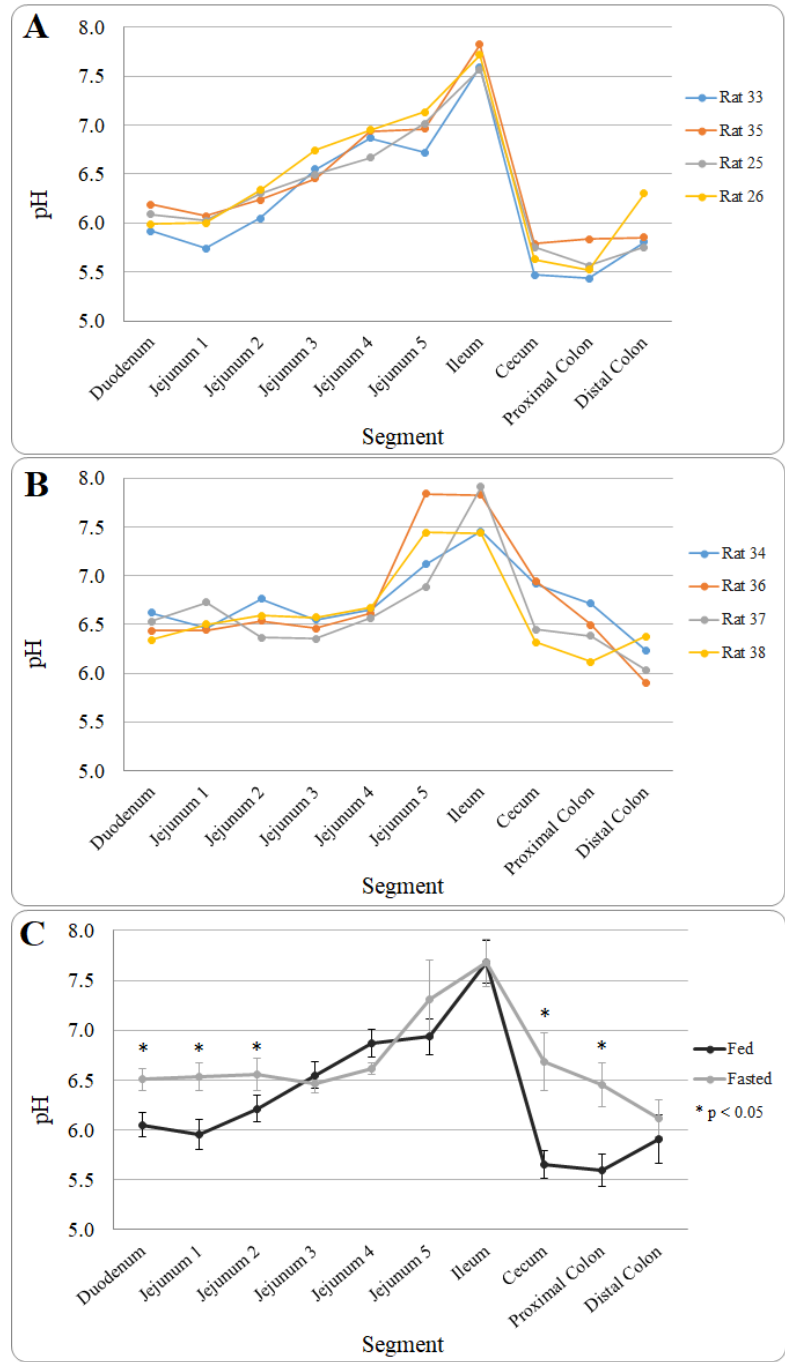


Figure 3.2 Average pH of contents along the intestine in rats. The pH averages are shown for each fed rat (A), each fasted rat (B), and a comparison of the fed versus fasted averages \pm std deviation (C). Data points for A and B are averages (n=3) of multiple measurements for the same animal/segment, while data points for C are averages (n=4) of multiple rats.

In fed rats, the pH began low at ~6 and gradually increased to ~7.5 in the ileum (Figure 3.4). The pH rapidly decreased to ~5.5, where it remained until the distal colon. In fasted rats, the pH started higher at ~6.5 and was maintained until the J4 segment. The ileum of fasted rats matched that of the fed group at ~7.5 before decreasing back to ~6.5 in the cecum and gradually declining along the colon. The fasted group had a significantly higher pH in the duodenum, J1, J2, cecum, and proximal colon segments.

3.5.2 Gastrointestinal Motility

No phenol red plugs were observed using Method 1. The use of charcoal in Method 2 (formulation #1) enabled visual detection of the plug along the intestine in fasted rats only. Results for Method 2 (formulation #1) are summarized in Table 3.4. Method 2 (formulation #2) allowed for the visual detection of the plug in both fed and fasted rats. Results for Method 2 (formulation #2) are summarized for individual fed and fasted rats in Table 3.5 and Table 3.6, respectively. Results for formulation #2 are summarized for the fed and fasted averages in Table 3.7 and Table 3.8, respectively. Comparisons between fed and fasted average distance traveled and length of the charcoal plug over time are shown in Figure 3.3 and Figure 3.4, respectively. Charcoal was clearly visible as a dark black plug, distinguishable from the brown intestinal contents. Visualization of the plug was possible from the duodenum to the ileum.

Table 3.4 Pilot charcoal study information.

Rat #	Group	Fast length (hr)	Time post dose (min)	Distance traveled (cm) [Segment]	Plug length (cm)
Rat 43	Fasted	14.7	37	38.8 [J2]	4.2
Rat 44	Fasted	14.9	100	108.8 [I]	5.8

D is the duodenum, J# is jejunum segment number #, and I is the ileum

Table 3.5 Individual fed charcoal study information

Rat #	Time post-dose (min)	Distance traveled (cm) [Segment]	Plug length (cm)
52	121	100.9 [J5]	29.4
53	100	87.9 [J3]	26.8
54	12	0.0	0.0
55	61	61.6 [J3]	13.4
56	44	64.8 [J3]	17.4
57	19	35.8 [J2]	5.2
58	74	72.2 [J3]	16.2
59	29	45.6 [J1]	2.6
60	31	47.1 [J2]	9.2
68	45	62.3 [J3]	4.1
69	125	99.3 [J5]	0.5
70	180	124.5 [I]	25.3
71	74	78.7 [J4]	24.2
77	62	65.8 [J3]	13.3
78	99	91.9 [J4]	19.1

D is the duodenum, J# is jejunum segment number #, and I is the ileum

Table 3.6 Individual fasted charcoal study information

Rat #	Fast length (hr)	Time post-dose (min)	Distance traveled (cm) [Segment]	Plug length (cm)
62	-	121	103.5 [J5]	9.45
63	-	21	23.6 [J1]	23.6
64	12.1	26	63.1 [J3]	12.7
65	11.8	181	124 [I]	7.8
66	12.0	101	86.5 [J5]	12.7
67	12.2	9	14.7 [J1]	4.7
72	12.1	9	15.9 [J1]	15.9
73	12.1	21	12.1 [J1]	12.1
74	13.0	23	31.4 [J1]	7.5
79	11.7	48	27.9 [J1]	7.8
86	11.9	102	92.7 [J4]	18.5
80	12.0	182	123 [J5]	22.2
84	12.2	120	124 [I]	12.0
85	11.9	76	87 [J4]	8.9
1*	12.1	45	17.9 [J1]	17.9
2*	12.4	13	13.5 [J1]	5.0

D is the duodenum, J# is jejunum segment number #, and I is the ileum. Fast length is the total time fasted.

Table 3.7 Average fed charcoal study information

Average time post-dose (hr)	Average distance traveled (m)	Average plug length (cm)
0.20	0.000	0.000
0.32	0.358	0.052
0.50	0.464	0.059
0.74	0.636	0.108
1.03	0.637	0.134
1.23	0.755	0.202
1.66	0.899	0.230
2.05	1.001	0.150
3.00	1.245	0.253

Table 3.8 Average fasted charcoal study information

Average time post-dose (hr)	Average distance traveled (m)	Average plug length (cm)
0.19	0.127	0.085
0.36	0.224	0.141
0.43	0.631	0.075
0.78	0.229	0.129
1.27	0.870	0.089
1.69	0.896	0.156
2.01	1.138	0.107
3.03	1.235	0.150

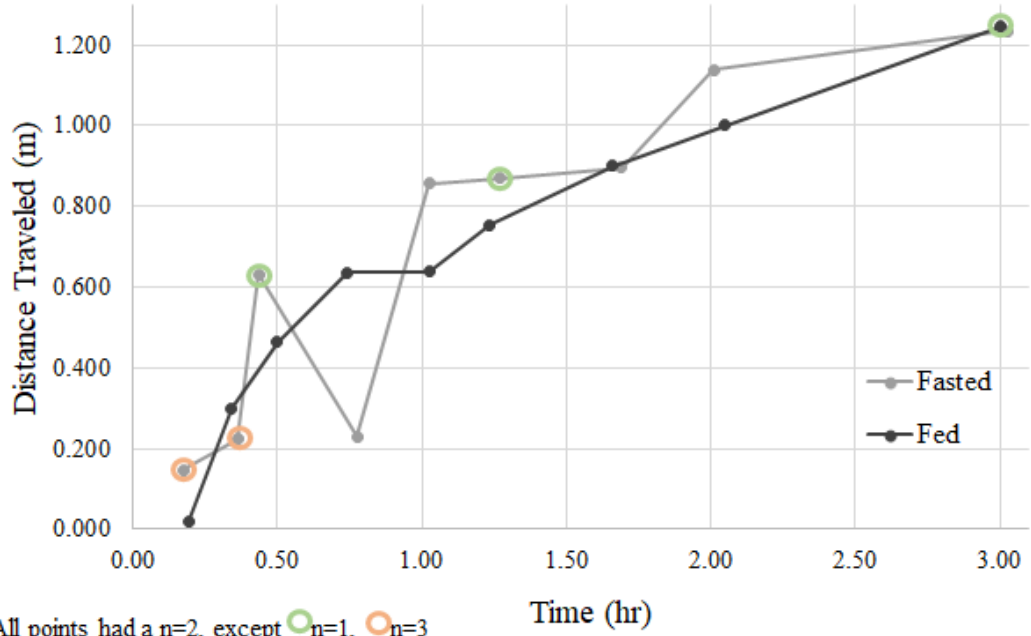


Figure 3.3 Fed versus fasted charcoal plug distance traveled over time

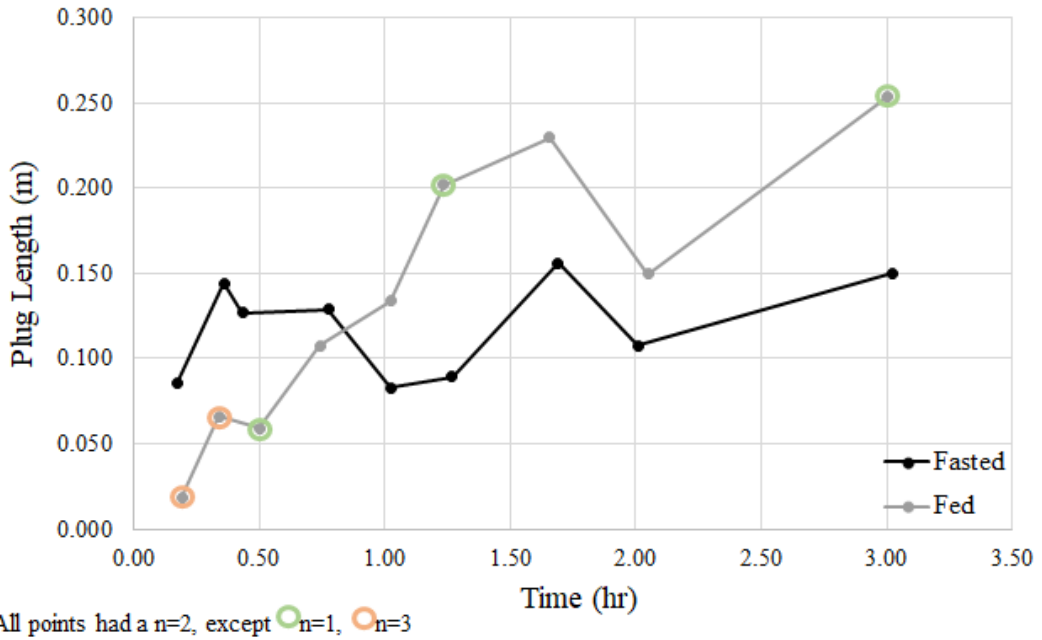


Figure 3.4 Fed versus fasted plug length over time

In both fed and fasted states, the velocity decreases as the charcoal plug moves along the intestine from the duodenum to the ileum, as shown in Table 3.9. For example, the velocity starts around 1 m/hr at 30 minutes and decreases to 0.26 m/hr in fed rats and 0.10 m/hr in fasted rats by three hours. While the plug length between the two feeding conditions differs, it is not statistically significant. There is an upward trend in fed rats. At the earliest time point, 10 minutes, the plug length is ~0.02 m, but by three hours it has increased to ~0.25 m. In contrast, the plug length remains relatively constant in fasted rats. From 10 minutes to three hours, all the measured time points have a measured plug length between 0.08 - 0.16 m.

Table 3.9 Fed versus fasted velocity data

Desired time point	Fed			Fasted		
	Average time (hr)	Distance (m)	Velocity (m/hr)	Average time (hr)	Distance (m)	Velocity (m/hr)
0.50	0.50	0.464	1.442	0.43	0.631	1.456
1.00	1.03	0.637	0.330	1.03	0.857	0.382
2.00	2.05	1.001	0.355	2.01	1.138	0.285
3.00	3.00	1.245	0.257	3.03	1.235	0.096

3.5.3 Intestinal Dimension Collection

The average lengths of the small and large intestines are listed in Table 3.10. The complete list of individual rat weights, total small intestinal lengths, single jejunum

segment lengths, and large intestine lengths are available in Appendix A. The average and individual data for the width of the lumen along the intestine are listed in Table 3.11.

Table 3.10 Average rat intestinal length data

Average total small intestine length (m) (n=43)	Average jejunum segment length (m) (n=43)	Average large Intestine length (m) (n=14)
1.19	0.212	0.159

Table 3.11 Width information for individual rats and averages

Width (m)						
Rat #	Duodenum	Jejunum 1	Jejunum 2	Jejunum 3	Ileum	Colon
2	0.0060	0.0100	0.0100	0.0100	0.0080	0.0140
3	0.0090	0.0090	0.0100	0.0095	0.0090	0.0090
4	0.0085	0.0100	0.0090	0.0090	0.0095	0.0140
5	0.0080	0.0080	0.0080	0.0080	0.0090	0.0105
6	0.0080	0.0090	0.0090	0.0090	0.0090	0.0110
AVG (n=5)	0.0079	0.0092	0.0092	0.0091	0.0089	0.0117

3.6 Discussion and Conclusion

The fasted group had an overall higher pH, which agrees with the literature (McConnell et al., 2008). In addition, the pH was within the pH 5 - 8 range reported in previous studies (Ward and Coates, 1987). The lower pH in the fed group could be associated with the presence of food in the collected luminal contents, but this is unlikely. The first

segments in fasted rats, which are the closest to the pellet pH, 5.93 ± 0.12 , contain the least estimated percentage of food (Table 3.3).

Method 1 was insufficient to measure the GI transit time in rats. The phenol red could not be visually evaluated once the intestinal lumen was exposed. This was most likely due to a pH related color change. Because it is a pH indicator, the color of phenol red ranges from yellow at pH values of < 6.4 to red at pH values of > 8.2

(<https://www.rsc.org/Merck-Index/monograph/m8630/phenolsulfonphthalein?q=authorize>, accessed on 01/24/2020). The rodent intestine had a pH range around 6 - 8, so at physiological pH, the color of the phenol red is likely yellow or orange. The intestines are either a pinkish hue, without food, or brown and orange, with lumen contents present (Appendix A). When analyzing visually, the phenol red is indistinguishable from the intestinal background due to the similarity in color.

Formulation #1, described in Method 2, provided a visible charcoal plug when dosed in fasted rats. However, there was no distinct plug when administered to fed rats. The increased presence of food in the stomach and intestines of fed rats likely led to the charcoal mixing with and being masked by food. Formulation #2 included a higher percentage of charcoal, accompanied by an increase in MC to keep the charcoal suspended. The percent of MC was kept as low as possible to prevent clogging the gavage needle and to reduce the amount of MC introduced to the rats. Using formulation #2, the dark black of the charcoal was noticeable against the light color of the lumen.

The velocity of the charcoal plug decreases as it goes along the rat intestine, which agrees with the literature (Varga, 1976; DeSesso and Jacobson, 2001). Furthermore, previous reports state gastric emptying was more rapid in fasted than fed humans and rats (Poulakos and Kent, 1973; Singh, 1999). While not statistically significant, the charcoal plug traveled further by the first time point in fasted rats compared to fed rats, matching the trend seen in the literature. One possibility for the similarity in GI transit time may be the incomplete fasting of rats. Rats are known to eat anything in their cage, including their bedding and feces, in the absence of food.

The pH data and intestinal dimension collected in this chapter were incorporated into the continuous intestine absorption model, Chapter 7. Intestinal dimensions were used to describe the segment distances and overall length of the intestine in the model. The pH data was incorporated into a series of logistic functions to describe the change in luminal pH along the intestine in both fed and fasted conditions. The distance traveled over time data was used to create a velocity data set. This velocity data set was used to create a series of logistic functions to describe the velocity along the length of the intestine for both fed and fasted conditions.

The addition of more rats to the GI motility study would give more confidence to the data set. Currently, most data points were performed in duplicate, so the charcoal data from a single rat has marked influence on the overall data set. Future studies could include adding at least one rat to obtain a minimum sample size of three rats for each time point.

Further refinement of the model to include intestinal transporter expression could better predict C-t profiles for drugs like GLY and DIG, known substrates of intestinal transporters. The transporter expression for Oatp1a5 is expected to be the highest in the proximal small intestine and fall along the intestine. The opposite should be seen for P-gp, whose expression is reported to be the highest in the distal regions of the small intestine (Brady et al., 2002). Matrix-assisted laser desorption/ionization could be utilized to determine the protein expression along the intestine under 12-hour fed and fasted conditions. More detailed descriptions are in Chapter 8.

CHAPTER 4: IN VITRO ADME AND IN VIVO IV DATA

4.1 Rationale

This chapter aims to determine the unbound fraction in microsomes (f_{um}) and to collect elimination and disposition information for the absorption model in Chapter 7. For a drug to have good permeability, it must partition into membranes. Compounds that are highly permeable exhibit extensive partitioning. As drugs partition into membranes, they show an experimentally observed delay in their release from the membrane (Nagar and Korzekwa, 2012). This impacts their passive diffusion and rate of entrance into the systemic circulation. In addition, extensive partitioning increases a drug's residence time in the membranes and the probability of being effluxed by P-gp, reducing their extent of absorption (Nagar, 2016).

Microsomes are vesicles of smooth endoplasmic reticulum created during tissue homogenization via differential centrifugation. They consist of unsorted membrane phospholipids, making them ideal for describing lipid partitioning. Additionally, microsomal partitioning data is relatively easy to collect (Korzekwa and Nagar, 2017). Microsomal binding can be determined using a variety of experimental methods, but equilibrium dialysis is considered the gold standard (Fessey, 2006).

For microsomes, it is assumed that 0.7 μL of lipid is available in a 1 mg/mL microsomal protein incubation (Korzekwa and Nagar, 2017). The f_{um} was used to determine the membrane partition constant of the drug (K_p) using the following equation:

$$K_p = \frac{1 - f_{um}}{0.0007 f_{um}} \quad \text{Equation 4.1}$$

The K_p was used in the continuous intestinal absorption model, Chapter 7, to calculate the radial diffusion out of the membranes:

$$Cl_o = \frac{Cl_i[x]}{K_p} \quad \text{Equation 4.2}$$

where Cl_o is the diffusional clearance out of membranes and Cl_i is the diffusional clearance into membranes. While many f_{um} values exist for GLY and DIG, there was no literature data available for AML. This made it necessary to determine the value in-house.

To simulate oral PK profiles, input functions generated by the absorption model were combined with systemic disposition functions. Systemic disposition functions describe a drug's distribution and elimination; information which is gathered using intravenous (IV) data. The IV data were fit using compartmental models.

4.2 Materials

Rat liver microsomes were purchased from SEKISUI XenoTech (Kansas City, KS). Potassium phosphate and EDTA were obtained from Fisher Scientific. Dialysis membrane and HT dialysis apparatus (model HTD96b) were obtained from H T Dialysis (Gales Ferry, CT). Male Sprague-Dawley single jugular cannulated rats weighing 239 – 250g were ordered from Charles River (Wilmington, MA). Sterile saline and syringes were ordered from FisherScientific (Pittsburgh, PA). Heparin was obtained from Sagent Pharmaceuticals (Schaumburg, IL). 23G needles and PEG-400 were from Sigma-Aldrich (St. Louis, MO). Isoflurane was ordered from Piramal Enterprises (Lexington, KY). Amlodipine was purchased from Alfa Asear (Haverhill, MA). Glyburide was from Frontier Scientific (Logan, UT). Digoxin was purchased from Tocris (Ellisville, MO). 1-methyl-2-pyrrolidinone was ordered from J.T baker (Allentown, PA).

4.3 Study Design

4.3.1 Microsomal Partitioning Assay

To achieve a 0.1 mg/mL microsomal solution, 20 mg/mL rat liver microsomes were diluted in 100 mM phosphate buffer with 0.1 mM EDTA at pH 7.4 (KPi buffer). An AML stock solution was prepared at 200 μ M in DMSO and diluted to 2 μ M in microsomes or KPi. The membrane, stored in 20% v/v ethanol in KPi buffer at 4°C, was rinsed twice before use with KPi buffer. Excess buffer was gently removed from the membrane, and the dialysis apparatus was assembled. To the receiving sides, 150 μ L KPi

buffer was added immediately to prevent membrane dehydration. To the sample side, 150 uL of drug in either microsomes or KPi buffer was added. Equilibrium dialysis was performed at 37°C and 5% CO₂ for 5 hours. The rotation speed was set to 100 rpm. Samples were analyzed by LC-MS/MS using the method described in Chapter 2.

Three controls were utilized to monitor the equilibrium dialysis runs. Drug-spiked KPi buffer was added in a dialysis well to monitor nonspecific binding to the membrane and wells. Additionally, this assured equilibrium between sample and receiving sides was reached. Drug degradation and matrix effects were monitored by two vials containing drug with and without 0.1 mg/mL microsomes. All controls were run simultaneously with samples and under the same conditions.

4.3.2 Animals

Male SD rats were singly housed under a reverse 12-hour light/dark cycle. Rats were acclimated for at least four days in the Temple University Health Sciences Campus animal housing facility and 30 minutes in the procedure room prior to the start of the study. Food and water were available ad libitum. All animal studies were performed with strict adherence to protocols approved by the Temple University IACUC.

4.3.3 Glyburide Pilot Study

GLY was pre-weighed, placed into separate tubes, and kept at -20°C until use to minimize freeze-thawing of the original bottle. Due to the poor solubility of GLY (4

mg/L in water), solutions were prepared using 70% 1-methyl-2-pyrrolidinone (NMP) in normal saline, the morning of the experiment. Rats (n=2) were administered a 5 mg/kg GLY solution into the jugular cannula, which was flushed with 100 U/mL heparinized saline to assure complete dosing. Blood samples (~0.2 mL) were collected via the jugular cannula into heparinized tubes at 0.08, 0.25, 0.5, 1, 2, 4, 6, and 24 hours post-dose. After each sampling, the loss of blood volume was supplemented with an equal volume of saline containing 100 U/mL heparin. Plasma was obtained by centrifugation at 10,000 g for 10 minutes at 4°C and kept at -20 °C until analyzed. Plasma samples were analyzed by LC-MS/MS using the method described in Chapter 2.

4.3.4 Glyburide and Amlodipine IV Study

GLY and AML were pre-weighed, placed into separate tubes, and kept at -20°C until use. Stock solutions were created in 100% NMP. Final drug solutions were prepared in 50% NMP, 20% PEG-400, and 30% MiliQ water, the morning of the experiment. Rats (n=3) were administered a combination of 4 mg/kg GLY and 2 mg/kg AML in solution into the jugular cannula, which was then flushed with 100 U/mL heparinized saline to assure the complete dosing of the animal. Blood samples (~0.2 mL) were collected via the jugular cannula into heparinized tubes at 0.08, 0.25, 0.5, 1, 2, 4, 6, 8, 10, and 12 hours post-dose. After each sampling, the loss of blood volume was supplemented with an equal volume of saline containing 100 U/mL heparin. Plasma was obtained by centrifugation at 5,000 g for 15 minutes at 4°C and kept at -20 °C until analysis. Plasma samples were analyzed by LC-MS/MS using the method described in Chapter 2.

4.3.5 Digoxin IV Study

DIG was pre-weighed and kept at room temperature until use. A stock solution of DIG was created in 100% NMP. The DIG stock was diluted to 15% NMP with saline. Rats (n=3) were dosed with a 0.25 mg/kg DIG solution into the jugular cannula, which was then flushed with 100 U/mL heparinized saline. Blood samples (~0.2 mL) were collected via the jugular cannula into heparinized tubes at 0.08, 0.25, 0.5, 0.75, 1, 2, 4, 6, and 8 hours post-dose. Plasma was obtained by centrifugation at 10,000 g for 10 minutes at 4°C and kept frozen at -20 °C until analyzed. Plasma samples were analyzed by LC-MS/MS using the protocol described in Chapter 2.

4.4 Data Analysis

4.4.1 F_{um}

The diluted unbound fraction was calculated using the following equation:

$$f_{u,d} = \frac{C_{buffer}}{C_{microsomes}} \quad \text{Equation 4.3}$$

where $f_{u,d}$ is the diluted unbound fraction, C_{buffer} is the concentration of drug in the buffer (receiver) side, and $C_{microsomes}$ is the concentration of drug in the microsomal (donor) side.

The $f_{u,d}$ was corrected to 1 mg/mL microsomes using the following equation:

$$f_{um} = \frac{1/D}{\left(\frac{1}{f_u} - 1\right) + 1/D} \quad \text{Equation 4.4}$$

where D is the dilution factor (Riccardi et al., 2018).

4.4.2 IV PK Studies

PK parameters and metrics were calculated using both compartmental and non-compartmental analysis (NCA) in Wolfram Mathematica 11.3. Data were analyzed using two approaches: average and naïve pooled. To obtain the average data, individual rats were analyzed separately and the PK parameters and metrics from each rat were averaged together. Average data were described using the mean and standard deviation. Naïve pooled data grouped individuals as if they were a single subject, thus were described as group median with no variation in the C-t dataset.

NCA clearance (CL) and volume of distribution (Vd) were determined using IV data. Because the complete dose is not assumed to be introduced into the systemic circulation when administered orally (PO), it is not appropriate to use PO data to CL or Vd (Gibaldi and Perrier, 1982). CL was calculated as:

$$CL = \frac{Dose_{IV}}{AUC_{IV}} \quad \text{Equation 4.5}$$

where $Dose_{IV}$ is the dose administered by IV route and AUC is the area under the curve for a drug dosed IV. The AUC was calculated using the log-linear trapezoidal rule. The AUC was extrapolated to infinity by C_{last}/λ , where C_{last} is the plasma concentration at the last time point and λ is the elimination rate constant. There are three volumes of distribution when using multi-compartment models: volume of the central compartment, volume at steady state, and the terminal volume. Of the three, the volume of distribution at steady state (V_{ss}) is the most valuable to calculate. The V_{ss} gives the best idea of the

relative degree of drug binding and has clinical use, such as calculating a loading dose (Toutain and Bousquet-Melou, 2004; Devi et al., 2015). The non-compartmental V_{ss} was calculated by the following equation:

$$V_{ss} = \frac{Dose_{IV} * MRT}{AUC_{IV}} \quad \text{Equation 4.6}$$

where MRT is the mean residence time. MRT is found by dividing the area under the first moment curve (AUCM) by the AUC. For compartmental modeling, both 2-compartment (2C) and 3-compartment (3C) models were fit to the data to describe the PK (Figure 4.1).

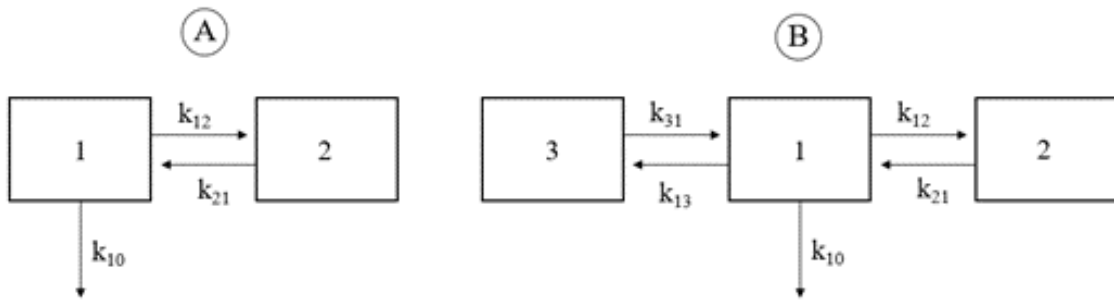


Figure 4.1 Schematic representation of compartmental models

A: 2-compartmental intravenous model **B:** 3-compartmental intravenous model.

Compartments are denoted by the numbers 1, 2, and 3. Distribution between compartments is described by first-order rate constants. k_{12} represents the distribution rate constant from compartment 1 to 2, k_{21} represents the distribution rate constant from compartment 2 to 1, k_{13} represents the distribution rate constant from compartment 1 to 3, k_{31} represents the distribution rate constant from compartment 3 to 1, and k_{10} represents the elimination rate constant

Drug administration and sampling were modeled from the central compartment.

Corrected Akaike's information criterion (AICc) was used to determine the better model

due to the smaller sample size ($n/p < 40$). AICc is defined by the following equation (Brewer et al., 2016):

$$AICc = AIC + \frac{2p(p + 1)}{n - p - 1} \quad \text{Equation 4.7}$$

where p is the number of model parameters estimated, n is the sample size (data points), and AIC is given as:

$$AIC = n * \log\left(\frac{WRSS}{n}\right) + 2p \quad \text{Equation 4.8}$$

where WRSS is the weighted residual sum of squares. The better model is indicated by a lower AICc value, assuming a difference of at least four. If the difference in AICc between models is less than four, residual analysis and model simplicity was used to determine the better model. Mean squared error (MSE) was calculated by the following equation:

$$MSE = SSE/(n - p) \quad \text{Equation 4.9}$$

where SSE is the sum of squared errors. Compartmental CL was calculated using (Equation 4.1) and Vss for the 2C (Equation 4.10) and 3C (Equation 4.11) IV models were calculated using the following equations:

$$V_{ss} = \frac{Dose\left[\left(\frac{A}{\alpha}\right)^2 + \left(\frac{B}{\beta}\right)^2\right]}{AUC^2} \quad \text{Equation 4.10}$$

$$V_{ss} = \frac{Dose\left[\left(\frac{A}{\alpha}\right)^2 + \left(\frac{B}{\beta}\right)^2 + \left(\frac{C}{\gamma}\right)^2\right]}{AUC^2} \quad \text{Equation 4.11}$$

where A, B, and C are constants and α , β , and γ are disposition rate constants. AUC is the area under the concentration-time curve, which was calculated for 2C (Equation 4.12) and 3C (Equation 4.13) models using the following equations:

$$AUC = \frac{A}{\alpha} + \frac{B}{\beta} \quad \text{Equation 4.12}$$

$$AUC = \frac{A}{\alpha} + \frac{B}{\beta} + \frac{C}{\gamma} \quad \text{Equation 4.13}$$

4.5 Results

4.5.1 F_{um}

The corrected unbound fraction in microsomes for AML ranged between 0.03 – 0.08. Each well was measured twice via LC-MS/MS and the averages of the two measurements are listed in Table 4.1.

Table 4.1 Microsomal binding assay results

Well #	AML
1	0.07
2	0.04
3	0.06
Average	0.057

4.5.2 GLY Pilot Study

The PK parameters and metrics analyzed by NCA for both rats are shown in Table 4.2.

The *in vivo* IV PK profiles of GLY were best described by a 2C model (Table 4.3, Figure 4.2). For both rats, the AICc for the 2C and 3C models were ~140 and infinity,

respectively. The MSE for the 2C models were ~3700, while the 3C models were ~2500.

The 2C model was chosen because the AICc indicated not enough data points were taken to determine a good 3C model fit. Additionally, 3C models did not converge to observed

rat data. The 2C model PK parameters and metrics analyzed for both rats are shown in

Table 4.4. Parameter estimates for 2C modeling for individual rats are shown in Table 4.5

Table 4.2 Non-compartmental PK parameters and metrics for GLY pilot study IV

	CL (mL/hr)	VD _{ss} (L)	k (hr ⁻¹)	t _{1/2} (hr)	AUC _(0 → infinity) (µg•hr/mL)
Rat 7	240.8	11.1	0.024	29.2	5.90
Rat 8	148.5	0.35	0.133	5.22	11.7

Table 4.3 Goodness of fit metrics for 2C and 3C models for GLY IV (n=2)

Goodness of fit metric	Rat 7		Rat 8	
	2C Model	3C Model	2C Model	3C Model
AICc	141.2	∞	137.4	∞
MSE	3718	2497	3743	2496
BIC	111.6	112.0	107.8	115.5
R ²	0.987	0.995	0.995	0.998

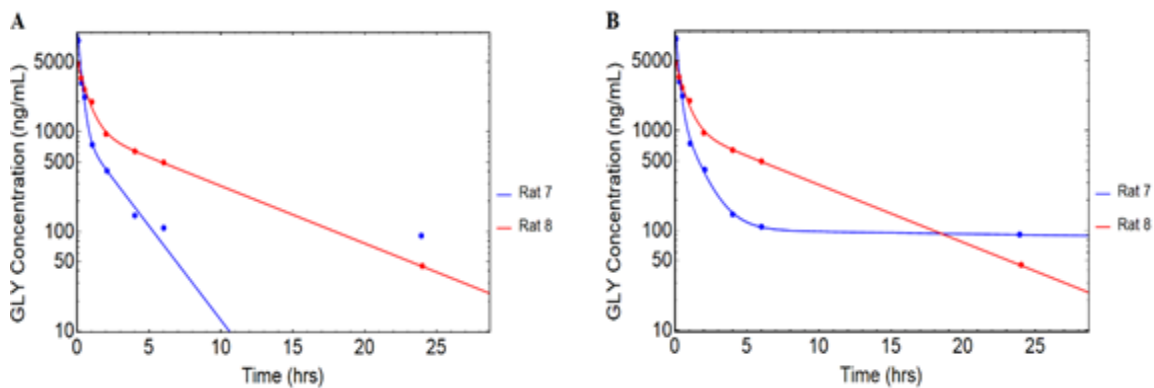


Figure 4.2 *In vivo* C-t profiles of GLY in SD rats (n=2) after an IV dose. **A:** 2-compartment model fitting **B:** 3-compartmental model fitting. Solid dots represent the observed concentrations from *in vivo* PK studies and the solid lines represent the predicted C-t profiles for individual rats.

Table 4.4 GLY pilot study IV PK parameters and metrics for 2C

	CL (mL/hr)	VD _{ss} (L)	k (hr ⁻¹)	t _{1/2} (hr)	AUC _(0 → infinity) (μg•hr/mL)
Rat 7	285	353	0.435	1.59	4.74
Rat 8	140.5	826	0.133	5.22	10.7

Table 4.5 Parameter estimates of GLY for 2C calculated for individual rats. Shown as estimate ± standard error.

	A (ng/mL)	α (hr ⁻¹)	B (ng/mL)	B (hr ⁻¹)
Rat 7	10125 ± 1149	4.14 ± 0.725	1000 ± 471	0.435 ± 0.170
Rat 8	3975 ± 346	1.55 ± 0.288	1079 ± 222	0.133 ± 0.0320

4.5.3 AML + GLY Study

The PK parameters and metrics analyzed for AML and GLY by NCA are listed in Table 4.6. The *in vivo* IV PK profiles of AML (Table 4.7) and GLY (Table 4.8) were best described by a 2C model. The AICc for the 2C and 3C models for AML were 68.7 and

115.5, respectively. The AICc for the 2C and 3C models for GLY were 126.3 and 157.9, respectively. For both AML and GLY, a 2C model best described the data, as evidence by a lower AICc (with a difference greater than 4). The 2C and 3C compartment models had similar visual fits for AML, while the 3C model seemed to be slightly better at capturing the last two terminal points than the 2C model for GLY (Figure 4.3). The 2C model PK parameters and metrics analyzed for AML and GLY are shown in Table 4.9.

For the 2C modeling, parameter estimates for AML for individual rats and the average of values are shown in Table 4.10. Parameter estimates for GLY for individual rats and the average of the parameter values are shown in Table 4.11. Parameter estimates of AML and GLY for 2C calculated for naïve pooled average were listed in Table 4.12.

Table 4.6 Non-compartmental PK parameters and metrics for AML and GLY IV (n=3)

	CL (mL/hr)	VD _{ss} (L)	k (hr ⁻¹)	t _{1/2} (hr)	AUC _(0 → infinity) (ng•hr/mL)
AML (average)	1520 ± 368	3019 ± 1370	0.237 ± 0.044	2.79 ± 0.26	365.3 ± 78.4
AML (naïve pooled)	1587	4446	0.290	2.43	407.2
GLY (average)	119.7 ± 10.1	348.3 ± 58.3	0.275 ± 0.058	2.61 ± 0.62	9892 ± 1635
GLY (naïve pooled)	122.9	367.8	0.340	2.04	9559

Table 4.7 Goodness of fit metrics for mean 2C and 3C models for AML IV

Goodness of fit metric	2C Model	3C Model
AICc	68.7	116
MSE	170	113
BIC	55.2	61.6
R ²	0.998	0.998

Table 4.8 Goodness of fit metrics for mean 2C and 3C models for GLY IV

Goodness of fit metric	2C Model	3C Model
AICc	126	158
MSE	6940	4629
BIC	113	104
R ²	0.999	0.999

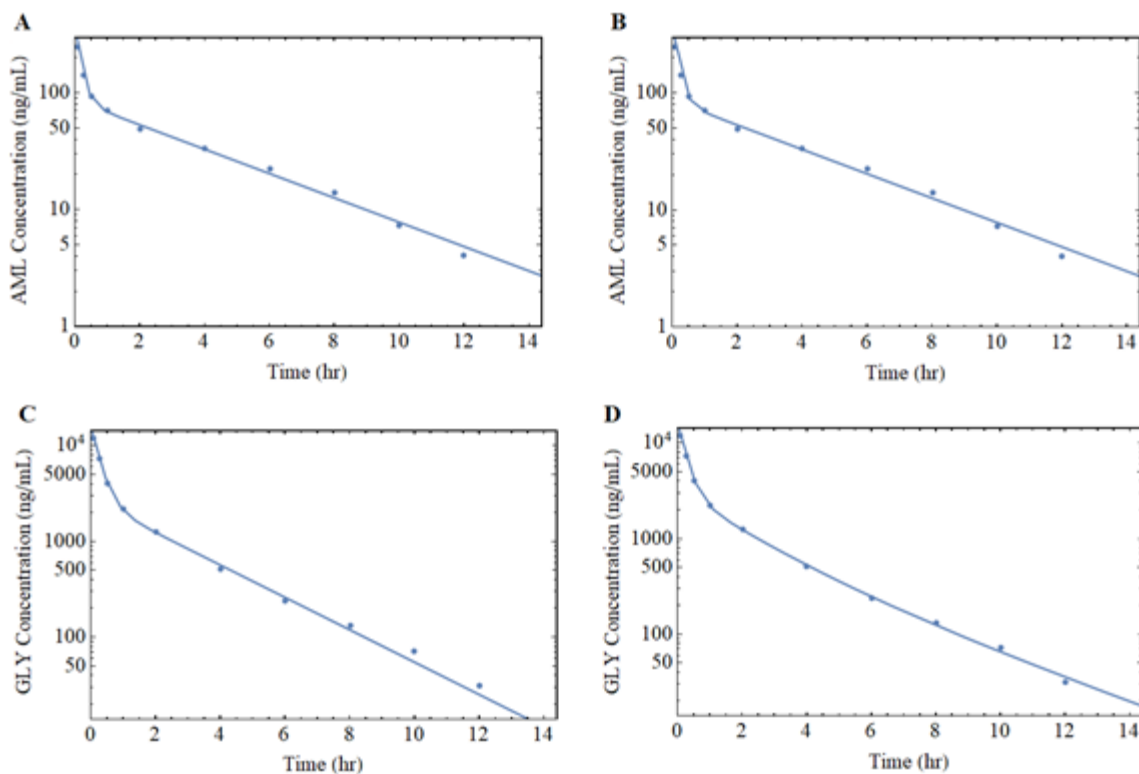


Figure 4.3 *In vivo* C-t profile of AML and GLY in SD rats (n=3) after an IV dose. **A:** 2-compartment model fitting for AML IV data **B:** 3-compartmental model fitting AML IV data **C:** 2-compartment model fitting for GLY IV data **D:** 3-compartmental model fitting GLY IV data. Solid dots represent the mean observed concentrations from *in vivo* PK studies and the solid line represents the predicted C-t profile

Table 4.9 PK parameters and metrics for AML and GLY IV for 2C (n=3)

	CL (mL/hr)	VD _{ss} (L)	k (hr ⁻¹)	t _{1/2} (hr)	AUC _(0 → infinity) (ng•hr/mL)
AML (average)	1454 ± 243	5642 ± 952	0.229 ± 0.032	3.06 ± 0.42	417 ± 116
AML (naïve pooled)	1437	5358	0.237	2.92	409
GLY (average)	113.0 ± 4.2	201.5 ± 41.5	0.401 ± 0.063	1.76 ± 0.29	10406 ± 115
GLY (naïve pooled)	112.4	201.2	0.390	1.79	10447

Table 4.10 Parameter estimates of AML for 2C calculated for individual rats and the average of values (n=3).
Shown as estimate \pm standard error for individual rats and the mean \pm standard deviation for the average.

Rat	A (ng/mL)	α (hr ⁻¹)	B (ng/mL)	β (hr ⁻¹)
63	460 \pm 68	6.50 \pm 1.18	108 \pm 11	0.230 \pm 0.030
66	195 \pm 13	6.05 \pm 0.63	77.2 \pm 3.3	0.263 \pm 0.010
67	197 \pm 15	3.69 \pm 0.48	61.0 \pm 5.4	0.175 \pm 0.020
Average	284 \pm 152	5.41 \pm 1.51	82.0 \pm 23.9	0.223 \pm 0.044

Table 4.11 Parameter estimates of GLY for 2C calculated for individual rats and the average of values (n=3).
Shown as estimate \pm standard error for individual rats and the mean \pm standard deviation for the average.

Rat	A (ng/mL)	α (hr ⁻¹)	B (ng/mL)	β (hr ⁻¹)
63	12130 \pm 507	3.86 \pm 0.29	377 \pm 252	0.408 \pm 0.022
66	14022 \pm 725	3.60 \pm 0.34	2780 \pm 419	0.460 \pm 0.044
67	13340 \pm 333	3.98 \pm 0.15	2073 \pm 106	0.334 \pm 0.013
Average	13164 \pm 958	3.81 \pm 0.19	1744 \pm 1235	0.401 \pm 0.063

Table 4.12 Parameter estimates of AML and GLY for 2C calculated for naïve pooled average rat (n=3)

Parameter	GLY		AML	
	Estimate	Standard Error	Estimate	Standard Error
A (ng/mL)	13.2	0.37	271	17.5
α (hr ⁻¹)	3.75	0.18	5.55	0.50
B (ng/mL)	2.70	0.16	86.0	3.84
β (hr ⁻¹)	0.39	0.02	0.24	0.01
k12 (hr ⁻¹)	1.65	0.10	3.38	0.16
k21 (hr ⁻¹)	0.96	0.06	1.51	0.09
k10 (hr ⁻¹)	1.52	0.04	0.88	0.02
Vc (mL)	73.9	1.76	1682	35.4

4.5.4 DIG Study

The PK parameters and metrics analyzed for DIG by NCA are listed in Table 4.13. The *in vivo* IV PK profile of DIG was best described by a 2C model (Table 4.14, Figure 4.4).

The AICc for the 2C and 3C models were 54.4 and 151.1, respectively. The MSE for the 2C model was 98.9 and 65.9 for the 3C model. The 2C model was chosen due to the lower AICc, with a difference between the two models of greater than 4. The 2C model

PK parameters and metrics analyzed for DIG are shown in Table 4.15. For the 2C modeling, parameter estimates for DIG for individual rats and the average of values are shown in Table 4.16. Parameter estimates for a 2C model fit the DIG naïve pooled average were listed in Table 4.17.

Table 4.13 Non-compartmental PK parameters and metrics for DIG (n=3)

	CL (mL/hr)	VD _{ss} (mL)	k (hr ⁻¹)	t _{1/2} (hr)	AUC _(0 → infinity) (ng•hr/mL)
Average	2290 ± 117	5506 ± 1956	0.396 ± 0.132	1.91 ± 0.73	107.8 ± 10.2
Naïve pooled	2233	4484	0.448	1.55	110.0

Table 4.14 Goodness of Fit Metrics for 2C and 3C Models for DIG IV

Goodness of fit metric	2C Model	3C Model
AICc	54.4	151
MSE	98.9	65.9
BIC	35.4	40.5
R ²	0.999	0.999

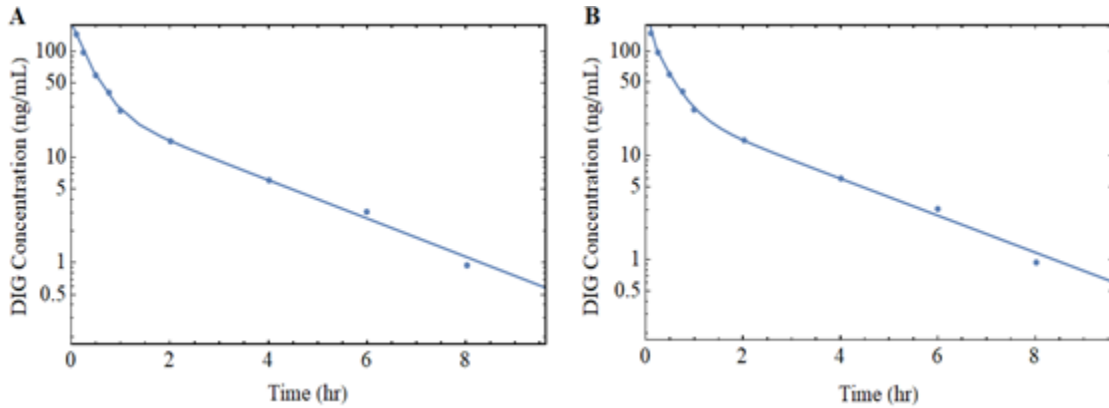


Figure 4.4 *In vivo* C-t profile of DIG in SD rats (n=3) after an IV dose.

A: 2-compartment model fitting **B:** 3-compartmental model fitting. Solid dots represent the mean observed concentrations from *in vivo* PK studies and the solid line represents the predicted C-t profile

Table 4.15 PK parameters and metrics for DIG for 2C (n=3)

	CL (mL/hr)	VD _{ss} (mL)	k (hr ⁻¹)	t _{1/2} (hr)	AUC _(0 → infinity) (ng•hr/mL)
Average	1933 ± 274	3437 ± 906	0.364 ± 0.115	2.07 ± 0.81	129.9 ± 22.9
Naïve pooled	1924	3032	0.417	1.66	127.7

Table 4.16 Parameter estimates of DIG for 2C calculated for naïve pooled average (n=3)

Parameter	Estimate	Standard Error
A (ng/mL)	155	5.37
α (hr-1)	3.06	0.21
B (ng/mL)	32.2	3.63
β (hr-1)	0.42	0.03
k ₁₂ (hr-1)	1.14	0.07
k ₂₁ (hr-1)	0.88	0.08
k ₁₀ (hr-1)	1.46	0.05
V _c (mL)	1315	34.8

Table 4.17 Parameter estimates of DIG for 2C calculated for individual rats and the average of values (n=3).
Shown as estimate \pm standard error for individual rats and the mean \pm standard deviation for the average.

Rat	A (ng/mL)	α (hr ⁻¹)	B (ng/mL)	β (hr ⁻¹)
58	200 \pm 22	3.70 \pm 0.75	24.5 \pm 10.5	0.432 \pm 0.123
59	125 \pm 17	2.39 \pm 0.57	30.4 \pm 13.8	0.489 \pm 0.115
60	152 \pm 5.7	2.36 \pm 0.18	20.5 \pm 4.2	0.231 \pm 0.050
Average	159 \pm 40	2.82 \pm 0.77	25.1 \pm 5.0	0.384 \pm 0.136

4.6 Discussion and Conclusion

The average f_{um} for AML was 0.06, indicating it is highly partitioned into microsomes.

This agrees with the literature which states that AML has a high membrane affinity (IC₅₀: 5.8 μ M) and protein binding (f_{up} : 2%) (Meredith and Elliott, 1992; Smith et al., 2010).

The GLY pilot study was performed with the formulation vehicle consisting of 70% NMP in saline. Additionally, drug would precipitate out of solution when at room temperature overnight. Therefore, a new formulation was devised for dosing GLY, using AML as a control. The 3C model AICc value of infinity suggests that more data points are needed to accurately fit the model to the data. In subsequent PK studies, more time points were measured to combat this issue.

For combined AML and GLY IV studies, a 2C model best described the PK of both drugs. The NCA and 2C model analyses of the PK parameters and metrics were not

significantly different for AML. For GLY, NCA and 2C model analysis of V_{dss} and AUC were not significantly different. The CL, k, and $t_{1/2}$ were significantly different with p-values of 0.049, 0.028, and 0.020, respectively. The calculations for k and $t_{1/2}$ are dependent on CL, so the differences in both metrics are likely due to the difference between the 2C and NCA values for CL. This disparity for this parameter may be due to the different equations used to calculate the value. Systemic disposition functions for the rat continuous intestine absorption model in Chapter 7 were generated using a 2C model for AML and GLY.

For DIG IV studies, a 2C model best described the PK of both drugs. The NCA and 2C model analyses of the PK parameters and metrics were not significantly different for DIG. The systemic disposition function was generated using a 2C model for DIG.

CHAPTER 5: FOOD EFFECTS ON GLY AND DIG ORAL ABSORPTION

5.1 Rationale

This chapter aims to determine the impact of food on the PK of AML, GLY, and DIG in SD rats. The amount of time between drug administration and the reintroduction of food was considered, along with the effect of a fasted versus fed state. Two feeding time points post drug dose were chosen to identify the impact of time fasted on a drug's PK profile. The AML, GLY, and DIG C-t profiles collected in this chapter were used to refine the rodent absorption model, detailed in Chapter 7.

PK studies are typically performed in fasted animals to reduce the inter-animal variability in C-t profiles (Melander, 1978; Singh et al., 2011; Small et al., 2015). Animals are usually fasted overnight between 12 and 18 hours, which is often noted (Vermeulen et al., 1997). However, most papers fail to specify when animals were fed after drug administration. Food effects may explain the inter-lab variability seen in PK profiles for the same drug at the same dose (Li et al., 2012; Jiang et al., 2015).

Food has been known to affect gastric emptying, small intestinal transit, pH, blood flow, transporter expression, and can even act as a mechanical barrier or binder. In the fasted state, the luminal pH decreases in humans, but luminal pH increases in rats (Ward and Coates, 1987; Klein, 2010). In rats, the fasted state impacts the gastric emptying rate by impeding emptying. Additionally, the transporter expression can be altered with

prolonged fasting. For example, P-gp gene and protein expression increased after a 12-hour fast in male rats (Dou et al., 2018).

There are conflicting reports of food effects on GLY PK in humans. Ootom et al. indicated that fasting before GLY administration led to an increase in C_{max} and AUC (Ootom et al., 2001). Other studies suggest that the administration of GLY with food does not alter its uptake (Sartor et al., 1982; Pearson, 1985). In humans, DIG administration with food is reported to slow the rate of absorption, though the extent of absorption remains unchanged (Johnson et al., 1978; GlaxoSmithKline, 2011). The presence of food impacts the extent of AML absorption in humans. The AUC and C_{max} were lower in the fed versus fasted groups (Hu et al., 2018; Wang et al., 2020).

Significant increases in corticosterone levels were seen in male SD rats between 12 and 16 hours of fasting (Nowland et al., 2011). Depressed gastric secretions and changes in intestinal motility have been reported when rats are placed under stress (Menguy, 1960; Williams et al., 1988). By 18 hours fasted, rats are reported to lose 10% of their body weight (Vermeulen et al., 1997). Liquids, like drug solutions, are reported to be mostly expelled from the rat stomach by 1 hour under fasted conditions. Over 50% of a phenol red solution was emptied after 20 minutes in fasted Wistar rats (Smits and Lefebvre, 1996). After 50 minutes, <15% of both technetium-99m labeled water and 4mM SDS remained in the stomach in fasted albino rats (Tomlin et al., 1993).

Based on the reported observations described above, the following experimental design was utilized. Two post-dose feeding times, thirty minutes and one hour, were chosen as they are more likely to impact drug emptying and potentially absorption. The time between dosing and food reintroduction was selected to minimize stomach content while reducing the time rats were food deprived. A 12-hour fast post-dose was chosen, as it was the shortest fasting time commonly used in PK studies. To maintain animal welfare and reduce physiological changes, the total fasting time was kept well under 16 hours.

Amlodipine (AML) is a BSC Class I drug, indicating high permeability and solubility. Therefore, the rate-limiting step to absorption is gastric emptying (Amidon et al., 1995). Conversely, a BCS Class II compound, like GLY, can be influenced by many variables, such as changes in media pH, GI motility, and transporter effects (Lobenberg et al., 2000; Li et al., 2012; Jiang et al., 2015).

There are three main benefits to administering both AML and GLY in the same dose. First, the coadministration of both drugs in a single solution allows for the collection of C-t data for two drugs without sacrificing additional animals. Second, AML acts as a positive control to confirm the experimental design works. Due to the numerous variables that can alter GLY absorption, coadministration with a BCS Class I drug like AML can highlight if unexpected GLY C-t profiles are due to experimental design or human error. Third, *in vivo* AML data can be used to make better C-t profile predictions for GLY using the continuous intestinal absorption model mentioned in Chapter 7. For example, as a

BCS Class I drug, transporter effects are not likely to alter AML uptake. Therefore, variability in transporter levels, which may influence GLY absorption, should not impact AML *in vivo* (Wu and Benet, 2005). Evidence suggests a possible pharmacodynamic but no PK interaction between AML and GLY. This potential pharmacodynamic interaction was acceptable to proceed with, as only a PK analysis was performed, and the interaction was not detrimental to animal health (Gari et al., 2017; Olapeju et al., 2018).

5.2 Materials

Male Sprague-Dawley single jugular cannulated rats weighing 239 – 250g were ordered from Charles River (Wilmington, MA). Sterile saline and syringes were ordered from FisherScientific (Pittsburgh, PA). Heparin was obtained from Sagent Pharmaceuticals (Schaumburg, IL). 23G needles and PEG-400 were from Sigma-Aldrich (St. Louis, MO). Isoflurane was ordered from Piramal Enterprises (Lexington, KY). Amlodipine was purchased from Alfa Aesar (Haverhill, MA). Glyburide was from Frontier Scientific (Logan, UT). Digoxin was purchased from Tocris (Ellisville, MO). 1-methyl-2-pyrrolidinone was ordered from J.T Baker (Allentown, PA).

5.3 Study Design

5.3.1 Animals

Male SD rats were singly housed under a reverse 12-hr light/dark cycle. Rats were acclimated for at least four days in the animal room of the Temple University Health

Sciences Campus animal housing facility and 30 minutes in the procedure room before the start of the study. Food and water were available ad libitum for fed groups. Food was removed from the cages of fasted groups 12 hours before the beginning of the study, and water was available ad libitum. For the combined AML and GLY food effect study, food was reintroduced at either 1 or 2 hours post-dose. For the DIG study, food was reintroduced into the animal's cages at either 30 or 60 minutes post-dose. The time the animals began eating was recorded. All animal studies were performed with strict adherence to protocols approved by the Temple University IACUC.

5.3.2 Glyburide Pilot Study

GLY was pre-weighed, placed into separate tubes, and kept at -20°C until use to minimize freeze-thawing of the original bottle. Due to the poor solubility of GLY (4mg/L in water), solutions were prepared using 70% 1-methyl-2-pyrrolidinone (NMP) in normal saline the morning of the experiment.

Rats (n=7) were orally administered 5 mg/kg of a 5 mg/mL solution of GLY (0.3 mL for a 300g rat). Blood samples (~0.2 mL) were collected into heparinized tubes at 0.08, 0.25, 0.5, 1, 2, 4, 6, 10, and 24 hours post-dose via jugular catheter. After each sampling, the loss of blood volume was supplemented with an equal volume of saline containing 100 U/mL heparin. Plasma was obtained by centrifugation at 10,000 g for 10 minutes at 4°C and kept at -20 °C until analyzed. Plasma samples were analyzed by LC-MS/MS with the protocol described in Chapter 2.

5.3.3 Glyburide and Amlodipine Food Effects Study

GLY and AML were pre-weighed, placed into separate tubes, and kept at -20°C until use. Stock solutions were created in 100% NMP. Final drug solutions were prepared in 50 – 55% NMP, 20% PEG-400, and 25 – 30% MiliQ water, the morning of the experiment.

SD rats (n=14) received a combination of 5 mg/kg GLY and 5 mg/kg AML in solution by oral gavage. The solution contained 3.75 mg/mL of each drug, so a 300g rat would receive a 0.4 mL dose. Blood samples (~0.2 ml) were collected via the jugular cannula into heparinized tubes at 0.17, 0.5, 1, 1.5, 2.5, 4, 6, 8, 10, and 24 hours post-dose. After each sampling, the loss of blood volume was supplemented with an equal volume of saline containing 100 U/mL heparin. Plasma was obtained by centrifugation at 5,000 g for 15 minutes at 4°C and kept at -20 °C until analysis. Plasma samples were analyzed by LC-MS/MS using the method described in Chapter 2.

5.3.4 Digoxin Food Effects Study

DIG was pre-weighed and kept at room temperature until use. A stock solution of DIG was created in 100% NMP and stored at 4°C between uses, but not exceeding one day. The DIG stock was diluted with saline to the final drug concentration and allowed to come to room temperature before dosing.

Rats (n=14) were orally administered 0.75 mg/kg of a 0.75 mg/mL solution of DIG in 15% NMP in saline, prepared the morning of the experiment (0.3 mL for a 300g rat).

Blood samples (~0.2 mL) were collected via the jugular cannula into heparinized tubes at 0.08, 0.25, 0.5, 0.75, 1, 2, 4, 6, 8, and 24 hours post-dose. After each sample, the loss of blood volume was supplemented with an equal volume of saline containing 100 U/mL heparin. Plasma was obtained by centrifugation at 10,000 g for 10 minutes at 4°C and kept frozen at -20 °C until analyzed. Plasma samples were analyzed by LC-MS/MS using the protocol described in Chapter 2.

5.4 Data Analysis

PK parameters and metrics were calculated using compartmental and non-compartmental analysis (NCA) in Wolfram Mathematica 11.3. Data were described using the mean and standard deviation (std dev). A one-way ANOVA was used to compare multiple groups. Post hoc analysis was conducted using Tukey's test. A p-value < 0.05 was considered significant. The following equation calculated the elimination rate constant (k):

$$k = \frac{1}{MRT} \quad \text{Equation 5.1}$$

The bioavailability (F) was calculated using both IV and PO data. The F depends on the dose and AUC for each route:

$$F = \frac{AUC_{PO} * Dose_{IV}}{AUC_{IV} * Dose_{PO}} \quad \text{Equation 5.2}$$

where AUC_{PO} is the area under the C-t curve for an orally administered dose, $Dose_{PO}$. The k_a was calculated by the following equation:

$$ka = \frac{1}{MAT} \quad \text{Equation 5.3}$$

where MAT is the mean absorption time. MAT is calculated by subtracting the MRT from an IV dose from the MRT of an oral dose.

For compartmental modeling, both 2-compartment (2C) and 3-compartment (3C) models were fit to the data to describe the PK (Figure 5.1). Absorption was assumed to be a first-order process and occurs faster than elimination ($ka > k$). A “gut” compartment was added to the perspective IV compartmental model scheme to describe oral administration. The AICc was used for model selection. Both the AICc (Equation 4.3) and MSE (Equation 4.5) were calculated as described in Chapter 4.

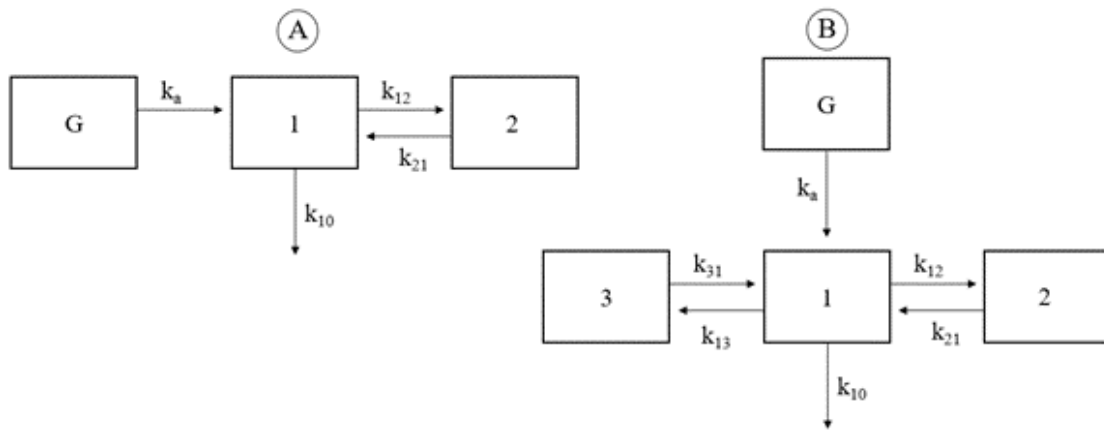


Figure 5.1 Schematic representation of compartmental models. **A:** 2-compartmental oral model **B:** 3-compartmental oral model. Compartments are denoted by the numbers 1, 2, 3, and the letter G (“gut”). First-order rate constants describe distribution between compartments. k_{12} represents the distribution rate constant from compartment 1 to 2, k_{21} represents the distribution rate constant from compartment 2 to 1, k_{13} represents the distribution rate constant from compartment 1 to 3, k_{31} represents the distribution rate constant from compartment 3 to 1, k_a represents the absorption rate constant, and k_{10} represents the elimination rate constant

5.5 Results

5.5.1 AML + GLY Study

Individual and average AML C-t profiles for 2-hours fasted rats are shown in Figure 5.2 and the NCA PK parameters and metrics are listed in Table 5.1. For 1-hour fasted rats, the C-t profiles for individual and average rats are shown in Figure 5.3. The NCA PK parameters and metrics are listed in Table 5.2. The C-t profiles and NCA PK parameters for fed rats are shown in Figure 5.4 and Table 5.3. Rat 79 and Rat 80 data did not contain a clear absorptive phase and had sporadic data, so they were excluded when averaging values and from the naïve pool.

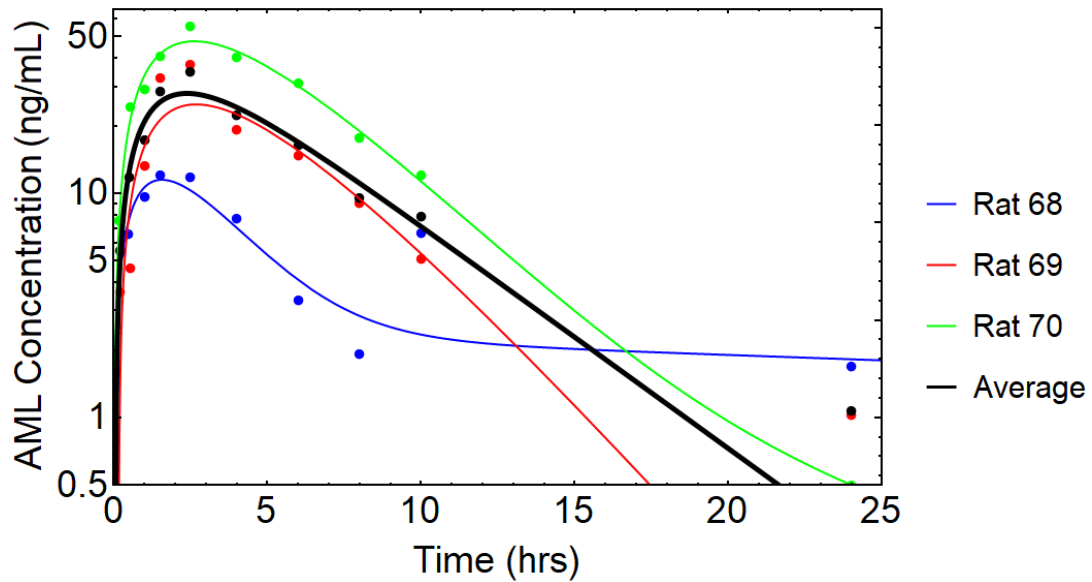


Figure 5.2 AML PO individual and average (n=3) PK C-t profiles for 2-hours fasted rats. Dots represent experimentally collect C-t data and lines represent a smoothed function to connect the experimental data. The bold, black line represents the naïve pooled average.

Table 5.1 PK parameters and metrics for AML PO for 2-hours fasted rats using NCA.
Individual rats are listed as single values and the average is the mean \pm std dev.

	Rat 68	Rat 69	Rat 70	Average \pm std dev
ka (hr ⁻¹)	0.142	0.251	0.279	0.224 \pm 0.072
F	0.246	0.167	0.344	0.252 \pm 0.089
Cmax (ng/mL)	12.1	37.5	55.4	35.0 \pm 21.8
tmax (hr)	1.50	2.50	2.50	2.17 \pm 0.58
AUC _(0-∞) (ng•hr/mL)	111	199	351	220 \pm 121

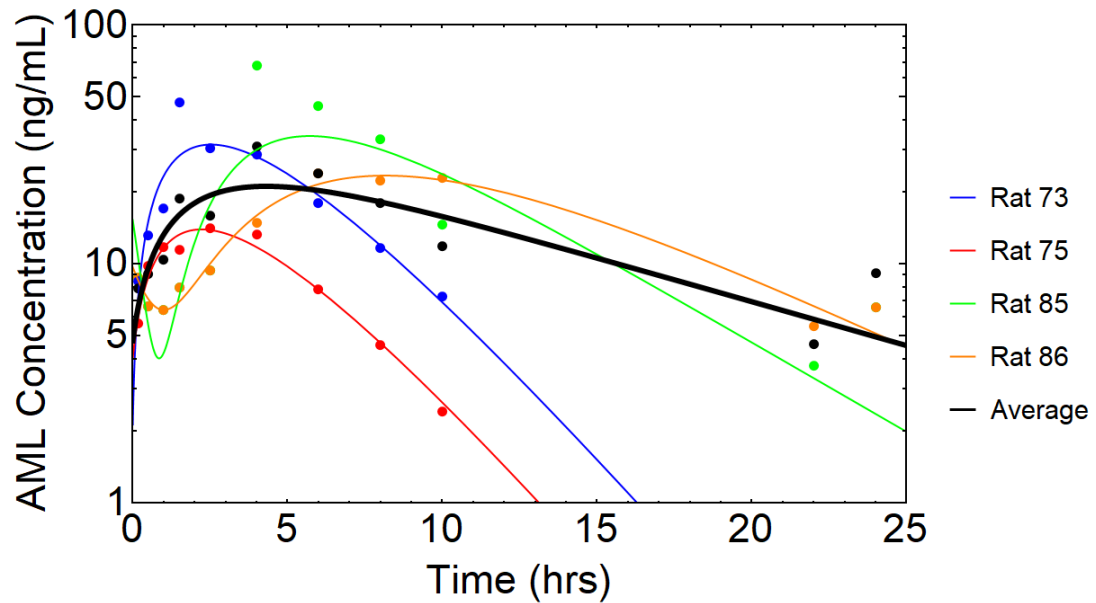


Figure 5.3 AML PO individual and average (n=4) PK C-t profiles for 1-hour fasted rats. Dots represent experimentally collect C-t data and lines represent a smoothed function to connect the experimental data. The bold, black line represents the naïve pooled average.

Table 5.2 PK parameters and metrics for AML PO for 1-hour fasted rats. Individual rats are listed as single values and the average is the mean \pm std dev.

	Rat 73	Rat 75	Rat 85	Rat 86	Average \pm std dev
ka (hr ⁻¹)	0.497	0.520	0.175	0.118	0.328 \pm 0.211
F	0.218	0.093	0.333	0.378	0.256 \pm 0.128
Cmax (ng/mL)	47.5	14.1	67.8	24.0	38.4 \pm 24.1
tmax (hr)	1.50	2.50	4.00	6.00	3.50 \pm 1.96
AUC _(0-∞) (ng•hr/mL)	205	87.0	395	325	253 \pm 136

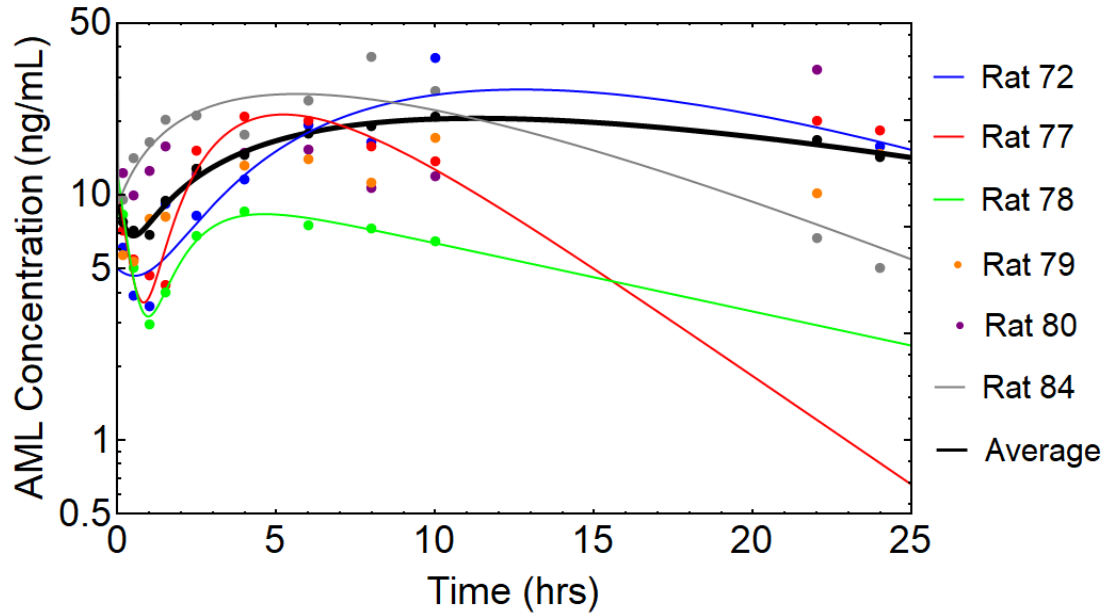


Figure 5.4 AML PO individual and average (n=4) PK C-t profiles for fed rats. Dots represent experimentally collect C-t data and lines represent a smoothed function to connect the experimental data. The bold, black line represents the naïve pooled average. Only experimentally obtained data points are shown for Rat 79 and Rat 80. Rat 79 and Rat 80 were not included in the naïve pooled average.

Table 5.3 PK parameters and metrics for AML PO for fed rats using NCA. Individual rats are listed as single values and the average is the mean \pm std dev.

	Rat 72	Rat 77	Rat 78	Rat 84	Average \pm std dev
ka (hr ⁻¹)	0.091	0.316	0.397	0.128	0.233 \pm 0.147
F	0.638	0.214	0.165	0.475	0.373 \pm 0.223
C _{max} (ng/mL)	36.3	20.8	8.52	36.4	25.5 \pm 13.5
t _{max} (hr)	10.0	4.00	4.00	8.00	6.50 \pm 3.00
AUC _(0-∞) (ng•hr/mL)	492	157	77.8	418	286 \pm 200

There was not a significant difference in any of the values when comparing the NCA averaged values. The naïve pooled averages for each feeding condition were compared, as shown in Figure 5.5 and Table 5.4. The C_{max} was similar across all groups. The average t_{max} increased as the fasting period decreased, shifting from ~2.5 hours for 2-hours fasted rats to ~22 hours for fed rats. The exposure was similar for fasted groups, while it was almost double for fed rats. The AUC was 233.6 and 284.1 ng hr/mL for 2-hours fasted and 1-hour fasted rats, respectively. When the rats were not denied food (fed group), the naïve pool average AUC was 407.9 ng hr/mL.

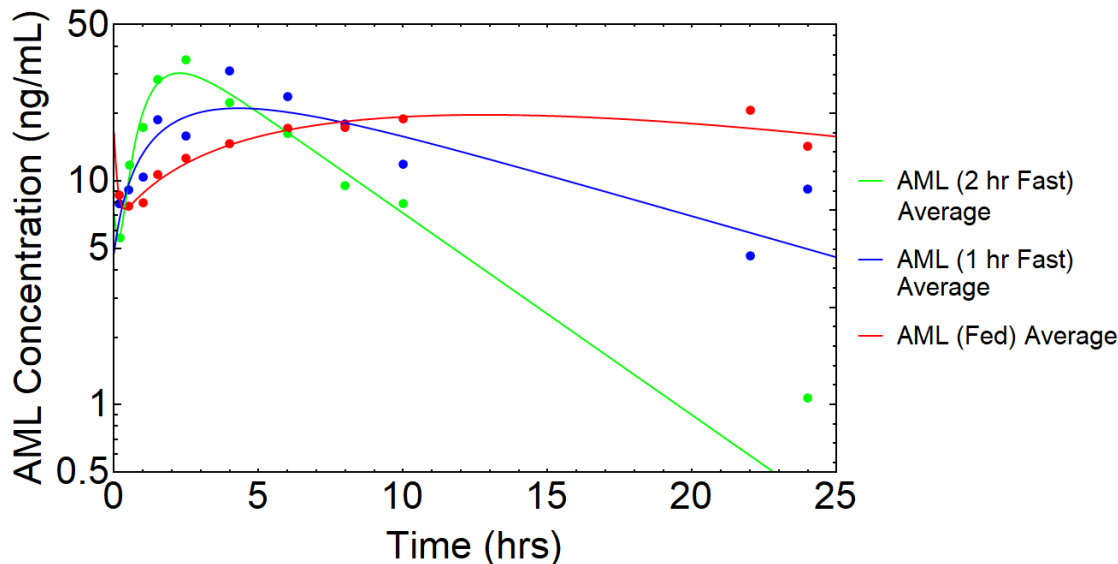


Figure 5.5 Comparison of average AML PK C-t profiles for fasted and fed rats. Dots represent experimentally collect C-t data and lines represent a smoothed function to connect the experimental data. Averages shown represent the naïve pooled averages.

Table 5.4 Comparison of average AML PK parameters and metrics for 2-hours fasted, 1-hour fasted, and fed rats.

	ka (hr ⁻¹)	F	C _{max} (ng/mL)	t _{max} (hr)	AUC _(0-∞) (ng•hr/mL)
Fast (2 hours)	0.228	0.204	34.9	2.50	233.6
Fast (1 hour)	0.160	0.307	31.2	4.00	284.1
Fed	0.095	0.666	20.6	10.0	407.9

Individual and average GLY C-t profiles for 2-hours fasted are shown in Figure 5.6 and the PK parameters and metrics are listed in Table 5.5. For 1-hour fasted rats, the C-t profiles for individual and average rats are shown in Figure 5.7. The NCA PK parameters and metrics are listed in Table 5.6. The C-t profiles and NCA PK parameters for fed rats are shown in Figure 5.8 and Table 5.7. Rat 72, Rat 78, and Rat 79 data did not contain a

clear absorptive phase and had sporadic data, so they were excluded when averaging values and from the naïve pool.

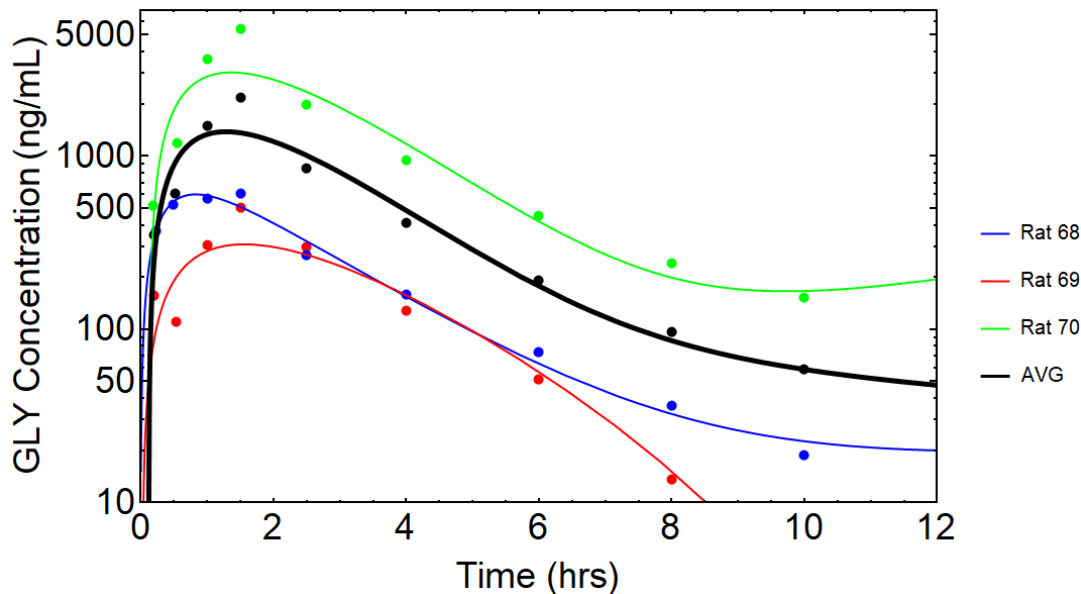


Figure 5.6 GLY PO individual and average (n=3) PK C-t profiles for 2-hours fasted rats. Dots represent experimentally collect C-t data and lines represent a smoothed function to connect the experimental data. The bold, black line represents the naïve pooled average.

Table 5.5 PK parameters and metrics for GLY PO 2-hours fasted rats using NCA. Individual rats are listed as single values and the average is the mean \pm std dev.

	Rat 68	Rat 69	Rat 70	Average \pm std dev
ka (hr ⁻¹)	1.18	1.84	0.840	1.23 \pm 0.51
F	0.153	0.107	0.892	0.402 \pm 0.441
Cmax (ng/mL)	606	505	3016	1326 \pm 1710
tmax (hr)	1.50	1.50	1.50	1.50 \pm 0.00
AUC _(0-∞) (ng•hr/mL)	1800	1263	11652	5017 \pm 5849

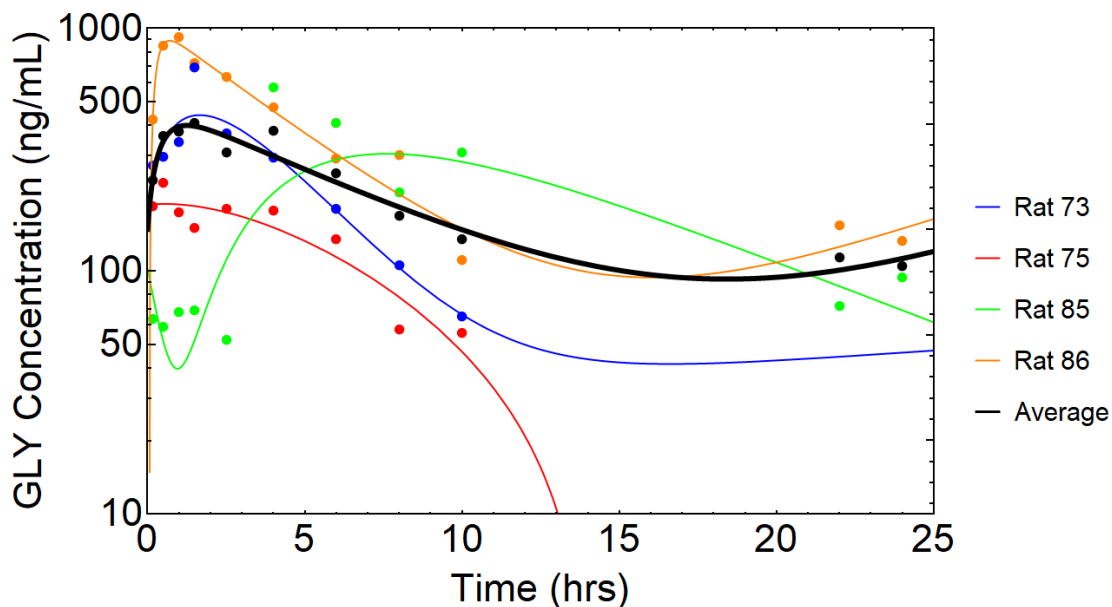


Figure 5.7 GLY PO individual and average (n=4) PK C-t profiles for 1-hour fasted rats. Dots represent experimentally collect C-t data and lines represent a smoothed function to connect the experimental data. The bold, black line represents the naïve pooled average.

Table 5.6 PK parameters and metrics for GLY PO 1-hour fasted rats using NCA. Individual rats are listed as single values and the average is the mean \pm std dev.

	Rat 73	Rat 75	Rat 85	Rat 86	Average \pm std dev
ka (hr ⁻¹)	0.471	0.283	0.094	0.035	0.221 \pm 0.198
F	0.207	0.111	0.397	0.523	0.310 \pm 0.185
Cmax (ng/mL)	691	180	572	922	591 \pm 310
tmax (hr)	1.50	2.50	4.00	1.00	2.25 \pm 1.32
AUC _(0-∞) (ng•hr/mL)	2436	1307	4674	6147	3641 \pm 2179

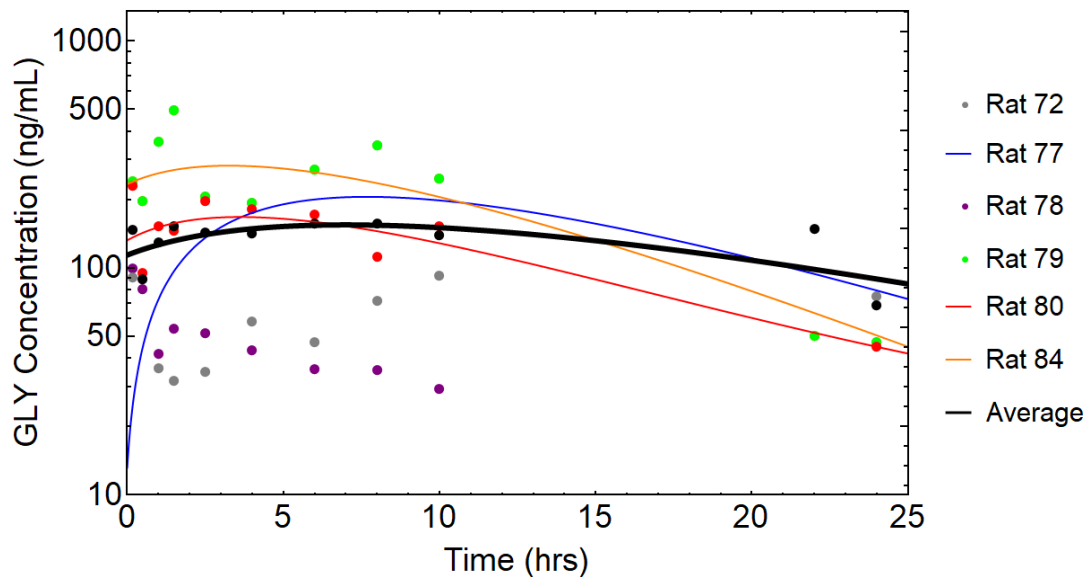


Figure 5.8 GLY PO individual and average (n=3) PK C-t profiles for fed rats. Dots represent experimentally collect C-t data and lines represent a smoothed function to connect the experimental data. The bold, black line represents the naïve pooled average. Only experimentally obtained data points are shown for Rat 72, Rat 78, and Rat 79. Rat 72, Rat 78, and Rat 79 were not included in the naïve pooled average.

Table 5.7 PK parameters and metrics for GLY PO fed rats using NCA. Individual rats are listed as single values and the average is the mean \pm std dev.

	Rat 72	Rat 77	Rat 78	Rat 79	Rat 80	Rat 84	Average \pm std dev
ka (hr ⁻¹)	0.051	0.114	0.392	0.429	0.132	0.249	0.165 \pm 0.073
F	0.186	0.354	0.037	0.039	0.347	0.176	0.292 \pm 0.101
C _{max} (ng/mL)	92.0	258	111	429	349	492	366 \pm 118
t _{max} (hr)	10.0	6.00	22.0	2.50	22.0	1.50	9.83 \pm 10.8
AUC _(0-∞) (ng•hr/mL)	2195	3567	433	457	2863	4281	3570 \pm 709

The averaged k_a for 2-hours fasted rats was significantly higher compared to the other two groups. The averaged t_{max} for fed rats was significantly higher compared to the other two groups. No other values were significantly different when comparing the averaged values. The naïve pooled averages for each feeding condition were compared, as shown in Figure 5.9 and Table 5.8.

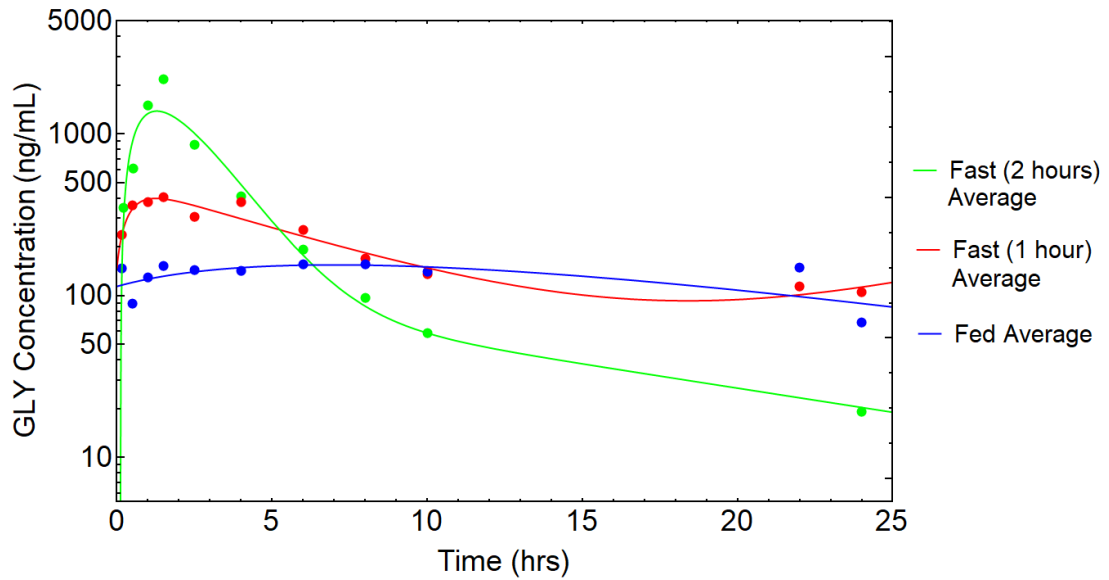


Figure 5.9 Comparison of average GLY PK C-t profiles for fasted and fed rats. Dots represent experimentally collect C-t data and lines represent a smoothed function to connect the experimental data. Averages shown represent the naïve pooled averages.

Table 5.8 Comparison of average GLY PK parameters and metrics for 2-hours fasted, 1-hour fasted, and fed rats using NCA.

	k_a (hr^{-1})	F	C_{max} (ng/mL)	t_{max} (hr)	$AUC_{(0-\infty)}$ (ng•hr/mL)
Fast (2 hours)	1.32	0.454	2183	1.46*	5352
Fast (1 hour)	0.020 [#]	0.374	407	1.50*	4413
Fed	0.122 [#]	0.340	640	6.70	4006

[#] statistically significant difference compared to 2 hour fasted rats, *statistically significant difference compared to fed rats. A $p < 0.05$ using Tukey's test was considered significant.

5.5.2 DIG Study

Individual and average DIG C-t profiles for 1-hour fasted rats are shown in Figure 5.10 and the NCA PK parameters and metrics are listed in Table 5.9. For 30-minute fasted rats, the C-t profiles for individual and average rats are shown in Figure 5.11. The NCA PK parameters and metrics are listed in Table 5.10. The C-t profiles and NCA PK parameters for fed rats are shown in Figure 5.12 and Table 5.11. Rat 49 data was very sporadic, so it was excluded when averaging values and from the naïve pool.

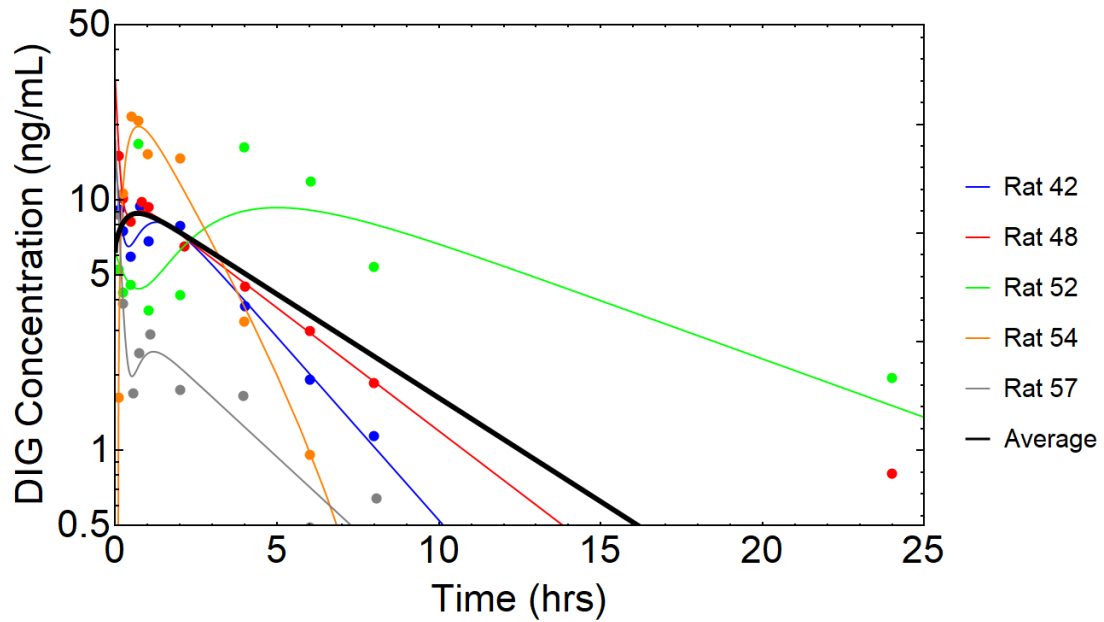


Figure 5.10 DIG PO individual and average (n=5) PK C-t profiles for 1-hour fasted rats. Dots represent experimental C-t data points and lines represent smoothed functions to join the dots. The average is the naïve pooled average.

Table 5.9 PK parameters and metrics for DIG in 1-hour fasted rats using NCA. Individual rats are listed as single values and the average is the mean \pm std dev.

	Rat 42	Rat 48	Rat 52	Rat 54	Rat 57	Average \pm std dev
ka (hr ⁻¹)	2.55	0.673	0.108	2.65	0.102	1.22 \pm 1.28
F	0.101	0.134	0.364	0.125	0.037	0.152 \pm 0.124
C _{max} (ng/mL)	9.42	10.1	16.8	21.5	8.76	13.3 \pm 5.60
t _{max} (hr)	0.77	0.25	0.72	0.50	0.10	0.47 \pm 0.29
AUC _(0-∞) (ng•hr/mL)	44.5	60.0	126.8	48.9	11.7	58.4 \pm 42.3

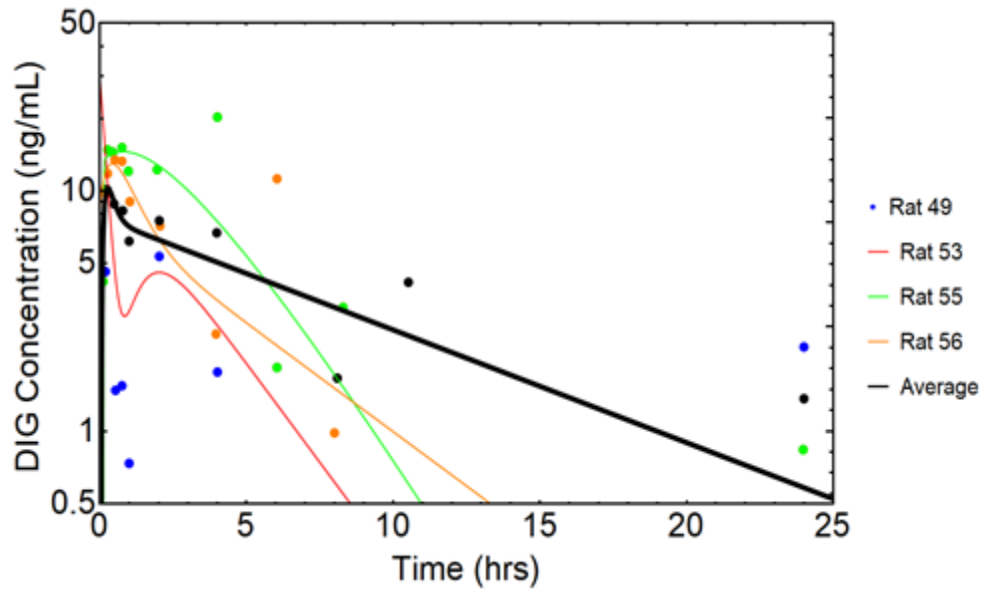


Figure 5.11 DIG PO individual and average (n=3) PK C-t profiles for 30-min fasted rats. Dots represent experimental C-t data points and lines represent smoothed functions to join the dots. The average is the naïve pooled average. Only experimentally obtained data points are shown for Rat 49. Rat 49 was not included in the naïve pooled average.

Table 5.10 PK parameters and metrics for DIG PO 30-min fasted rats using NCA. Individual rats are listed as single values and the average is the mean \pm std dev.

	Rat 49	Rat 53	Rat 55	Rat 56	Average \pm std dev
ka (hr ⁻¹)	0.018	0.26	0.854	1.13	1.22 \pm 1.28
F	0.152	0.072	0.318	0.120	0.152 \pm 0.124
C _{max} (ng/mL)	5.33	16.1	20.2	13.5	13.8 \pm 6.3
t _{max} (hr)	2.03	0.18	4.00	0.52	1.68 \pm 1.74
AUC _(0-∞) (ng•hr/mL)	50.2	42.7	105	48.7	58.4 \pm 42.3

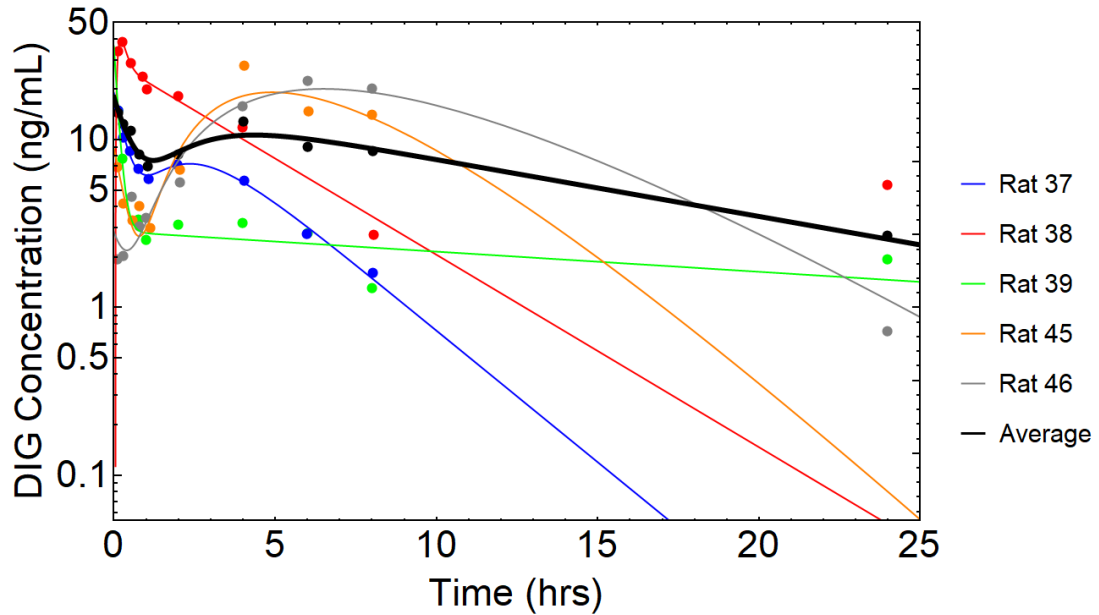


Figure 5.12 DIG PO individual and average (n=5) PK C-t profiles for fed rats. Dots represent experimental C-t data points and lines represent smoothed functions to join the dots. The average is the naïve pooled average.

Table 5.11 PK parameters and metrics for DIG PO fed rats using NCA.
Individual rats are listed as single values and the average is the mean \pm std dev.

	Rat 37	Rat 38	Rat 39	Rat 45	Rat 46	Average \pm std dev
ka (hr ⁻¹)	0.897	0.539	0.672	0.224	2.940	1.05 \pm 1.08
F	0.121	0.287	0.084	0.414	0.620	0.305 \pm 0.220
C _{max} (ng/mL)	1.05	14.62	0.37	5.57	16.40	7.6 \pm 7.5
t _{max} (hr)	1.67	2.23	1.95	3.73	0.99	2.11 \pm 1.01
AUC _(0-∞) (ng•hr/mL)	40.4	162.2	24.6	118.4	200.7	109.3 \pm 76.1

None of the parameters or metrics were significantly different between groups for DIG.

The average naïve pooled for each feeding condition were compared, as shown in Figure 5.9 and Table 5.8.

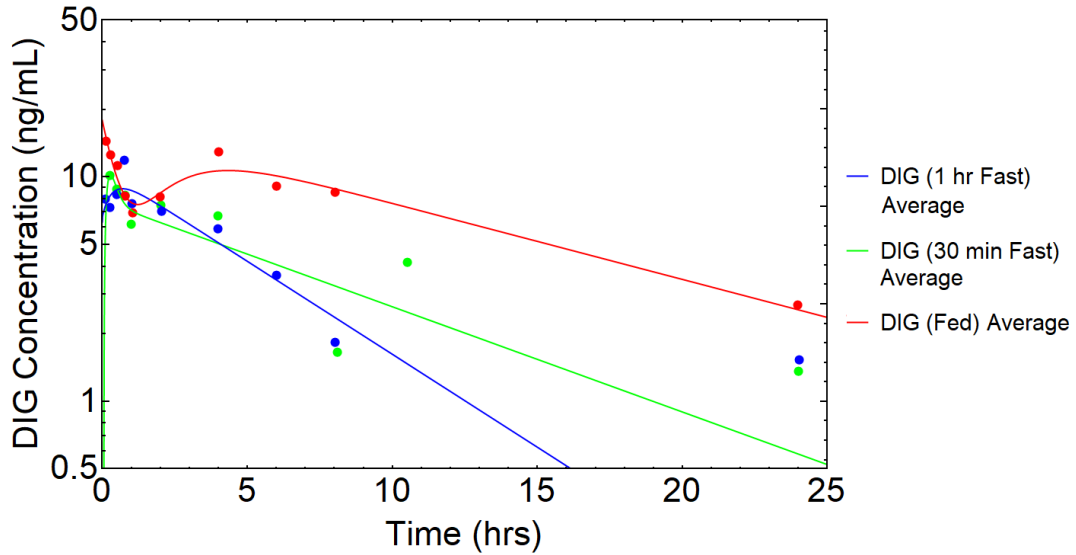


Figure 5.13 Comparison of average DIG PK C-t profiles for fasted and fed rats. Dots represent experimentally collect C-t data and lines represent a smoothed function to connect the experimental data. Averages shown represent the naïve pooled averages.

Table 5.12 Comparison of average DIG PK parameters and metrics for 1-hour fasted, 30-min fasted, and fed rats using NCA.

	ka (hr ⁻¹)	F	C _{max} (ng/mL)	t _{max} (hr)	AUC _(0-∞) (ng•hr/mL)
Fast (1 hour)	0.050	0.144	11.8	0.750	69.8
Fast (30 min)	0.132	0.188	0.62	9.60	79.5
Fed	0.107	0.598	2.05	11.6	158

5.6 Discussion and Conclusion

For naive pooled AML, the F for the fasted groups were smaller than those of the fed group, while the ka was increased. This agrees with the literature, which states that the presence of food leads to delayed gastric emptying. This delayed emptying leads to a decrease in ka. This was seen for fed rats, which had a lower ka than fasted groups. As described in Chapter 1, the F will proportionally affect the C_{max} and AUC. The exposure for fasted groups was decreased, as expected but the C_{max} was unaffected. This was likely due to the increase in ka. While the amount absorbed may have decreased, this was compensated for by the increase in the rate the drug was taken up by the intestines. Additionally, the increase in ka influenced the t_{max} by shortening the time to C_{max} for fasted groups.

The same rats were used for GLY as AML and the observed increased ka for fasted groups was expected. For averaged GLY values, the ka for the 2-hours fasted rats was significantly higher compared to other groups using Tukey's test. The increased ka led to

an increase in C_{max} for the 2-hours fasted naïve pool average. The t_{max} was significantly higher in the fed rat group compared to the other groups using Tukey's test. The AUC was not different between groups, which was expected since the F was similar for all feeding conditions.

For naïve pooled DIG, the F for fed rats was around double that of fasted groups. This led to a proportional increase in AUC. There were no distinguishable differences in k_a or C_{max} , likely due to the high variability in these values, which led to overlapping values across feeding groups. The t_{max} was shorter for the 1-hour fasted rat group compared to the 30-minute fasted and fed group, when looking at the naïve pooled average. This was not expected as there was no alteration in k_a to influence the t_{max} . Given the difference in t_{max} was not statistically significant and the data had large variability, the difference in t_{max} may not be physiologically relevant.

An overall trend seen for all three drugs was a decrease in variability and more clean data as the fasting length increased. Compared to fed rats, fasted rats have a more distinct absorption and elimination phase. As mentioned in Chapter 1, this emphasizes the importance of dosing while fasted to reduce variability and improve PK parameter estimations. In addition, this underscores the value of performing food effect studies to better understand a drug's PK.

CHAPTER 6: PARTICLE SIZE EFFECTS ON GLY ORAL DISPOSITION

6.1 Rationale

This chapter aims to determine the influence of particle size on the PK profile of GLY. Physiochemical and formulation properties of the drug, along with physiological factors, dictate its absorption. For BSC Class II drugs like GLY, absorption is limited by dissolution rate. As mentioned in Chapter 1, particle size influences drug absorption by influencing the dissolution rate. Therefore, BCS Class II drugs in suspension can benefit from a decrease in particle size, resulting in increased dissolution and uptake into the systemic circulation (Tsume et al., 2014). To better understand and model the influence of particle size on absorption profiles using the rodent model, Chapter 7, *in vivo* PK studies utilizing multiple well-characterized particle sizes were performed.

In vitro dissolution studies reveal that the dissolution of GLY was improved with a reduction in particle size (Valleri et al., 2004; Wang et al., 2017). The increase in dissolution rate can be seen by improved absorption *in vivo*. A 3.5 mg micronized formulation provided greater GLY serum concentrations than a 5 mg non-micronized formulation in humans (Arnqvist et al., 1983). Similarly, decreasing the particle size of GLY led to a shorter t_{max} and significantly increased C_{max} in SD rats (Wang et al., 2017).

Drug characterization should be performed before dosing in animals. Laser diffraction is a commonly used method for determining drug particle size due to its rapid, reliable, and reproducible output (Ma et al., 2002). Laser diffraction uses a beam of light to hit a sample, causing the light to scatter at a specific angle. The angle of scatter is measured and corresponds to the particle size. This method uses the Fraunhofer or Mie theories to calculate size (Murphy et al., 2018). Both theories assume the particles are spheres, which should be confirmed by another form of measurement. Scanning electron microscopy (SEM) can be used to validate whether a drug is spherical. SEM uses a focused electron beam to scan a defined area of the surface of a particle. The emitted signals are processed to form a 3-D image depicting the surface topography and shape of the particle (Luo, 2018).

To achieve the desired particle size for the work here, jet milling was used. Jet milling blasts the drug with high-velocity nitrogen gas in a grinding chamber, causing the particles to collide and fracture (Saleem and Smyth, 2010). While this is a common method for micronization, alterations to the crystalline structure can occur, leading to changes in dissolution (Guinot and Leveiller, 1999). X-ray diffraction (XRD) can be used to characterize the drug's polymorph and identify if any alterations have occurred due to the milling process (Loh et al., 2015). A cathode-ray tube produces electrons that bombard the sample, producing X-ray spectra. The spectra are detected and processed (Bunaciu et al., 2015).

A portion of the drug passes into the solution when creating a drug suspension, while the rest remains undissolved. The solubilized portion can be easily absorbed *in vivo* due to GLY's high permeability, while the remaining drug must be dissolved. Therefore, it is essential to distinguish the percent soluble, as the absorption kinetics for the portion in solution would be different from that in suspension (Ahmed, 2015). In the rodent absorption model detailed in Chapter 7, the drug in suspension underwent a dissolution step before becoming available for absorption.

6.2 Materials

Male Sprague-Dawley single jugular cannulated rats weighing 239 – 250g were ordered from Charles River (Wilmington, MA). Sterile saline and syringes were ordered from FisherScientific (Pittsburgh, PA). Heparin was obtained from Sagent Pharmaceuticals (Schaumburg, IL). 23G needles were ordered from Sigma-Aldrich (St. Louis, MO). Isoflurane was ordered from Piramal Enterprises (Lexington, KY). Glyburide was from Combi-blocks (San Diego, CA).

6.3 Study Design

6.3.1 Animals

Male SD rats were singly housed under a reverse 12-hr light/dark cycle. Rats were acclimated for at least four days in the Temple University Health Science Campus animal housing facility and 30 minutes in the procedure room prior to the start of the study. They

were provided food and water *ad libitum*. Food was removed from the cages of fasted groups 12 hours before the beginning of the study and reintroduced 2 hours after dosing. All animal studies were performed with strict adherence to protocols approved by the Temple University IACUC.

6.3.2 Drug and Formulation Preparation

Bulk glyburide with an average particle size of 67.1 μm (Appendix B) was micronized by jet milling by Particle Solutions (24 Hagerty Blvd, West Chester, PA 19382). Pace Analytical (600 Markley St, Norristown, PA 19401) measured the particle size and distribution of GLY using laser diffraction. XRD was performed to assure no polymorph changes occurred from jet milling, and SEM was done to confirm the drug particles are spherical. Pace Analytical designed the formulation to be dosed into rats. This formulation was the same as the formulation used for physicochemical characterization to minimize any formulation-dependent changes to the drug particle size and shape. This allows for the best description of the drug that was administered to the rats.

The dosing consistency was established by creating two 10 mg/mL suspensions (~2 mL) of each particle size. Three samples of 0.4 mL GLY were removed from each stock using a gavage needle attached to a syringe. The suspension was vortexed between samplings. Samples were diluted 1:400 in ACN to obtain detectable concentrations within a validated linear range on the LC-MS/MS. The diluted samples were added to a tube containing two and a half times the volume of IS in ACN. This mixture was analyzed by

LC-MS/MS using the method described in Chapter 2. Because the exact concentrations aren't necessary, the dosing consistency was determined by comparing peak area ratios of GLY to GLY-d3.

Three suspensions of each particle size were created to determine the percent solubilized. The suspensions were centrifuged at 15,000 g for 10 minutes. The clear top layer was removed and diluted 1:100 with ACN. The diluted samples were added to a tube containing two and a half times the volume of IS in ACN. The mixture was analyzed by LC-MS/MS using the method described in Chapter 2.

The total drug amount consists of the drug in both solution and suspension. The percent of drug in solution and was determined using the following equation:

$$P_{Sol} = \frac{D_{Sol}}{D_T} \times 100 \quad \text{Equation 5.1}$$

where P_{Sol} is the percent of GLY in solution, D_T is the total amount of drug (10 mg), and D_{Sol} is the amount of drug in solution, which was calculated by:

$$D_{Sol} = \frac{C_{Sol}}{V_{Sol}} \quad \text{Equation 5.2}$$

where C_{Sol} is the concentration of GLY in solution and V_{Sol} is the volume of the solution (1 mL).

6.3.3 PK Study

Rats were divided into two groups containing five animals each. Rats were administered either of two micronized samples: Sample A, with a mean particle size of 4.1 μm , or Sample B, with a mean particle size of 42.7 μm (Table 6.1). The formulation was 0.5% w/w methylcellulose A15 (MC) and 0.5% w/w polysorbate 80. Fresh dosing vehicle was prepared the night before. MC and polysorbate 80 were added to distilled water and stirred overnight to allow the MC to dissolve fully.

Table 6.1 Mean and distributions for particle sizes

	Dv(10) (μm)	Dv(50) (μm)	Dv(90) (μm)	Span	Specific surface area (m^2/kg)
Sample A	1.67	4.10	8.82	1.74	1875
Sample B	8.02	42.7	117	2.56	328.2

The GLY suspension was vortexed before each dose is drawn to assure proper drug distribution in the suspension. Rats were administered 10 mg/kg of a 10 mg/mL suspension of either particle size by oral gavage. Blood samples (~0.2 mL) were collected via the jugular cannula into pre-heparinized tubes at 0.17, 0.5, 1, 1.5, 2.5, 4, 6, 8, 12, 16, 20, 24 hours post-dose. After each sampling, the loss of blood volume was supplemented with an equal volume of saline containing 100 U/mL heparin. Plasma was obtained by centrifugation at 2,000 g for 15 minutes at 4°C and kept at -20 °C until analysis. Plasma samples were analyzed by LC-MS/MS using the method described in Chapter 2.

6.4 Data Analysis

PK parameters and metrics for oral PK data were calculated using compartmental and NCA analysis as described in Chapter 5. Data were described using the mean and standard deviation. The dosing consistency, percent solubilized, and particle size group data were analyzed using an Independent Samples t-test. A p-value < 0.05 was considered significant.

6.5 Results

6.5.1 Drug and Formulation Preparation

Peak area ratios were not significantly different between samples taken from the same stock or between stocks with the same particle size. There was a significant difference between stocks from different particle sizes, as shown in Table 6.2. GLY concentrations in solution and thus the percent of GLY solubilized were not significantly different between stocks of the same particle size or between particle sizes, as shown in Table 6.3. The average percent of GLY in solution ranged between 0.125 – 0.176% and 0.141 – 0.367% for Sample A and Sample B formulations, respectively.

Table 6.2 Dosing consistency measured using GLY to GLY-d4 peak area ratios

	Sample A (4.1 μm)		Sample B (42.7 μm)	
	Stock #1	Stock #2	Stock #1	Stock #2
Run #1	10.50	10.30	8.58	9.15
Run #2	10.50	10.80	9.63	8.28
Run #3	10.40	10.60	8.75	8.38
Average \pm std dev	10.47 \pm 0.06	10.57 \pm 0.25	8.99 \pm 0.56*	8.60 \pm 0.48*

*statistically different from Sample A using Independent Samples t-test with a p-value <0.001

Table 6.3 Percent of GLY in solution

	Sample A (%)			Sample A (%)		
	Stock #1	Stock #2	Stock #3	Stock #1	Stock #2	Stock #3
Run #1	0.199	0.224	0.232	0.340	0.130	0.123
Run #2	0.082	0.111	0.241	0.370	0.495	0.195
Run #3	0.094	0.103	0.050	0.203	0.565	0.106
Average \pm std dev	0.125 \pm 0.06	0.147 \pm 0.07	0.176 \pm 0.10	0.304 \pm 0.09	0.397 \pm 0.23	0.141 \pm 0.01

6.5.2 PK Study

The individual C-t profiles and PK metrics for Sample A (4.1 μm) are shown in Figure 6.1 and Table 6.4, respectively. Using NCA, the individual values for k_a ranged from 0.099 – 0.451 hr^{-1} . The F varied around 0.08 – 0.63 and the average C_{max} ranged from 176 – 996 ng/mL . The t_{max} was around 2.5 – 8.0 hr. Lastly the AUC ranged from around 1950 – 7300 ng hr/mL .

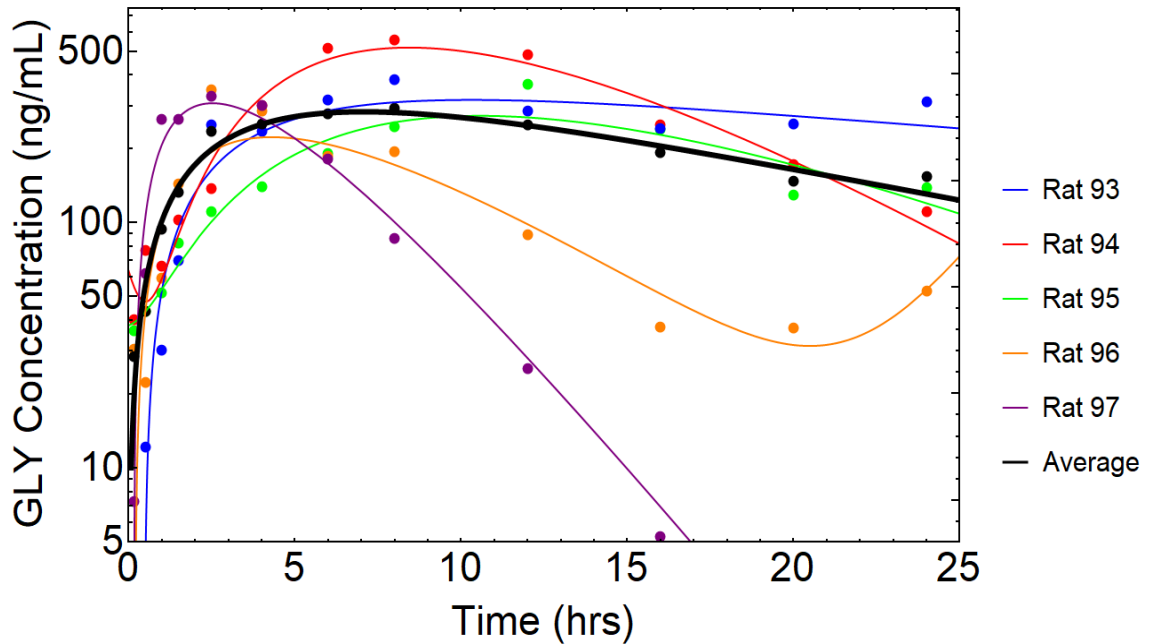


Figure 6.1 PO individual and average (n=5) PK C-t profiles for Sample A (4.1 μm). Dots represent experimentally collect C-t data and lines represent a smoothed function to connect the experimental data. The bold, black line represents the naïve pooled average.

Table 6.4 Individual PK parameter and metrics for Sample A (4.1 μm) using NCA

	Rat 93	Rat 94	Rat 95	Rat 96	Rat 97
k_a (hr^{-1})	0.099	0.116	0.101	0.175	0.451
F	0.626	0.302	0.219	0.095	0.075
C_{max} (ng/mL)	383	558	367	349	326
t_{max} (hr)	8.0	8.0	8.0	2.5	2.5
$AUC_{(0-\infty)}$ (ng•hr/mL)	6358	7284	4799	2736	1949

The individual C-t profiles and NCA PK metrics for the Sample B (42.7 μm) are shown in Figure 6.2 and Table 6.5, respectively. The individual values for k_a range from 0.125 – 0.413 hr^{-1} and the F ranged from 0.02 – 0.085. The C_{max} ranged from 57.0 – 159 ng/mL , and the t_{max} was around 0.17 – 8.0 hr. The AUC ranged around 400 - 2000 ng hr/mL .

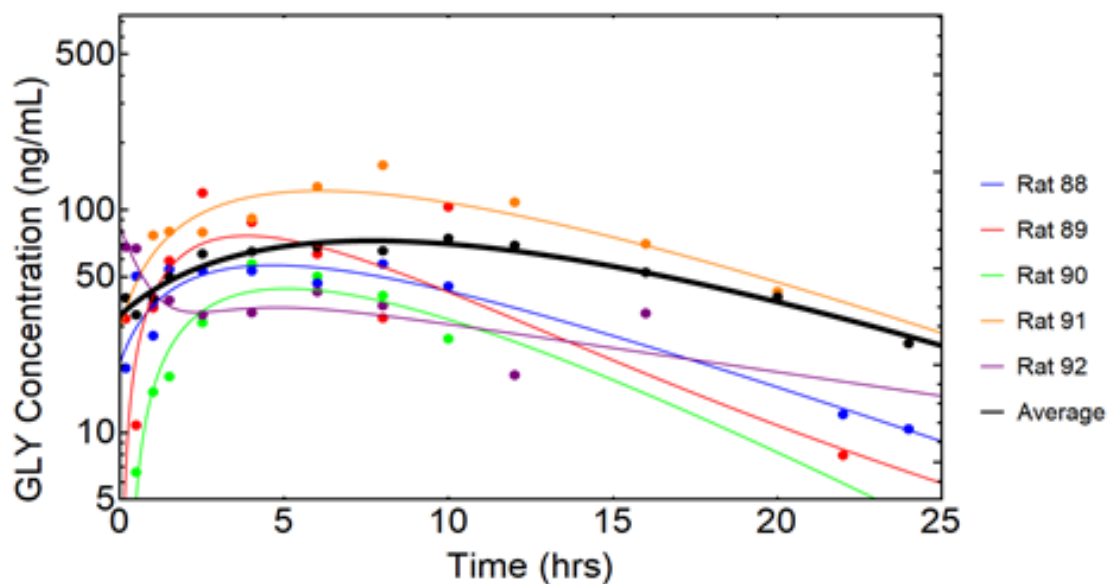


Figure 6.2 PO individual and average (n=5) PK C-t profiles for Sample B (42.7 μm). Dots represent experimentally collect C-t data and lines represent a smoothed function to connect the experimental data. The bold, black line represents the naïve pooled average.

Table 6.5 Individual PK parameter and metrics for Sample B (42.7 μm) using NCA

	Rat 88	Rat 89	Rat 90	Rat 91	Rat 92
k_a (hr^{-1})	0.166	0.413	0.363	0.125	0.220
F	0.035	0.046	0.022	0.085	0.038
C_{max} (ng/mL)	57.0	119	57.0	159	68.4
t_{max} (hr)	8.0	2.5	4.0	8.0	0.17
$\text{AUC}_{(0-\infty)}$ ($\text{ng}\cdot\text{hr/mL}$)	893	901	395	1985	536

The average PK parameters and metrics for the Sample A and Sample B are shown in Table 6.6 and Table 6.7, respectively. The average k_a and t_{max} were not significantly different between formulations. Using NCA, the C_{max} was significantly different between particle sizes (396.6 ng/mL, Table 6.6 vs 92.1 ng/mL, Table 6.7, Independent t-test, p-value 0.004). For the F, there was a difference in the means that was significant NCA (0.263, Table 6.6 vs 0.060, Table 6.7, Independent t-test, p-value 0.02). Lastly, there was no significant difference in AUC between groups significant when using NCA.

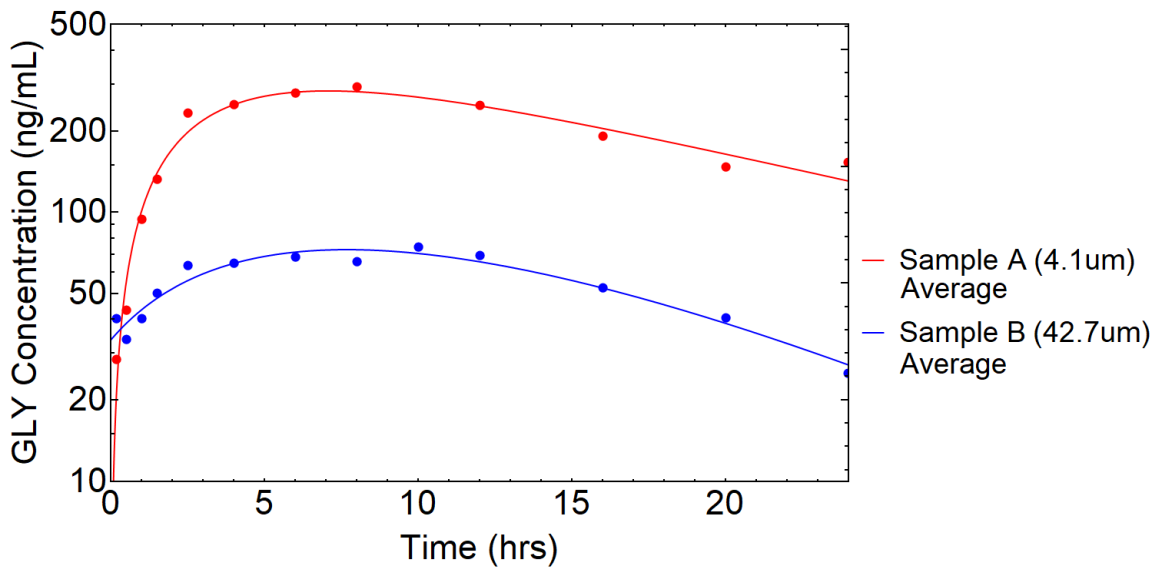


Figure 6.3 Comparison of average PK C-t profiles for Sample A and Sample B

Table 6.6 Average PK parameter and metrics for Sample A (4.1 μm) using NCA

	GLY (average)	GLY (naïve pooled)
ka (hr^{-1})	0.188 ± 0.150	0.111
F	0.263 ± 0.223	0.277
Cmax (ng/mL)	396.6 ± 92.7	271.4
tmax (hr)	5.8 ± 3.0	8.0
AUC _(0-∞) (ng•hr/mL)	4625 ± 2282	4999

Table 6.7 Average PK parameter and metrics for Sample B (42.7 μm)

	GLY (average)	GLY (naïve pooled)
ka (hr^{-1})	0.267 ± 0.142	0.117
F	0.047 ± 0.027	0.060
Cmax (ng/mL)	92.1 ± 45.3	74.2
tmax (hr)	4.53 ± 3.45	10.0
AUC _(0-∞) (ng•hr/mL)	1044 ± 671	1312

6.6 Discussion and Conclusion

Dosing consistency was established using a single stock and between stocks of the same particle size. Drug suspensions are heterogenous mixtures, so particles may gradually sink to the bottom of the container they occupy. Before administering GLY to animals, it was essential to establish dosing consistency. This assured each rat received the same amount of drug, allowing plasma concentrations to be pooled and the averaging of PK parameters and metrics. The percent of GLY in solution will dictate the percent available

for absorption and can be used to determine the percent in suspension. This is important to define, as drug in suspension will need to undergo an additional, dissolution step before becoming available for absorption. For Sample A and Sample B, there was no significant difference in percent in solution.

As the sample size decreased from Sample B (42.7 μm) to Sample A (4.1 μm), the F increased around 4.5X from 0.06 to 0.277. The C_{max} rose around 4X, from 74.2 ng/mL to 271.4 ng/mL. Similarly, the AUC for Sample A (~1300 ng hr/mL) was ~4.5X higher than that of Sample B (~6000 ng hr/mL). As mentioned previously, the F is expected to increase as the particle size decreases, due to an increase in dissolution rate. Due to the influence of F on the C_{max} and AUC, the relatively proportional changes in these values were anticipated.

6.7 Acknowledgments

I would like to thank Dr. Raymond Stevens (Particle Solutions, West Chester, PA) for his work creating the micronized samples from bulk glyburide. Additionally, I want to acknowledge Robert Tuohy (Pace Analytical, Norristown, PA) for his work on the drug characterization and formulation development.

CHAPTER 7: RODENT CONTINUOUS INTESTINAL ABSORPTION MODEL

7.1 Rationale

The aim of this chapter was to develop and refine a continuous intestinal model to predict drug absorption in rats. The anatomical data collected in Chapter 3 were input into the model. Similarly, the membrane partitioning data and systemic disposition functions from Chapter 4 were incorporated. The model was fit to the oral PK data from Chapter 5 and Chapter 6, and specific parameters were optimized. Any additional necessary physiological or physicochemical data were taken from the literature.

PK modeling typically divides the body into separate compartments. Classical compartmental models depict the intestine as a distinct mathematical compartment, with absorption described as a single first-order process. Physiologically-based pharmacokinetic (PBPK) models are more mechanistic. The compartments represent specific organs or tissues which are connected by blood flows. Simpler PBPK models also represent the gut as a single compartment attached to a liver compartment by the portal vein blood flow (Lin and Wong, 2017). More elaborate compartmental modeling, such as the Advanced Compartmental Absorption and Transit (ACAT) model, breaks the intestine into a series of compartments. The drug moves along the intestine from compartment to compartment in a first-order process. In a solid formulation, the drug is released and dissolved in an irreversible and reversible manner,

respectively. The ACAT model is a hybrid model, as the absorption compartments connect to the rest of the body, which is represented as classical central and peripheral compartments (Huang et al., 2009). Elaborate models, like the ACAT model, consider physiological factors (pH, gastric emptying, intestinal transit, and transporter expression levels) and physicochemical factors (pKa, particle size, and solubility) to better predict absorption. This model uses ordinary differential equations to understand drug movement in the body.

Another approach is to consider the intestine to be a continuous compartment. Absorption is modeled as a change in drug concentration along distance (x) and over time (t) (Nagar et al., 2017). This can be achieved with partial differential equations (PDEs), which were revisited due to the advancements in computational power and speed. The continuous intestinal absorption model is based on the basic convection-diffusion equation:

$$\frac{d}{dt} C(x, t) = D \frac{d^2}{dx^2} C(x, t) - \frac{Q}{\pi r^2} \frac{d}{dx} C(x, t) - \sum_{i=1}^n k_i C(x, t) \quad \text{Equation 6.1}$$

where drug concentration (C) varies as a function of both distance (x) and time (t), D is the drug molecule diffusion coefficient, Q is the bulk fluid flow rate, r is the radius of the intestinal lumen, and k_i is the first-order rate constant for the i th radial transfer process. The first term describes axial diffusion, the spread of the drug pulse due to

intestinal drug mixing. The second term describes convection, the axial bulk movement of the pulse, and the last term describes radial diffusion. This approach also includes relevant physiological and physicochemical factors. This model further includes an explicit enterocyte apical membrane and intercellular lipid compartments in the radial direction.

The creation of a continuous intestinal model could be beneficial for the prediction of absorption in preclinical studies. Rats are a commonly used preclinical species for PK studies. Rats also show similar intestinal permeability and drug absorption as humans (Cao et al., 2006). However, the usefulness of rat studies is diminished by species-specific transporters and metabolizing enzymes. A model that could account for the species-specific differences would be advantageous. The collection of rich physiological and PK data to develop and refine a rodent model would be more time-efficient and cost-effective than doing the same in humans.

Species differences in physiology would be valuable to include in a rat absorption model. While the human stomach is a single gastric organ, the rat stomach has two separate portions divided by a limiting ridge (Kararli, 1995; DeSesso and Jacobson, 2001). This could contribute to differences in gastric emptying and drug dumping into the duodenum. Humans have a gallbladder that releases concentrated bile when chyme is present, typically after meals. Rats do not possess a gallbladder, so dilute bile continuously flows into the small intestine. The human jejunum makes up ~40% of the

small intestine, but the jejunum comprises ~90% of the rat small intestine. The cecum makes up 26% of the large intestine in rats but only 5% in humans. Additionally, rats do not have Kerckring's folds, which increases the absorptive surface area in humans. Permeability or solubility differences could exist due to dissimilarities in pH. While both humans and rats have a similar overall trend in pH around 6 – 8, humans have a gastric pH around 1 – 2.5, while rats have a more alkaline gastric pH around 3 – 4 (Ward and Coates, 1987; Evans et al., 1988).

The rodent absorption model describes the intestine as a continuous, concentric set of cylinders. The drug enters as a plug from the stomach into the duodenum (10 cm), moves along the gut through the jejunum (106 cm), ileum (3 cm), and colon (16 cm) before leaving the body. The small intestine has a radius of 0.79 cm in the duodenum, 0.92 cm in the jejunum, 0.89 cm in the ileum, and 1.17 cm in the colon (Figure 6.1). As the plug travels along the axial direction, it does so with a fluctuating velocity, measured *in vivo* in Chapter 3.

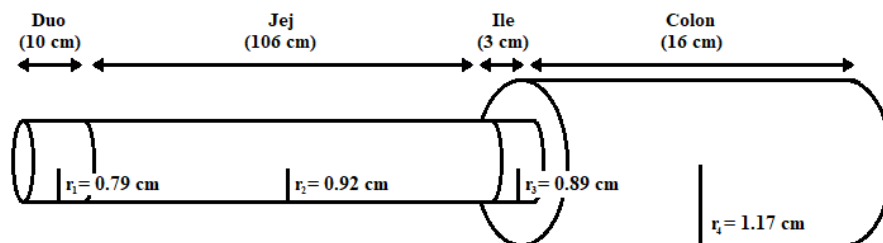


Figure 7.1 Depiction of the rat intestine as a continuous cylinder. Duo is the duodenum, Jej is the jejunum, Ile is the ileum, r_1 is the radius of the Duo, r_2 is the radius of the Jej, r_3 is the radius of the Ile, and r_4 is the radius of the Colon

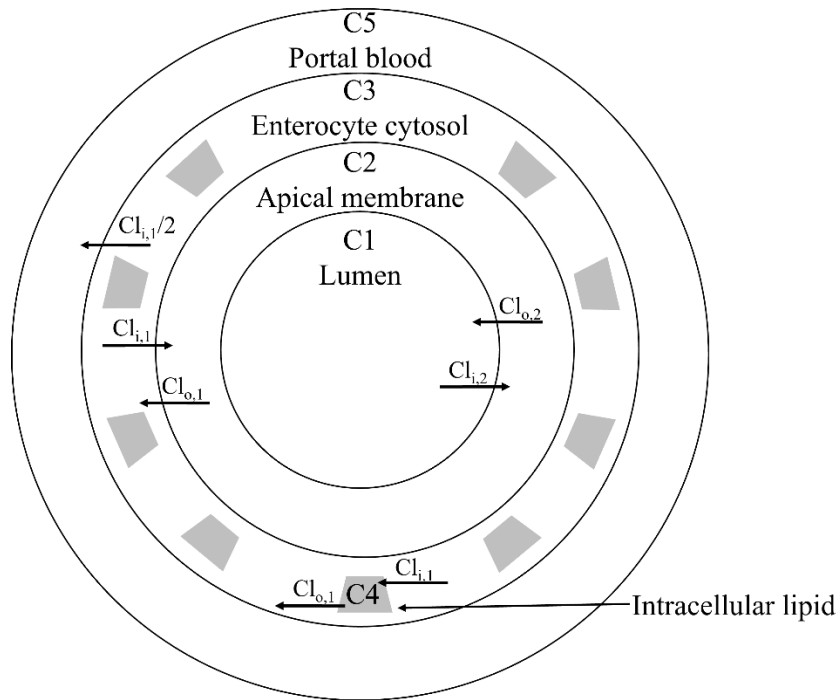


Figure 7.2 Depiction of the radical compartments comprising the concentric cylinders of the rat intestine

The drug also travels in a radial direction as it is absorbed. The drug can reversibly move from the lumen (C1), through the apical enterocyte membrane (C2), into the enterocyte cytosol (C3), where it has the option to go into intracellular lipids (C4). In the final step, the drug irreversibly moves into the basolateral blood (C5) (Figure 6.2). Movement in and out of compartments is expressed by diffusional clearance terms Cl_i and Cl_o , respectively.

7.2 Methods

Table 7.1 Input parameters and their sources

Experimentally obtained parameter	Optimized parameter	Literature Parameters
Luminal pH	Drug bolus (plug) length	Drug nature
Length of intestine	Caco-2 scaling factor	pKa
Radii of intestine	Stomach emptying lag time	Fraction unbound in microsomes
Velocity of the drug bolus		Total bioavailability
		Drug solubility
		Microvilli factors
		Fraction absorbed
		Apparent permeability

The whole drug plug moves in an axial direction through the intestine. The transit rate slows along the length, with the slowest velocity occurring in the large intestine. The velocity data was collected in Chapter 3 and is further discussed in section 7.4. The cross-sectional area for the enterocyte apical membrane (Equation 6.2) and cytosol (Equation 6.3) were determined. The surface area of the small intestine and colon was multiplied by width of the plasma membrane (35 \AA) and the diameter of an enterocyte ($20 \text{ }\mu\text{m}$), respectively, to obtain the following equations:

$$a_{mem}(x) = (35 * 10^{-10})sa_{lumen}(x) \quad \text{Equation 6.2}$$

$$a_{cyt}(x) = (20 * 10^{-6})sa_{villi}(x) \quad \text{Equation 6.3}$$

where $sa_{lumen}(x)$ is the surface area of the lumen (accounting for villi and microvilli) along the distance (x), while sa_{villi} , is the surface area (accounting for villi) along the distance (x). The surface areas and microvilli factors were obtained from the literature (Wood, 1944; Mayhew and Middleton, 1985). Because microvilli are only present on the apical surface of epithelial cells, only the apical membrane includes both villi and microvilli (Walton et al., 2016). The cross-sectional area for cytosolic lipids was calculated, assuming lipids make up 7% of membranes by volume:

$$a_{lip}(x) = (15 * 10^{-7})sa_{villi}(x) \quad \text{Equation 6.4}$$

The plug experiences peristalsis as it moves along the intestine, causing the plug to diffuse axially. The effective axial diffusion is a function of velocity, as show in the following equation:

$$dif(x) = 0.005(0.5 + 0.5 \tan(75(x - .025))) * vel(x) \quad \text{Equation 6.5}$$

The apparent permeability (P_{app}) is calculated based on Caco-2 data. To account for species differences and the transition from *in vitro* to *in vivo*, a Caco-2 scaling factor was altered to best fit the experimental C-t data. The pH along the intestine (pH) was collected in Chapter 3 and further discussed in section 7.4. For neutral drugs, the P_{app} remains constant along the intestine. Permeability for acids and bases depend on the pH of the lumen and pKa. The P_{app} for acids (Equation 6.6) and bases (Equation 6.7) were calculated using the following equations:

$$Papp_a(x) = \frac{Papp_{scaled}}{1 + 10^{ma/10(pH_c - pKa)}} \quad \text{Equation 6.6}$$

$$* \frac{1}{1 + 10^{ma/10(pH(x) - pKa)}}$$

$$Papp_b(x) = \frac{Papp_{scaled}}{1 + 10^{mb/10(pKa - pH_c)}} \quad \text{Equation 6.7}$$

$$* \frac{1}{1 + 10^{mb/10(pKa - pH(x))}}$$

where $Papp(x)$ is the apparent permeability along the intestine, $Papp_{scaled}$ is the scaled Caco-2 permeability of a specific drug, ma is the slope of permeability versus pH for acids, and mb is the slope of permeability versus pH for bases, pH_c is the pH at which the Caco-2 experiments were conducted, pKa is the pKa for the drug (the pH at which the drug is 50% ionized), and $pH(x)$ is the pH of the intestine at distance x .

The movement of drug between compartments is described by diffusional clearances $Cl_i(x)$ and $Cl_o(x)$. Movement of drug into the membrane is the product of permeability and surface area:

$$Cl_{i,1}(x) = 2Papp(x) * sa_{lumen}(x) \quad \text{Equation 6.8}$$

$$Cl_{i,2}(x) = 2Papp_2(x) * sa_{lumen}(x) \quad \text{Equation 6.9}$$

$$Cl_{i,3}(x) = 4Papp(x) * 100sa_{lumen}(x) \quad \text{Equation 6.10}$$

where $Cl_{i,2}(x)$ is the diffusional clearance when radial diffusion is the rate limiting step, and $Papp_2$ is the modified apparent permeability when radial diffusion is the rate limiting step. $Papp_2$ (Equation 6.11) is modified by a radial diffusion function (Equation 6.12) to slow radial diffusion in the terminal colon:

$$Papp_2(x) = \frac{Papp(x) * f_{raddiff}(x)}{Papp(x) + f_{raddiff}(x)} \quad \text{Equation 6.11}$$

$$f_{raddiff}(x) = 0.025(1 - (1 - 0.014) \tan[2(x - 5)])) * (1 - \tan[50(x - 1.2)])) \quad \text{Equation 6.12}$$

The $Cl_{i,3}(x)$ is the diffusional clearance for the intracellular lipid compartment. It is assumed that the plasma membrane makes up ~0.1% of total cell volume, while the intracellular lipids comprise ~10%. To account for this difference, the $sa[x]$ was multiplied by a factor of 100.

The diffusional clearance out of the membranes is dependent on membrane partitioning. For drugs that are comfortable remaining in the lipophilic membranes, an experimentally observed time lag in drug movement is present (Korzekwa et al., 2012). Therefore, radial diffusion out of the membranes (Equation 6.13) and membrane partitioning (Equation 6.14) can be explained by the following equations:

$$Cl_o(x) = Cl_i(x)/Kp \quad \text{Equation 6.13}$$

$$Kp = \frac{1 - f_{um}}{0.0007 f_{um}} \quad \text{Equation 6.14}$$

where f_{um} is the fraction unbound in microsomes. The f_{um} values were collected from the literature or experimentally. The drug is released from the stomach in a pulse after a lag time. The initial velocity in the duodenum was achieved by:

$$pulse(t) = C_0 * V_{corr} * uppulse(t) \quad \text{Equation 6.15}$$

where C_0 is the initial concentration (Equation 6.16), V_{corr} is a volume correction factor, (Equation 6.17) and $uppulse(t)$ is the input from the stomach (Equation 6.18):

$$C_0 = dose/V_{s,o} \quad \text{Equation 6.16}$$

$$V_{corr} = \frac{V_{s,o}}{PL_t * \pi * r_1^2 * Vel0} \quad \text{Equation 6.17}$$

$$uppulse(t) = 0.5 (\tan[300(t - lag)] - \tan[100(t - (PL_t + lag))]) \quad \text{Equation 6.18}$$

where $V_{s,o}$ is the volume of water introduced into the stomach with the drug (1mL/kg), PL_t is the stomach pulse length (initially set to 0.3 hr), $Vel0$ is the velocity at $x=0$, and lag is the time lag before the drug pulse is released from the stomach (initially set to 0.1 hr). Drug solution disposition in the rat intestine was modeled for drug concentrations in the lumen, $C1(x,t)$, apical membrane, $C2(x,t)$, enterocyte cytosol, $C3(x,t)$, and optional intracellular lipids, $C4(x,t)$, with the following PDEs:

$$\begin{aligned} \frac{d}{dt} C1(x, t) = & dif(x) \frac{d^2}{dx^2} C1(x, t) + \left(-vel(x) + \frac{d}{dx} dif(x) + \right. \\ & \left. \frac{dif(x)}{a(x)} \frac{d}{dx} a(x) \right) \frac{d}{dx} C1(x, t) + \left(-\frac{d}{dx} vel(x) - \right. \\ & \left. \frac{vel(x)}{a(x)} \frac{d}{dx} a(x) \right) C1(x, t) - \frac{Cl_{i,2}(x)}{a(x)} C1(x, t) + \frac{Cl_{o,2}(x)}{a(x)} C2(x, t) \end{aligned} \quad \text{Equation 6.19}$$

$$\begin{aligned} \frac{d}{dt} C2(x, t) = & \frac{Cl_{i,2}(x)}{a_{mem}(x)} C1(x, t) - \\ & \left(\frac{Cl_{o,1}(x) + Cl_{o,2}(x)}{a_{mem}(x)} \right) C2(x, t) + \frac{Cl_{i,1}(x)}{a_{mem}(x)} C3(x, t) \end{aligned} \quad \text{Equation 6.20}$$

$$\begin{aligned} \frac{d}{dt} C3(x, t) = & \frac{Cl_{o,1}(x)}{a_{cyt}(x)} C2(x, t) - \frac{Cl_{i,1}(x)}{a_{cyt}(x)} C3(x, t) - \\ & \frac{Cl_{i,1}(x)}{2a_{cyt}(x)} C3(x, t) + \frac{Cl_{i,3}(x)}{2a_{cyt}(x)} C3(x, t) + \frac{Cl_{o,3}(x)}{a_{cyt}(x)} C4(x, t) \end{aligned} \quad \text{Equation 6.21}$$

$$\frac{d}{dt} C4(x, t) = \frac{Cl_{i,1}(x)}{a_{lip}(x)} C3(x, t) - \frac{Cl_{o,3}(x)}{a_{lip}(x)} C4(x, t) \quad \text{Equation 6.22}$$

where, $C1(t, 0) = \text{pulse}(t)$, $C1(0, x) = \text{pulse}(0)$, $C1(t, 1.4) = 0$,

$C2(0, x) = 0$, $C2(t, 0) = 0$, $C2(t, 1.4) = 0$, $C3(0, x) = 0$, $C3(t, 0) = 0$, $C3(t, 1.4) = 0$, $C4(t, 0) = 0$, $C4(0, x) = 0$, $C4(t, 1.4) = 0$.

For a drug in suspension, a dissolution step is needed before the drug can be absorbed.

The equation to describe the dissolution of drug particles was proposed by Wang and Flanagan:

$$f_{diss}(x, t) = (8C_{part}(x, t)\pi D \sqrt[3]{\frac{3C_{solid}(x, t)}{4\pi\rho C_{part}(x, t)}})(S - C1(x, t)) \quad \text{Equation 6.23}$$

where C_{part} is the drug particle concentration, D is the drug diffusion coefficient, C_{solid} is the solid drug concentration, p is the density of the drug particles, and S is the drug solubility in pH 7.4 buffer. The amount of drug in a particle was determined by dividing C_{solid} by C_{part} . To keep a constant number of particles in the system, dissolution occurs until C_{solid} is 0.001% of its initial value (C_{slim}). This was done so particles could precipitate if the concentration of drug in the lumen (C_1) exceeds the drug solubility.

As mentioned previously, a portion of the drug is dissolved in a suspension. A single stomach compartment was modeled to release drug in solution in a zero-order (Equation 6.24) and first-order manner (Equation 6.25):

$$pulse_{soln,0}(t) = C_{sol}V_{corr,0}((0.5 + 0.5 \tan[150(t - lag)] - (0.5 + 0.5 \tan[150(t - (PL_t + lag))])) \quad \text{Equation 6.24}$$

$$pulse_{soln,1}(t) = C_{0,corr}(0.5 + 0.5 \tan[150(t - (PL_t + lag))]) e^{-k_1(t - (PL_t + lag))} \quad \text{Equation 6.25}$$

where C_{sol} is the drug solubility, $V_{corr,0}$ is the volume correction factor the zero-order stomach pulse (Equation 6.26), $C_{0,corr}$ is a correction factor for the first-order stomach pulse for a solution (Equation 6.27), and k_1 is the stomach elimination rate constant.

$$V_{corr,0} = \frac{vol(0) * FP_0}{\pi r_0^2 PL_t vel(0)} \quad \text{Equation 6.26}$$

$$C_{0,corr} = \frac{(FP_1 * dose_{soln}/V_{stom})}{(\pi r_0^2 vel(0)/Cl_{stomach})} \quad \text{Equation 6.27}$$

where $vol(0)$ is the volume of the dose, FP_0 is the fraction of the solution dose that is emptied in a zero-order process, r_0^2 is the radius of intestine at distance =0, $vel(0)$ is the velocity at time = 0, FP_1 is the fraction of the solution dose that is emptied in a first-order process, $dose_{soln}$ is the dose that is in solution, V_{stom} is the volume of the stomach, and Cl_{stom} is the clearance from the stomach. The undissolved portion also leaves in both a zero-order (Equation 6.28) and first-order manner (Equation 6.29):

$$pulse_{sus,0}(t) = C_{sol}V_{corr,0}((0.5 + 0.5 \tan[150(t - lag)] - (0.5 + 0.5 \tan[150(t - (PL_t + lag))])) \quad \text{Equation 6.28}$$

$$pulse_{sus,1}(t) = C_{02,corr}(0.5 + 0.5 \tan[150(t - (PL_t + lag))]) e^{-k_1(t-(PL_t+lag))} \quad \text{Equation 6.29}$$

where $C_{02,corr}$ is the correction factor for the first-order stomach pulse for a suspension:

$$C_{02,corr} = \frac{(FP_2 * dose_{sus}/V_{stom})}{(\pi r_0^2 vel(0)/Cl_{stomach})} \quad \text{Equation 6.30}$$

where FP_2 is the fraction of the suspension dose that is emptied in a first-order process, and $dose_{sus}$ is the solid dose in the suspension. As only dissolved drug can enter the apical membrane, $C_2(x,t)$, $C_3(x,t)$, and $C_4(x,t)$ use the same PDEs as mentioned above (Equation 6.20 – 6.22) for a solution dose. Lastly, the particle pulse (undissolved drug)

into the stomach was described in a zero-order (Equation 6.31) and first-order manner (Equation 6.32):

$$pulse_{part,0}(t) = C_{p,0}V_{corr,0}((0.5 + 0.5 \tan[150(t - lag)] - (0.5 + 0.5 \tan[150(t - (PL_t + lag))])) \quad \text{Equation 6.31}$$

$$pulse_{part,1}(t) = C_{03,corr}(0.5 + 0.5 \tan[150(t - (PL_t + lag))]) e^{-k_1(t - (PL_t + lag))} \quad \text{Equation 6.32}$$

where $C_{p,0}$ is the particle number (Equation 6.33) and $C_{03,corr}$ is the correction factor for the first-order particle pulse into the stomach (Equation 6.34):

$$C_{p,0} = \left(\frac{(dose_{sus}/p)}{\frac{4}{3}\pi PS^3} \right) / vol(0) \quad \text{Equation 6.33}$$

$$C_{03,corr} = \frac{\left(\frac{FP_2(dose_{sus}/p)}{\frac{4}{3}\pi PS^3 V_{stom}} \right)}{\left(\frac{\pi r_0^2 vel(0)}{Cl_{stomach}} \right)} \quad \text{Equation 6.34}$$

where PS is the particle size of the drug. To describe the absorption disposition for solid drug, the following equations were used:

$$\begin{aligned} \frac{d}{dt} Cp1(x, t) = dif(x) \frac{d^2}{dx^2} Cp1(x, t) + \left(-vel(x) + \frac{d}{dx} dif(x) + \right. \\ \left. \frac{dif(x)}{a(x)} \frac{d}{dx} a(x) \right) \frac{d}{dx} Cp1(x, t) + \left(-\frac{d}{dx} vel(x) - \right. \\ \left. \frac{vel(x)}{a(x)} \frac{d}{dx} a(x) \right) Cp1(x, t) \end{aligned} \quad \text{Equation 6.35}$$

$$\begin{aligned}
\frac{d}{dt} Cs1(x, t) = dif(x) \frac{d^2}{dx^2} Cs1(x, t) + \left(-vel(x) + \frac{d}{dx} dif(x) + \right. \\
\left. \frac{dif(x)}{a(x)} \frac{d}{dx} a(x) \right) \frac{d}{dx} Cs1(x, t) + \left(-\frac{d}{dx} vel(x) - \right. \\
\left. \frac{vel(x)}{a(x)} \frac{d}{dx} a(x) \right) Cs1(x, t) - (0.5(1 + \tan[3(Cs1(x, t) - \\
C_{slim}])) + (0.5(1 + \tan[-75(C_{sol} - C1(x, t))]))(8Cp1(x, t)\pi D^3 \sqrt{\frac{3Cs1(x, t)}{4\pi p Cp1(x, t)}})(C_{sol} - \\
C1(x, t))
\end{aligned}$$

Equation 6.36

$$\begin{aligned}
\frac{d}{dt} C1(x, t) = dif(x) \frac{d^2}{dx^2} C1(x, t) + \left(-vel(x) + \frac{d}{dx} dif(x) + \right. \\
\left. \frac{dif(x)}{a(x)} \frac{d}{dx} a(x) \right) \frac{d}{dx} C1(x, t) + \left(-\frac{d}{dx} vel(x) - \right. \\
\left. \frac{vel(x)}{a(x)} \frac{d}{dx} a(x) \right) C1(x, t) - \frac{Cl_{i,2}(x)}{a(x)} C1(x, t) + \frac{Cl_{o,2}(x)}{a(x)} C2(x, t) + (0.5(1 + \\
\tan[3(Cs1(x, t) - C_{slim}])) + (0.5(1 + \tan[-75(C_{sol} - \\
C1(x, t))]))(8Cp1(x, t)\pi D^3 \sqrt{\frac{3Cs1(x, t)}{4\pi p Cp1(x, t)}})(C_{sol} - C1(x, t))
\end{aligned}$$

Equation 6.37

where $Cp1(t, 0) = pulsepart,0(t) + pulsepart,1(t)$, $Cp1(0, x) = pulsesoln,0(0) e^{-10x}$, $Cp1(t, 1.4) = 0$, $Cs1(t, 0) = pulsesus,0(t) + pulsesus,1(t)$, $Cs1(0, x) = pulsesus,0(0) e^{-10x}$, $Cs1(t, 1.4) = 0$, $C1(t, 0) = pulsesoln,0(t) + pulse_{soln,1}(t)$, $C1(0, x) = pulse_{soln,0}(0) e^{-10x}$, and $C1(t, 1.4) = 0$.

7.3 Data Analysis

The naïve pooled C-t data collected from Chapter 5 and 6 were plotted. The IV data from Chapter 4 was used to estimate clearance and distribution and were fixed as disposition functions. The predicted curves were normalized to the observed AUC, by optimizing the

first-pass metabolism (FgFh) value to obtain the experimental AUC. Therefore, only the rate of absorption and shape of the C-t profiles were predicted.

A sensitivity analysis was performed for each of the fasted/fed states and particle sizes for AML, GLY, and DIG. This analysis determines the parameters that are the most influential to C-t profile predictions and within which range of values they have the most impact. The exposure overlap coefficient (EOC) was used to compare the observed and predicted C-t profiles. The EOC calculates the overlapping portions of two separate AUCs with zero indicating no overlap and one meaning complete overlap. The absolute fold error (AFE) in Cmax and tmax for predicted and observed data were calculated.

7.4 Results

As mentioned previously, the drug plug moves in an axial direction through the intestine. The velocity data was determined in Chapter 3. The radius of the intestinal segment influenced the velocity and was used to create the expression for velocity:

$$\begin{aligned}
 vel(x) = \frac{a1}{a(x)} & \left(2.4 - \frac{1.96}{1 + e^{-20(-0.45+x)}} - \frac{0.19}{1 + e^{-15(-1.05+x)}} \right. \\
 & \left. - \frac{0.11}{1 + e^{-25(-1.3+x)}} - \frac{0.09}{1 + e^{-25(-1.399+x)}} \right)
 \end{aligned}$$

Equation 6.40

where a1 is the cross-sectional area at radius r1 and a(x) is the cross-sectional area as a function of distance (x) (Equation 6.2).

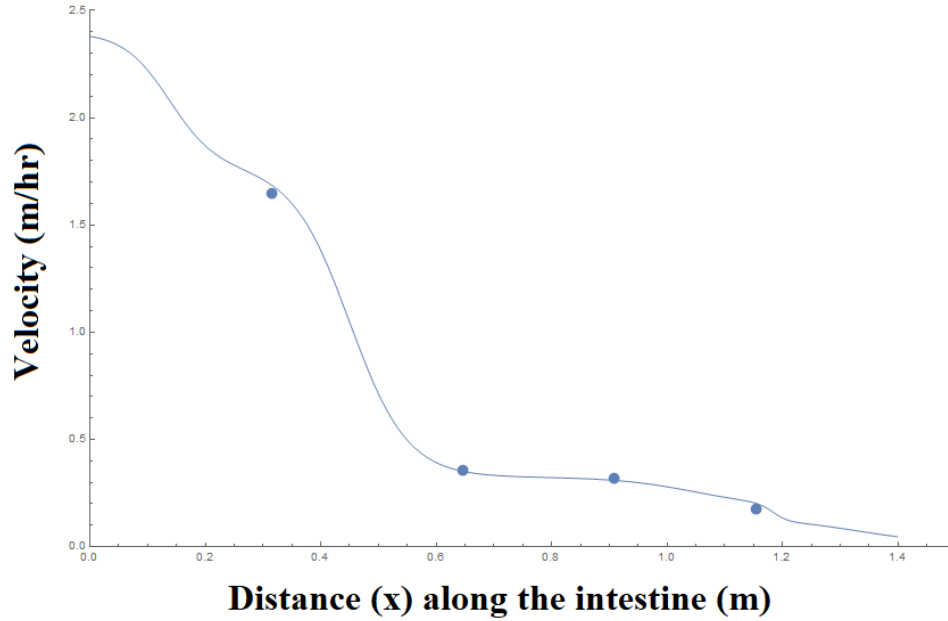


Figure 7.3 Function of velocity along the distance (x) of the rat intestine

The pH along the intestine, collected experimentally in Chapter 3, was described as a combination of logistic functions for fasted (Equation 6.39) and fed (Equation 6.40) states:

$$pH_{ft}(x) = 6.5 - \frac{0.4}{1+e^{-75(-1.32+x)}} - \frac{1.2}{1+e^{-75(-1.25+x)}} + \frac{0.4}{1+e^{-50(-1.1+x)}} + \frac{0.7}{1+e^{-15(-1+x)}} + \frac{0.1}{1+e^{-2(-.761+x)}} \quad \text{Equation 6.39}$$

$$pH_{fd}(x) = 6 + \frac{0.3}{1+e^{-30(-1.3+x)}} - \frac{2.1}{1+e^{-150(-1.25+x)}} + \frac{0.8}{1+e^{-50(-1.15+x)}} + \frac{0.7}{1+e^{-10(-.67+x)}} + \frac{0.3}{1+e^{-10(-.37+x)}} - \frac{0.1}{1+e^{-10(-.15+x)}} \quad \text{Equation 6.40}$$

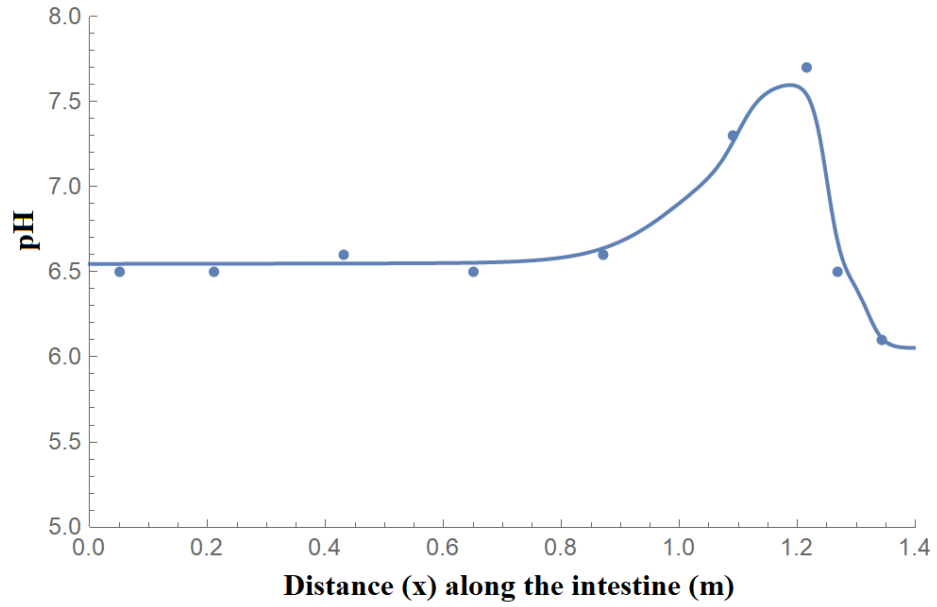


Figure 7.4 Function of fasted pH along distance (x) of the rat intestine

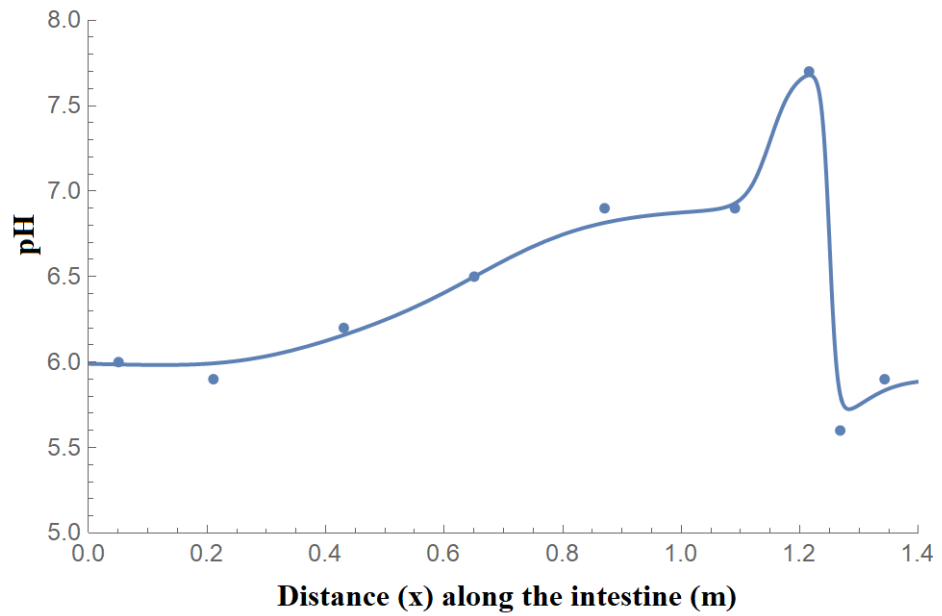


Figure 7.5 Function of fed pH along distance (x) of the rat intestine

The cross-sectional surface area was determined by the experimental radii along the intestine and described by:

$$a(x) = a1 + \frac{a2-a1}{1+e^{-25(-0.15+x)}} \frac{a3-a2}{1+e^{-20(-1.2+x)}} \frac{a4-a3}{1+e^{-75(-1.23+x)}} \quad \text{Equation 6.40}$$

where a_2 is the cross-sectional area at radius r_2 , a_3 is the cross-sectional area at radius r_3 , and a_4 is the cross-sectional area at radius r_4 .

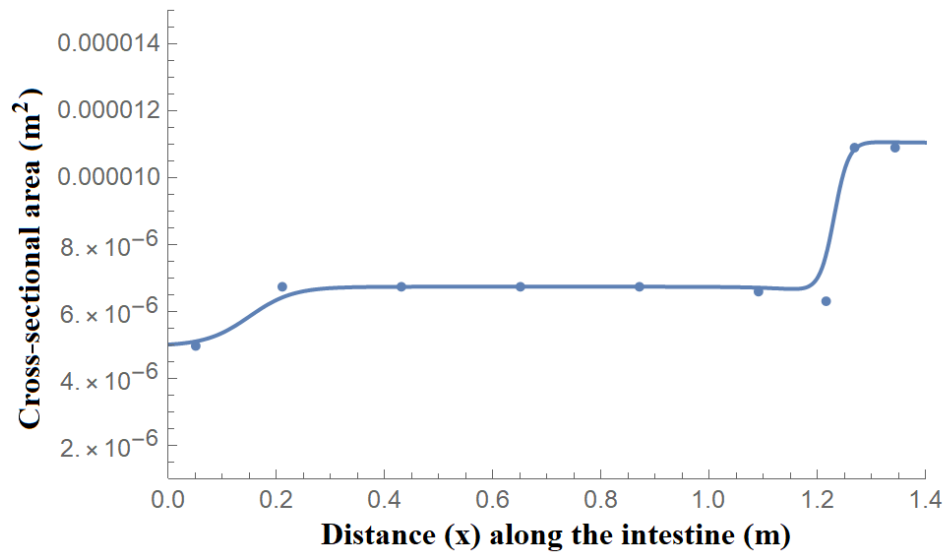


Figure 7.6 Function of cross-sectional area along distance (x) of the rat intestine

7.4.1 AML Food Effects

A sensitivity analysis was performed for Caco-2 scaling factor (Caco-2 sf), plug length (PL_t), and stomach lag time (lag). Initial values for Caco-2 sf, PL_t , and lag were 2.4, 0.3 hr, and 0.1 hr, respectively. First, the Caco-2 sf and PL_t were varied between 0.003 – 12 and 0.06 – 1.5 hr, respectively. The EOC values for the initial and extreme boundaries are

show in Table 7.2. To minimize number of runs, lag time was only varied for the top three Caco-2 sf/ PL_t combinations. Lag was varied between 0.005 – 0.5 hr.

Table 7.2 Caco-2 sf and PL_t combinations for AML fasted and fed rats. Lag time was set to 0.1 hr for all modeling attempts. Bold values are the top three EOCs for each feeding condition.

Caco-2 sf	PL _t (hr)	Fast 2 hr	Fast 1 hr	Fed
0.12	0.06	0.555	0.679	0.919
0.12	0.3	0.550	0.675	0.915
0.12	1.5	0.529	0.653	0.896
0.48	0.06	0.633	0.765	0.980
0.48	0.3	0.628	0.760	0.978
0.48	1.5	0.602	0.733	0.962
1.2	0.06	0.734	0.874	0.900
1.2	0.3	0.728	0.869	0.901
1.2	1.5	0.690	0.832	0.910
2.4	0.06	0.843	0.914	0.781
2.4	0.3	0.835	0.914	0.783
2.4	1.5	0.790	0.899	0.802
4.8	0.06	0.872	0.835	0.632
4.8	0.3	0.870	0.835	0.634
4.8	1.5	0.823	0.848	0.660
12	0.06	0.840	0.691	0.486
12	0.3	0.841	0.697	0.488
12	1.5	0.851	0.749	0.515

The EOCS, AFE for t_{max}, and AFE for C_{max} for rats fasted 2 hours are shown in Table 7.3. The best combinations had a Caco-2 sf greater than the initial value of 2.4. As the PL_t decreased, the EOC increased, though the difference was minor. Lag time did not

play a large role on EOC, tmax AFE, or Cmax AFE. For 2-hours fasted rats (Figure 7.7), the best combination of values for Caco-2 sf, PL_t, and lag were 4.8, 0.06, and 0.005, respectively. The EOC improved from 0.835 to 0.877. The AFEs for tmax and Cmax improved from 1.72 to 1.04 and 1.68 to 1.22, respectively.

Table 7.3 Top Caco-2 sf, PL_t, and lag combinations for AML (fasted 2 hours)

Caco-2 sf	PL _t (hr)	lag (hr)	EOC	AFE tmax	AFE Cmax
4.8	0.06	0.1	0.872	1.16	1.26
		0.01	0.872	1.12	1.26
		0.005	0.877	1.04	1.22
		0.5	n/a	n/a	n/a
4.8	0.3	0.1	0.870	1.16	1.25
		0.01	0.873	1.12	1.25
		0.005	0.875	1.08	1.24
		0.5	0.841	1.36	1.25
12	1.5	0.1	0.851	1.14	1.11
		0.01	0.854	1.19	1.11
		0.005	0.856	1.19	1.11
		0.5	0.811	1.08	1.19

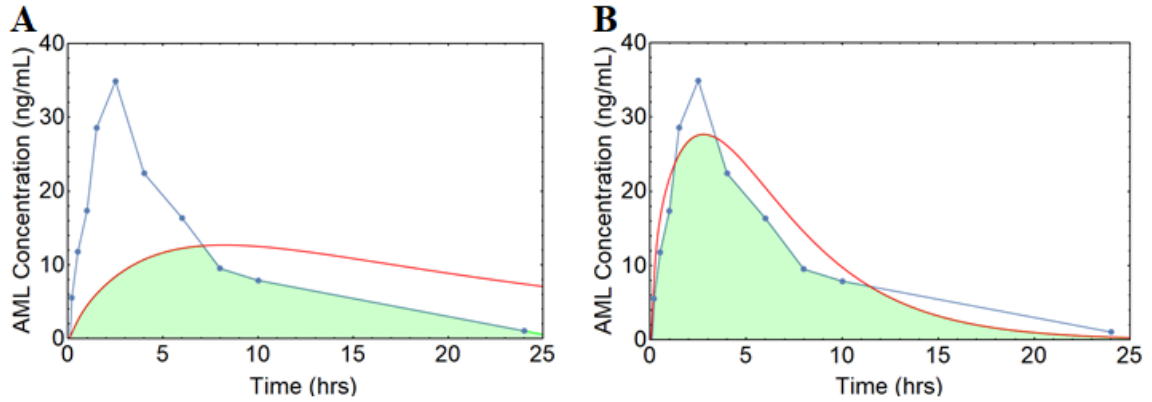


Figure 7.7 Predicted versus observed C-t profiles for 2-hours fasted rats dosed a 5 mg/kg AML solution for (A) initial and (B) best parameter value combination.

The blue line represents the observed C-t profile, the blue dots represent the observed C-t data collected from the literature, the red line represents the predicted C-t profile, and the green shading is the overlapping portion of the two C-t profiles.

The EOCS, AFE for t_{max} , and AFE for C_{max} for rats fasted 1 hour are shown in Table 7.4. The top three best parameter combinations had a Caco-2 sf of 2.4. As the PL_t increases, the EOC decreases, though this effect is minor. Lag time did not play a large role on EOC, t_{max} AFE, or C_{max} AFE. For 1-hour fasted rats (Figure 7.8), the best combination of values for Caco-2 sf, PL_t , and lag were 2.4, 0.06, and 0.01, respectively. The EOC remained constant at 0.914. The AFE for t_{max} improved from 1.08 to 1.05. The AFE for C_{max} remained at 1.22.

Table 7.4 Top Caco-2 sf, PL_t, and lag combinations for AML (fasted 1 hour)

Caco-2 sf	PL _t (hr)	lag (hr)	EOC	AFE tmax	AFE Cmax
2.4	0.06	0.1	0.914	1.05	1.22
		0.01	0.914	1.03	1.22
		0.005	0.907	1.08	1.17
		0.5	0.909	1.15	1.22
2.4	0.3	0.1	0.914	1.08	1.22
		0.01	0.914	1.05	1.22
		0.005	0.912	1.03	1.21
		0.5	0.906	1.18	1.22
2.4	1.5	0.1	0.899	1.25	1.22
		0.01	0.902	1.23	1.22
		0.005	0.904	1.20	1.22
		0.5	0.881	1.30	1.21

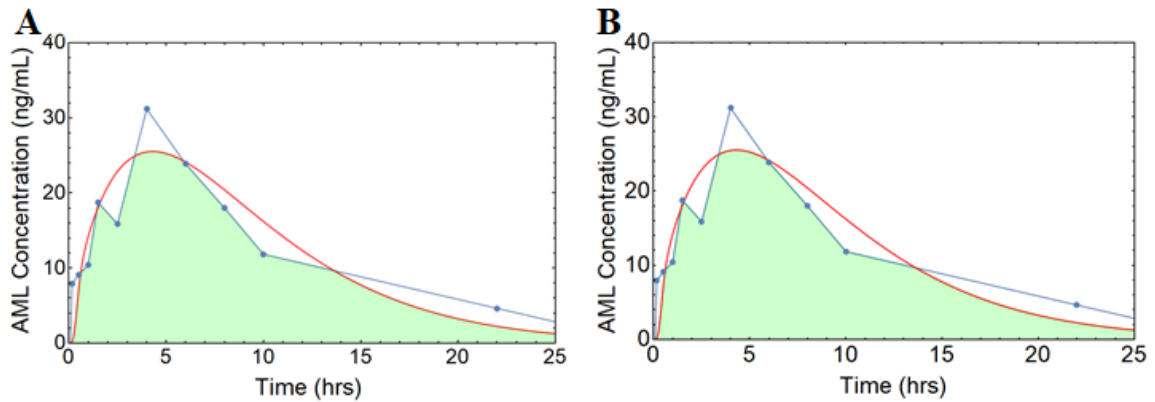


Figure 7.8 Predicted versus observed C-t profiles for 1-hour fasted rats dosed a 5 mg/kg AML solution for (A) initial and (B) best parameter value combination. The blue line represents the observed C-t profile, the blue dots represent the observed C-t data collected from the literature, the red line represents the predicted C-t profile, and the green shading is the overlapping portion of the two C-t profiles.

The EOCS, AFE for tmax, and AFE for Cmax for fed rats are shown in Table 7.5. The top three best parameter combinations had a Caco-2 sf of 0.48. As the PL_t increases, the EOC decreases, though this effect is minor. Lag time did not play a large role on EOC, tmax AFE, or Cmax AFE. For fed rats (Figure 7.9), the best combination of values for Caco-2 sf, PL_t, and lag were 0.48, 0.06, and 0.01, respectively. The EOC increased from 0.783 to 0.980. The AFE for tmax improved from 1.85 to 1.01. The AFE for Cmax improved from 1.38 to 1.00.

Table 7.5 Top Caco-2 sf, PL_t, and lag combinations for AML (fed)

Caco-2 sf	PL _t (hr)	lag (hr)	EOC	AFE tmax	AFE Cmax
0.48	0.06	0.1	0.980	1.00	1.01
		0.01	0.980	1.02	1.02
		0.005	0.962	1.16	1.01
		0.5	0.971	1.04	1.00
0.48	0.3	0.1	0.978	1.01	1.01
		0.01	0.980	1.00	1.01
		0.005	0.977	1.05	1.01
		0.5	0.967	1.06	1.01
0.48	1.5	0.1	0.962	1.07	1.01
		0.01	0.965	1.07	1.01
		0.005	0.966	1.05	1.01
		0.5	0.948	1.11	1.03

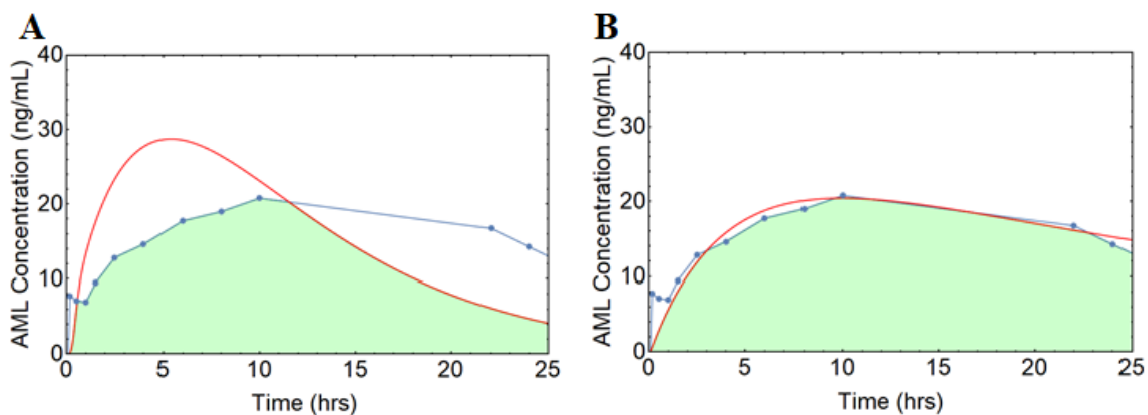


Figure 7.9 Predicted versus observed C-t profiles for fed rats dosed a 5 mg/kg AML solution for (A) initial and (B) best parameter value combination. The blue line represents the observed C-t profile, the blue dots represent the observed C-t data collected from the literature, the red line represents the predicted C-t profile, and the green shading is the overlapping portion of the two C-t profiles.

The pH function for fasted and fed animals was reversed to determine the influence of pH on predictions. The best fit combination was used to compare EOCs. For AML, the use of the fasted pH function in modeling attempts yielded higher EOCs for fasted rat groups. For fed rats, the EOC was higher when using the fed pH function. This can be seen in Table 7.6.

Table 7.6 EOC values for fasted and fed rat groups using different pH functions. The best fit parameters for Caco-2 sf, PL_i, and lag were used for comparisons. The higher EOC values are bolded.

Fast 2 hr		Fast 1 hr		Fed	
Fast pH	Fed pH	Fast pH	Fed pH	Fast pH	Fed pH
0.913	0.865	0.914	0.912	0.949	0.981

7.4.2 GLY Food Effects

A sensitivity analysis was performed for Caco-2 sf, PL_t , and lag. Initial values for Caco-2 sf, PL_t , and lag were 2.4, 0.3 hr, and 0.1 hr, respectively. For 1-hour fasted and fed rats, the Caco-2 sf was varied between 0.0001 – 12. For 2-hours fasted rats, the Caco-2 sf was varied between 0.01 – 12. Lower values of Caco-2 sf weren't run for 2-hours fasted rats because the EOCs for all PL_t begin to decrease as the Caco-2 sf decreased. The EOC values for the initial and extreme boundaries are show in Table 7.7. To minimize number of runs, lag time was only varied for the top three Caco-2 sf/ PL_t combinations. Lag was varied between 0.005 – 0.5 hr.

Table 7.7 Caco-2 sf and PL_t combinations for GLY fasted and fed rats. Lag time was set to 0.1 hr for all modeling attempts. Bold values are the top three EOCs for each feeding condition.

Caco-2 sf	PL _t (hr)	Fast 2 hr	Fast 1 hr	Fed
0.0001	0.06	n/a	0.704	0.872
0.0001	0.3	n/a	0.698	0.867
0.0001	1.5	n/a	0.670	0.847
0.0003	0.06	n/a	0.706	0.906
0.0003	0.3	n/a	0.700	0.901
0.0003	1.5	n/a	0.676	0.877
0.001	0.06	n/a	0.811	0.897
0.001	0.3	n/a	0.803	0.894
0.001	1.5	n/a	0.769	0.882
0.003	0.06	n/a	0.900	0.801
0.003	0.3	n/a	0.893	0.796
0.003	1.5	n/a	0.858	0.796
0.01	0.06	0.539	0.810	0.591
0.01	0.3	0.606	0.807	0.593
0.01	1.5	0.539	0.794	0.604
0.12	0.06	0.757	0.483	0.317
0.12	0.3	0.791	0.492	0.321
0.12	1.5	0.890	0.538	0.344
0.48	0.06	0.639	0.452	0.299
0.48	0.3	0.672	0.461	0.305
0.48	1.5	0.897	0.505	0.333
1.2	0.06	0.617	0.445	0.297
1.2	0.3	0.651	0.456	0.304
1.2	1.5	0.892	0.506	0.332
2.4	0.06	0.609	0.444	0.296
2.4	0.3	0.644	0.454	0.304
2.4	1.5	0.886	0.504	0.332

Table 7.7 Caco-2 sf and PL_t combinations for GLY fasted and fed rats (continued).

Caco-2 sf	PL _t (hr)	Fast 2 hr	Fast 1 hr	Fed
4.8	0.06	0.609	0.442	0.297
4.8	0.3	0.641	0.453	0.304
4.8	1.5	0.883	0.504	0.332
12	0.06	0.606	0.445	0.298
12	0.3	0.640	0.453	0.304
12	1.5	0.881	0.503	0.332

The EOCS and AFE for t_{max} and C_{max} for 2-hours fasted rats are shown in Table 7.8.

All the top three combinations had a PL_t of 1.5 hr. The lag time influenced the EOC, with the best lag time being 0.1 hr, followed by 0.01 hr. The top three combinations had a Caco-2 sf equal to or less than the initial value. Overall, Caco-2 sf did not play a large role on EOC, t_{max} AFE, or C_{max} AFE. For 2-hours fasted (Figure 7.10), the best combination of values for Caco-2 sf, PL_t, and lag were 0.48, 1.5, and 0.1, respectively. The EOC improved from 0.644 to 0.897. The best combination captured the t_{max}, improving the AFE, which went from 3.75 to 1.07. Additionally, the AFE for C_{max} improved from 2.43 to 1.09.

Table 7.8 Top Caco-2 sf, PL_t, and lag combinations for GLY (fasted 2 hours)

Caco-2 sf	PL _t (hr)	lag (hr)	EOC	AFE tmax	AFE Cmax
0.48	1.5	0.1	0.897	1.07	1.09
		0.01	0.884	1.00	1.06
		0.005	0.881	1.00	1.05
		0.5	0.773	1.53	1.22
1.2	1.5	0.1	0.892	1.07	1.07
		0.01	0.866	1.00	1.07
		0.005	0.863	1.00	1.06
		0.5	0.796	1.40	1.22
2.4	1.5	0.1	0.886	1.07	1.08
		0.01	0.857	1.00	1.08
		0.005	0.855	1.00	1.08
		0.5	0.823	1.33	1.13

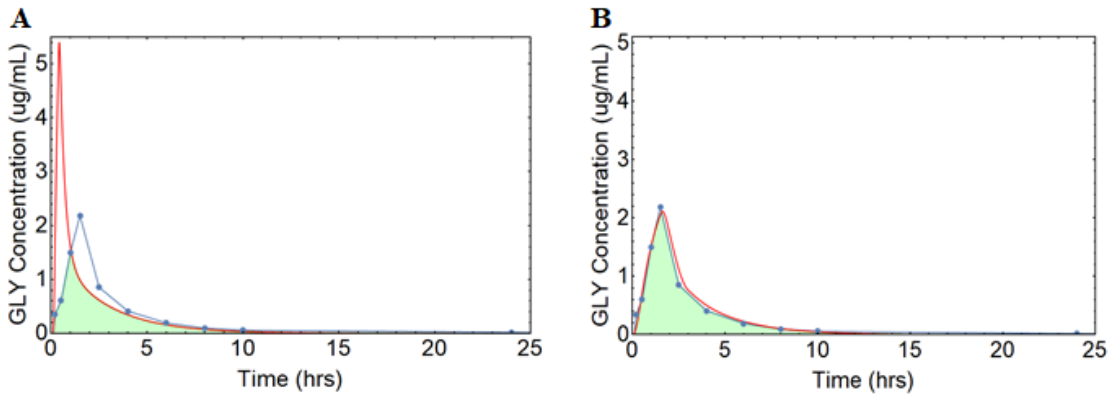


Figure 7.10 Predicted versus observed C-t profiles for 2-hours fasted rats dosed a 5 mg/kg GLY solution for (A) initial and (B) best parameter value combination. The blue line represents the observed C-t profile, the blue dots represent the observed C-t data collected from the literature, the red line represents the predicted C-t profile, and the green shading is the overlapping portion of the two C-t profiles.

The EOCS and AFE for tmax and Cmax for 1-hour fasted rats are shown in Table 7.9.

All the top three combinations had a Caco-2 sf of 0.003 hr. As the PL_t decreases, the EOC increases, though this trend is minor. The lag had little influence on the EOC, tmax AFE, or Cmax AFE. For 1-hour fasted rats (Figure 7.11), the best combination of values for Caco-2 sf, PL_t, and lag were 0.003, 0.06, and 0.01, respectively. The EOC improved from 0.454 to 0.871. The best combination captured the tmax, improving the AFE, which went from 3.75 to 1.00. Additionally, the AFE for Cmax improved from 10.12 to 1.47.

Table 7.9 Top Caco-2 sf, PL_t, and lag combinations for GLY (fasted 1 hour)

Caco-2 sf	PL _t (hr)	lag (hr)	EOC	AFE tmax	AFE Cmax
0.003	0.06	0.1	0.870	1.07	1.47
		0.01	0.871	1.00	1.47
		0.005	0.866	1.07	1.52
		0.5	0.856	1.33	1.48
0.003	0.3	0.1	0.868	1.13	1.47
		0.01	0.869	1.07	1.47
		0.005	0.868	1.07	1.49
		0.5	0.868	1.07	1.49
0.003	1.5	0.1	0.848	1.47	1.48
		0.01	0.852	1.60	1.45
		0.005	0.854	1.60	1.45
		0.5	0.815	1.93	1.54

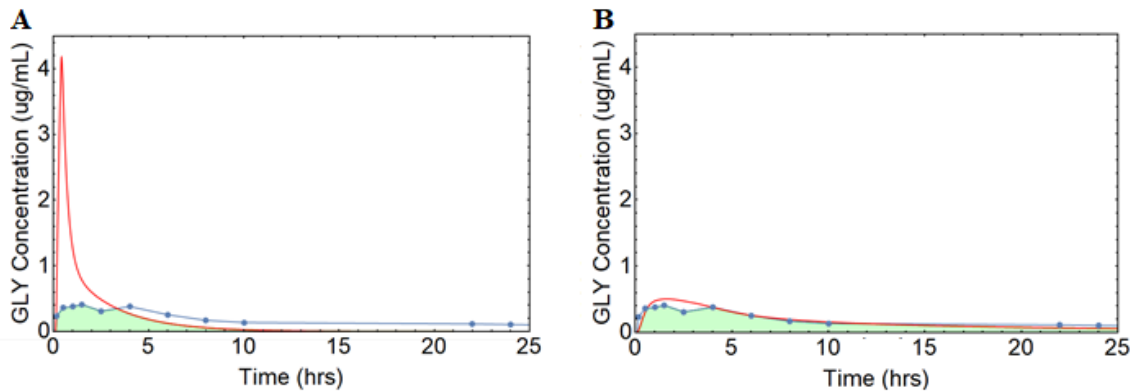


Figure 7.11 Predicted versus observed C-t profiles for 1-hour fasted rats dosed a 5 mg/kg GLY solution for (A) initial and (B) best parameter value combination. The blue line represents the observed C-t profile, the blue dots represent the observed C-t data collected from the literature, the red line represents the predicted C-t profile, and the green shading is the overlapping portion of the two C-t profiles.

The EOCS and AFE for t_{max} and C_{max} for fed rats are shown in Table 7.10. All the top three combinations had a C_{aco-2} sf of 0.003 hr. The PL_t and lag had little influence on the EOC, t_{max} AFE, or C_{max} AFE. For fed rats (Figure 7.12), the best combination of values for C_{aco-2} sf, PL_t , and lag were 0.003, 0.06, and 0.01, respectively. The EOC improved from 0.304 to 0.802. The best combination captured the t_{max} , improving the AFE, which went from 15.00 to 1.28. Additionally, the AFE for C_{max} improved from 20.35 to 1.58.

Table 7.10 Top Caco-2 sf, PL_t, and lag combinations for GLY (fed)

Caco-2 sf	PL _t (hr)	lag (hr)	EOC	AFE tmax	AFE Cmax
0.003	0.06	0.1	0.801	1.25	1.58
		0.01	0.802	1.28	1.58
		0.005	0.799	1.30	1.60
		0.5	0.797	1.15	1.59
0.003	0.3	0.1	0.800	1.22	1.59
		0.01	0.801	1.25	1.59
		0.005	0.800	1.25	1.59
		0.5	0.795	1.11	1.60
0.003	1.5	0.1	0.796	1.07	1.59
		0.01	0.797	1.09	1.59
		0.005	0.797	1.09	1.59
		0.5	0.791	1.00	1.60

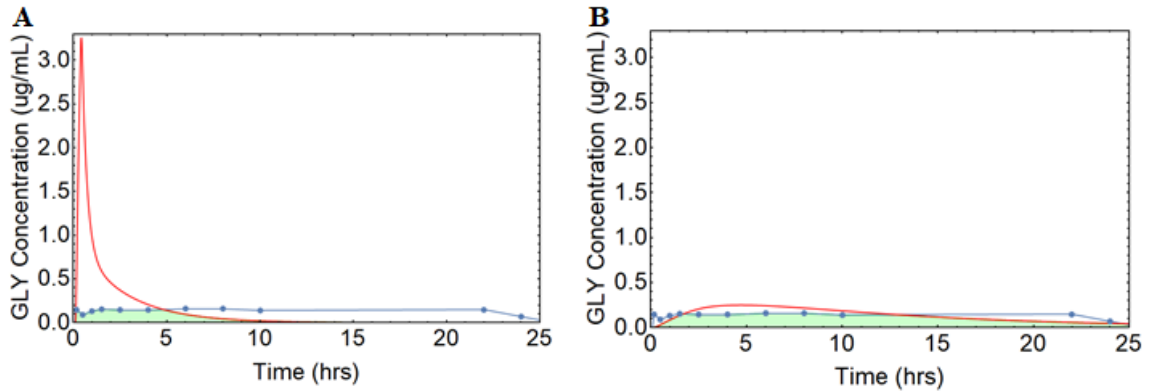


Figure 7.12 Predicted versus observed C-t profiles for fed rats dosed a 5 mg/kg GLY solution for (A) initial and (B) best parameter value combination. The blue line represents the observed C-t profile, the blue dots represent the observed C-t data collected from the literature, the red line represents the predicted C-t profile, and the green shading is the overlapping portion of the two C-t profiles.

7.4.3 DIG Food Effects

A sensitivity analysis was performed for Caco-2 sf, PL_t , and lag. Initial values for Caco-2 sf, PL_t , and lag were 2.4, 0.3 hr, and 0.1 hr, respectively. The Caco-2 sf was varied between 0.003 – 12. The EOC values for the initial and extreme boundaries are show in Table 7.7. To minimize number of runs, lag time was only varied for the top three Caco-2 sf/ PL_t combinations. Lag was varied between 0.005 – 0.5 hr.

Table 7.11 Caco-2 sf and PL_t combinations for DIG fasted and fed rats. Lag time was set to 0.1 hr for all modeling attempts. Bold values are the top three EOCs for each feeding condition.

CACO-2	PL _t	Fast 1 hr	Fast 30 min	Fed
0.003	0.06	0.626	0.659	0.800
0.003	0.3	0.621	0.646	0.795
0.003	1.5	0.597	0.589	0.772
0.01	0.06	0.693	0.659	0.874
0.01	0.3	0.686	0.646	0.867
0.01	1.5	0.655	0.589	0.836
0.12	0.06	0.714	0.899	0.600
0.12	0.3	0.701	0.893	0.600
0.12	1.5	0.664	0.839	0.614
0.48	0.06	0.564	0.662	0.400
0.48	0.3	0.565	0.657	0.403
0.48	1.5	0.586	0.702	0.440
1.2	0.06	0.507	0.573	0.360
1.2	0.3	0.510	0.573	0.363
1.2	1.5	0.549	0.623	0.394
2.4	0.06	0.491	0.545	0.351
2.4	0.3	0.498	0.555	0.356
2.4	1.5	0.532	0.602	0.383
4.8	0.06	0.483	0.531	0.346
4.8	0.3	0.492	0.548	0.352
4.8	1.5	0.541	0.617	0.386
12	0.06	0.477	0.522	0.345
12	0.3	0.489	0.541	0.350
12	1.5	0.546	0.626	0.388

The EOCs and AFEs for t_{max} and C_{max} for 1-hour fasted rats are shown in Table 7.12. The top three best parameter combinations had a Caco-2 sf of 0.12. The PL_t and lag had little influence on the EOC, t_{max} AFE, or C_{max} AFE. For 1-hour fasted rats (Figure 7.13), the best combination of values for Caco-2 sf, PL_t , and lag were 0.12, 0.06, and 0.005, respectively. The EOC improved from 0.498 to 0.727. The best combination did not capture the t_{max} , with the AFE increasing from 1.17 to 2.00. The AFE for C_{max} improved from 4.82 to 1.16.

Table 7.12 Top Caco-2 sf, PL_t , and lag combinations for DIG (fasted 1 hour)

Caco-2 sf	PL_t (hr)	lag (hr)	EOC	AFE t_{max}	AFE C_{max}
0.12	0.06	0.1	0.714	2.29	1.14
		0.01	0.725	2.14	1.15
		0.005	0.727	2.00	1.16
		0.5	0.673	2.86	1.14
0.12	0.3	0.1	0.701	2.43	1.14
		0.01	0.711	2.29	1.14
		0.005	0.713	2.29	1.15
		0.5	0.664	3.00	1.13
0.12	1.5	0.1	0.664	3.57	1.10
		0.01	0.671	3.43	1.10
		0.005	0.673	3.43	1.10
		0.5	0.631	4.14	1.17

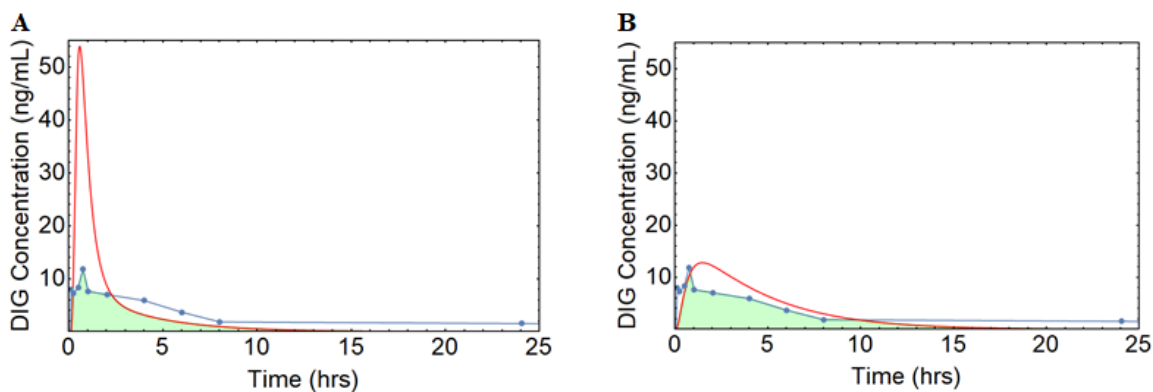


Figure 7.13 Predicted versus observed C-t profiles for 1-hour fasted rats dosed a 0.75 mg/kg DIG solution for (A) initial and (B) best parameter value combination. The blue line represents the observed C-t profile, the blue dots represent the observed C-t data collected from the literature, the red line represents the predicted C-t profile, and the green shading is the overlapping portion of the two C-t profiles.

The EOCs and AFEs for t_{max} and C_{max} for 30-minute fasted rats are shown in Table 7.13. The top three best parameter combinations had a $Caco-2$ sf of 0.12. As the PL_t and lag value decreases, the EOC increases, though the trend is minor. Overall, the PL_t and lag had little influence on the EOC, t_{max} AFE, or C_{max} AFE. For 30-minute fasted rats (Figure 7.14), the best combination of values for $Caco-2$ sf, PL_t , and lag were 0.12, 0.06, and 0.01, respectively. The EOC improved from 0.555 to 0.904. The best combination did not capture the t_{max} , with the AFE increasing from 2.00 to 5.00. The AFE for C_{max} improved from 3.65 to 1.03.

Table 7.13 Top Caco-2 sf, PL_t, and lag combinations for DIG (fasted 30 min)

Caco-2 sf	PL _t (hr)	lag (hr)	EOC	AFE tmax	AFE Cmax
0.12	0.06	0.1	0.899	5.33	1.03
		0.01	0.904	5.00	1.03
		0.005	0.903	4.67	1.02
		0.5	0.867	6.67	1.01
0.12	0.3	0.1	0.893	5.67	1.02
		0.01	0.898	5.33	1.02
		0.005	0.898	5.33	1.02
		0.5	0.851	7.00	1.00
0.12	1.5	0.1	0.839	8.33	1.02
		0.01	0.853	8.00	1.03
		0.005	0.856	8.00	1.03
		0.5	0.775	9.67	1.06

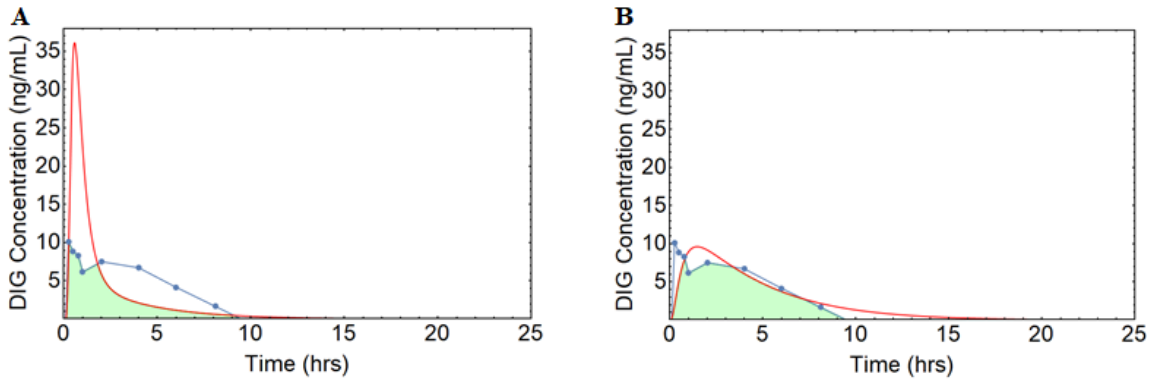


Figure 7.14 Predicted versus observed C-t profiles for 30-minute fasted rats dosed a 0.75 mg/kg DIG solution for (A) initial and (B) best parameter value combination. The blue line represents the observed C-t profile, the blue dots represent the observed C-t data collected from the literature, the red line represents the predicted C-t profile, and the green shading is the overlapping portion of the two C-t profiles.

The EOCs and AFEs for t_{max} and C_{max} for fed rats are shown in Table 7.14. The top three best parameter combinations had a $Caco-2$ sf of 0.01. As the PL_t and lag value decreases, the EOC increases, though the trend is minor. Overall, the PL_t and lag had little influence on the EOC, t_{max} AFE, or C_{max} AFE. For fed rats (Figure 7.15), the best combination of values for $Caco-2$ sf, PL_t , and lag were 0.01, 0.06, and 0.005, respectively. The EOC improved from 0.356 to 0.892. The best combination did not capture the t_{max} , with the AFE increasing from 3.00 to 26.50. The AFE for C_{max} improved from 9.45 to 1.38.

Table 7.14 Top $Caco-2$ sf, PL_t , and lag combinations for DIG (fed)

$Caco-2$ sf	PL_t (hr)	lag (hr)	EOC	AFE t_{max}	AFE C_{max}
0.01	0.06	0.1	0.874	28.50	1.39
		0.01	0.888	27.00	1.38
		0.005	0.892	26.50	1.38
		0.5	0.852	30.50	1.38
0.01	0.3	0.1	0.867	29.00	1.39
		0.01	0.877	28.00	1.39
		0.005	0.881	27.50	1.38
		0.5	0.846	31.00	1.37
0.01	1.5	0.1	0.836	32.50	1.37
		0.01	0.843	31.50	1.37
		0.005	0.846	31.50	1.37
		0.5	0.814	34.50	1.35

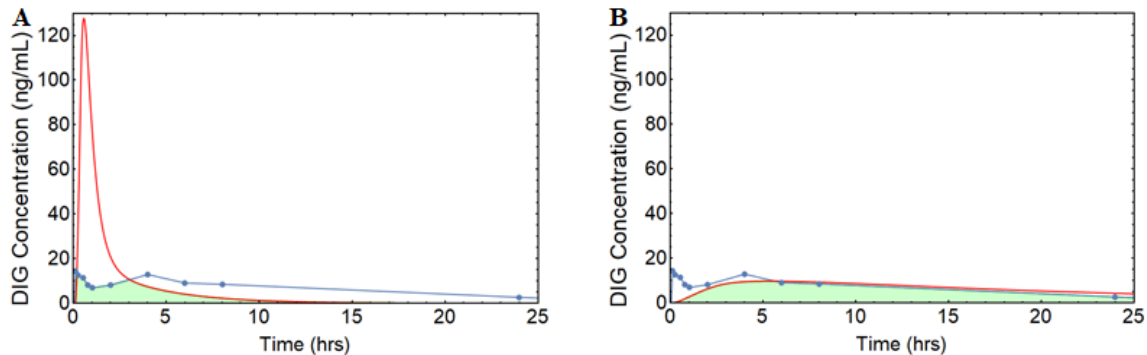


Figure 7.15 Predicted versus observed C-t profiles for fed rats dosed a 0.75 mg/kg DIG solution for (A) initial and (B) best parameter value combination. The blue line represents the observed C-t profile, the blue dots represent the observed C-t data collected from the literature, the red line represents the predicted C-t profile, and the green shading is the overlapping portion of the two C-t profiles.

7.5 Discussion and Conclusion

For all three drugs, the Caco-2 sf was the most impactful parameter. For AML, the Caco-2 sf was at or above 0.48 for all groups, while for the other drugs, GLY and DIG, the Caco-2 sf was at or below 0.48. As mentioned previously, the Caco-2 sf was multiplied by the Caco-2 permeability data (m/hr) to accommodate for differences in permeability between species and moving from *in vitro* to *in vivo*. Given the highly permeable and soluble nature of AML, a higher Caco-2 sf compared to the other drugs was expected as this will greatly increase permeability and drug moving from C1 into C2 of the model. Additionally, the lower Caco-2 sf for GLY and DIG may indicate the presence of transporter effects, as both drugs are known substrates of transporters. In the intestines, GLY is taken up by OATP2B1 and effluxed by BCRP and P-gp (El-Kattan and Varma, 2011; Estudante et al., 2013). DIG is a substrate for P-gp in both rats and humans (El-

Kattan and Varma, 2011; Suzuki et al., 2014). The incorporation of transporters could assist in bettering model predictions of these two drugs.

For AML, as fasting time decreases, the Caco-2 sf decreases. Gastric emptying is delayed when rats are fed, leading to a decrease in k_a and resulting in a decrease in C_{max} . For the rat continuous intestinal absorption model, decreasing the Caco-2 sf mimics a decrease in permeability, also resulting in a slower entrance into the systemic circulation (k_a) and C_{max} . Therefore, using smaller Caco-2 sf values to model groups with decreased fasting times leads to better predictions.

The best PL_t was 0.06 for all AML groups, with a smaller PL_t being associated with a larger EOC. For highly permeable and soluble compounds, as soon as the drug gets dumped into the intestines, it can be absorbed. Therefore, the smaller PL_t was expected. Lastly, the lag time was 0.01 hr for fed and 1-hour fasted rats, while the 2-hours fasted rats had a lag of 0.005 hr. As mentioned previously, gastric emptying is delayed when fasting time decreases. So, the longer lag time for fed and 1-hour fasted rats compared to 2-hours fasted rats is expected. Overall AML was well predicted by the rat continuous intestinal absorption model (EOCs > 0.87).

For GLY, the Caco-2 sf was 0.003 for fed and 1-hour fasted rats, while the Caco-2 sf for 2-hours fasted rats was variable, but larger than that of the other two groups (0.48 – 2.4). As mentioned previously with AML, the lower Caco-2 sf for groups with decreased

fasting times is expected. The best PL_t was 0.06 hr for fed and 1-hour fasted groups, while it was higher for 2-hours fasted rats (1.5 hr). The longer PL_t for the 2-hours fasted group may be compensating for the much larger Caco-2 sf. A longer lag time will delay input into the systemic circulation. Conversely, a larger Caco-2 sf will mimic increased permeability and shorten the time into the systemic circulation. This compensation may also be occurring for the lag time. The lag for fed and 1-hour fasted groups was 0.01 hr, while it was higher (0.1 hr) for 2-hours fasted rats. This was not expected, as gastric emptying delays were expected to lengthen the lag for groups with decreased fasting times. Overall GLY was well predicted by the rat continuous intestinal absorption model (EOCs > 0.80).

For DIG, fasted rat groups had a best fit Caco-2 sf of 0.12, while for the fed group, this value was 0.01. This trend of lower Caco-2 sf values for groups with decreased fasting time was seen for all drugs. The best PL_t and lag was 0.06 hr and 0.005 hr for all groups. Overall DIG was well predicted by the rat continuous intestinal absorption model (EOCs > 0.70), with two of the three groups having an EOC close to 0.90.

The influence of particle size on the dissolution rate and absorption of a drug using the rat continuous intestinal absorption model is ongoing. Two particle sizes, Sample A (4.1 μ m) and Sample B (42.7 μ m) are being utilized.

CHAPTER 8: FUTURE STUDIES

8.1 Anatomical Data Collection

Currently, the GI transit data only includes two animals per timepoint. Future studies could include the addition of at least one rat to each timepoint, allowing for increased confidence in the transit values and the calculation of a standard deviation. This is especially important in the initial time points where drug is present in the portions of the intestine where the surface area is greatest.

Further refinement of the model to include intestinal transporter expression could better predict C-t profiles for drugs like GLY and DIG, known substrates of intestinal transporters. The transporter expression for Oatp1a5 is expected to be the highest in the proximal small intestine and fall along the intestine. The opposite should be seen for P-gp, whose expression is reported to be the highest in the distal regions of the small intestine (Brady et al., 2002). Matrix-assisted laser desorption/ionization (MALDI) could be utilized to determine the protein expression along the intestine under 12-hour fed and fasted conditions.

GLY is a substrate for OATP2B1 in humans and Oatp1a5, previously known as Oatp3, in rats. Administration of grapefruit juice, an OATP2B1 inhibitor, in conjunction with GLY has been shown to reduce uptake *in vitro* (Sato et al., 2005). However, this was not able to be reproduced *in vivo* (Lilja et al., 2007). In rats, naringin, a component of citrus fruits

and inhibitor of Oapt1a5, reduced GLY uptake both *in vitro* and *in vivo* (Jiang et al., 2015). GLY is also a substrate of P-gp, and alterations in protein expression could lead to species-specific changes in drug PK. In humans, administration of GLY along with a P-gp inhibitor led to an increase in AUC and C_{max} (Semple et al., 1986; Lilja et al., 2007), though there is little evidence suggesting P-gp induction or inhibition is influential in GLY absorption in rats (Devi et al., 2015).

DIG is a well-known substrate for P-gp in both humans and rats, with inhibition or induction of the transporter leading to *in vivo* effects on PK. Patients pretreated with rifampin, a P-gp inducer, for ten days prior to DIG administration, experienced a significant decrease in AUC and C_{max}. The t_{max} was significantly prolonged in the rifampin treatment group (Greiner et al., 1999). Increasing doses of quinidine, a P-gp inhibitor, and the use of *mdr1a*(-/-) rats led to an increase in AUC and C_{max} (Suzuki et al., 2014). Recently, Dou et al. showed that P-gp expression might be altered by food consumption. Male Wistar rats showed a significant increase in *mdr1a* gene and P-gp protein expression when fasted for 12 hours compared to a fed state. The opposite was true for female rats (Dou et al., 2018).

One of the most prevalent methods to quantify protein levels is Western blotting. This method separates proteins based on molecular weight and identifies the protein of interest by labeling them with antibodies (Mahmood and Yang, 2012). LC-MS/MS is another frequently used method for protein quantification and can determine the absolute amount

of protein (Pan et al., 2009). In both methods, samples are often homogenates.

Homogenization releases proteases from the cytosol, which can degrade proteins in a sample. In addition, spatial fidelity is lost when a sample is homogenized (Zubair et al., 2016).

Matrix-assisted laser desorption/ionization (MALDI) can preserve the spatial information of proteins and provide relative levels of protein expression. MALDI provides relevant *in vivo* information as it can be performed on whole tissues (Nilsson et al., 2017). However, it is difficult to measure proteins with a weight > 25kDa. This occurs due to inefficient solubilization in the matrix solution, indicating improper extraction from tissue, and increased difficulty in ionizing larger proteins (Gilmore and Seah, 2000; Franck et al., 2010). For larger proteins, *in situ* trypsin digestion of proteins into smaller peptides allows for better identification. In addition to increased extraction and ionization, multiple peptides can be monitored for a single protein (Zubair et al., 2016). Trypsin digestion is needed for both rat P-gp, ~141kDa, and Oatp1a5, ~75kDa (Silverman et al., 1991; Ding et al., 2017). Peptide sequences will be chosen based on the criteria mentioned in Table 8.1 (Oswald et al., 2013).

Table 8.1 Peptide Sequence Criteria

Criteria	Reasoning
Mass within the mass range of the spectrometer	Establish the ability to detect the peptide
At least seven amino acids	Assure protein specificity
No post-translation modifications	Secure the identity of the peptide
Amino acid exchanges due to genetic polymorphism must be less than 1%	Secure the identity of the peptide
Not located in the transmembrane region	Ensure efficient trypsin digestion
No repeats of arginine and lysine	Reduce the chance of a missed cleavage
Not contain methionine, cysteine and tryptophan	Improve stability of the peptide
Protein/ species specificity confirmed by BLAST	Assure protein specificity

8.2 Food Effects

In human PK studies, food effect studies are conducted to determine the presence of food-drug interactions (Koziolek et al., 2019). For the fasted condition, participants are denied food overnight, typically ~10 hours (Cheng and Wong, 2020). For the food effect studies in Chapter 5, rats were kept in cages with bedding and their feces. This is a common practice in rat PK studies. While the food was removed from their cages, rats are known to eat anything available to them. This includes their bedding and engaging in coprophagy (Wang et al., 2016; Gregor et al., 2020). Future studies could be performed in metabolic cages, where the rats are not able to access anything to eat. The rats would then achieve a complete fast, like that of human studies.

8.3 Particle Size

Three particle sizes were created by Particle Solutions (West Chester, PA) and characterized by Pace Analytical (Norristown, PA). Only two of the three particle sizes were dosed in rats: Sample A (mean particle size of 4.1 μ m) and Sample B (mean particle size of 42.7 μ m). The third sample, Sample C, has a mean size of 67.1 μ m (Table 8.2). While the mean particle size of Sample C is close to that of Sample B, the specific surface area is half of that of Sample B (328 m²/kg). The third particle size could provide a more detailed description of the influence of a drug particle's surface area on its PK profile.

Table 8.2 Mean and distribution data for Sample C

	Dv(10) (μ m)	Dv(50) (μ m)	Dv(90) (μ m)	Span	Specific surface area (m ² /kg)
Sample C	17.6	67.1	151	1.981	178

8.4 Rat Continuous Intestinal Absorption Model

The current model encompasses many important physiological and physicochemical characteristics that impact absorption. Future additions could include a more detailed description of the lumen. This includes those mentioned previously, such as transporters and improved velocity data.

Another consideration is the incorporation of enterohepatic recycling. This could be achieved by the creation of a bile compartment that accumulates drug over time before being dumped back into the luminal compartment around distance $(x)=0$.

REFERENCES

- Abernethy DR (1992) Pharmacokinetics and Pharmacodynamics of Amlodipine. **80**:31–36.
- Abuhelwa AY, Williams DB, Upton RN, and Foster DJR (2017) Food, gastrointestinal pH, and models of oral drug absorption. *European Journal of Pharmaceutics and Biopharmaceutics* **112**:234-248.
- Agoram B, Woltoz WS, and Bolger MB (2001) Predicting the impact of physiological and biochemical processes on oral drug bioavailability. *Advanced Drug Delivery Reviews* **50**:S41-S67.
- Ahmed T (2015) *Basic Pharmacokinetic Concepts and Some Clinical Applications*. InTech, Rijeka, Croatia.
- Akula P and Lakshmi PK (2018) Effect of pH on weakly acidic and basic model drugs and determination of their ex vivo transdermal permeation routes. *Brazilian Journal of Pharmaceutical Sciences* **54**:8.
- Amidon GL, Lennernas H, Shah VP, and Crison JR (1995) A Theoretical Basis For A Biopharmaceutic Drug Classification - The Correlation Of In-Vitro Drug Product Dissolution And In-Vivo Bioavailability. *Pharmaceutical Research* **12**:413-420.
- Arnqvist HJ, Karlberg BE, and Melander A (1983) Pharmacokinetics and effects of glibenclamide in two formulations, HB 419 and HB 420, in type 2 diabetes. *Annals of Clinical Research* **15**:21-25.
- Beresford AP, Macrae PV, and Stopher DA (1988a) METABOLISM OF AMLODIPINE IN THE RAT AND THE DOG - A SPECIES-DIFFERENCE. *Xenobiotica* **18**:169-182.
- Beresford AP, McGibney D, Humphrey MJ, Macrae PV, and Stopher DA (1988b) METABOLISM AND KINETICS OF AMLODIPINE IN MAN. *Xenobiotica* **18**:245-254.
- Berginc K, Zakelj S, and Kristl A (2010) In vitro interactions between aged garlic extract and drugs used for the treatment of cardiovascular and diabetic patients. *European Journal of Nutrition* **49**:373-384.
- Brady JM, Cherrington NJ, Hartley DP, Buist SC, Li N, and Klaassen CD (2002) Tissue distribution and chemical induction of multiple drug resistance genes in rats. *Drug Metabolism and Disposition* **30**:838-844.

- Brage R, Cortijo J, Esplugues J, Esplugues JV, Martibonmati E, and Rodriguez C (1986) Effects of calcium-channel blockers on gastric-emptying and acid-secretion of the rat in vivo. *British Journal of Pharmacology* **89**:627-633.
- Brewer MJ, Butler A, and Cooksley SL (2016) The relative performance of AIC, AIC(C) and BIC in the presence of unobserved heterogeneity. *Methods in Ecology and Evolution* **7**:679-692.
- Brockmeier D, Grigoleit HG, and Leonhardt H (1985) Absorption Of Glibenclamide From Different Sites Of The Gastrointestinal-Tract. *European Journal of Clinical Pharmacology* **29**:193-197.
- Bunaciu AA, Udristioiu EG, and Aboul-Enein HY (2015) X-Ray Diffraction: Instrumentation and Applications. *Critical Reviews in Analytical Chemistry* **45**:289-299.
- Caldwell JH and Cline CT (1976) BILIARY-EXCRETION OF DIGOXIN IN MAN. *Clinical Pharmacology & Therapeutics* **19**:410-415.
- Camilleri M and Linden DR (2016) Measurement of Gastrointestinal and Colonic Motor Functions in Humans and Animals. *Cellular and Molecular Gastroenterology and Hepatology* **2**:412-428.
- Cao XH, Gibbs ST, Fang LY, Miller HA, Landowski CP, Shin HC, Lennernas H, Zhong YQ, Amidon GL, Yu LX, and Sun DX (2006) Why is it challenging to predict intestinal drug absorption and oral bioavailability in human using rat model. *Pharmaceutical Research* **23**:1675-1686.
- Caron G, Ermondi G, Damiano A, Novaroli L, Tsinman O, Ruell JA, and Avdeef A (2004) Ionization, lipophilicity, and molecular modeling to investigate permeability and other biological properties of amlodipine. *Bioorganic & Medicinal Chemistry* **12**:6107-6118.
- Cheng LS and Wong H (2020) Food Effects on Oral Drug Absorption: Application of Physiologically-Based Pharmacokinetic Modeling as a Predictive Tool. *Pharmaceutics* **12**.
- Christfort JF, Strindberg S, Plum J, Hall-Andersen J, Janfelt C, Nielsen LH, and Mullertz A (2019) Developing a predictive in vitro dissolution model based on gastrointestinal fluid characterisation in rats. *European Journal of Pharmaceutics and Biopharmaceutics* **142**:307-314.

- Chu KR, Lee E, Jeong SH, and Park ES (2012) Effect of particle size on the dissolution behaviors of poorly water-soluble drugs. *Archives of Pharmacal Research* **35**:1187-1195.
- Cohen AF, Kroon R, Schoemaker R, Hoogkamer H, and Vanvliet A (1991) Influence Of Gastric-Acidity On The Bioavailability Of Digoxin. *Annals of Internal Medicine* **115**:540-545.
- da Graca JRV, Parente CC, Fiuza RF, da Silva PAF, Mota BT, Salles LD, Silva CMD, da Silva MTB, de Oliveira RB, and dos Santos AA (2015) Subtotal nephrectomy inhibits the gastric emptying of liquid in awake rats. *Physiological Reports* **3**:10.
- Dahan A, Miller JM, and Amidon GL (2009) Prediction of Solubility and Permeability Class Membership: Provisional BCS Classification of the World's Top Oral Drugs. *Aaps Journal* **11**:740-746.
- Darvari R and Boroujerdi M (2004) Concentration dependency of modulatory effect of amlodipine on P-glycoprotein efflux activity of doxorubicin - a comparison with tamoxifen. *Journal of Pharmacy and Pharmacology* **56**:985-991.
- Dasgupta A (2012) Challenges in Therapeutic Drug Monitoring of Digoxin and Other Anti-Arrhythmic Drugs, in: *Therapeutic Drug Monitoring: Newer Drugs and Biomarkers* (Dasgupta A ed), pp 219-241, Elsevier Academic Press Inc, San Diego.
- Deloose E and Tack J (2016) Redefining the functional roles of the gastrointestinal migrating motor complex and motilin in small bacterial overgrowth and hunger signaling. *American Journal of Physiology-Gastrointestinal and Liver Physiology* **310**:G228-G233.
- DeSesso JM and Jacobson CF (2001) Anatomical and physiological parameters affecting gastrointestinal absorption in humans and rats. *Food and Chemical Toxicology* **39**:209-228.
- Devi PRS, Reddy AG, Rao GS, Kumar C, and Boobalan G (2015) Pharmacokinetic interaction of curcumin and glibenclamide in diabetic rats. *Veterinary World* **8**:508-511.
- Ding J, Wang J, Xiang Z, Diao WY, Su MX, Shi WW, Wan T, and Han XD (2017) The organic anion transporting polypeptide 1a5 is a pivotal transporter for the uptake of microcystin-LR by gonadotropin-releasing hormone neurons. *Aquatic Toxicology* **182**:1-10.

- Doherty JE, Flanigan WJ, Murphy ML, Bulloch RT, Dalrymple GL, Beard OW, and Perkins Wh (1970) Tritiated Digoxin .14. Enterohepatic Circulation, Absorption, And Excretion Studies In Human Volunteers. *Circulation* **42**:867-+.
- Dou L, Mai Y, Madla CM, Orlu M, and Basit AW (2018) P-glycoprotein expression in the gastrointestinal tract of male and female rats is influenced differently by food. *European Journal of Pharmaceutical Sciences* **123**:569-575.
- Duan JZ (2010) Drug-Drug Interaction Pattern Recognition. *Drugs in R&D* **10**:9-24.
- El-Kattan A and Varma M (2011) Oral Absorption, Intestinal Metabolism and Human Oral Bioavailability, in: *Topics on Drug Metabolism*.
- Estudante M, Morais JG, Soveral G, and Benet LZ (2013) Intestinal drug transporters: An overview. *Advanced Drug Delivery Reviews* **65**:1340-1356.
- Evans DF, Pye G, Bramley R, Clark AG, Dyson TJ, and Hardcastle JD (1988) Measurement Of Gastrointestinal Ph Profiles In Normal Ambulant Human-Subjects. *Gut* **29**:1035-1041.
- Fallingborg J (1999) Intraluminal pH of the human gastrointestinal tract. *Danish Medical Bulletin* **46**:183-196.
- Fares H, DiNicolantonio JJ, O'Keefe JH, and Lavie CJ (2016) Amlodipine in hypertension: a first-line agent with efficacy for improving blood pressure and patient outcomes. *Open Heart* **3**:7.
- Faulkner JK, McGibney D, Chasseaud LF, Perry JL, and Taylor IW (1986) The Pharmacokinetics Of Amlodipine In Healthy-Volunteers After Single Intravenous And Oral Doses And After 14 Repeated Oral Doses Given Once Daily. *British Journal of Clinical Pharmacology* **22**:21-25.
- Fessey R, Austin, R., Barton, P., Davis, A., and Wenlock, M. (2006) The Role of Plasma Protein Binding in Drug Discovery, in: *Pharmacokinetic Profiling in Drug Research* (Acta VHC ed).
- Fleisher D, Li C, Zhou Y, Pao LH, and Karim A (1999) Drug, meal and formulation interactions influencing drug absorption after oral administration - Clinical implications. *Clinical Pharmacokinetics* **36**:233-254.
- Franck J, Longuespee R, Wisztorski M, Van Remoortere A, Van Zeijl R, Deelder A, Salzet M, McDonnell L, and Fournier I (2010) MALDI mass spectrometry imaging of proteins exceeding 30 000 daltons. *Medical Science Monitor* **16**:BR293-BR299.

- Gari M, Debbarma RR, Majhee L, and Subhankar C (2017) Effect of amlodipine on blood glucose level in euglycemic and streptozotocin induced diabetic Albino rats and its pharmacodynamic interaction with glibenclamide. *International Journal of Basic & Clinical Pharmacology* **6**.
- Gault MH, Charles JD, Sugden DL, and Kepkey DC (1977) HYDROLYSIS OF DIGOXIN BY ACID. *Journal of Pharmacy and Pharmacology* **29**:27-32.
- Gibaldi M and Perrier D (1982) *Pharmacokinetics 2nd Edition*. Informa Healthcare USA, Inc., New York, NY.
- Gilmore IS and Seah MP (2000) Ion detection efficiency in SIMS: dependencies on energy, mass and composition for microchannel plates used in mass spectrometry. *International Journal of Mass Spectrometry* **202**:217-229.
- GlaxoSmithKline (2011)
https://www.accessdata.fda.gov/drugsatfda_docs/label/2011/020405s006lbl.pdf.
- Gregor A, Fragner L, Trajanoski S, Li W, Sun X, Weckwerth W, Konig J, and Duszka K (2020) Cage bedding modifies metabolic and gut microbiota profiles in mouse studies applying dietary restriction. *Scientific Reports* **10**.
- Greiner B, Eichelbaum M, Fritz P, Kreichgauer HP, Von Richter O, Zundler J, and Kroemer HK (1999) The role of intestinal P-glycoprotein in the interaction of digoxin and rifampin. *Journal of Clinical Investigation* **104**:147-153.
- Guinot S and Leveiller F (1999) The use of MTDSC to assess the amorphous phase content of a micronised drug substance. *International Journal of Pharmaceutics* **192**:63-75.
- Hartmann C, Massart DL, and McDowall RD (1994) An Analysis Of The Washington Conference Report On Bioanalytical Method Validation. *Journal of Pharmaceutical and Biomedical Analysis* **12**:1337-1343.
- Hatanaka S, Kondoh M, Kawarabayashi K, and Furuhashi K (1994) The Measurement Of Gastric-Emptying In Conscious Rats By Monitoring Serial Changes In Serum Acetaminophen Level. *Journal of Pharmacological and Toxicological Methods* **31**:161-165.
- Helander HF and Fandriks L (2014) Surface area of the digestive tract - revisited. *Scandinavian Journal of Gastroenterology* **49**:681-689.
- Holt K, Ye M, Nagar S, and Korzekwa K (2019) Prediction of Tissue-Plasma Partition Coefficients Using Microsomal Partitioning: Incorporation into Physiologically

based Pharmacokinetic Models and Steady-State Volume of Distribution Predictions. *Drug Metabolism and Disposition* **47**:1050-1060.

- Hu CY, Hu X, Wang CH, Zhao ZR, Gao D, Chen XP, Zhou DL, Huang Y, Li L, and Zhang L (2018) Bioequivalence and Pharmacokinetics of Bisoprolol-Amlodipine 5 mg/5 mg Combination Tablet versus Bisoprolol 5 mg Tablet and Amlodipine 5mg Tablet: An Open-Label, Randomized, Two-Sequence Crossover Study in Healthy Chinese Subjects. *Clinical Drug Investigation* **38**:1145-1154.
- Huang WL, Lee SL, and Yu LX (2009) Mechanistic Approaches to Predicting Oral Drug Absorption. *Aaps Journal* **11**:217-224.
- Hutchinson L, Sinclair M, Reid B, Burnett K, and Callan B (2018) A descriptive systematic review of salivary therapeutic drug monitoring in neonates and infants. *British Journal of Clinical Pharmacology* **84**:1089-1108.
- Jeffrey P, Burrows M, and Bye A (1987) Does The Rat Have An Empty Stomach After An Overnight Fast. *Laboratory Animals* **21**:330-334.
- Jiang SW, Zhao WM, Chen Y, Zhong ZY, Zhang MA, Li F, Xu P, Zhao KJ, Li Y, Liu L, and Liu XD (2015) Paroxetine decreased plasma exposure of glyburide partly via inhibiting intestinal absorption in rats. *Drug Metabolism and Pharmacokinetics* **30**:240-246.
- Johnson BF, Ogrady J, Sabey GA, and Bye C (1978) Effect Of A Standard Breakfast On Digoxin Absorption In Normal Subjects. *Clinical Pharmacology & Therapeutics* **23**:315-319.
- Junghanns J and Muller RH (2008) Nanocrystal technology, drug delivery and clinical applications. *International Journal of Nanomedicine* **3**:295-309.
- Kararli TT (1995) Comparison Of The Gastrointestinal Anatomy, Physiology, And Biochemistry Of Humans And Commonly Used Laboratory-Animals. *Biopharmaceutics & Drug Disposition* **16**:351-380.
- Kato R, Fujwara A, Kawai T, Moriguchi J, Nakagawa M, Tsukura Y, Uchida K, Amano F, Hirotsu Y, Ijiri Y, and Tanaka K (2008) Changes in digoxin pharmacokinetics treated with lipopolysaccharide in Wistar rats. *Biological & Pharmaceutical Bulletin* **31**:1221-1225.
- Khadka P, Ro J, Kim H, Kim I, Kim JT, Kim H, Cho JM, Yun G, and Lee J (2014) Pharmaceutical particle technologies: An approach to improve drug solubility, dissolution and bioavailability. *Asian Journal of Pharmaceutical Sciences* **9**:304-316.

- Kirby BJ, Kalthorn T, Hebert M, Easterling T, and Unadkat JD (2008) Sensitive and specific LC-MS assay for quantification of digoxin in human plasma and urine. *Biomedical Chromatography* **22**:712-718.
- Klein S (2010) The Use of Biorelevant Dissolution Media to Forecast the In Vivo Performance of a Drug. *Aaps Journal* **12**:397-406.
- Knapp BK, Bauer LL, Swanson KS, Tappenden KA, and Fahey GC (2013) Soluble Fiber Dextran and Soluble Corn Fiber Supplementation Modify Indices of Health in Cecum and Colon of Sprague-Dawley Rats. *Nutrients* **5**:396-410.
- Koc E (2020) Calcium and Sodium Channel Blockers and Gastrointestinal Motility. *Cyprus Journal of Medical Sciences* **5**:295-298.
- Korzekwa K and Nagar S (2017) Drug Distribution Part 2. Predicting Volume of Distribution from Plasma Protein Binding and Membrane Partitioning. *Pharmaceutical Research* **34**:544-551.
- Korzekwa KR, Nagar S, Tucker J, Weiskircher EA, Bhoopathy S, and Hidalgo IJ (2012) Models to Predict Unbound Intracellular Drug Concentrations in the Presence of Transporters. *Drug Metabolism and Disposition* **40**:865-876.
- Kothare PA, Soon DKW, Linnebjerg H, Park S, Chan C, Yeo A, Lim M, Mace KE, and Wise SD (2005) Effect of exenatide on the steady-state pharmacokinetics of digoxin. *Journal of Clinical Pharmacology* **45**:1032-1037.
- Koup JR, Jusko WJ, Elwood CM, and Kohli RK (1975) Digoxin Pharmacokinetics - Role Of Renal-Failure In Dosage Regimen Design. *Clinical Pharmacology & Therapeutics* **18**:9-21.
- Koziolek M, Alcaro S, Augustijns P, Basit AW, Grimm M, Hens B, Hoad CL, Jedamzik P, Madla CM, Maliepaard M, Marciani L, Maruca A, Parrott N, Pavek P, Porter CJH, Reppas C, van Riet-Nales D, Rubbens J, Stelova M, Trevaskis NL, Valentova K, Vertzoni M, Cepo DV, and Corsetti M (2019) The mechanisms of pharmacokinetic food-drug interactions - A perspective from the UNGAP group. *European Journal of Pharmaceutical Sciences* **134**:31-59.
- Kramer WG, Kolibash AJ, Lewis RP, Bathala MS, Visconti JA, and Reuning RH (1979) Pharmacokinetics Of Digoxin - Relationship Between Response Intensity And Predicted Compartmental Drug Levels In Man. *Journal of Pharmacokinetics and Biopharmaceutics* **7**:47-61.

- Kwak HH, Kim JO, Chung HK, Choi SM, Kim JH, Kwon JW, Yoo M, Lee JH, and Lee MG (2006) Pharmacokinetics of oral amlodipine orotate in vagotomized dogs. *Biopharmaceutics & Drug Disposition* **27**:141-145.
- Lai SK, Wang YY, and Hanes J (2009) Mucus-penetrating nanoparticles for drug and gene delivery to mucosal tissues. *Advanced Drug Delivery Reviews* **61**:158-171.
- Lan T, Rao A, Haywood J, Davis CB, Han C, Garver E, and Dawson PA (2009) Interaction of Macrolide Antibiotics with Intestinally Expressed Human and Rat Organic Anion-Transporting Polypeptides. *Drug Metabolism and Disposition* **37**:2375-2382.
- Lee JH, Kim EJ, Kwon JW, Yoo M, and Lee MG (2006) Negligible pharmacokinetic interaction between oral DA-8159, a new erectogenic, and amlodipine in rats. *Biopharmaceutics & Drug Disposition* **27**:125-131.
- Lee WC, Yang HW, Lee YJ, Jung SH, Choi GY, Go H, Kim A, and Cha SW (2008) Brunner's gland hyperplasia: Treatment of severe diffuse nodular hyperplasia mimicking a malignancy on pancreatic-duodenal area. *Journal of Korean Medical Science* **23**:540-543.
- Lennernas H (2007) Intestinal permeability and its relevance for absorption and elimination. *Xenobiotica* **37**:1015-1051.
- Levine RR (1970) Factors Affecting Gastrointestinal Absorption Of Drugs. *American Journal of Digestive Diseases* **15**:171-+.
- Li R, Bi YA, Vildhede A, Scialis RJ, Mathialagan S, Yang X, Marroquin LD, Lin J, and Varma MVS (2017) Transporter-Mediated Disposition, Clinical Pharmacokinetics and Cholestatic Potential of Glyburide and Its Primary Active Metabolites. *Drug Metabolism and Disposition* **45**:737-747.
- Li Y, Wei Y, Zhang F, Wang D, and Wu X (2012) Changes in the pharmacokinetics of glibenclamide in rats with streptozotocin-induced diabetes mellitus. *Acta Pharmaceutica Sinica B* **2**:198-204.
- Lilja JJ, Niemi M, Fredrikson H, and Neuvonen PJ (2007) Effects of clarithromycin and grapefruit juice on the pharmacokinetics of glibenclamide. *British Journal of Clinical Pharmacology* **63**:732-740.
- Lin HC and Visek WJ (1991) Large Intestinal Ph And Ammonia In Rats - Dietary-Fat And Protein Interactions. *Journal of Nutrition* **121**:832-843.

- Lin L and Wong H (2017) Predicting Oral Drug Absorption: Mini Review on Physiologically-Based Pharmacokinetic Models. *Pharmaceutics* **9**:14.
- Lisalo E (1977) Clinical Pharmacokinetics Of Digoxin. *Clinical Pharmacokinetics* **2**:1-16.
- Liu HY, Liu L, Li J, Mei D, Duan R, Hu N, Guo HF, Zhong ZY, and Liu XD (2012) Combined Contributions of Impaired Hepatic CYP2C11 and Intestinal Breast Cancer Resistance Protein Activities and Expression to Increased Oral Glibenclamide Exposure in Rats with Streptozotocin-Induced Diabetes Mellitus. *Drug Metabolism and Disposition* **40**:1104-1112.
- Lobenberg R, Kramer J, Shah VP, Amidon GL, and Dressman JB (2000) Dissolution testing as a prognostic tool for oral drug absorption: Dissolution behavior of glibenclamide. *Pharmaceutical Research* **17**:439-444.
- Loh ZH, Samanta AK, and Heng PWS (2015) Overview of milling techniques for improving the solubility of poorly water-soluble drugs. *Asian Journal of Pharmaceutical Sciences* **10**:255-274.
- Lowes S, Jersey J, Shoup R, Garofolo F, Savoie N, Mortz E, Needham S, Caturla MC, Steffen R, Sheldon C, Hayes R, Samuels T, Di Donato L, Kamerud J, Michael S, Lin ZP, Hillier J, Moussallie M, Teixeira LD, Rocci M, Buonarati M, Truog J, Hussain S, Lundberg R, Breau A, Zhang TY, Jonker J, Berger N, Gagnon-Carignan S, Nehls C, Nicholson R, Hilhorst M, Karnik S, de Boer T, Houghton R, Smith K, Cojocar L, Allen M, Harter T, Fatmi S, Sayyarpour F, Vija J, Malone M, and Heller D (2011) Recommendations on: internal standard criteria, stability, incurred sample reanalysis and recent 483s by the Global CRO Council for Bioanalysis. *Bioanalysis* **3**:1323-1332.
- Luo QS (2018) Electron Microscopy and Spectroscopy in the Analysis of Friction and Wear Mechanisms. *Lubricants* **6**:19.
- Ma ZH, Merkus HG, van der Veen HG, Wong M, and Searlett B (2002) On-line measurement of particle size and shape using laser diffraction. *Particle & Particle Systems Characterization* **18**:243-247.
- Mahmood T and Yang P-C (2012) Western Blot: Technique, Theory, and Trouble Shooting. *North American Journal of Medical Sciences* **4**:429-434.
- Malm-Erjefalt M, Ekblom M, Vouis J, Zdravkovic M, and Lennernas H (2015) Effect on the Gastrointestinal Absorption of Drugs from Different Classes in the

- Biopharmaceutics Classification System, When Treating with Liraglutide. *Molecular Pharmaceutics* **12**:4166-4173.
- Manallack DT, Prankerd RJ, Yuriev E, Oprea TI, and Chalmers DK (2013) The significance of acid/base properties in drug discovery. *Chemical Society Reviews* **42**:485-496.
- Maurer AH, Camilleri M, Donohoe K, Knight LC, Madsen JL, Mariani G, Parkman HP, and Van Dolsen J (2013) The SNMMI and EANM Practice Guideline for Small-Bowel and Colon Transit 1.0. *Journal of Nuclear Medicine* **54**:2004-2013.
- Mayhew TM and Middleton C (1985) Crypts, Villi And Microvilli In The Small-Intestine Of The Rat - A Stereological Study Of Their Variability Within And Between Animals. *Journal of Anatomy* **141**:1-17.
- McConnell EL, Basit AW, and Murdan S (2008) Measurements of rat and mouse gastrointestinal pH fluid and lymphoid tissue, and implications for in-vivo experiments. *Journal of Pharmacy and Pharmacology* **60**:63-70.
- Melander A (1978) Influence of food on the bioavailability of drugs. *Clinical Pharmacokinetics* **3**:337-351.
- Menguy R (1960) Effects Of Restraint Stress On Gastric Secretion In The Rat. *American Journal of Digestive Diseases* **5**:911-916.
- Meredith PA and Elliott HL (1992) Clinical Pharmacokinetics Of Amlodipine. *Clinical Pharmacokinetics* **22**:22-31.
- Mistri HN, Jangid AG, and Shrivastav PS (2007) Liquid chromatography tandem mass spectrometry method for simultaneous determination of antidiabetic drugs metformin and glyburide in human plasma. *Journal of Pharmaceutical and Biomedical Analysis* **45**:97-106.
- Mitra A and Kesisoglou F (2013) Impaired Drug Absorption Due to High Stomach pH: A Review of Strategies for Mitigation of Such Effect To Enable Pharmaceutical Product Development. *Molecular Pharmaceutics* **10**:3970-3979.
- Mouly S and Paine MF (2003) P-glycoprotein increases from proximal to distal regions of human small intestine. *Pharmaceutical Research* **20**:1595-1599.
- Mudie DM, Samiei N, Marshall DJ, Amidon GE, and Bergstrom CAS (2020) Selection of In Vivo Predictive Dissolution Media Using Drug Substance and Physiological Properties. *Aaps Journal* **22**:13.

- Murphy TF, Schade CT, and Zwiren AD (2018) Using Light And Electron Microscopy, Computed Tomography, And Light Scattering To Evaluate Additive Manufacturing Powders And Parts. *International Journal of Powder Metallurgy* **54**:23-37.
- Nagar S and Korzekwa K (2012) Commentary: Nonspecific Protein Binding versus Membrane Partitioning: It Is Not Just Semantics. *Drug Metabolism and Disposition* **40**:1649-1652.
- Nagar S, Korzekwa RC, and Korzekwa K (2017) Continuous Intestinal Absorption Model Based on the Convection-Diffusion Equation. *Molecular Pharmaceutics* **14**:3069-3086.
- Nagar SaK, K. (2016) Drug Distribution. Part 1. Models to Predict Membrane Partitioning. *Pharmaceutical Research* **34**:535–543.
- Naraharisetti SB, Kirby BJ, Hebert MF, Easterling TR, and Unadkat JD (2007) Validation of a sensitive LC-MS assay for quantification of glyburide and its metabolite 4-transhydroxy glyburide in plasma and urine: An OPRU Network study. *Journal of Chromatography B-Analytical Technologies in the Biomedical and Life Sciences* **860**:34-41.
- Neerati P and Gade J (2011) Influence of atorvastatin on the pharmacokinetics and pharmacodynamics of glyburide in normal and diabetic rats. *European Journal of Pharmaceutical Sciences* **42**:285-289.
- Neuhoff S, Ungell AL, Zamora I, and Artursson P (2003) pH-dependent bidirectional transport of weakly basic drugs across Caco-2 monolayers: Implications for drug-drug interactions. *Pharmaceutical Research* **20**:1141-1148.
- Niebergall PJ, Goyan JE, and Milosovich G (1963) Dissolution Rate Studies .2. Dissolution Of Particles Under Conditions Of Rapid Agitation. *Journal of Pharmaceutical Sciences* **52**:236-&.
- Nilsson A, Peric A, Strimfors M, Goodwin RJA, Hayes MA, Andren PE, and Hilgendorf C (2017) Mass Spectrometry Imaging proves differential absorption profiles of well-characterised permeability markers along the crypt-villus axis. *Scientific Reports* **7**:10.
- Nowland MH, Hugunin KMS, and Rogers KL (2011) Effects of Short-Term Fasting in Male Sprague-Dawley Rats. *Comparative Medicine* **61**:138-144.

- Obembe AO, Okon VE, Ofutet EO, and Ayitu RA (2015) Effect of Fasting on Intestinal Motility and Transit in Albino Wistar Rats. *Trends in Medical Research* **10**:63-68.
- Ochs HR, Greenblatt DJ, Bodem G, and Harmatz JS (1978) Dose-Independent Pharmacokinetics Of Digoxin In Humans. *American Heart Journal* **96**:507-511.
- Ogle CW, Cho CH, Tong MC, and Koo MWL (1985) The Influence Of Verapamil On The Gastric Effects Of Stress In Rats. *European Journal of Pharmacology* **112**:399-404.
- Oiestad EL, Johansen U, Opdal MS, Bergan S, and Christophersen AS (2009) Determination of Digoxin and Digitoxin in Whole Blood. *Journal of Analytical Toxicology* **33**:372-378.
- Olapeju BI, Inanemo OEK, and Enitome BE (2018) Effects of amlodipine and valsartan on glibenclamide-treated streptozotocin-induced diabetic rats. *Biomedicine & Pharmacotherapy* **106**:566-574.
- Olsen KM, Kearns GL, and Kemp SF (1995) Glyburide Protein-Binding And The Effect Of Albumin Glycation In Children, Young-Adults, And Older Adults With Diabetes. *Journal of Clinical Pharmacology* **35**:739-745.
- Oswald S, Groer C, Drozdik M, and Siegmund W (2013) Mass Spectrometry-Based Targeted Proteomics as a Tool to Elucidate the Expression and Function of Intestinal Drug Transporters. *Aaps Journal* **15**:1128-1140.
- Otoom S, Hasan M, and Najib N (2001) The bioavailability of glyburide (glibenclamide) under fasting and feeding conditions: a comparative study. *International Journal of Pharmaceutical Medicine* **15**:117-120.
- Pan S, Aebersold R, Chen R, Rush J, Goodlett DR, McIntosh MW, Zhang J, and Brentnall TA (2009) Mass Spectrometry Based Targeted Protein Quantification: Methods and Applications. *Journal of Proteome Research* **8**:787-797.
- Pearson JG (1985) Pharmacokinetics Of Glyburide. *American Journal of Medicine* **79**:67-71.
- Peddireddy MKR (2010) In vivo Methods for Evaluation of Drugs for the Treatment of Gastrointestinal Motility Disorders. *Indian Journal of Pharmaceutical Education and Research* **44**:42-48.
- Poulakos L and Kent TH (1973) Gastric Emptying And Small Intestinal Propulsion In Fed And Fasted Rats. *Gastroenterology* **64**:962-967.

- Prior H, Ewart L, Bright J, and Valentin JP (2012) Refinement of the Charcoal Meal Study by Reduction of the Fasting Period. *Atla-Alternatives to Laboratory Animals* **40**:99-107.
- Rausl D, Fotaki N, Zanoski R, Vertzoni M, Cetina-Cizmek B, Khan MZI, and Reppas C (2006) Intestinal permeability and excretion into bile control the arrival of amlodipine into the systemic circulation after oral administration. *Journal of Pharmacy and Pharmacology* **58**:827-836.
- Read NW, Aljanabi MN, Holgate AM, Barber DC, and Edwards CA (1986) Simultaneous Measurement Of Gastric-Emptying, Small-Bowel Residence And Colonic Filling Of A Solid Meal By The Use Of The Gamma-Camera. *Gut* **27**:300-308.
- Riccardi K, Ryu S, Lin J, Yates P, Tess D, Li R, Singh D, Holder BR, Kapinos B, Chang G, and Di L (2018) Comparison of Species and Cell-Type Differences in Fraction Unbound of Liver Tissues, Hepatocytes, and Cell Lines. *Drug Metabolism and Disposition* **46**:415-421.
- Rubbens J, Mols R, Brouwers J, and Augustijns P (2018) Exploring gastric drug absorption in fasted and fed state rats. *International Journal of Pharmaceutics* **548**:636-641.
- Rydberg T, Jonsson A, and Melander A (1995) COMPARISON OF THE KINETICS OF GLYBURIDE AND ITS ACTIVE METABOLITES IN HUMANS. *Journal of Clinical Pharmacy and Therapeutics* **20**:283-295.
- Saleem IY and Smyth HDC (2010) Micronization of a Soft Material: Air-Jet and Micro-Ball Milling. *Aaps Pharmscitech* **11**:1642-1649.
- Salphati L and Benet LZ (1998) Effects of ketoconazole on digoxin absorption and disposition in rat. *Pharmacology* **56**:308-313.
- Salphati L and Benet LZ (1999) Metabolism of digoxin and digoxigenin digitoxosides in rat liver microsomes: involvement of cytochrome P4503A. *Xenobiotica* **29**:171-185.
- Samala S and Veeresham C (2016) Pharmacokinetic and Pharmacodynamic Interaction of Boswellic Acids and Andrographolide with Glyburide in Diabetic Rats: Including Its PK/PD Modeling. *Phytotherapy Research* **30**:496-502.
- Saperstein S, Edgren RA, Jung D, Mroszczak EJ, Lee GJL, Dorr A, Pritchard R, Kushinsky S, Fong JC, and Combs DL (1989) Pharmacokinetics Of Norethindrone - Effect Of Particle-Size. *Contraception* **40**:731-740.

- Sartor G, Lundquist I, Melander A, Schersten B, and Wahlinboll E (1982) Improved Effect Of Glibenclamide On Administration Before Breakfast. *European Journal of Clinical Pharmacology* **21**:403-408.
- Satoh H, Yamashita F, Tsujimoto M, Murakami H, Koyabu N, Ohtani H, and Sawada Y (2005) Citrus juices inhibit the function of human organic anion-transporting polypeptide OATP-B. *Drug Metabolism and Disposition* **33**:518-523.
- Schulz M, Iwersen-Bergmann S, Andresen H, and Schmoldt A (2012) Therapeutic and toxic blood concentrations of nearly 1,000 drugs and other xenobiotics. *Critical Care* **16**:4.
- Scotcher D, Jones CR, Galetin A, and Rostami-Hodjegan A (2017) Delineating the Role of Various Factors in Renal Disposition of Digoxin through Application of Physiologically Based Kidney Model to Renal Impairment Populations. *Journal of Pharmacology and Experimental Therapeutics* **360**:484-495.
- Semple CG, Omile C, Buchanan KD, Beastall GH, and Paterson KR (1986) Effect Of Oral Verapamil On Glibenclamide Stimulated Insulin-Secretion. *British Journal of Clinical Pharmacology* **22**:187-190.
- Shoghi E, Fuguet E, Bosch E, and Rafols C (2013) Solubility-pH profiles of some acidic, basic and amphoteric drugs. *European Journal of Pharmaceutical Sciences* **48**:291-300.
- Shohin IE, Ramenskaya GV, Vasilenko GF, and Malashenko EA (2010) In Vitro Dissolution Kinetics of Amlodipine Tablets Marketed in Russia Under Biowaiver Conditions. *Dissolution Technologies* **17**:20-22.
- Shore PA, Brodie BB, and Hogben CAM (1957) THE GASTRIC SECRETION OF DRUGS - A PH PARTITION HYPOTHESIS. *Journal of Pharmacology and Experimental Therapeutics* **119**:361-369.
- Silverman JA, Raunio H, Gant TW, and Thorgeirsson SS (1991) CLONING AND CHARACTERIZATION OF A MEMBER OF THE RAT MULTIDRUG RESISTANCE (MDR) GENE FAMILY. *Gene* **106**:229-236.
- Singh BN (1999) Effects of food on clinical pharmacokinetics. *Clinical Pharmacokinetics* **37**:213-255.
- Singh RP, Sabarinath S, Gautam N, Gupta RC, and Singh SK (2011) Pharmacokinetic study of the novel, synthetic trioxane antimalarial compound 97-78 in rats using an LC-MS/MS method for quantification. *Arzneimittelforschung-Drug Research* **61**:120-125.

- Singh SK, Srinivasan KK, Gowthamarajan K, and Narayan GB (2010) Development and validation of discriminatory dissolution procedure for poorly soluble glyburide. *Asian Journal of Pharmaceutics* **4**:8.
- Small DS, Zhang W, Royalty J, Cannady EA, Downs D, Friedrich S, and Suico JG (2015) A Multidose Study to Examine the Effect of Food on Evacetrapib Exposure at Steady State. *Journal of Cardiovascular Pharmacology and Therapeutics* **20**:483-489.
- Small H, Gardner I, Jones HM, Davis J, and Rowland M (2011) Measurement of Binding of Basic Drugs to Acidic Phospholipids Using Surface Plasmon Resonance and Incorporation of the Data into Mechanistic Tissue Composition Equations to Predict Steady-State Volume of Distribution. *Drug Metabolism and Disposition* **39**:1789-1793.
- Smith DA, Di L, and Kerns EH (2010) The effect of plasma protein binding on in vivo efficacy: misconceptions in drug discovery. *Nature Reviews Drug Discovery* **9**:929-939.
- Smits GJM and Lefebvre RA (1996) Influence of aging on gastric emptying of liquids, small intestine transit, and fecal output in rats. *Experimental Gerontology* **31**:589-596.
- Souza MAN, Souza M, Palheta RC, Cruz PRM, Medeiros BA, Rola FH, Magalhaes PJC, Troncon LEA, and Santos AA (2009) Evaluation of gastrointestinal motility in awake rats: a learning exercise for undergraduate biomedical students. *Advances in Physiology Education* **33**:343-348.
- Stokes AM, Lavie NL, Keowen ML, Gaschen L, Gaschen FP, Barthel D, and Andrews FM (2012) Evaluation of a wireless ambulatory capsule (SmartPill (R)) to measure gastrointestinal tract pH, luminal pressure and temperature, and transit time in ponies. *Equine Veterinary Journal* **44**:482-486.
- Stopher DA, Beresford AP, Macrae PV, and Humphrey MJ (1988) THE METABOLISM AND PHARMACOKINETICS OF AMLODIPINE IN HUMANS AND ANIMALS. *Journal of Cardiovascular Pharmacology* **12**:S55-S59.
- Suksridechacin NK, P, Chamniansawat S, and N T (2020) Effect of prolonged omeprazole administration on segmental intestinal Mg²⁺ absorption in male Sprague-Dawley rats. *World Journal of Gastroenterology* **26**:1142-1155.
- Sun J, Wang F, Sui Y, She ZN, Zhai WJ, Wang CL, and Deng YH (2012) Effect of particle size on solubility, dissolution rate, and oral bioavailability: evaluation

using coenzyme Q(10) as naked nanocrystals. *International Journal of Nanomedicine* **7**:5733-5744.

Suzuki M, Komura H, Yoshikawa T, Enya S, Nagao A, Takubo H, and Kogayu M (2014) Characterization of gastrointestinal absorption of digoxin involving influx and efflux transporter in rats: application of *mdr1a* knockout (-/-) rats into absorption study of multiple transporter substrate. *Xenobiotica* **44**:1039-1045.

Suzuyama N, Katoh M, Takeuchi T, Yoshitomi S, Higuchi T, Asashi S, and Yokoi T (2007) Species differences of inhibitory effects on P-glycoprotein-mediated drug transport. *Journal of Pharmaceutical Sciences* **96**:1609-1618.

Takara K, Matsubara M, Yamamoto K, Minegaki T, Takegami S, Takahashi M, Yokoyama T, and Okumura K (2012) Differential effects of calcium antagonists on ABCG2/BCRP-mediated drug resistance and transport in SN-38-resistant HeLa cells. *Molecular Medicine Reports* **5**:603-609.

Tannergren C, Bergendal A, Lennernas H, and Abrahamsson B (2009) Toward an Increased Understanding of the Barriers to Colonic Drug Absorption in Humans: Implications for Early Controlled Release Candidate Assessment. *Molecular Pharmaceutics* **6**:60-73.

Taskar KS, Mariappan TT, Kurawattimath V, Gautam SS, Mullapudi TVR, Sridhar SK, Kallem RR, Marathe P, and Mandlekar S (2017) Unmasking the Role of Uptake Transporters for Digoxin Uptake Across the Barriers of the Central Nervous System in Rat. *Journal of Central Nervous System Disease* **9**:7.

Taub ME, Mease K, Sane RS, Watson CA, Chen LF, Ellens H, Hirakawa B, Reyner EL, Jani M, and Lee CA (2011) Digoxin Is Not a Substrate for Organic Anion-Transporting Polypeptide Transporters OATP1A2, OATP1B1, OATP1B3, and OATP2B1 but Is a Substrate for a Sodium-Dependent Transporter Expressed in HEK293 Cells. *Drug Metabolism and Disposition* **39**:2093-2102.

Tiwari G and Tiwari R (2010) Bioanalytical method validation: An updated review. *Pharmaceutical Methods* **1**:25-38.

Tomlin J, Brown N, Ellis A, Carlsson A, Bogentoft C, and Read NW (1993) THE EFFECT OF LIQUID FIBER ON GASTRIC-EMPTYING IN THE RAT AND HUMANS AND THE DISTRIBUTION OF SMALL-INTESTINAL CONTENTS IN THE RAT. *Gut* **34**:1177-1181.

Tougas G, Eaker EY, Abell TL, Abrahamsson H, Boivin M, Chen JD, Hocking MP, Quigley EMM, Koch KL, Tokayer AZ, Stanghellini V, Chen Y, Huizinga JD,

- Ryden J, Bourgeois I, and McCallum RW (2000) Assessment of gastric emptying using a low fat meal: Establishment of international control values. *American Journal of Gastroenterology* **95**:1456-1462.
- Toutain PL and Bousquet-Melou A (2004) Volumes of distribution. *Journal of Veterinary Pharmacology and Therapeutics* **27**:441-453.
- Tsume Y, Mudie DM, Langguth P, Amidon GE, and Amidon GL (2014) The Biopharmaceutics Classification System: Subclasses for in vivo predictive dissolution (IPD) methodology and IVIVC. *European Journal of Pharmaceutical Sciences* **57**:152-163.
- Valleri M, Mura P, Maestrelli F, Cirri M, and Ballerini R (2004) Development and evaluation of glyburide fast dissolving tablets using solid dispersion technique. *Drug Development and Industrial Pharmacy* **30**:525-534.
- van den Bosch HM, Bungler M, de Groot PJ, van der Meijde J, Hooiveld GJ, and Muller M (2007) Gene expression of transporters and phase I/II metabolic enzymes in murine small intestine during fasting. *Bmc Genomics* **8**:12.
- Varga F (1976) Transit Time Changes with Age in the Gastrointestinal Tract of the Rat. *Digestion* **14**:319-324.
- Varma MVS, Scialis RJ, Lin J, Bi YA, Rotter CJ, Goosen TC, and Yang X (2014) Mechanism-Based Pharmacokinetic Modeling to Evaluate Transporter-Enzyme Interplay in Drug Interactions and Pharmacogenetics of Glyburide. *Aaps Journal* **16**:736-748.
- Varum FJO, Hatton GB, and Basit AW (2013) Food, physiology and drug delivery. *International Journal of Pharmaceutics* **457**:446-460.
- Vdoviakova K, Petrovova E, Maloveska M, Kresakova L, Teleky J, Elias MZJ, and Petrasova D (2016) Surgical Anatomy of the Gastrointestinal Tract and Its Vasculature in the Laboratory Rat. *Gastroenterology Research and Practice*:11.
- Vermeulen JK, Vries AD, Schlingmann F, and Remie R (1997) Food deprivation: common sense or nonsense? *Animal Technology* **48**.
- Vincent J, Harris SI, Foulds G, Dogolo LC, Willavize S, and Friedman HL (2000) Lack of effect of grapefruit juice on the pharmacokinetics and pharmacodynamics of amlodipine. *British Journal of Clinical Pharmacology* **50**:455-463.
- Walton KD, Freddo AM, Wang S, and Gumucio DL (2016) Generation of intestinal surface: an absorbing tale. *Development* **143**:2261-2272.

- Wang LJ, Liu WX, Zhang ZJ, and Tian Y (2018) Validated LC-MS/MS method for the determination of amlodipine enantiomers in rat plasma and its application to a stereoselective pharmacokinetic study. *Journal of Pharmaceutical and Biomedical Analysis* **158**:74-81.
- Wang R, Zhang H, Sun S, Wang YY, Chai YF, and Yuan YF (2016) Effect of Ginkgo Leaf Tablets on the Pharmacokinetics of Amlodipine in Rats. *European Journal of Drug Metabolism and Pharmacokinetics* **41**:825-833.
- Wang SC, Lu KY, Chen SM, and Young TK (2001) Gastric emptying and intestinal transit of liquid and solid markers in rats with chronic uremia. *Chinese Journal of Physiology* **44**:81-87.
- Wang TT, Wang YN, Lin SS, Fang L, Lou S, Zhao D, Zhu JJ, Yang QG, and Wang Y (2020) Evaluation of pharmacokinetics and safety with bioequivalence of Amlodipine in healthy Chinese volunteers: Bioequivalence Study Findings. *Journal of Clinical Laboratory Analysis* **34**.
- Wang YJ, Yang WQ, Fu Q, Guo ZB, Sun BJ, Liu W, Liu YX, Mu SM, Guo MR, Li JR, Pu XH, and He ZG (2017) The role of particle size of glyburide crystals in improving its oral absorption. *Drug Delivery and Translational Research* **7**:428-438.
- Ward FW and Coates ME (1987) GASTROINTESTINAL PH MEASUREMENT IN RATS - INFLUENCE OF THE MICROBIAL-FLORA, DIET AND FASTING. *Laboratory Animals* **21**:216-222.
- Wei H, Dalton C, Di Maso M, Kanfer I, and Lobenberg R (2008) Physicochemical characterization of five glyburide powders: A BCS based approach to predict oral absorption. *European Journal of Pharmaceutics and Biopharmaceutics* **69**:1046-1056.
- Williams CL, Villar RG, Peterson JM, and Burks TF (1988) STRESS-INDUCED CHANGES IN INTESTINAL TRANSIT IN THE RAT - A MODEL FOR IRRITABLE BOWEL SYNDROME. *Gastroenterology* **94**:611-621.
- Wood HO (1944) The surface area of the intestinal mucosa in the rat and in the cat. *Journal of Anatomy* **78**:103-105.
- Wu CY and Benet LZ (2005) Predicting drug disposition via application of BCS: Transport/absorption/elimination interplay and development of a biopharmaceutics drug disposition classification system. *Pharmaceutical Research* **22**:11-23.

- Yao M, Zhang HJ, Chong SH, Zhu MS, and Morrison RA (2003) A rapid and sensitive LC/MS/MS assay for quantitative determination of digoxin in rat plasma. *Journal of Pharmaceutical and Biomedical Analysis* **32**:1189-1197.
- Yazdani M, Briggs K, Jankovsky C, and Hawi A (2004) The "high solubility" definition of the current FDA Guidance on Biopharmaceutical Classification System may be too strict for acidic drugs. *Pharmaceutical Research* **21**:293-299.
- Yu LX, Crison JR, and Amidon GL (1996) Compartmental transit and dispersion model analysis of small intestinal transit flow in humans. *International Journal of Pharmaceutics* **140**:111-118.
- Zhang CY, Gao ZQ, Niu LJ, and Chen XX (2018) Effects of triptolide on pharmacokinetics of amlodipine in rats by using LC-MS/MS. *Pharmaceutical Biology* **56**:132-137.
- Zhang HX, Han XY, Li YQ, Li HG, and Guo XC (2019) Effects of Danshen tablets on pharmacokinetics of amlodipine in rats. *Pharmaceutical Biology* **57**:306-309.
- Zhou X, Rougee LRA, Bedwell DW, Cramer JW, Mohutsky MA, Calvert NA, Moulton RD, Cassidy KC, Yumibe NP, Adams LA, and Ruterbories KJ (2016) Difference in the Pharmacokinetics and Hepatic Metabolism of Antidiabetic Drugs in Zucker Diabetic Fatty and Sprague-Dawley Rats. *Drug Metabolism and Disposition* **44**:1184-1192.
- Zhu YL, Wang F, Li Q, Zhu MS, Du A, Tang W, and Chen WQ (2014) Amlodipine Metabolism in Human Liver Microsomes and Roles of CYP3A4/5 in the Dihydropyridine Dehydrogenation. *Drug Metabolism and Disposition* **42**:245-249.
- Zimmermann T, Laufen H, Yeates R, Scharpf F, Riedel KD, and Schumacher T (1999) The pharmacokinetics of extended-release formulations of calcium antagonists and of amlodipine in subjects with different gastrointestinal transit times. *Journal of Clinical Pharmacology* **39**:1021-1031.
- Zubair F, Laibinis PE, Swisher WG, Yang JH, Spraggins JM, Norris JL, and Caprioli RM (2016) Trypsin and MALDI matrix pre-coated targets simplify sample preparation for mapping proteomic distributions within biological tissues by imaging mass spectrometry. *Journal of Mass Spectrometry* **51**:1168-1179.
- Zuber R, Anzenbacherova E, and Anzenbacher P (2002) Cytochromes P450 and experimental models of drug metabolism. *Journal of Cellular and Molecular Medicine* **6**:189-198.

APPENDIX A- INDIVIDUAL ANATOMIC DATA

The complete list of pH measurements, rat weight, the exact length of each segment, total time fasted, and percentage estimate of food content for the fasted group.

Rat 34					
Intestinal Segment	% food in the lumen	Length	pH 1	pH 2	pH 3
Duodenum	0	10.0	6.62	6.61	6.63
Jejunum 1	0	23.8	6.47	6.41	6.49
Jejunum 2	25	23.8	6.79	6.76	6.73
Jejunum 3	25	23.8	6.59	6.55	6.50
Jejunum 4	25/50	23.8	6.66	6.63	6.67
Jejunum 5		23.8	7.09	7.09	7.17
Ileum	75/100	3.0	7.52	7.48	7.36
Cecum	100	-	6.75	7.02	6.98
Proximal Colon	100	17.0	6.68	6.71	6.76
Distal Colon	100		6.26	6.23	6.21
Weight:	373g		Time of fast:		8:15 PM
			Time of sacrificed:		9:10 AM

Rat 36					
Intestinal Segment	% food in the lumen	Length	pH 1	pH 2	pH 3
Duodenum	0	10.0	6.38	6.47	6.45
Jejunum 1	25	20.0	6.43	6.46	6.44
Jejunum 2	25	20.0	6.49	6.56	6.56
Jejunum 3	25	20.0	6.45	6.47	6.45
Jejunum 4	25	20.0	6.63	6.63	6.58
Jejunum 5	25/50	20.0	7.85	7.85	7.82
Ileum	100	3.0	7.72	7.85	7.91
Cecum	100	-	6.94	6.95	6.95
Proximal Colon	100	17.0	6.48	6.60	6.40
Distal Colon	100		5.90	5.91	5.89
Weight:	346g		Time of fast:		7:12 PM
			Time of sacrificed:		7:25 AM

Rat 37					
Intestinal Segment	% food in the lumen	Length	pH 1	pH 2	pH 3
Duodenum	0/25	10.0	6.41	6.60	6.58
Jejunum 1	0/25	19.5	6.62	6.78	6.78
Jejunum 2	50/75	19.5	6.35	6.39	6.35
Jejunum 3	75/100	19.5	6.33	6.37	6.35
Jejunum 4	75/100	19.5	6.48	6.62	6.59
Jejunum 5	50	19.5	6.83	6.93	6.89
Ileum	25/50	3.0	7.90	8.03	7.80
Cecum	100	-	6.43	6.44	6.48
Proximal Colon	100	16.0	6.39	6.42	6.34
Distal Colon	0/25		6.03	6.09	5.98
Weight:	323 g		Time of fast:		7:40 PM
			Time of sacrificed:		8:10 AM

Rat 38					
Intestinal Segment	% food in the lumen	Length	pH 1	pH 2	
Duodenum	0/25	10.0	6.34		
Jejunum 1	0/25	20.0	6.50		
Jejunum 2	0/25	20.0	6.59		
Jejunum 3	0/25	20.0	6.57		
Jejunum 4	50/75	20.0	6.67		
Jejunum 5	50/75	20.0	7.40	7.48	
Ileum	100	3.0	7.39	7.48	
Cecum	100	-	6.30	6.34	
Proximal Colon	100	-	6.07	6.16	
Distal Colon	50		6.33	6.42	
Weight:	308 g		Time of fast:		9:35 PM
			Time of sacrificed:		10:27 AM

The complete list of pH measurements, rat weight, the exact length of each segment, total time fasted, and percentage estimate of food content for the fed group.

Rat 25				
Intestinal Segment	Length	pH 1	pH 2	pH 3
Duodenum	10.0	6.08	6.10	
Jejunum 1	22.5	6.01	6.04	
Jejunum 2	22.5	6.31	6.29	
Jejunum 3	22.5	6.39	6.60	
Jejunum 4	22.5	6.60	6.73	
Jejunum 5	22.5	7.03	7.00	
Ileum	3.0	7.57	7.57	7.72
Cecum	-	5.75	5.76	5.76
Proximal Colon	* no measurement	5.57	5.56	5.56
Distal Colon		5.74	5.77	

Rat 26				
Intestinal Segment	Length	pH 1	pH 2	pH 3
Duodenum	10.0	6.01	5.97	
Jejunum 1	22.5	6.02	5.98	
Jejunum 2	22.5	6.36	6.31	
Jejunum 3	22.5	6.7	6.79	
Jejunum 4	22.5	6.91	6.99	
Jejunum 5	22.5	7.07	7.2	
Ileum	3.0	7.72	7.72	7.98
Cecum	-	5.65	5.61	5.65
Proximal Colon	20.0	5.54	5.51	5.58
Distal Colon		6.3	6.3	6.38

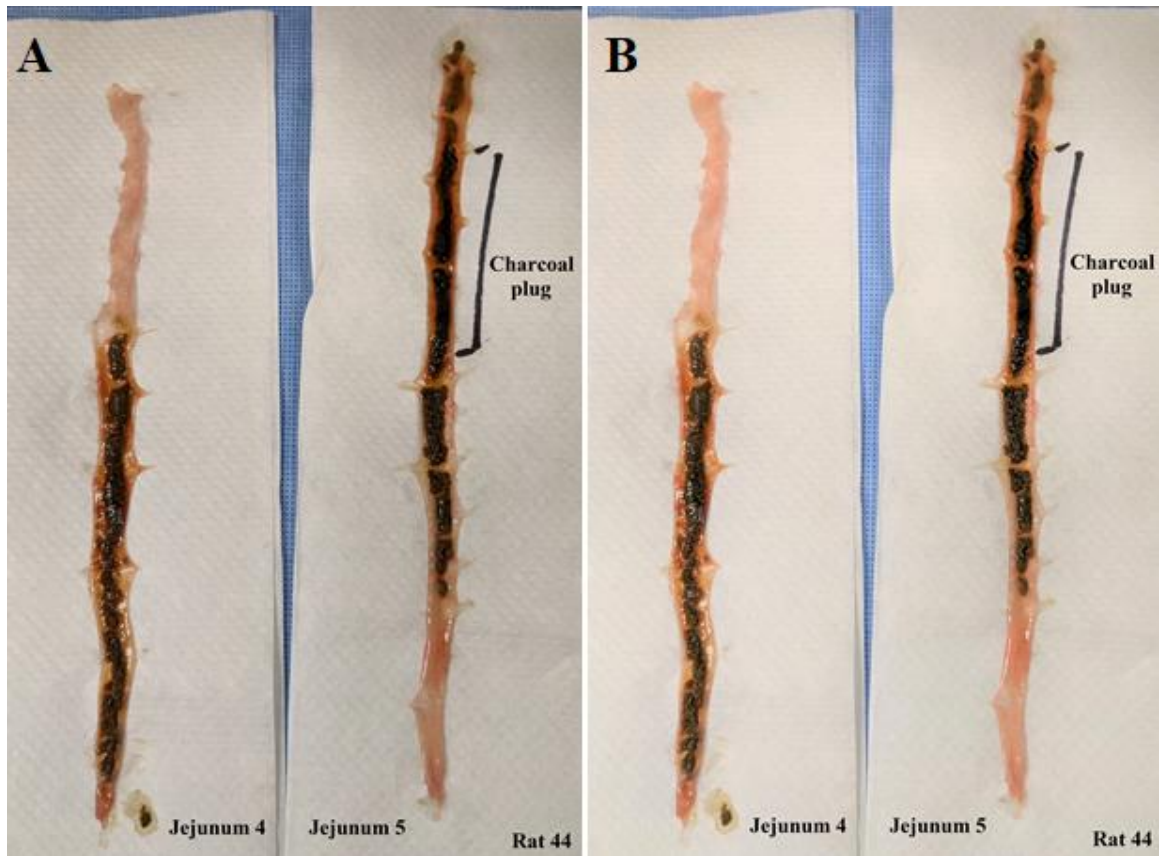
Rat 33					
Intestinal Segment	% food in the lumen	Length	pH 1	pH 2	pH 3
Duodenum	25	10.0	5.87	5.91	5.98
Jejunum 1	25/50	21.0	5.74	5.72	5.76
Jejunum 2	50	21.0	6.08	6.03	6.04
Jejunum 3	75/100	21.0	6.47	6.58	6.59
Jejunum 4	100	21.0	6.69	6.91	7.00
Jejunum 5	75/100	21.0	6.58	6.70	6.88
Ileum	100	3.0	7.20	7.91	7.68
Cecum	100	-	5.42	5.48	5.50
Proximal Colon	100	19.0	5.38	5.46	5.46
Distal Colon	100		5.84	5.80	5.77
Weight:	367 g				

Rat 35					
Intestinal Segment	% food in the lumen	Length	pH 1	pH 2	pH 3
Duodenum	0	10	6.24	6.13	6.2
Jejunum 1	25	21	6.15	6.02	6.05
Jejunum 2	25/50	21	6.36	6.17	6.18
Jejunum 3	50/75	21	6.54	6.49	6.34
Jejunum 4	50/75	21	6.91	6.98	6.93
Jejunum 5	75/100	21	7.01	6.89	6.99
Ileum	100	3	7.63	7.86	7.98
Cecum	100	-	5.86	5.72	5.78
Proximal Colon	100	16	5.93	5.76	5.81
Distal Colon	100		5.84	5.85	5.87
Weight:	342 g				

Full physiological data of rats collected during Chapter 3.

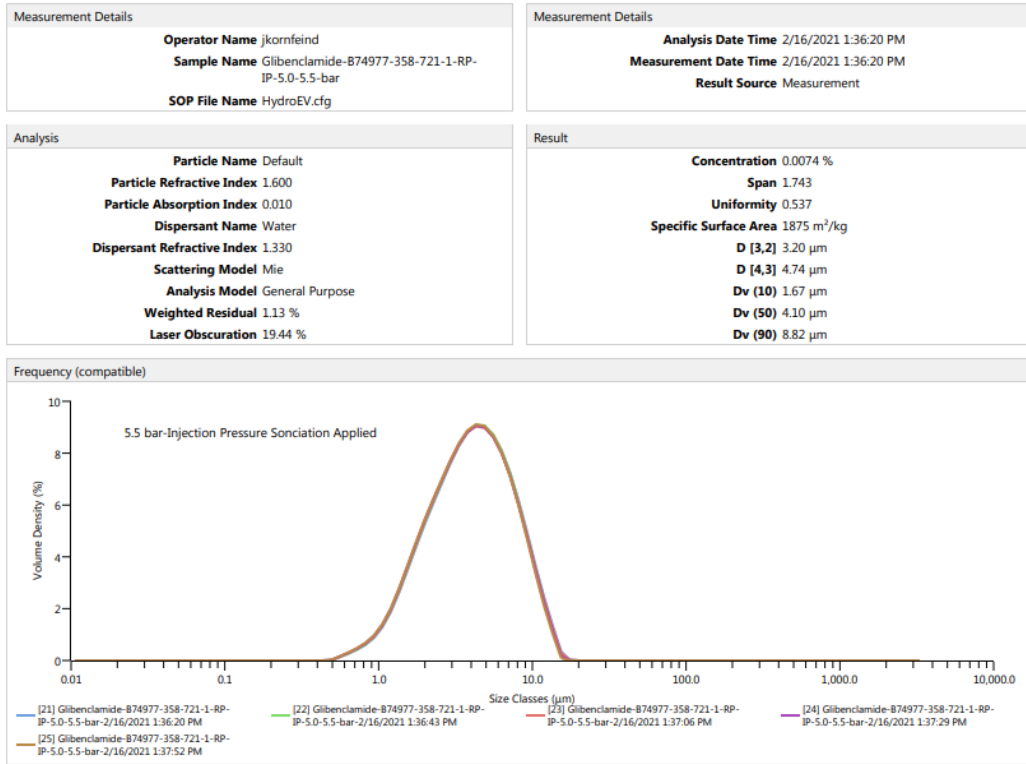
Physiological data				
Rat	Weight (grams)	Total Length of Small Intestine (cm)	Single jejunum segment (cm)	Length of Large Intestine (cm)
25	-	125.5	22.5	-
26	-	125.5	22.5	20
33	367.0	118	21.0	19
34	373.0	132	23.8	17
35	342.0	118	21.0	16
36	346.0	113	20.0	17
37	323.0	110.5	19.5	16
38	308.0	113	20.0	-
52	349.1	126	22.6	14
53	312.5	119	21.2	15
55	317.5	120	21.4	16
56	389.9	128	23.0	14
57	364.1	111	19.6	13
58	371.5	110	19.4	14
59	355.7	124	22.2	-
60	391.6	112	19.8	15
62	371.0	118	21.0	-
63	346.5	116	20.6	-
64	331.5	101	20.2	-
65	318.2	124	22.2	-
66	328.9	102	17.8	17
67	318.1	107	18.8	-
68	317.9	117	20.8	-
69	321.9	117	20.8	-
70	341.8	124.5	22.3	-
71	334.2	115	20.4	-
72	359.0	130	23.4	-
73	328.2	128	23.0	-
74	345.6	120	21.4	-
75	341.4	124	22.4	-
77	362.0	114	20.2	-

78	351.7	116	20.6	-
79	376.0	116	20.6	-
80	381.1	125	22.4	-
84	354.0	124	22.2	-
85	409.1	130	23.4	-
86	401.0	126	22.6	-
94	386.1	126	22.6	-
95	346.1	121	21.6	-
96	369.2	118	21.0	-
97	346.1	118	21.0	-
1*	318.0	109	19.2	-
2*	294.2	117	20.8	-



Images of Charcoal Plug in the J5 Segment of Rat 44. Images of Charcoal Plug in the J5 Segment of Rat 44. The original image (A) and the same image with the light increased by 50% using Microsoft Photos Version 2018.18011.15918.0 (B).

APPENDIX B- PARTICLE SIZE CHARACTERIZATION



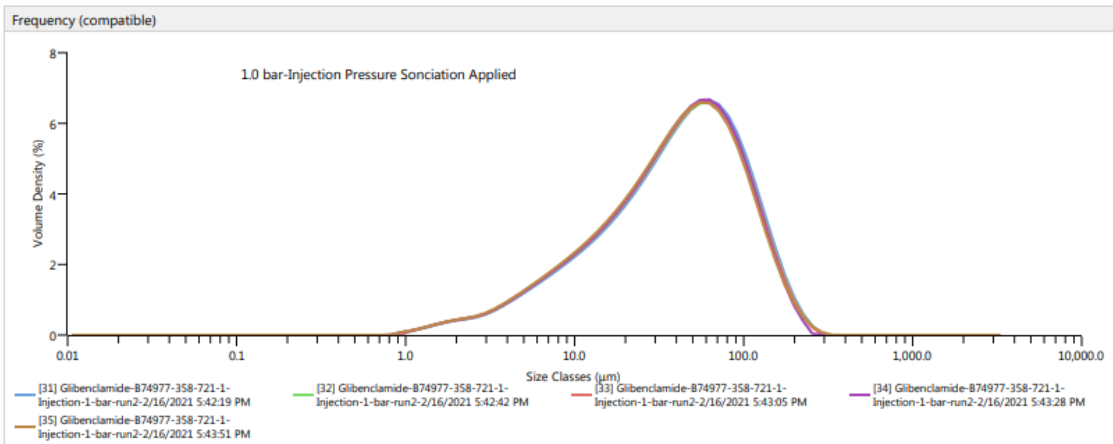
Sample A particle size analysis

Measurement Details	
Operator Name	jkornfeind
Sample Name	Glibenclamide-874977-358-721-1- Injection-1-bar-run2
SOP File Name	HydroEV.cfg

Measurement Details	
Analysis Date Time	2/16/2021 5:42:19 PM
Measurement Date Time	2/16/2021 5:42:19 PM
Result Source	Measurement

Analysis	
Particle Name	Default
Particle Refractive Index	1.600
Particle Absorption Index	0.010
Dispersant Name	Water
Dispersant Refractive Index	1.330
Scattering Model	Mie
Analysis Model	General Purpose
Weighted Residual	0.24 %
Laser Obscuration	17.34 %

Result	
Concentration	0.0399 %
Span	2.558
Uniformity	0.796
Specific Surface Area	328.2 m ² /kg
D [3,2]	18.3 μm
D [4,3]	54.3 μm
Dv (10)	8.02 μm
Dv (50)	42.7 μm
Dv (90)	117 μm



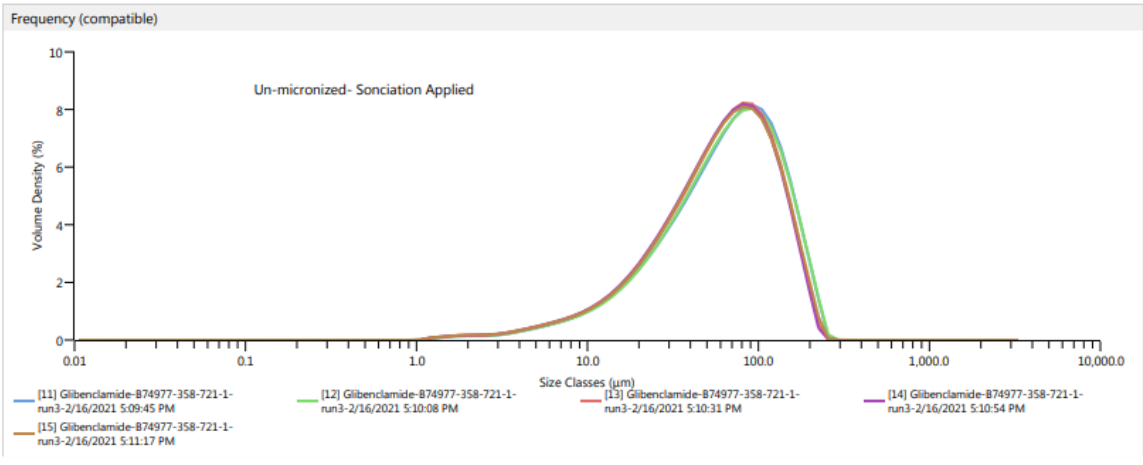
Sample B particle size analysis

Measurement Details	
Operator Name	jkornfeind
Sample Name	Glibenclamide-874977-358-721-1-run3
SOP File Name	HydroEV.cfg

Measurement Details	
Analysis Date Time	2/16/2021 5:09:45 PM
Measurement Date Time	2/16/2021 5:09:45 PM
Result Source	Measurement

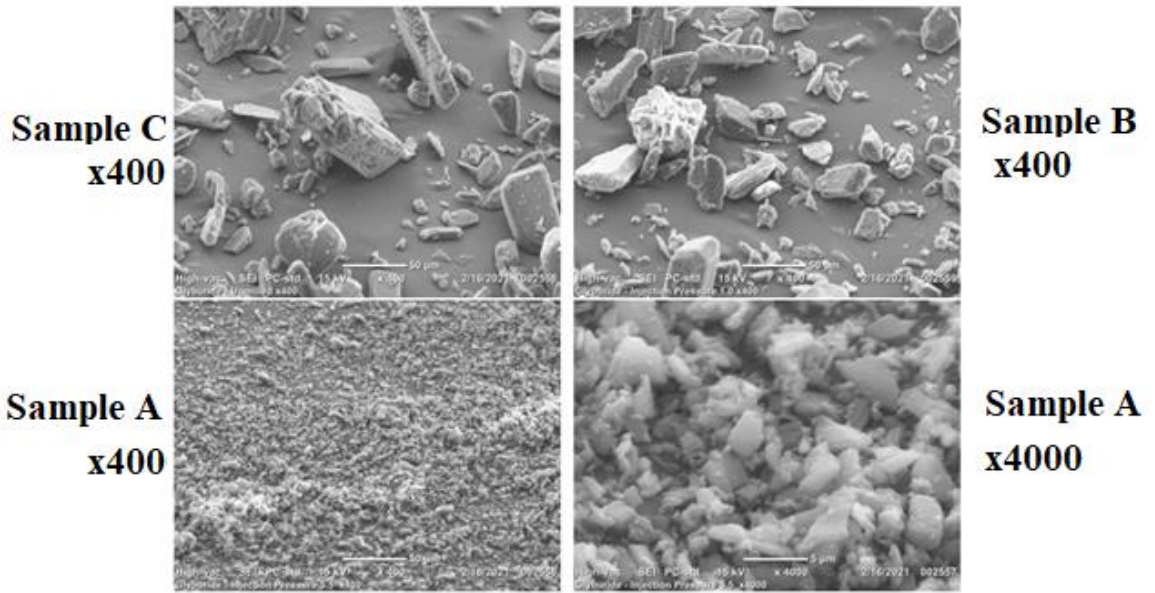
Analysis	
Particle Name	Default
Particle Refractive Index	1.600
Particle Absorption Index	0.010
Dispersant Name	Water
Dispersant Refractive Index	1.330
Scattering Model	Mie
Analysis Model	General Purpose
Weighted Residual	1.55 %
Laser Obscuration	5.20 %

Result	
Concentration	0.0215 %
Span	1.981
Uniformity	0.610
Specific Surface Area	178.0 m ² /kg
D [3,2]	33.7 μm
D [4,3]	76.5 μm
Dv (10)	17.6 μm
Dv (50)	67.1 μm
Dv (90)	151 μm



Sample C particle size analysis

Scanning Electron Microscopy



Scanning electron microscopy images of Sample A (4.1 μm), Sample B (42.7 μm), and Sample C (67.1 μm) of GLY.

APPENDIX C- EXAMPLE SOLUTION NOTEBOOK

Attached PDF

```
In[69996]:= ClearAll["Global`*"];
In[69997]:= Needs["NDSolve`FEM`"];
In[69998]:= SetDirectory["/Users/brave/Dropbox/My PC (DESKTOP-M528K7I)/Desktop"];
In[69999]:= datafile = "CCR.rat.abs.data.soln.07.28.xlsx";
```

```
In[70000]:= sheet = 1;
```

```
In[70001]:= compd = 5;
```

```
In[70002]:= cacosf = 4.8;
```

Drug specific parameters

```
In[70003]:= {drug, f, fabs, fabscol, papp0, sol1, sol2, rho, fumics, dose1,
             vol0, dose2, inftime, xp2, ph0, pkaa, pkab, ma, mb, acidflag, baseflag} =
             Import[datafile, {"Data", sheet, compd + 1, Range[1, 21]}]
```

```
Out[70003]:= {AML-fast 2hr, 0.5, 64., 100., 7.43, 0.744, 0.744,
             1.33, 0.06, 1.5, 1., 0.6, 0.01, 4., 7.4, 1., 9.1, 4., 4., 0., 1.}
```

Solubility (mg/m³)

```
In[70004]:= sol1 = sol1 1000000;
```

```
In[70005]:= sol2 = sol2 1000000.;
```

Rho (mg/m³)

```
In[70006]:= rho = rho 1000000000;
```

Fraction unbound in microsomes at 1 mg/mL

fumics;

CACO2 Papp in m/hr (cm/sec*36 = m/hr)

```
In[70008]:= papp0 = papp0 36 × 10-6.;
```

```
In[70009]:= papp0 = papp0 cacosf;
```

Drug dose in mg (for abs model, ng for PK), vol in m³, infusion time in hr

```
In[70010]:= vol0 = vol0 10-6
```

```
Out[70010]:= 1. × 10-6
```

Plug length time in m/(m/hr)

```
In[70011]:= pl1 = 0.06; (*stomach pulse length*)
```

```
In[70012]:= lag = 0.1; (*stomach emptying lag time*)
```

Concentration in Dosing solution mg/L=g/m³ (g/m³)

```
In[70013]:= C0 = dose1 / vol0;
```

Rat Physiology

Radii (m)

duodenum, J1, J2, J3, J4, J5, ileum, proximal colon, and distal colon

circumference (cm) from in-house experimental *scaleradii = radii (m) [scaleradii to make circumference in cm to radii in meters]

```
In[70014]:= scaleradii = 0.01 / (2 π);
```

```
In[70015]:= r1 = 0.79 scaleradii;
r2 = 0.92 scaleradii;
r3 = 0.92 scaleradii;
r4 = 0.92 scaleradii;
r5 = 0.92 scaleradii;
r6 = 0.91 scaleradii;
r7 = 0.89 scaleradii;
r8 = 1.17 scaleradii;
r9 = 1.17 scaleradii;
```

Distances (m)

Distances measured in-house (specific aim #2) in meters. Distance is where the segment ends (cumulative). Ex: jej2 = duo + jej1 + jej2

```
In[70024]:= d0 = 0.0005;
duo = 0.1005;
jej1 = 0.3125;
jej2 = 0.5255;
jej3 = 0.7375;
jej4 = 0.9495;
jej5 = 1.1615;
ile = 1.1915;
proxcol = 1.2715;
distcol = 1.4305;
```

Cross sectional area (m²)

From radii listed above

```
In[70034]:= xa1 = π r1^2;
```

```
In[70035]:= xa2 = π r2^2;
```

```
In[70036]:= xa3 = π r3^2;
```

```
In[70037]:= xa4 = π r4^2;
```

```
In[70038]:= xa5 = π r5^2;
```

```
In[70039]:= xa6 = π r6^2;
```

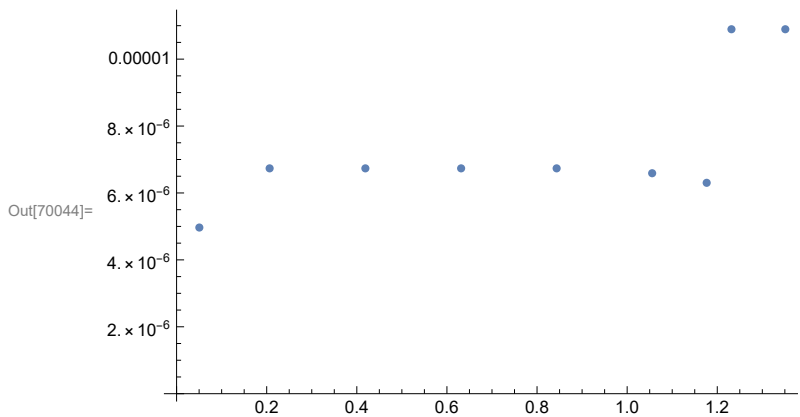
```
In[70040]:= xa7 = π r7^2;
```

```
In[70041]:= xa8 = π r8^2;
```

```
In[70042]:= xa9 = π r9^2;
```

```
In[70043]:= xat = {{(duo - d0) / 2 + d0, xa1}, {(jej1 - duo) / 2 + duo, xa2},
  {(jej2 - jej1) / 2 + jej1, xa3}, {(jej3 - jej2) / 2 + jej2, xa4},
  {(jej4 - jej3) / 2 + jej3, xa5}, {(jej5 - jej4) / 2 + jej4, xa6}, {(ile - jej5) / 2 + jej5, xa7},
  {(proxcol - ile) / 2 + ile, xa8}, {(distcol - proxcol) / 2 + proxcol, xa9}};
```

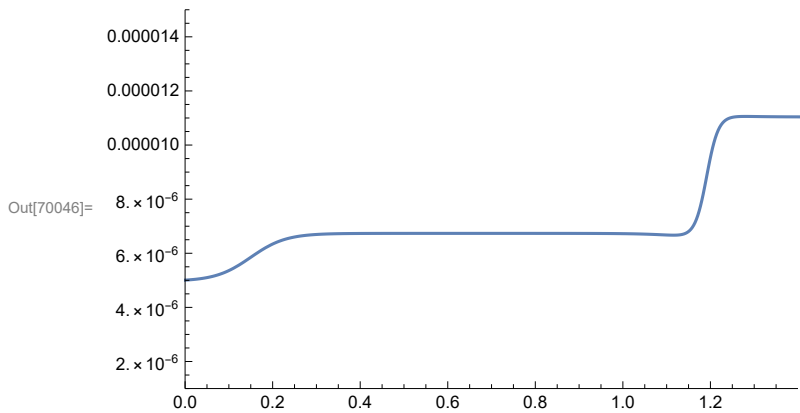
```
In[70044]:= plot2 = ListPlot[xat]
```



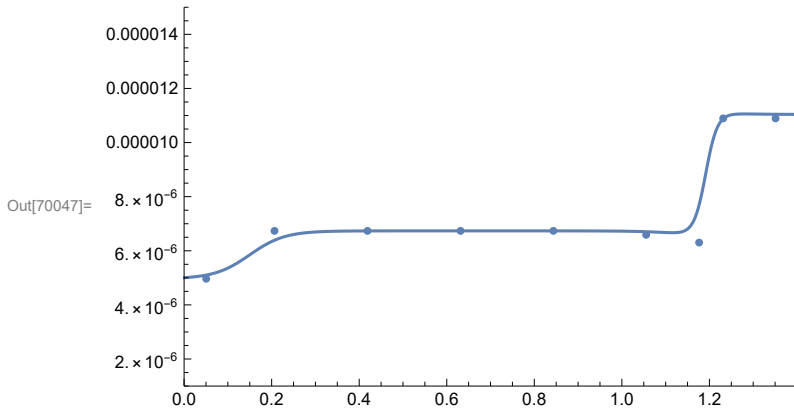
```
In[70045]:= xa[x] = xa1 + (xa2 - xa1) / (1 + e^-25 (x-0.15)) +
  (xa7 - xa6) / (1 + e^-20 (x-jej5)) + ((xa8 - xa7)) / (1 + e^-75 (x-ile))
```

```
Out[70045]= 4.96643 × 10-6 +  $\frac{4.59003 \times 10^{-6}}{1 + e^{-75 (-1.1915+x)}}$  -  $\frac{2.86479 \times 10^{-7}}{1 + e^{-20 (-1.1615+x)}}$  +  $\frac{1.76901 \times 10^{-6}}{1 + e^{-25 (-0.15+x)}}$ 
```

```
In[70046]:= plot1 = Plot[Evaluate[xa[x]], {x, 0, 10}, PlotRange -> {{0, 1.40}, {0.000001, 0.000015}}]
```



In[70047]:= Show[plot1, plot2]



In[70048]:= dxa[x] = D[xa[x], x]

$$\text{Out[70048]} = \frac{0.000344252 e^{-75(-1.1915+x)}}{(1 + e^{-75(-1.1915+x)})^2} - \frac{5.72958 \times 10^{-6} e^{-20(-1.1615+x)}}{(1 + e^{-20(-1.1615+x)})^2} + \frac{0.0000442252 e^{-25(-0.15+x)}}{(1 + e^{-25(-0.15+x)})^2}$$

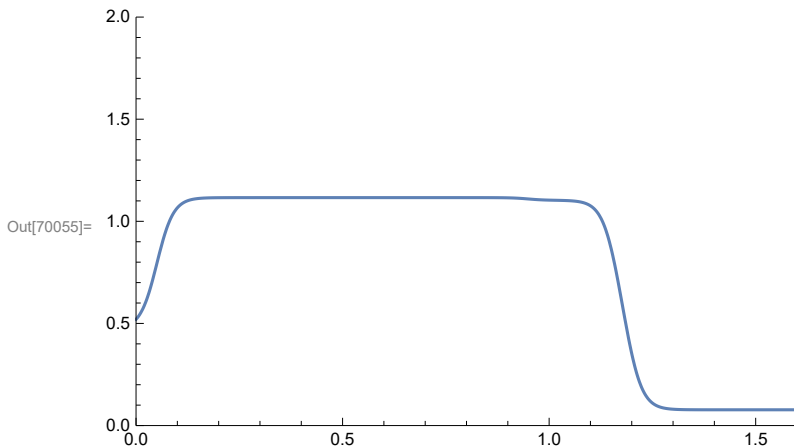
SA per length (or circumference) in m²/m

In[70049]:= **sa1 = 0.47242;**
sa2 = 1.116;
sa3 = 1.103;
sa4 = 0.615;
sa5 = 0.0772;

$$\text{In[70054]} = \text{sa}[x] = \text{sa1} + \frac{\text{sa2} - \text{sa1}}{(1 + e^{-50(x - (d0+d00)/2)})} - \frac{\text{sa2} - \text{sa3}}{(1 + e^{-50(x - \text{je}j4)})} - \frac{\text{sa3} - \text{sa4}}{(1 + e^{-50(x - \text{je}j5)})} - \frac{\text{sa4} - \text{sa5}}{(1 + e^{-50(x - \text{i}le)})}$$

$$\text{Out[70054]} = 0.47242 - \frac{0.5378}{1 + e^{-50(-1.1915+x)}} - \frac{0.488}{1 + e^{-50(-1.1615+x)}} - \frac{0.013}{1 + e^{-50(-0.9495+x)}} + \frac{0.64358}{1 + e^{-50(-0.0505+x)}}$$

In[70055]:= Plot[Evaluate[sa[x]], {x, 0, 1.6}, PlotRange -> {{0, 1.6}, {0, 2}}]

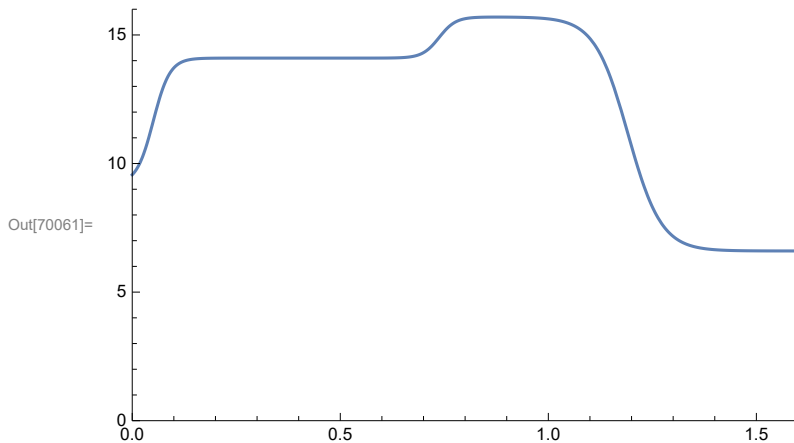


Microvilli factor as a function of x

```
In[70056]:= mf1 = 9.2;
mf2 = 14.1;
mf3 = 15.7;
mf4 = 6.6;
```

```
In[70060]:= mf[x] = mf1 + (mf2 - mf1) / (1 + e-50 (x - (d0+du0)/2)) -
(mf2 - mf3) / (1 + e-50 (x - jeJ3)) - (mf3 - mf4) / (1 + e-25 (x - ile));
```

```
In[70061]:= Plot[Evaluate[mf[x]], {x, 0, 1.6}, PlotRange -> {{0, 1.6}, {0, 16}}]
```



Cross sectional surface areas of cells (m²)

Cell: SA of the small intestine/ colon was multiplied by the diameter of an enterocyte (20 μm) [20 μm = 0.000020 meters]

Membrane: SA of the small intestine/ colon was multiplied by width of the plasma membrane (35 Å) [35 Å = 0.0000000035 meters]

Microvilli are only present on apical surface of epithelial cells, so only apical membrane includes villi and microvilli (not divided by mf [microvilli factor])

Lipids: SA of the small intestine/ colon was multiplied by width of cytosolic lipids (assuming they make up 7% of enterocyte volume)

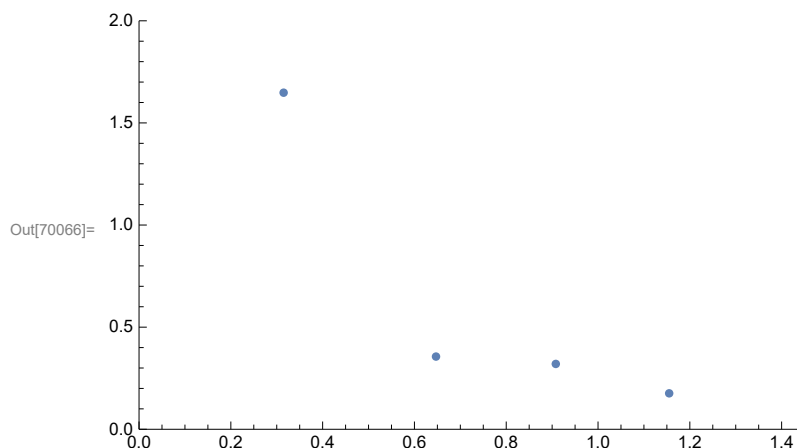
```
In[70062]:= xacell[x] = sa[x] / mf[x] 0.000020;
xamem[x] = sa[x] 0.0000000035;
xalip[x] = sa[x] / mf[x] 0.0000015;
```

Axial Velocity (m/hr)

Velocity data measured in-house (specific aim #2)

```
In[70065]:= veltab = {{0.315, 1.648}, {0.647, 0.356}, {0.908, 0.320}, {1.155, 0.176}};
```

In[70066]:= **plot2 = ListPlot[veltab, PlotRange -> {{0, 1.44}, {0, 2}}]**

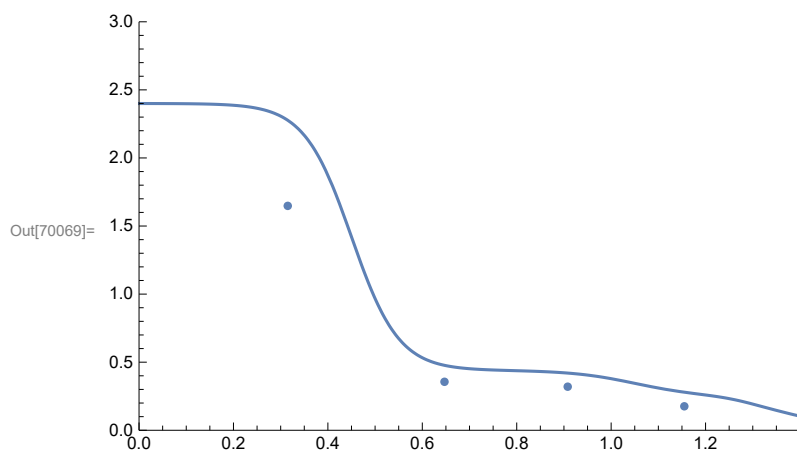


In[70067]:= **vel[x] = 2.4 - (2.4 - .440) / (1 + e^{-20(x-.45)}) -**
(0.340 - 0.15) / (1 + e^{-15(x-1.05)}) - (0.11) / (1 + e^{-25(x-1.3)}) - (0.09) / (1 + e^{-25(x-1.399)})

Out[70067]=
$$2.4 - \frac{0.09}{1 + e^{-25(-1.399+x)}} - \frac{0.11}{1 + e^{-25(-1.3+x)}} - \frac{0.19}{1 + e^{-15(-1.05+x)}} - \frac{1.96}{1 + e^{-20(-0.45+x)}}$$

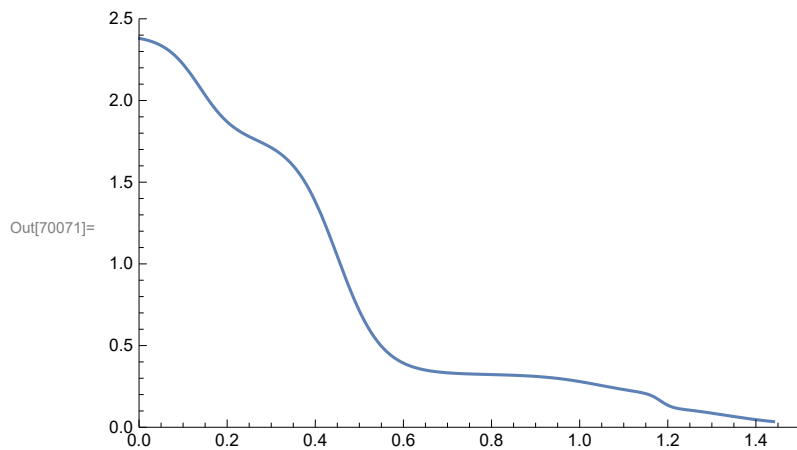
In[70068]:= **plot1 = Plot[Evaluate[vel[x]], {x, 0, 1.44}, PlotRange -> {{0, 1.4}, {0, 3}}];**

In[70069]:= **Show[plot1, plot2]**

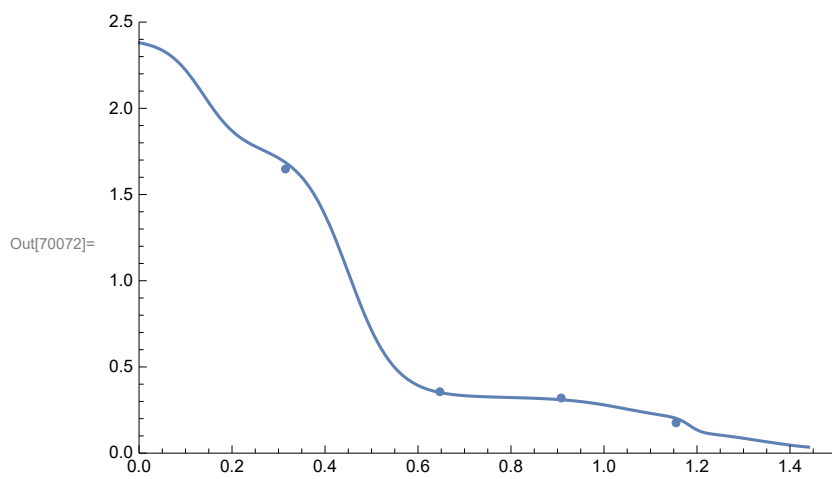


In[70070]:= **vel2[x] = (vel[x]) (xa1 / xa[x]);**

```
In[70071]:= plot3 = Plot[Evaluate[vel2[x]], {x, 0, 1.44}, PlotRange -> {{0, 1.5}, {0, 2.5}}]
```



```
In[70072]:= Show[plot3, plot2]
```

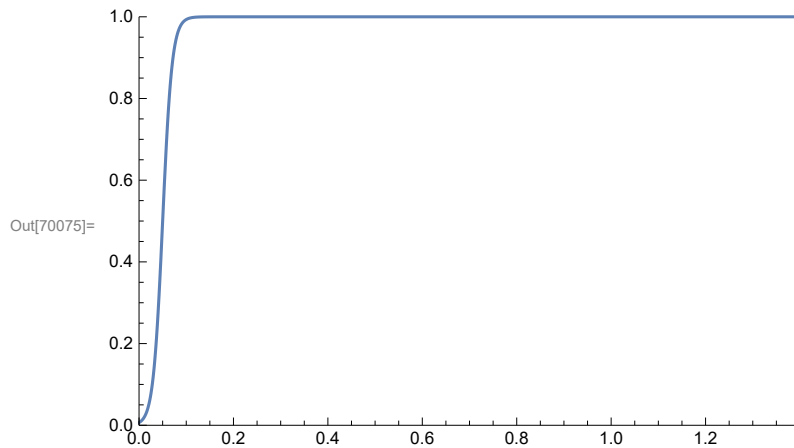


```
In[70073]:= dvel[x] = D[vel2[x], x];
```

```
In[70074]:= Plot[Evaluate[dvel[x]], {x, 0, 1.44}, PlotRange -> {{0, 1.4}, {0, 1.2}}];
```

Axial Diffusion rate constant
Effective diffusion in m²/hr

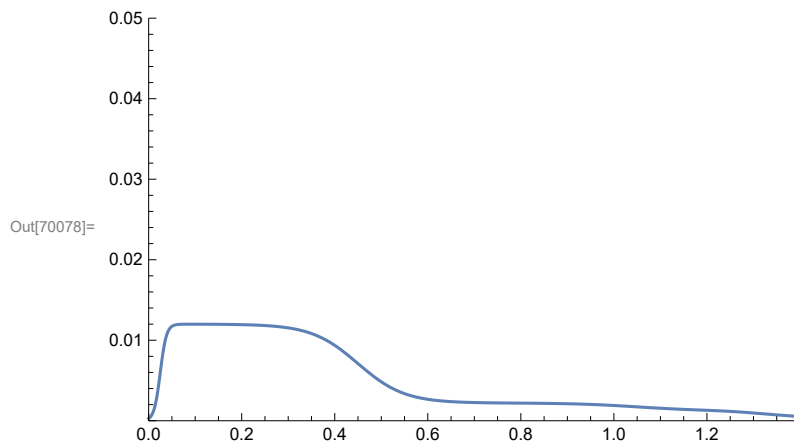
In[70075]:= **Plot**[$0.5 + (0.5) \operatorname{Tanh}[50. (x - 0.05)]$], {x, 0, 1.4}, **PlotRange** → {{0, 1.4}, {0, 1}}



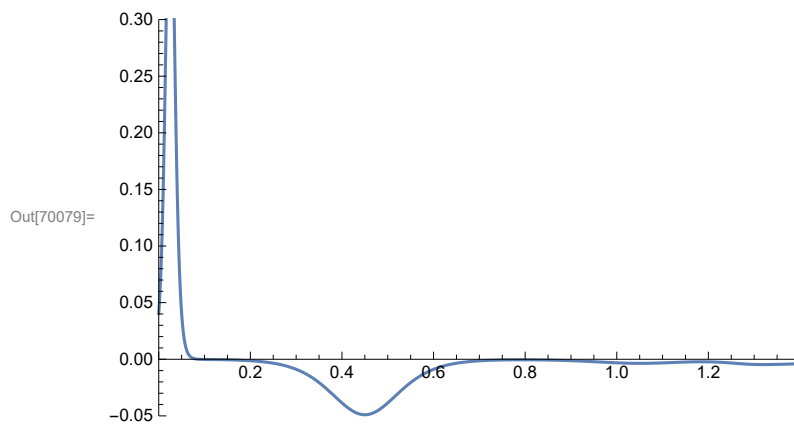
In[70076]:= **dif2**[x] = $0.005 (0.5 + 0.5 \operatorname{Tanh}[75. (x - 0.025)]) \operatorname{vel}[x]$;

In[70077]:= **ddif2**[x] = **D**[dif2[x], x];

In[70078]:= **Plot**[**Evaluate**[dif2[x]], {x, 0, 1.4}, **PlotRange** → {{0, 1.4}, {0, .05}}



In[70079]:= **Plot**[**Evaluate**[ddif2[x]], {x, 0, 1.44}, **PlotRange** → {{0, 1.4}, {- .05, .3}}

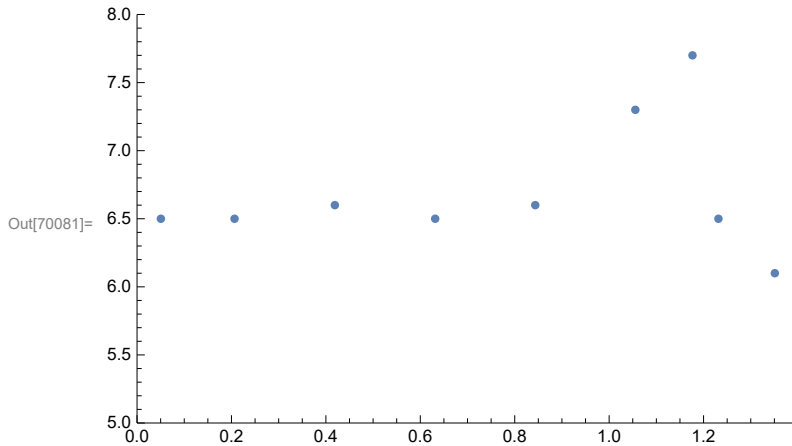


pH Fasted and Fed

The pH was measured for fasted and fed animals in-house (specific aim #2).

```
In[70080]:= phfasttab = { {(d0 + duo) / 2}, 6.5}, { (duo + jej1) / 2}, 6.5}, { (jej1 + jej2) / 2}, 6.6},
  { (jej2 + jej3) / 2}, 6.5}, { (jej3 + jej4) / 2}, 6.6}, { (jej4 + jej5) / 2}, 7.3},
  { (jej5 + ile) / 2}, 7.7}, { (ile + proxcol) / 2}, 6.5}, { ((proxcol + distcol) / 2), 6.1}};
```

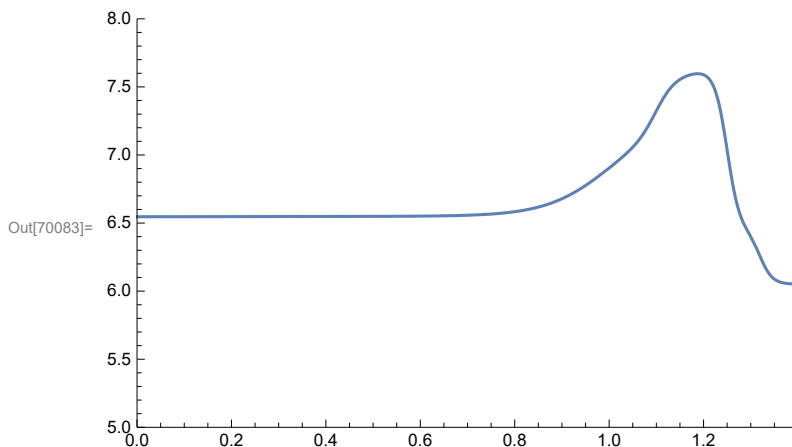
```
In[70081]:= plot2 = ListPlot[phfasttab, PlotRange -> {{0, 1.4}, {5, 8}}]
```



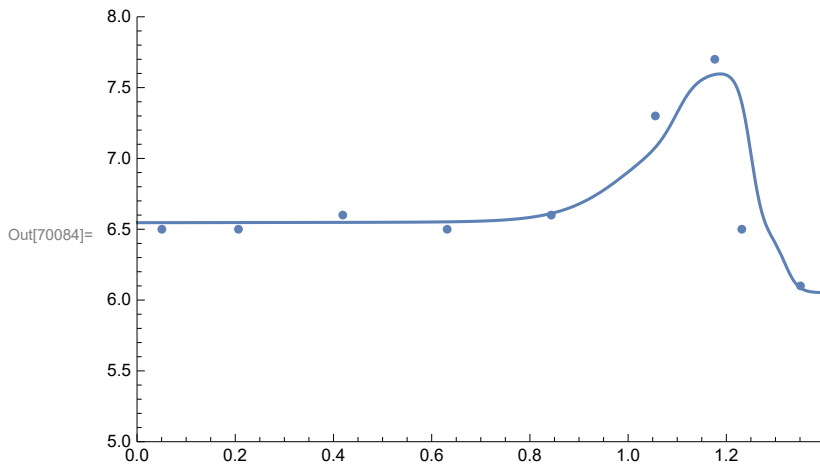
```
In[70082]:= phfast[x] = phfasttab[[1, 2]] + (phfasttab[[5, 2]] - phfasttab[[1, 2]]) / (1 + e-0.2(x-jej3)) +
  (phfasttab[[6, 2]] - phfasttab[[5, 2]]) / (1 + e-15(x-1)) +
  (phfasttab[[7, 2]] - phfasttab[[6, 2]]) / (1 + e-50(x-1.1)) +
  (phfasttab[[8, 2]] - phfasttab[[7, 2]]) / (1 + e-75(x-1.25)) +
  (phfasttab[[9, 2]] - phfasttab[[8, 2]]) / (1 + e-75(x-1.32))
```

```
Out[70082]= 6.5 -  $\frac{0.4}{1 + e^{-75(-1.32+x)}}$  -  $\frac{1.2}{1 + e^{-75(-1.25+x)}}$  +  $\frac{0.4}{1 + e^{-50(-1.1+x)}}$  +  $\frac{0.7}{1 + e^{-15(-1+x)}}$  +  $\frac{0.1}{1 + e^{-0.2(-0.7375+x)}}$ 
```

```
In[70083]:= plot1 = Plot[Evaluate[phfast[x]], {x, 0, 1.4}, PlotRange -> {{0, 1.4}, {5, 8}}]
```

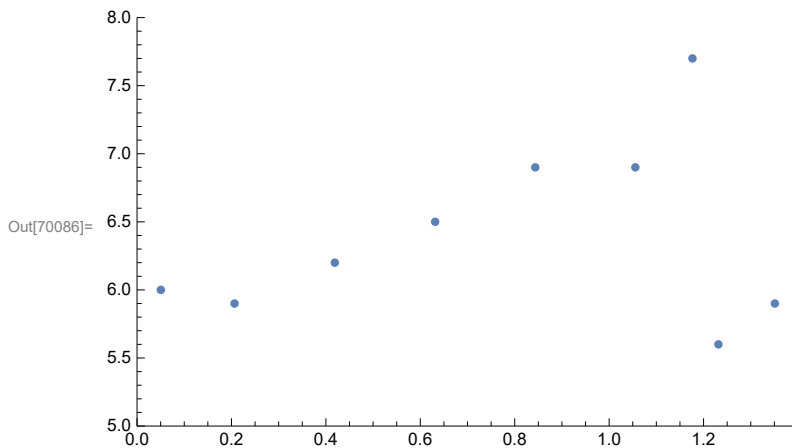


In[70084]:= Show[plot1, plot2]



In[70085]:= phfedtab = {{(d0 + duo) / 2}, 6.0}, {(duo + jej1) / 2}, 5.9}, {(jej1 + jej2) / 2}, 6.2},
 {{(jej2 + jej3) / 2}, 6.5}, {(jej3 + jej4) / 2}, 6.9}, {(jej4 + jej5) / 2}, 6.9},
 {{(jej5 + ile) / 2}, 7.7}, {(ile + proxcol) / 2}, 5.6}, {(proxcol + distcol) / 2}, 5.9}};

In[70086]:= plot2 = ListPlot[phfedtab, PlotRange -> {{0, 1.4}, {5, 8}}]

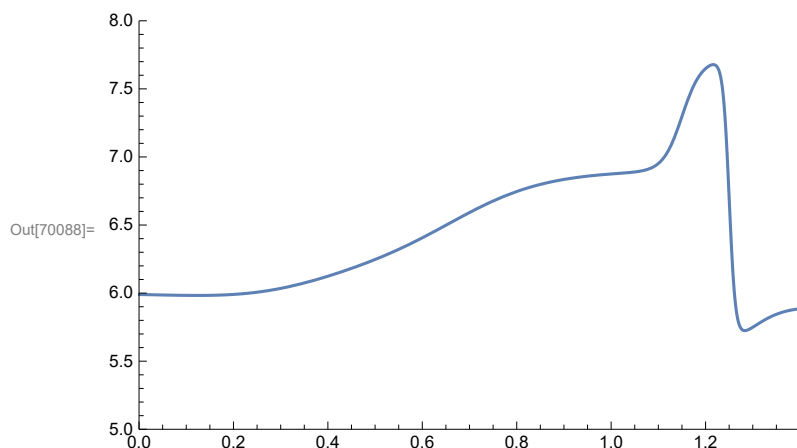


In[70087]:= phfed[x] = phfedtab[[1, 2]] + (phfedtab[[2, 2]] - phfedtab[[1, 2]]) / (1 + e^{-10(x-.15)}) +
 (phfedtab[[3, 2]] - phfedtab[[2, 2]]) / (1 + e^{-10(x-.37)}) +
 (phfedtab[[5, 2]] - phfedtab[[3, 2]]) / (1 + e^{-10(x-.67)}) +
 (phfedtab[[7, 2]] - phfedtab[[6, 2]]) / (1 + e^{-50(x-1.15)}) +
 (phfedtab[[8, 2]] - phfedtab[[7, 2]]) / (1 + e^{-150(x-1.25)}) +
 (phfedtab[[9, 2]] - phfedtab[[8, 2]]) / (1 + e^{-30(x-1.3)})

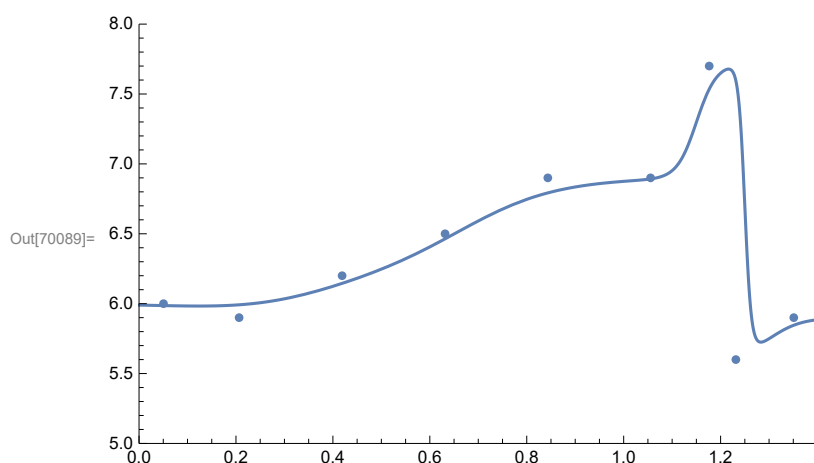
Out[70087]=
$$6. + \frac{0.3}{1 + e^{-30(-1.3+x)}} - \frac{2.1}{1 + e^{-150(-1.25+x)}} +$$

$$\frac{0.8}{1 + e^{-50(-1.15+x)}} + \frac{0.7}{1 + e^{-10(-0.67+x)}} + \frac{0.3}{1 + e^{-10(-0.37+x)}} - \frac{0.1}{1 + e^{-10(-0.15+x)}}$$

```
In[70088]:= plot1 = Plot[Evaluate[phfed[x]], {x, 0, 1.4}, PlotRange -> {{0, 1.4}, {5, 8}}]
```



```
In[70089]:= Show[plot1, plot2]
```



Papp(x) with the modified FN method (i.e. including the non-linear part of the pH logPapp curve)-
assuming fasted conditions

Permeability v pH slope profiles do not correspond to the neutral fraction (which would give a slope of 10 in the linear pH range),
but have an average slope of 4.1 ± 2.1 for acids (ma) and 3.9 ± 2.4 for bases (mb)

```
In[70093]:= ma;  
mb;
```

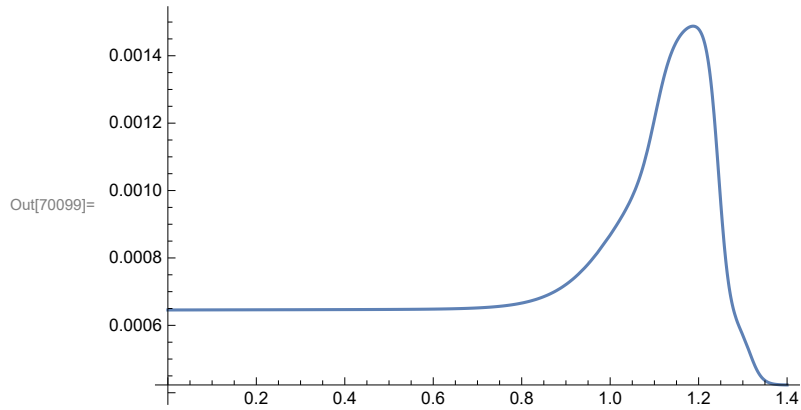
```
In[70095]:= fn[x] = 1 / (1 + acidflag (10^ (ma / 10 (phfast[x] - pkaa))) +  
baseflag (10^ (mb / 10 (pkab - phfast[x]))));
```

```
In[70096]:= fn0 = 1 / (1 + acidflag (10^ (ma / 10 (ph0 - pkaa))) + baseflag (10^ (mb / 10 (pkab - ph0))));
```

```
In[70097]:= p = papp0 / fn0;
```

```
In[70098]:= papp[x] = p fn[x];
```

```
In[70099]:= Plot[Evaluate[papp[x]], {x, 0, 1.4}]
```



Radial diffusion rate constant

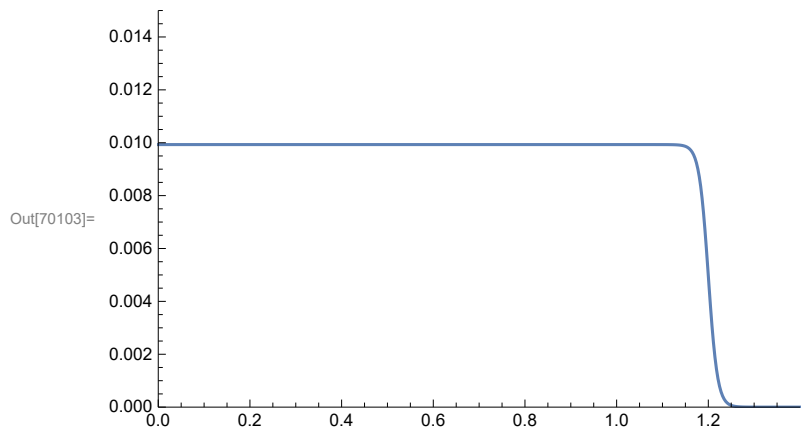
Effective diffusion rate in 1 dimension (m/hr), accounting for 8X increase due to mixing

```
In[70100]:= ClearAll[diffr1]
```

```
In[70101]:= diffrad = 0.01;
```

```
In[70102]:= diffr1[x] = 0.5 diffrad (1 - (1 - 0.014) Tanh[2. (x - 5.)]) 0.5 (1 - Tanh[50 (x - 1.2)]);
```

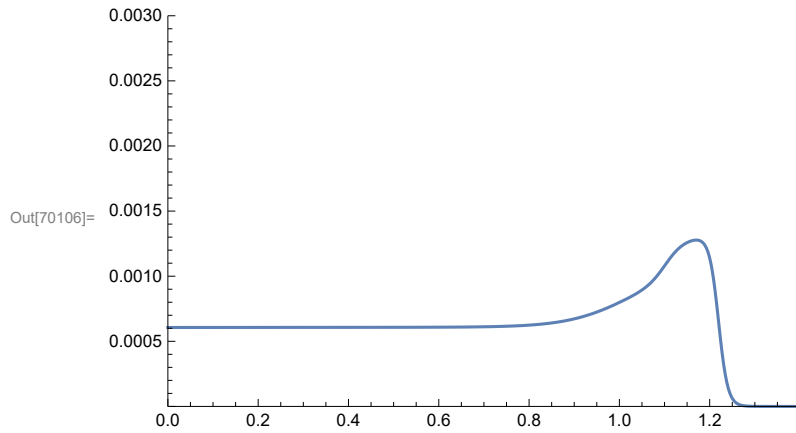
```
In[70103]:= Plot[Evaluate[diffr1[x]], {x, 0, 10}, PlotRange -> {{0, 1.4}, {0, 0.015}}]
```



```
In[70104]:= Evaluate[diffr1[x] /. x -> {1.0, 1.4}];
```

```
In[70105]:= papp2[x] = diffr1[x] × papp[x] / (diffr1[x] + papp[x]);
```

```
In[70106]:= Plot[Evaluate[papp2[x]], {x, 0, 10}, PlotRange -> {{0, 1.4}, {0, 0.003}}]
```



Drug Parameters

Partition coefficient based on 0.7 uL lipid per 1 mg microsomal protein

```
In[70107]:= Kp = ((1 - fumics) / fumics) (1 / 0.0007);
```

```
In[70108]:= cli[x] = 4 papp[x] × sa[x];
```

```
In[70109]:= clo[x] = cli[x] / Kp;
```

```
In[70110]:= cli2[x] = 4 papp2[x] × sa[x];
```

```
In[70111]:= clo2[x] = cli2[x] / Kp;
cli3[x] = 4 papp[x] 100 sa[x];
clo3[x] = cli3[x] / Kp;
```

Solution Pulse in stomach w lag

Velocity leaving stomach (m/hr)

```
In[70114]:= vel0 = vel[x] /. x → 0;
```

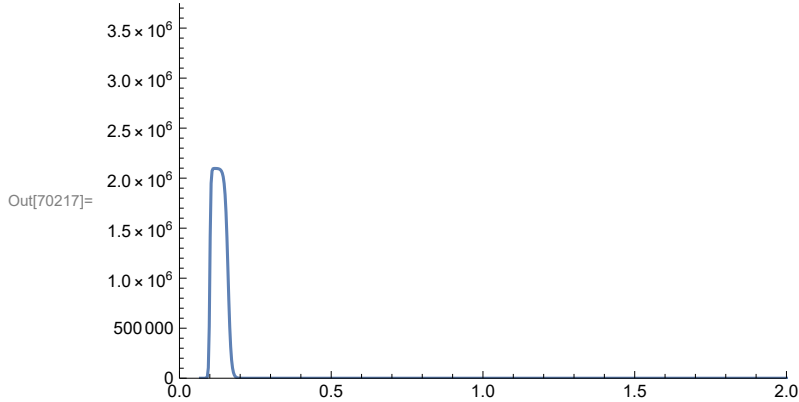
```
In[70115]:= volcor = vol0 / ( $\pi$  r1^2 p11 vel0);
```

Use a single smoothed pulse input function

```
In[70116]:= upulse1[t] = 0.5 (Tanh[300. (t - lag)] - Tanh[100. (t - (p11 + lag))]);
```

```
In[70117]:= pulse1[t] = C0 volcor upulse1[t];
```

```
In[70217]:= Plot[Evaluate[pulse1[t]], {t, 0, 10}, PlotRange -> {{0, 2}, {0, 2.5 dose1 / vol0}}]
```



```
In[70119]:= NIntegrate[pulse1[t] vel0 xa1, {t, 0, 1.0}];
```


```
In[70120]:= c10 = Evaluate[pulse1[t] /. t -> 0];
```

```
In[70121]:= coordx = Join[0. + Range[0, 450] / 3000, 0.15 + Range[1, 250] / 1000,
  0.40 + Range[1, 40] / 200, 0.6 + Range[1, 15.0] / 100.0, 0.75 + Range[1, 13] / 20.0];
```


```
In[70122]:= Length[coordx];
```

PDEs Solution Dose


```
In[70123]:= soln = NDSolve[{
  D[C1[t, x], t] == dif2[x] × D[C1[t, x], {x, 2}] +
    (-vel2[x] + ddif2[x] + dif2[x] × dxa[x] / xa[x]) D[C1[t, x], x] +
    C1[t, x] (-dvel[x] - (dxa[x] / xa[x]) vel2[x]) - cli2[x] × C1[t, x] / xa[x] +
    clo2[x] × C2[t, x] / xa[x], D[C2[t, x], t] == cli2[x] × C1[t, x] / xamem[x] -
    (clo[x] + clo2[x]) C2[t, x] / xamem[x] + cli[x] × C3[t, x] / xamem[x],
  D[C3[t, x], t] == clo[x] × C2[t, x] / xacell[x] - cli[x] × C3[t, x] / xacell[x] - cli3[x] ×
    C3[t, x] / xacell[x] + clo3[x] × C4[t, x] / xacell[x] - (cli[x] / 2) C3[t, x] / xacell[x],
  D[C4[t, x], t] == -clo3[x] × C4[t, x] / xalip[x] + cli3[x] × C3[t, x] / xalip[x],
  {
    C1[t, 0] == pulse1[t], C1[0, x] == c10, C1[t, 1.4] == 0,
    C2[0, x] == 0, C2[t, 0] == 0, C2[t, 1.4] == 0, C3[0, x] == 0, C3[t, 0] == 0,
    C3[t, 1.4] == 0, C4[t, 0] == 0, C4[0, x] == 0, C4[t, 1.4] == 0}},
  {C1, C2, C3, C4}, {t, 0, 24}, {x, 0, 1.4}, (*MaxStepSize->0.005,*)
  (*Method->{"FiniteElement", "MeshOptions" -> {MaxCellMeasure -> 0.0005}} *)
  Method -> {"PDEDiscretization" -> {"MethodOfLines",
    (*"DiscretizedMonitorVariables" -> True, *) "SpatialDiscretization" ->
    {"TensorProductGrid", "Coordinates" -> {coordx}, "DifferenceOrder" -> 2}}}]
```

```
Out[70123]= {{C1 → InterpolatingFunction[ Domain: {{0., 24.}, {0., 1.4}} Output: scalar ],  

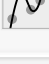
Data not in notebook; Store now »  

C2 → InterpolatingFunction[ Domain: {{0., 24.}, {0., 1.4}} Output: scalar ],  

Data not in notebook; Store now »  

C3 → InterpolatingFunction[ Domain: {{0., 24.}, {0., 1.4}} Output: scalar ],  

Data not in notebook; Store now »  

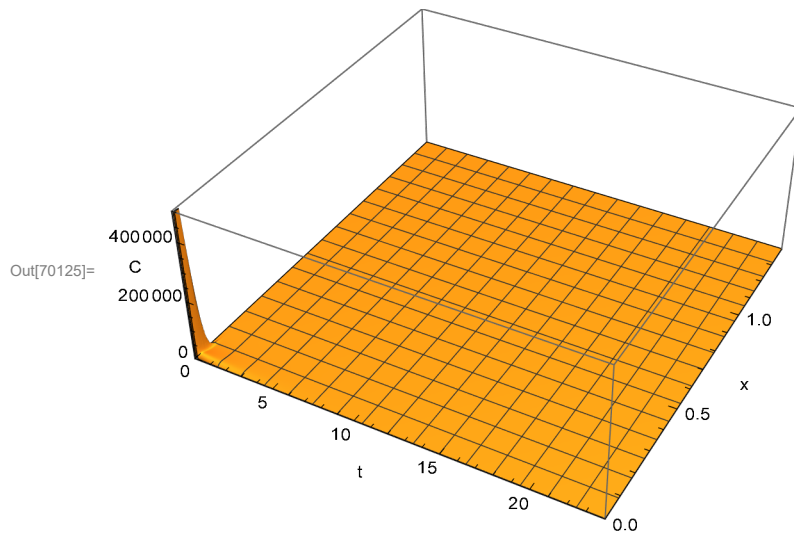
C4 → InterpolatingFunction[ Domain: {{0., 24.}, {0., 1.4}} Output: scalar ]}}
```

```
In[70124]:= C1[0.2, .0] /. soln;
```

```
In[70125]:= plot1 = Plot3D[C1[t, x] /. soln, {t, 0, 24},  

{x, 0, 1.4}, PlotRange → {{0, 24}, {0, 1.4}, {-2000, 500000}},  

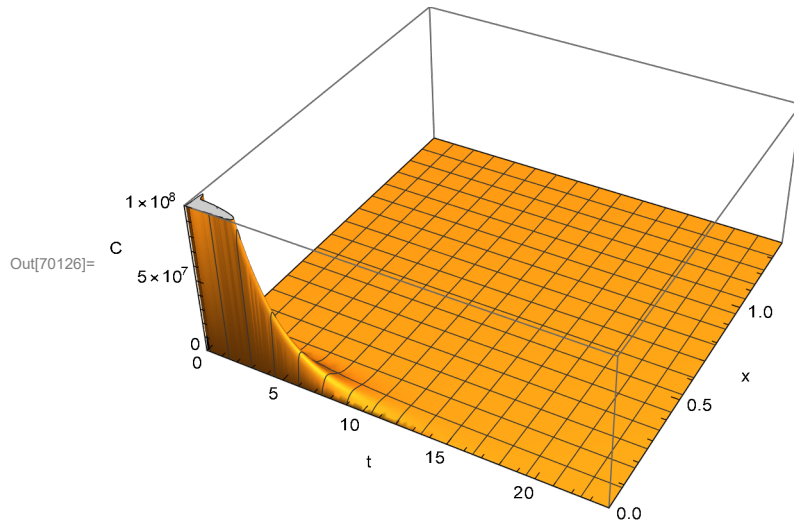
AxesLabel → {"t", "x", "C"}, MaxRecursion → 7]
```



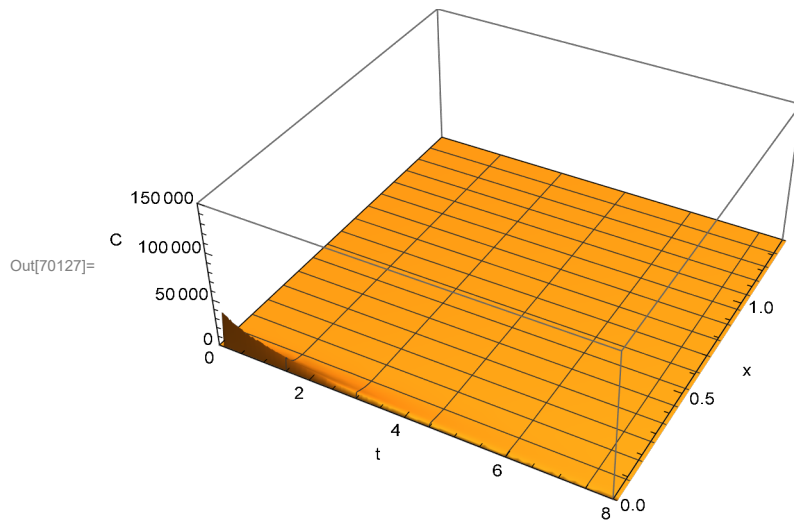
```
In[70126]:= plot4 = Plot3D[C2[t, x] /. soln, {t, 0, 24},  

{x, 0, 1.4}, PlotRange → {{0, 24}, {0, 1.4}, {-1000, 100000000}},  

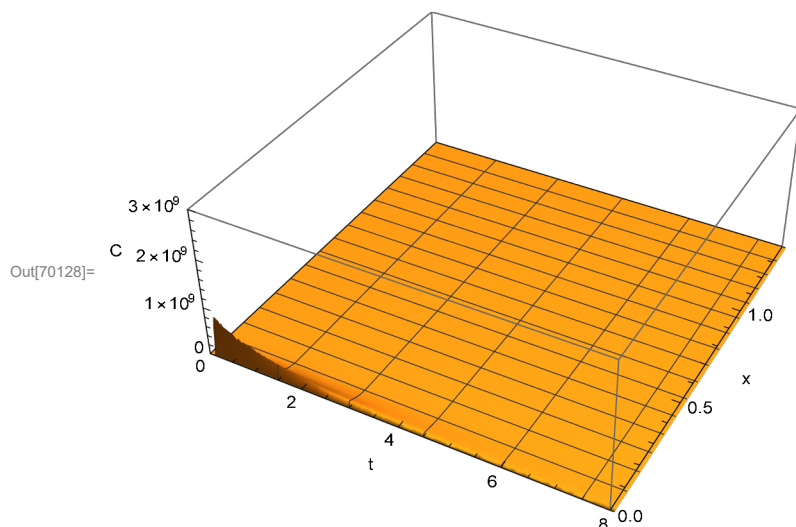
AxesLabel → {"t", "x", "C"}, MaxRecursion → 7]
```



```
In[70127]:= plot5 = Plot3D[C3[t, x] /. soln, {t, 0, 24},
  {x, 0, 1.4}, PlotRange -> {{0, 8}, {0, 1.4}, {-100, 150000}},
  AxesLabel -> {"t", "x", "C"}, MaxRecursion -> 7]
```



```
In[70128]:= plot6 = Plot3D[C4[t, x] /. soln, {t, 0, 24},
  {x, 0, 1.4}, PlotRange -> {{0, 8}, {0, 1.4}, {-100, 3000000000}},
  AxesLabel -> {"t", "x", "C"}, MaxRecursion -> 7]
```



```
In[70129]:= amtout = NIntegrate[ ((cli[x] / 2) C3[t, x]) /. soln[[1]], {t, 0, 24},
  {x, 0, 1.4}, AccuracyGoal -> 7, Method -> "AdaptiveQuasiMonteCarlo"]
```

Out[70129]= 1.49794

```
In[70130]:= residC1 = NIntegrate[ (C1[24, x] × xa[x]) /. soln[[1]],
  {x, 0, 1.4}, AccuracyGoal -> 7, Method -> "AdaptiveQuasiMonteCarlo"]
```

Out[70130]= 8.41623×10^{-8}

```
In[70131]:= residC2 = NIntegrate[ (C2[24, x] × xamem[x]) /. soln[[1]],
  {x, 0, 1.4}, AccuracyGoal -> 7, Method -> "AdaptiveQuasiMonteCarlo"]
```

Out[70131]= 1.19718×10^{-6}

```
In[70132]:= residC3 = NIntegrate[ (C3[24, x] × xacell[x]) /. soln[[1]],
  {x, 0, 1.4}, AccuracyGoal -> 7, Method -> "AdaptiveQuasiMonteCarlo"]
```

Out[70132]= 2.31099×10^{-8}

```
In[70133]:= residC4 = NIntegrate[ (C4[24, x] × xalip[x]) /. soln[[1]],
  {x, 0, 1.4}, AccuracyGoal -> 7, Method -> "AdaptiveQuasiMonteCarlo"]
```

Out[70133]= 0.0000389725

```
In[70134]:= total = amtout + residC1 + residC2 + residC3 + residC4
```

Out[70134]= 1.49799

```
In[70135]:= facalc = amtout / total
```

Out[70135]= 0.999973

```
In[70136]:= total / dose1
```

Out[70136]= 0.998657

```
In[70137]:= (*ClearAll[c42]*)
```

```
In[70138]:= ClearAll[c5]
```

C4 is dA/Dt in mg/hr

```
In[70139]:= c5[t_] = NIntegrate[ ((cli[x] / 2) C3[t, x]) /. soln[[1]],
  {x, 0, 1.4}, AccuracyGoal -> 7, Method -> "AdaptiveQuasiMonteCarlo"]
```

```
Out[70139]= NIntegrate[  $\frac{1}{2}$  cli[x] × C3[t, x] /. soln[[1]],
  {x, 0, 1.4}, AccuracyGoal -> 7, Method -> AdaptiveQuasiMonteCarlo ]
```


```
In[70140]:= c5t1 = Table[{t, If[c5[t] < 0, 0, c5[t]]}, {t, 0, 2, 0.05}];
```

```
In[70141]:= c5t2 = Table[{t, If[c5[t] < 0, 0, c5[t]]}, {t, 3, 24, 1.}];
```

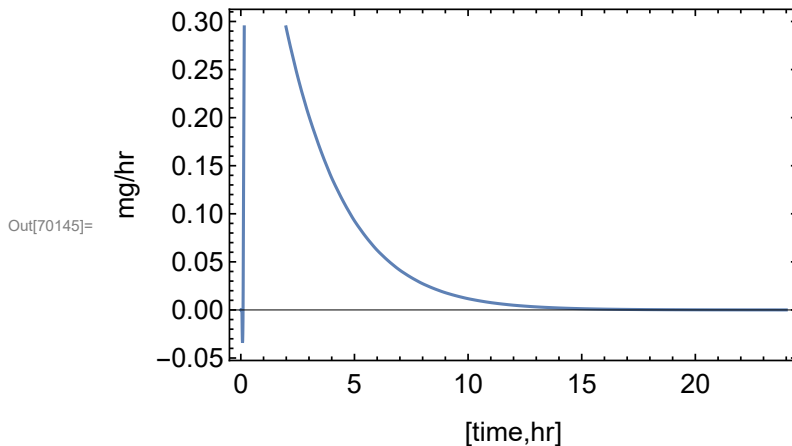
```
In[70142]:= c5t3 = Table[{t, 0}, {t, 25., 200., 10.0}];
```

```
In[70143]:= c5t = Join[c5t1, c5t2(*,c5t3*)];
```

```
In[70144]:= c5fun = Interpolation[c5t, InterpolationOrder -> 2]
```

```
Out[70144]= InterpolatingFunction[  Domain: {{0., 24.}}
  Output: scalar ]
```

```
In[70145]:= plot6 = Plot[Evaluate[c5fun[t]], {t, 0, 24},
  PlotRange -> {{0, 8}, {0, 1.2 Max[Table[c5t1[[i, 2]], {i, 1, 100}]]}},
  (*Epilog->{PointSize[Medium],Point[c4t]},*) Frame -> True,
  FrameStyle -> Directive[Black, 14, Thickness[0.003]],
  LabelStyle -> (FontFamily -> "Arial"), Framelabel -> {"[time,hr]", "mg/hr"}]
```



```
In[70146]:= Integrate[c5fun[t], {t, 0, 24}];
```

Apply to drug PK model for an IV dose- 2C model

```
In[70147]:= ClearAll[modelpkiv1, modelpkiv2, modelpko1, modelIV, fitiv, dataIV]
```

Data in hr, ng/mL - in house collection (n=3); dose - 2 mg/kg for a 300 g rat.

```
In[70148]:= dataIV = {{0.0933, 246.266}, {0.266, 140.66}, {0.511, 93.3}, {1., 70.7}, {2.010, 48.93},
  {4., 33.4}, {6.02, 22.33}, {8.016, 14.01}, {10., 7.30}, {12., 4.045}};
```

```
In[70149]:= nt = Length[dataIV];
```

```

In[70150]:= colort = {Red, Blue, Orange, Green, Purple, Cyan, Brown};

In[70151]:= k10init = 1;
            k12init = 4;
            k21init = 1.5;
            V1init = 1000.;

In[70155]:= doseiv = 1000000 dose2 ; (*in ng*)

In[70156]:= modelIV[k12_?NumericQ, k21_?NumericQ, k10_?NumericQ, V1_?NumericQ, te_?NumericQ] :=
            (modeliv[k12, k21, k10, V1, te] =
              (Xc[te] / V1) /. First[NDSolve[{Xc'[t] == - (k12 + k10) Xc[t] + k21 Xp1[t],
              Xp1'[t] == k12 Xc[t] - k21 Xp1[t],
              Xc[0] == doseiv,
              Xp1[0] == 0},
              {Xc, Xp1}, {t, 0, 35}, MaxSteps -> 10000, PrecisionGoal -> ∞]])

In[70157]:= fitiv = NonlinearModelFit[dataIV, modelIV[k12, k21, k10, V1, te],
            {{k12, k12init}, {k21, k21init}, {k10, k10init}, {V1, V1init}},
            {te}, PrecisionGoal -> ∞, MaxIterations -> 10000, Weights -> (1 / #2 &)]

Out[70157]= FittedModel[modelIV[3.79766, 1.62191, 0.915213, 1606.08, te]]

```

In[70158]:= **fitiv["ParameterTable"]**

	Estimate	Standard Error	t-Statistic	P-Value
k12	3.79766	0.115422	32.9024	5.24372×10^{-8}
k21	1.62191	0.101747	15.9406	3.86958×10^{-6}
k10	0.915213	0.0344475	26.5684	1.87701×10^{-7}
V1	1606.08	57.1591	28.0985	1.34454×10^{-7}

In[70159]:= **fitiv["RSquared"]**

Out[70159]= **0.998332**

In[70160]:= **fitiv["AICc"]**

Out[70160]= **68.5088**

In[70161]:= **TableForm[fitiv["CorrelationMatrix"]]**

Out[70161]//TableForm=

1.	0.178909	0.289208	-0.635838
0.178909	1.	-0.325473	0.26806
0.289208	-0.325473	1.	-0.74874
-0.635838	0.26806	-0.74874	1.

In[70162]:= **k12 = fitiv["BestFitParameters"][[1, 2]];**

In[70163]:= **k21 = fitiv["BestFitParameters"][[2, 2]];**

In[70164]:= **k10 = fitiv["BestFitParameters"][[3, 2]];**

In[70165]:= **V1 = fitiv["BestFitParameters"][[4, 2]];**

In[70166]:= **fitiv["FitResiduals"]**

Out[70166]= **{-1.55442, 1.64255, 2.85587, 1.04588,
-5.0229, 0.180918, 2.02531, 1.52624, -0.397759, -0.683135}**

In[70167]:= **fitiv["PredictedResponse"]**

Out[70167]= **{247.82, 139.017, 90.4441, 69.6541, 53.9529, 33.2191, 20.3047, 12.4838, 7.69776, 4.72813}**

In[70168]:= **ClearAll[modelpkiv2];**

```
modelpkiv2 = First[NDSolve[{Xc'[t] == -(k12 + k10) Xc[t] + k21 Xp1[t],  
Xp1'[t] == k12 Xc[t] - k21 Xp1[t],  
Xc[0] == doseiv,  
Xp1[0] == 0},  
{Xc, Xp1}, {t, 0, 35}, MaxSteps -> 10000, PrecisionGoal -> ∞];
```

In[70170]:= **CL = k10 V1**

Out[70170]= **1469.91**

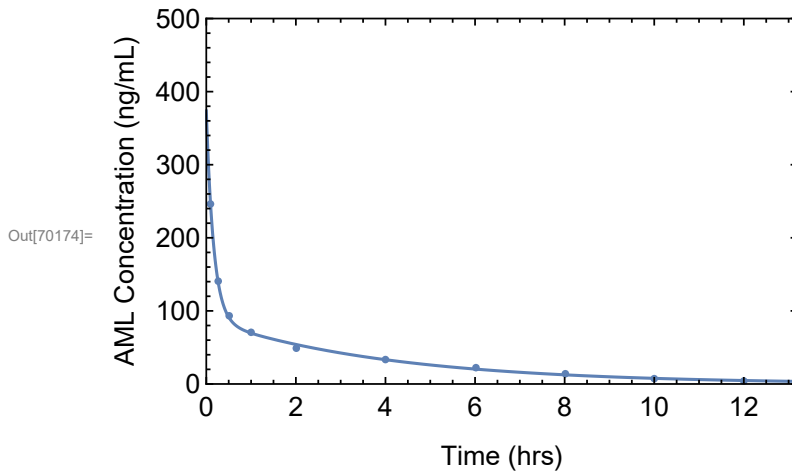
In[70171]:= **beta = 1 / 2 ((k12 + k21 + k10) - ((k12 + k21 + k10)^2 - 4 k21 k10)^0.5)**

Out[70171]= **0.243699**

```
In[70172]:= plot1 = Plot[(Xc[t] / V1) /. modelpkiv2, {t, 0, 1.1 dataIV[[nt, 1]]},
  PlotRange -> {{0, 1.1 dataIV[[nt, 1]]}, {0, 500.}}, Frame -> True,
  FrameStyle -> Directive[Black, 14, Thickness[0.003]], LabelStyle ->
  (FontFamily -> "Arial"), FrameLabel -> {"Time (hrs)", "AML Concentration (ng/mL)"}];
```

```
In[70173]:= plot2 = ListPlot[dataIV, PlotRange -> {{0, 24}, {0, 15.}}];
```

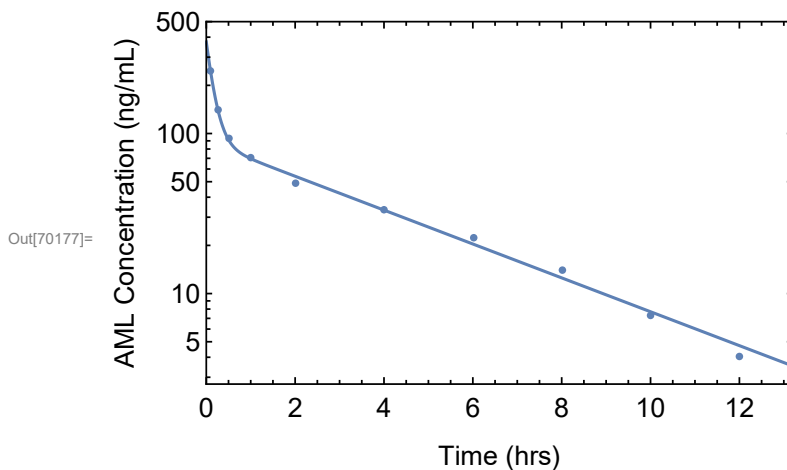
```
In[70174]:= Show[plot1, plot2]
```



```
In[70175]:= plot3 = LogPlot[(Xc[t] / V1) /. modelpkiv2, {t, 0, 1.1 dataIV[[nt, 1]]},
  PlotRange -> {{0, 1.1 dataIV[[nt, 1]]}, {0, 500}}, Frame -> True,
  FrameStyle -> Directive[Black, 14, Thickness[0.003]], LabelStyle ->
  (FontFamily -> "Arial"), FrameLabel -> {"Time (hrs)", "AML Concentration (ng/mL)"}];
```

```
In[70176]:= plot4 = ListLogPlot[dataIV];
```

```
In[70177]:= Show[plot3, plot4]
```



Oral PK inputs (5mg/kg dose-fasted 2hr). Data in ng/ml and hr

```
In[70178]:= dataP0 = {{0.203, 5.55}, {0.52, 11.82}, {1.0, 17.35}, {1.5, 28.55}, {2.5, 34.90},
  {4.0, 22.41}, {6.0, 16.37}, {8.0, 9.517}, {10.0, 7.908}, {24.0, 1.065}};
```

```
In[70179]:= nt = Length[dataP0];
```

$$F = Fa * Fg * Fh$$

```
In[70180]:= fgfh = f / facalc
```

```
Out[70180]= 0.500013
```

Drug VD in mL

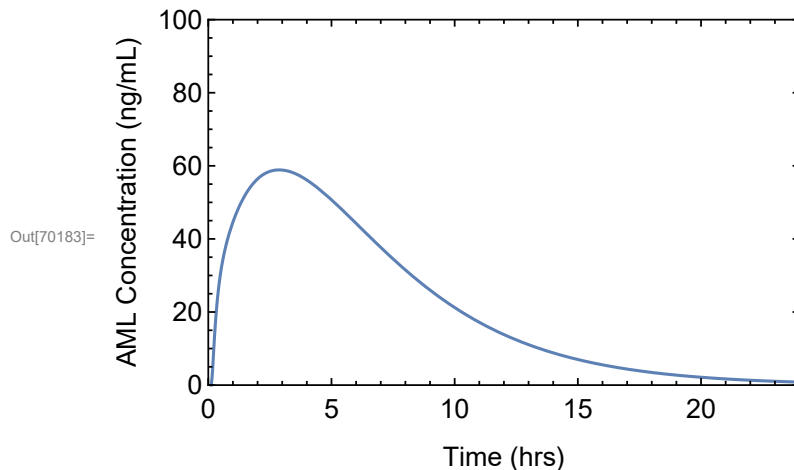
```
In[70181]:= ClearAll[modelpko1];
```

```
modelpko1 =
```

```
First[NDSolve[{Xc'[t] == 1000000 fgfh c5fun[t] - (k12 + k10) Xc[t] + k21 Xp1[t],
  Xp1'[t] == k12 Xc[t] - k21 Xp1[t],
  Xc[0] == 0,
  Xp1[0] == 0},
  {Xc, Xp1}, {t, 0, 35}, MaxSteps -> 100000, PrecisionGoal -> ∞];
```

```
In[70183]:= plotpk1 =
```

```
Plot[(Xc[t] / V1) /. modelpko1, {t, 0, 24}, PlotRange -> {{0, 24}, {0, 100}}, Frame -> True,
  FrameStyle -> Directive[Black, 14, Thickness[0.003]], LabelStyle -> (FontFamily -> "Arial"),
  FrameLabel -> {"Time (hrs)", "AML Concentration (ng/mL)"}]
```



```
Show[plotpk1, ListPlot[dataP0]];
```

```
In[70185]:= ClearAll[dataP02, interpP0, plotintP0, aucon];
```

```
In[70186]:= npo = Length[dataP0];
```

```
In[70187]:= auciv = NIntegrate[(Xc[t] / V1) /. modelpkiv2, {t, 0, 24}]
```

```
Out[70187]= 407.147
```

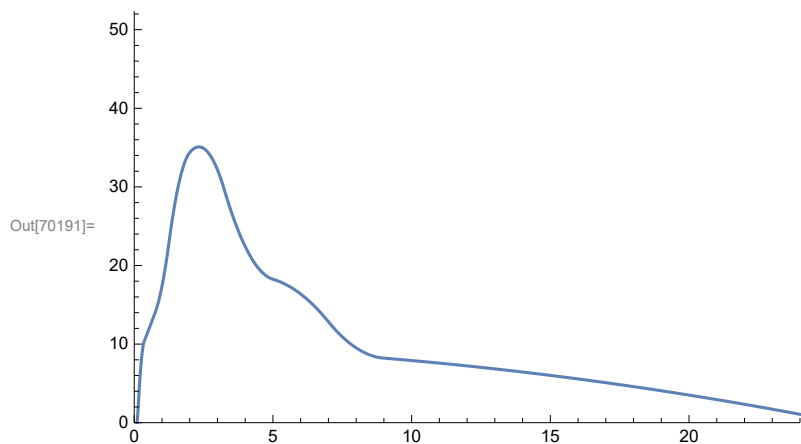
```
In[70188]:= dataP02 = Join[{{0, 0}, {Min[0.1, dataP0[[1, 1]] / 2], 0}}, dataP0];
```

```
In[70189]:= ymax = Max[Flatten[dataP0][[2 ;; 2 npo ;; 2]]]
```

```
Out[70189]= 34.9
```

```
In[70190]:= interpP0 = Interpolation[dataP02, InterpolationOrder -> 2, Method -> "Spline"];
```

```
In[70191]:= plotintP0 = Plot[Evaluate[interpP0[t]],
  {t, 0, 1.2 dataP0[[npo, 1]]}, PlotRange -> {{0, dataP0[[npo, 1]]}, {0, 1.5 ymax}}]
```



In[70192]:= **aucintP0n = NIntegrate[interpP0[t], {t, 0, dataP0[[npo, 1]]}]**

Out[70192]= 247.252

In[70193]:= **aucon = NIntegrate[Xc[t] / V1 /. modelpko1, {t, 0, dataP0[[npo, 1]]}]**

Out[70193]= 512.992

In[70194]:= **overlap = NIntegrate[Min[interpP0[t], (aucintP0n / aucon) ((Xc[t] / V1) /. modelpko1)],
{t, 0, dataP0[[npo, 1]]}]**

Out[70194]= 210.268

In[70195]:= **(aucintP0n / aucon)**

Out[70195]= 0.481981

In[70196]:= **overlap / aucintP0n**

Out[70196]= 0.850419

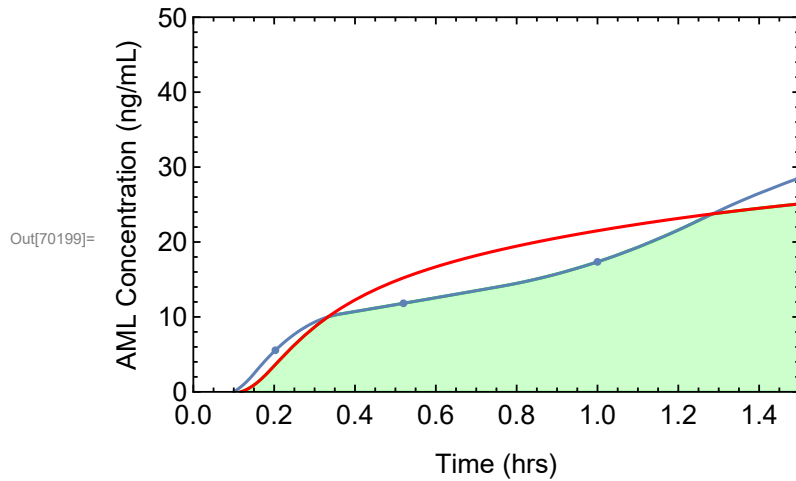
```

In[70197]:= plotnormsimPO = Plot[Evaluate[(aucintPOn / aucon) ((Xc[t] / V1) /. modelpko1)],
  {t, 0, 1.5}, PlotRange -> {{0, 1.5}, {0, 1.5 Max[dataPO2]}}, PlotStyle -> Red];

In[70198]:= plotoverlap = Plot[Min[interpPO[t], (aucintPOn / aucon) ((Xc[t] / V1) /. modelpko1)],
  {t, 0, 24}, PlotRange -> {{0, 1.5}, {0, 50}}, PlotStyle -> Green, Filling -> Axis,
  Frame -> True, FrameStyle -> Directive[Black, 14, Thickness[0.003]], LabelStyle ->
  (FontFamily -> "Arial"), FrameLabel -> {"Time (hrs)", "AML Concentration (ng/mL)"}];

In[70199]:= Show[plotoverlap, plotintPO, plotnormsimPO, ListPlot[dataPO]]

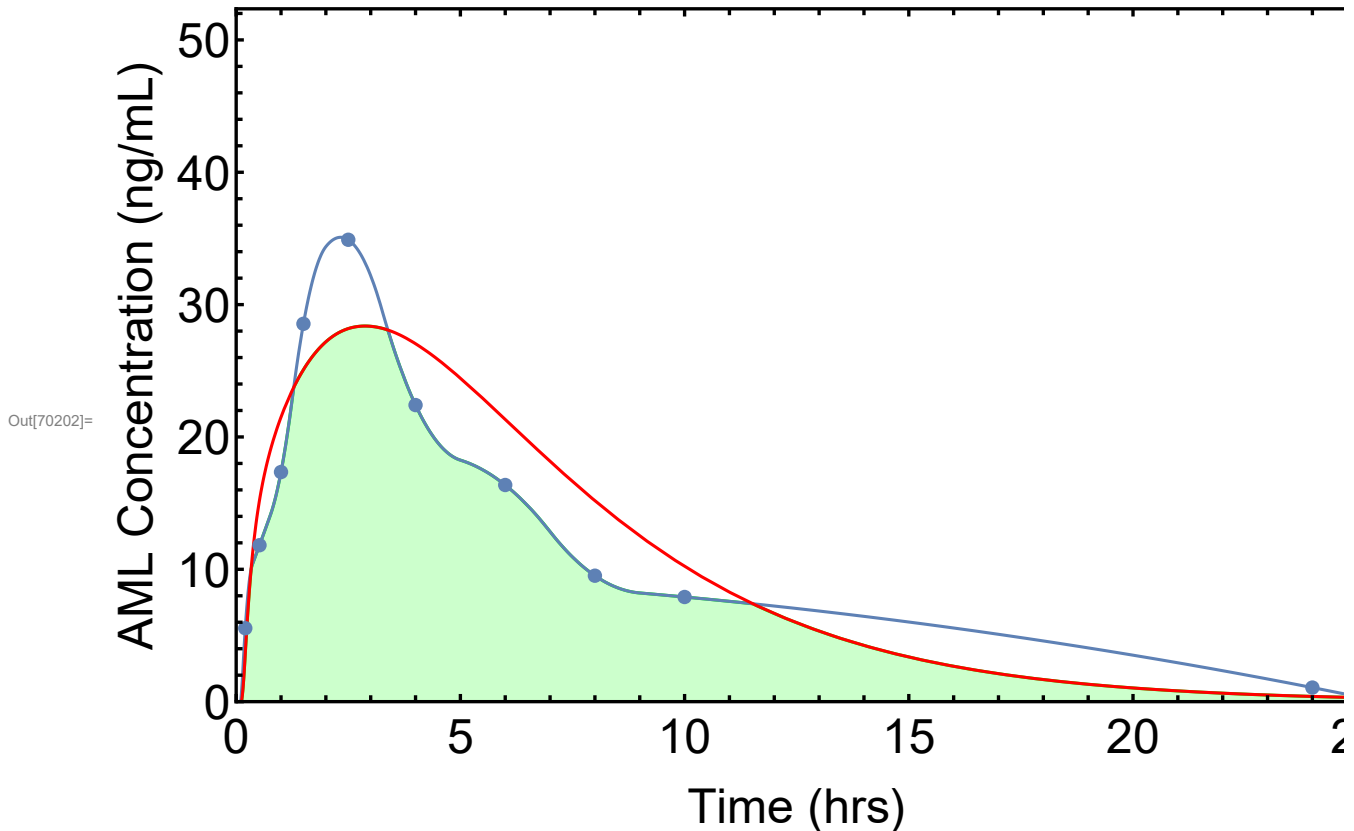
```



```

In[70200]:= plotoverlap3 = Plot[Min[interpP0[t], (aucintP0n / aucon) ((Xc[t] / V1) /. modelpko1)],
  {t, 0, 50}, PlotRange -> {{0, 25}, {0, 1.5 ymax}}, PlotStyle -> Green, Filling -> Axis,
  Frame -> True, FrameStyle -> Directive[Black, 25, Thickness[0.003]], LabelStyle ->
  (FontFamily -> "Arial"), FrameLabel -> {"Time (hrs)", "AML Concentration (ng/mL)"}];
plotnormsimP03 = Plot[Evaluate[(aucintP0n / aucon) ((Xc[t] / V1) /. modelpko1)],
  {t, 0, 30}, PlotRange -> {{0, 25}, {0, 50}}, PlotStyle -> Red];
Show[plotoverlap3, plotintP0, plotnormsimP03, ListPlot[dataP0]]

```



Calculate experimental oral AUC by extending the oral data to infinity (assume 1st order terminal elimination).

```

In[70203]:= auctailo = dataP02[[npo + 1, 2]] / beta

```

```

Out[70203]= 32.4498

```

```

In[70204]:= aucpo = aucintP0n + auctailo

```

```

Out[70204]= 279.702

```

```

In[70205]:= fcalc = aucpo dose2 / (auciv dose1)

```

```

Out[70205]= 0.274793

```

Calculate Cmax and Tmax, exp and pred

```

In[70206]:= ClearAll[cmax, intt];

```

```

In[70207]:= intt = Table[{i, interpP0[i]}, {i, 0, dataP02[[npo + 1, 1]], 0.1}];

```

```
In[70208]:= itt2 = Flatten[intt];
```

```
In[70209]:= cmax = Max[itt2[[2 ;; Length[itt2] - 1 ;; 2]]]
```

```
Out[70209]= 35.0801
```

```
In[70210]:= tmax = Flatten[Position[intt, cmax]][[1]] / 10 - 0.1
```

```
Out[70210]= 2.3
```

```
In[70211]:= predt = Table[{i, Evaluate[(aucintP0n / aucon) ((Xc[i] / V1) /. modelpko1)]},  
  {i, 0, dataP02[[npo + 1, 1]], 0.1}];
```

```
In[70212]:= predt2 = Flatten[predt];
```

```
In[70213]:= cmaxpred = Max[predt2[[2 ;; Length[predt2] - 1 ;; 2]]]
```

```
Out[70213]= 28.379
```

```
In[70214]:= tmaxpred = Flatten[Position[predt, cmaxpred]][[1]] / 10 - 0.1
```

```
Out[70214]= 2.9
```

APPENDIX D- EXAMPLE SUSPENSION NOTEBOOK

Attached PDF

```

In[1]:= ClearAll["Global`*"];
In[2]:= Needs["NDSolve`FEM` "]
In[3]:= SetDirectory["/Users/korzekwa/Dropbox/Casey Manuscript "];
In[4]:= datafile = "CCR.rat.abs.data.soln.08.03.xlsx";
In[5]:= sheet = 1;
In[6]:= compd = 8;
In[7]:= cacof = 2.4;
      Drug specific parameters
In[8]:= {drug, f, fabs, fabscol, papp0, sol1, sol2, rho, fumics, dose1, vol0, dose2,
      inftime, xp2, ph0, pkaa, pkab, ma, mb, acidflag, baseflag, difc, psize} =
      Import[datafile, {"Data", sheet, compd + 1, Range[1, 23]}]
Out[8]:= {GLY (42.7 um), 0.05, 67., 100., 18.9, 0.006, 0.006, 1.33, 0.72,
      3., 1., 1.2, 0.01, 4., 7.4, 5.1, 1., 1., 4., 1., 0., 2.24 × 10-6, 42.7}

In[9]:= (*papp0=100 papp0*)
      Drug dose in mg

In[10]:= (*f=.15*)
      Solubility (mg/m^3)

In[11]:= sol1 = sol1 1 000 000 ;
In[12]:= sol2 = sol2 1 000 000. ;
      Rho (mg/m^3)

In[13]:= rho = rho 1 000 000 000 ;
      Particle size m

In[14]:= psize = psize 10 ^-6
Out[14]= 0.0000427
      difc in m^2/hr

In[15]:= difc
Out[15]= 2.24 × 10-6
      Fraction unbound in microsomes at 1 mg/mL

In[16]:= fumics = 0.89
Out[16]= 0.89
      CACO2 Papp in m/hr (cm/sec*36 = m/hr)

In[17]:= papp0 = papp0 36 × 10 ^-6. ;

```

```
In[18]:= papp0 = papp0 cacosf ;
```

Drug dose in mg (for abs model, ug for PK), vol in m³, infusion time in hr

```
In[19]:= vol0 = vol0 10 ^ -6
```

```
Out[19]= 1. × 10-6
```

Plug length time in m /(m/hr)

```
In[20]:= pl1 = 0.3;(*stomach pulse length*)
```

```
In[21]:= lag = 0.1 ;
```

Concentration in Dosing solution mg/L=g/m³ (g/m³)

```
In[22]:= C0 = dose1 / vol0
```

```
Out[22]= 3. × 106
```

Rat Physiology

Radii (m)

duodenum, J1, J2, J3, J4, J5, ileum, proximal colon, and distal colon

circumference (cm) from in-house experimental *scaleradii = radii (m) [scaleradii to make circumference in cm to radii in meters]

```
In[23]:= scaleradii = 0.01 / (2 π)
```

```
Out[23]= 0.00159155
```

```

In[24]:= r1 = 0.79 scaleradii ;
         r2 = 0.92 scaleradii ;
         r3 = 0.92 scaleradii ;
         r4 = 0.92 scaleradii ;
         r5 = 0.92 scaleradii ;
         r6 = 0.91 scaleradii ;
         r7 = 0.89 scaleradii ;
         r8 = 1.17 scaleradii ;
         r9 = 1.17 scaleradii ;

```

Distances (m)

Distances measured in-house (specific aim #2) in meters. Distance is where the segment ends (cumulative). Ex: jej2 =duo + jej1+ jej2

```

In[33]:= d0 = 0.0005 ;
         duo = 0.1005 ;
         jej1 = 0.3125 ;
         jej2 = 0.5255 ;
         jej3 = 0.7375 ;
         jej4 = 0.9495 ;
         jej5 = 1.1615 ;
         ile = 1.1915 ;
         proxcol = 1.2715 ;
         distcol = 1.4305 ;

```

Cross sectional area (m²)

From radii listed above

```

In[43]:= xa1 = π r1 ^ 2

```

```

Out[43]= 4.96643 × 10-6

```

```

In[44]:= xa2 = π r2 ^ 2 ;

```

```

In[45]:= xa3 = π r3 ^ 2 ;

```

```

In[46]:= xa4 = π r4 ^ 2 ;

```

```

In[47]:= xa5 = π r5 ^ 2 ;

```

```

In[48]:= xa6 = π r6 ^ 2 ;

```

```

In[49]:= xa7 = π r7 ^ 2 ;

```

```

In[50]:= xa8 = π r8 ^ 2 ;

```

```

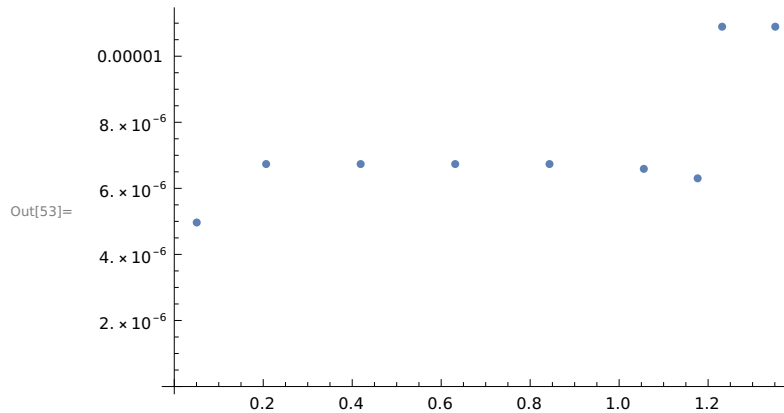
In[51]:= xa9 = π r9 ^ 2 ;

```

```
In[52]:= xat = {{{(duo - d0)/2 + d0, xa1}, {(jej1 - duo)/2 + duo, xa2},
  {(jej2 - jej1)/2 + jej1, xa3}, {(jej3 - jej2)/2 + jej2, xa4},
  {(jej4 - jej3)/2 + jej3, xa5}, {(jej5 - jej4)/2 + jej4, xa6}, {(ile - jej5)/2 + jej5, xa7},
  {(proxcol - ile)/2 + ile, xa8}, {(distcol - proxcol)/2 + proxcol, xa9}}
```

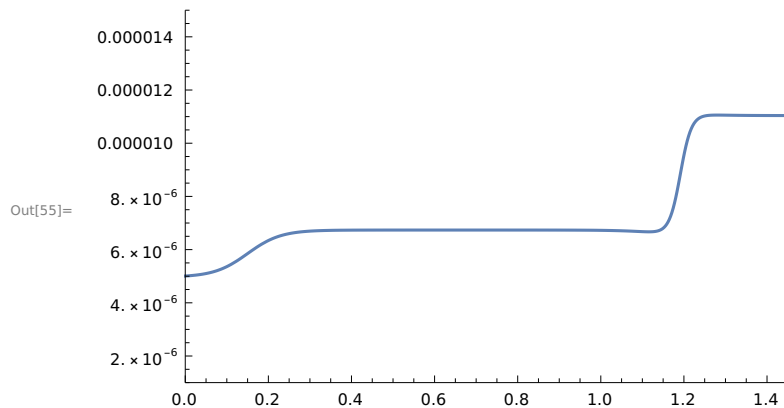
```
Out[52]:= {{0.0505, 4.96643 × 10-6}, {0.2065, 6.73544 × 10-6}, {0.419, 6.73544 × 10-6},
  {0.6315, 6.73544 × 10-6}, {0.8435, 6.73544 × 10-6}, {1.0555, 6.58981 × 10-6},
  {1.1765, 6.30333 × 10-6}, {1.2315, 0.0000108934}, {1.351, 0.0000108934}}
```

```
In[53]:= plot2 = ListPlot[xat]
```

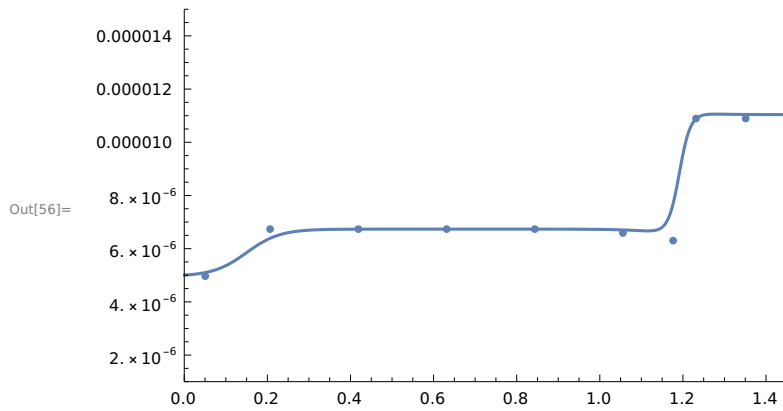


```
In[54]:= xa[x] = xa1 + (xa2 - xa1) / (1 + e-25(x-0.15)) + (xa7 - xa6) / (1 + e-20(x-jej5)) + ((xa8 - xa7)) / (1 + e-75(x-ile));
```

```
In[55]:= plot1 = Plot[Evaluate[xa[x]], {x, 0, 10}, PlotRange -> {{0, 1.450}, {0.000001, 0.000015}}]
```



In[56]:= Show[plot1, plot2]



In[57]:= dxa[x] = D[xa[x], x]

Out[57]=

$$\frac{0.000344252 e^{-75 \cdot (-1.1915 + x)}}{(1 + e^{-75 \cdot (-1.1915 + x)})^2} - \frac{5.72958 \times 10^{-6} e^{-20 \cdot (-1.1615 + x)}}{(1 + e^{-20 \cdot (-1.1615 + x)})^2} + \frac{0.0000442252 e^{-25 \cdot (-0.15 + x)}}{(1 + e^{-25 \cdot (-0.15 + x)})^2}$$

SA per length (or circumference) in m²/m

In[58]:= sa1 = 0.47242 ;

sa2 = 1.116 ;

sa3 = 1.103 ;

sa4 = 0.615 ;

sa5 = 0.0772 ;

In[63]:= sa[x] = sa1 + (sa2 - sa1) / (1 + e^{-50 (x-(d0+duo)/2)}) -
 (sa2 - sa3) / (1 + e^{-50 (x-je4)}) - (sa3 - sa4) / (1 + e^{-50 (x-je5)}) - (sa4 - sa5) / (1 + e^{-50 (x-ile)})

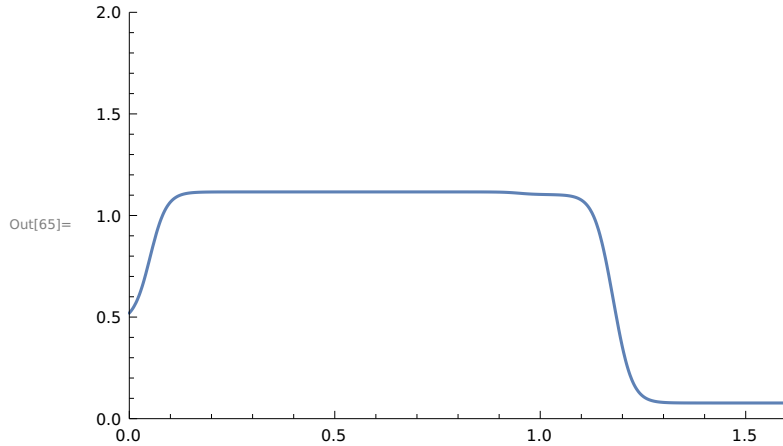
Out[63]=

$$0.47242 - \frac{0.5378}{1 + e^{-50 \cdot (-1.1915 + x)}} - \frac{0.488}{1 + e^{-50 \cdot (-1.1615 + x)}} - \frac{0.013}{1 + e^{-50 \cdot (-0.9495 + x)}} + \frac{0.64358}{1 + e^{-50 \cdot (-0.0505 + x)}}$$

In[64]:= sa[x] /. x -> 0

Out[64]= 0.520125

In[65]:= Plot[Evaluate[sa[x]], {x, 0, 1.6}, PlotRange -> {{0, 1.6}, {0, 2}}



microvilli factor as a function of x

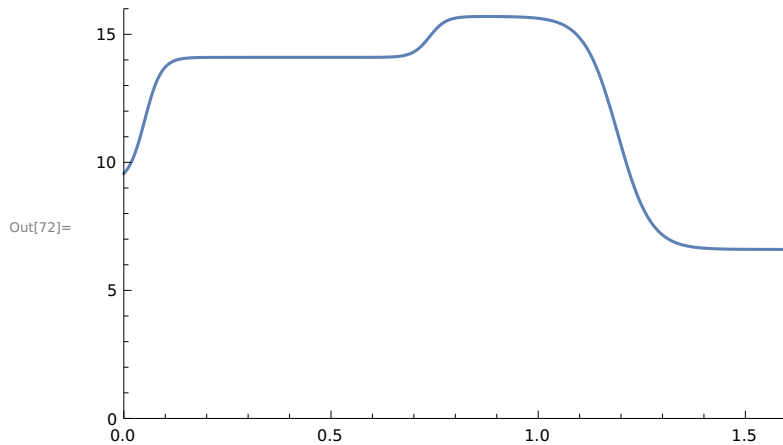
```
In[66]:= mf1 = 9.2 ;
mf2 = 14.1 ;
mf3 = 15.7 ;
mf4 = 6.6 ;
```

```
In[70]:= mf[x] =
mf1 + (mf2 - mf1) / (1 + e-50 (x-(d0+d0o)/2)) - (mf2 - mf3) / (1 + e-50 (x-je3)) - (mf3 - mf4) / (1 + e-25 (x-ile));
```

```
In[71]:= mf[x] /. x -> 0
```

Out[71]= 9.56321

```
In[72]:= Plot[Evaluate[mf[x]], {x, 0, 1.6}, PlotRange -> {{0, 1.6}, {0, 16}}]
```



Cross sectional surface areas of cells (m²)

Cell: SA of the small intestine/ colon was multiplied by the diameter of an enterocyte (20 μm) [20 μm = 0.000020 meters]

Membrane: SA of the small intestine/ colon was multiplied by width of the plasma membrane (35 Å) [35 Å = 0.000000035 meters]

Microvilli are only present on apical surface of epithelial cells, so only apical membrane includes villi and microvilli (not divided by mf [microvilli factor])

Lipids: SA of the small intestine/ colon was multiplied by width of cytosolic lipids (assuming they make up 7% of enterocyte volume)

```
In[73]:= xacell[x] = sa[x]/mf[x] 0.000020 ;
xamem[x] = sa[x] 0.0000000035 ;
xalip[x] = sa[x]/mf[x] 0.0000015 ;
```

Axial Velocity m/hr

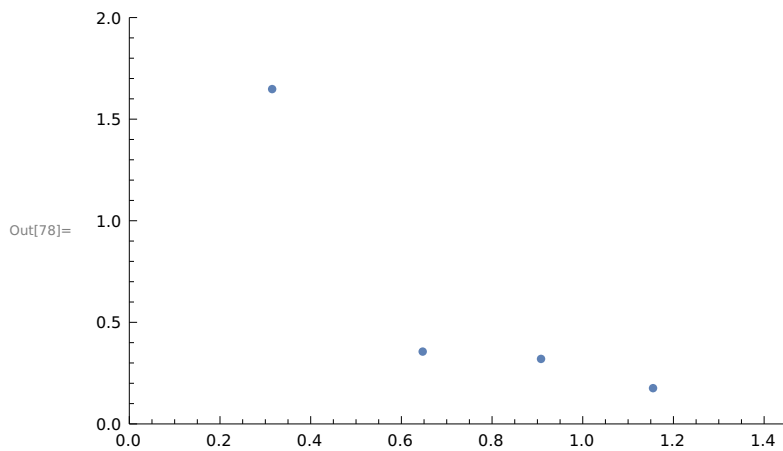
Velocity (Varga et al. 1976: veltabV, and in-house data: veltab)

```
In[76]:= veltabV = {{0.153, 0.9}, {0.45, 0.47}, {0.67, 0.15}, {1.03, .083}, {1.25, .01}}
veltab = {{0.315, 1.648}, {0.647, 0.356}, {0.908, 0.320}, {1.155, 0.176}}
```

```
Out[76]:= {{0.153, 0.9}, {0.45, 0.47}, {0.67, 0.15}, {1.03, 0.083}, {1.25, 0.01}}
```

```
Out[77]:= {{0.315, 1.648}, {0.647, 0.356}, {0.908, 0.32}, {1.155, 0.176}}
```

```
In[78]:= plot2 = ListPlot[veltab, PlotRange -> {{0, 1.45}, {0, 2}}]
```

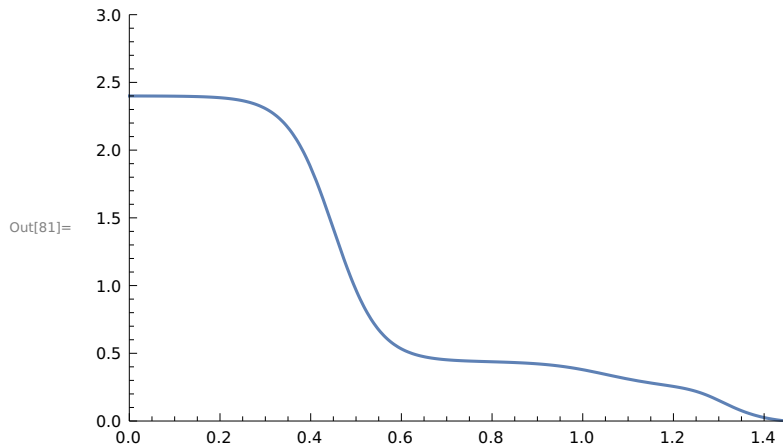


```
In[79]:= vel[x] = 2.4 - (2.4 - .440) / (1 + e-20(x-.45)) -
(0.340 - 0.15) / (1 + e-15(x-1.05)) - (0.13) / (1 + e-30(x-1.3)) - (0.139) / (1 + e-20(x-1.35));
```

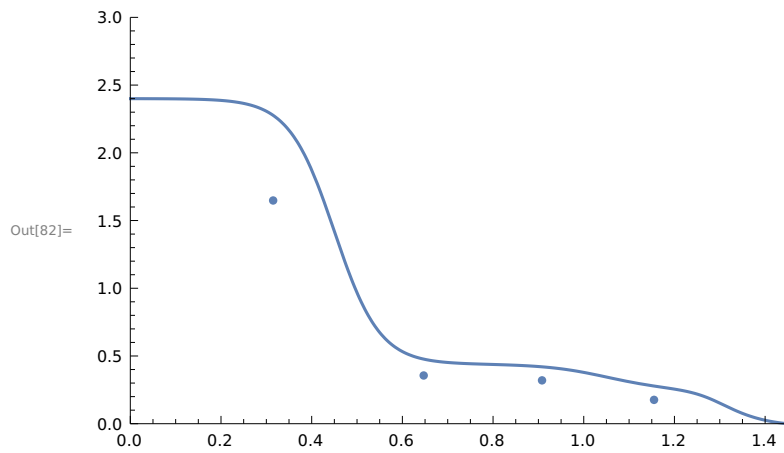
```
In[80]:= vel[x] /. x -> 1.45
```

```
Out[80]= -0.000532689
```

```
In[81]:= plot1 = Plot[Evaluate[vel[x], {x, 0, 1.45}], PlotRange -> {{0, 1.45}, {0, 3}}]
```



In[82]:= Show[plot1, plot2]



In[83]:= vel1 = vel[x] /. x → 0

Out[83]= 2.39976

In[84]:= vel2[x] = (vel[x]) (xa1 / xa[x]);

In[85]:= vel2[x] /. x → 1.33

Out[85]= 0.04702

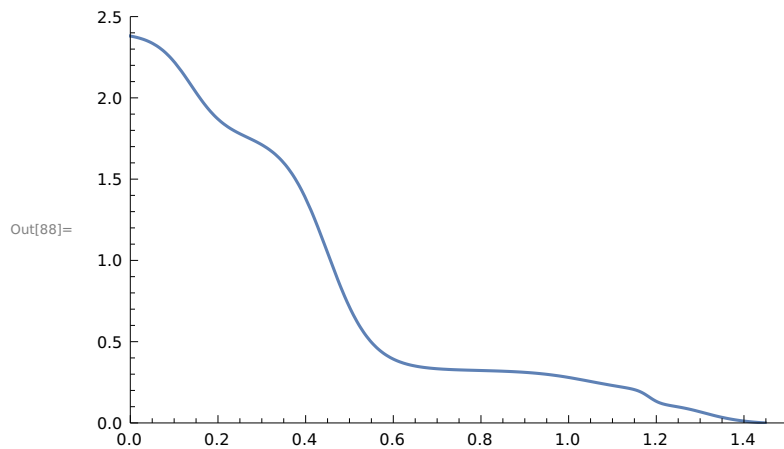
In[86]:= vel2[x] /. x → 0

Out[86]= 2.38028

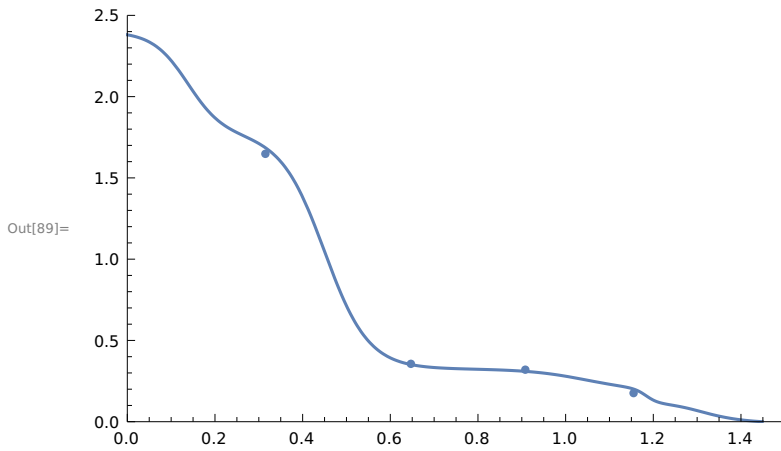
In[87]:= vel2[x] /. x → 1.45

Out[87]= -0.000239637

In[88]:= plot3 = Plot[Evaluate[vel2[x], {x, 0, 1.45}], PlotRange → {{0, 1.5}, {0, 2.5}}]



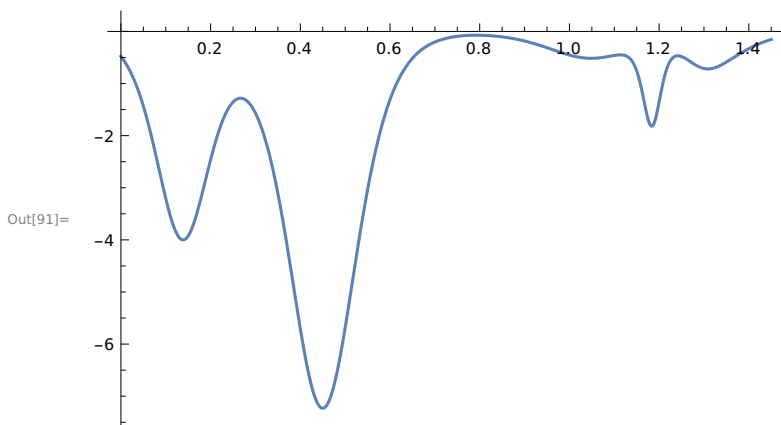
In[89]:= Show[plot3, plot2]



In[90]:= dvel[x] = D[vel2[x], x]

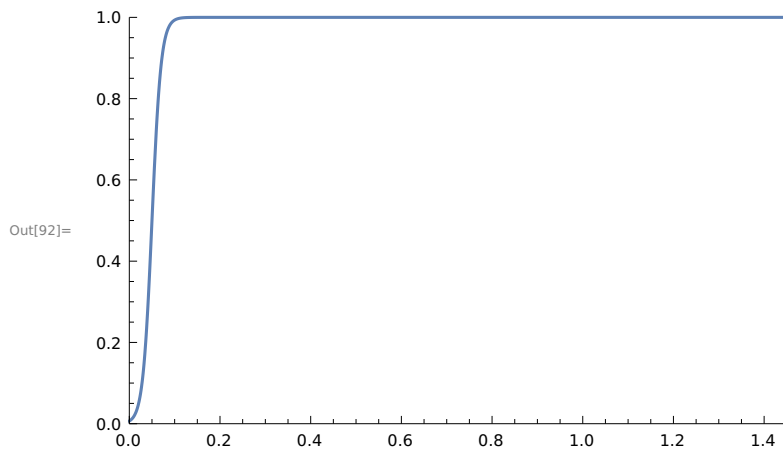
$$\text{Out[90]=} -\left(4.96643 \times 10^{-6} \times \left(2.4 - \frac{0.139}{1 + e^{-20 \cdot (-1.35 + x)}} - \frac{0.13}{1 + e^{-30 \cdot (-1.3 + x)}} - \frac{0.19}{1 + e^{-15 \cdot (-1.05 + x)}} - \frac{1.96}{1 + e^{-20 \cdot (-0.45 + x)}}\right) \right. \\ \left. \left(\frac{0.000344252 e^{-75 \cdot (-1.1915 + x)}}{(1 + e^{-75 \cdot (-1.1915 + x)})^2} - \frac{5.72958 \times 10^{-6} e^{-20 \cdot (-1.1615 + x)}}{(1 + e^{-20 \cdot (-1.1615 + x)})^2} + \frac{0.0000442252 e^{-25 \cdot (-0.15 + x)}}{(1 + e^{-25 \cdot (-0.15 + x)})^2} \right) \right) / \\ \left(4.96643 \times 10^{-6} + \frac{4.59003 \times 10^{-6}}{1 + e^{-75 \cdot (-1.1915 + x)}} - \frac{2.86479 \times 10^{-7}}{1 + e^{-20 \cdot (-1.1615 + x)}} + \frac{1.76901 \times 10^{-6}}{1 + e^{-25 \cdot (-0.15 + x)}} \right)^2 + \\ \frac{4.96643 \times 10^{-6} \left(-\frac{2.78 e^{-20 \cdot (-1.35 + x)}}{(1 + e^{-20 \cdot (-1.35 + x)})^2} - \frac{3.9 e^{-30 \cdot (-1.3 + x)}}{(1 + e^{-30 \cdot (-1.3 + x)})^2} - \frac{2.85 e^{-15 \cdot (-1.05 + x)}}{(1 + e^{-15 \cdot (-1.05 + x)})^2} - \frac{39.2 e^{-20 \cdot (-0.45 + x)}}{(1 + e^{-20 \cdot (-0.45 + x)})^2} \right)}{4.96643 \times 10^{-6} + \frac{4.59003 \times 10^{-6}}{1 + e^{-75 \cdot (-1.1915 + x)}} - \frac{2.86479 \times 10^{-7}}{1 + e^{-20 \cdot (-1.1615 + x)}} + \frac{1.76901 \times 10^{-6}}{1 + e^{-25 \cdot (-0.15 + x)}}$$

In[91]:= Plot[Evaluate[dvel[x], {x, 0, 1.45}]] (*, PlotRange -> {{0, 1.45}, {0, 1.2}} *)



Axial Diffusion rate constant
effective diffusion in m²/hr

In[92]:= `Plot[0.5 + (0.5) Tanh[50. (x - 0.05)], {x, 0, 1.45}, PlotRange -> {{0, 1.45}, {0, 1}}]`



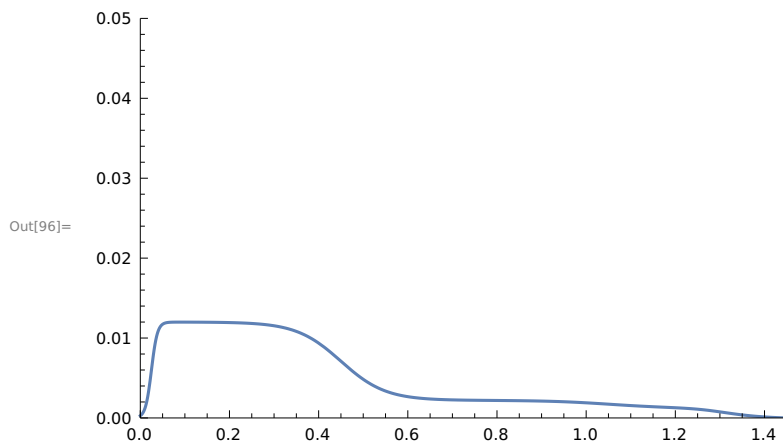
In[93]:= `dif2[x] = 0.005 * (0.5 + 0.5 Tanh[75. (x - 0.025)]) vel[x];`

In[94]:= `dif2[x] /. x -> 0.`

Out[94]= 0.000275701

In[95]:= `ddif2[x] = D[dif2[x], x];`

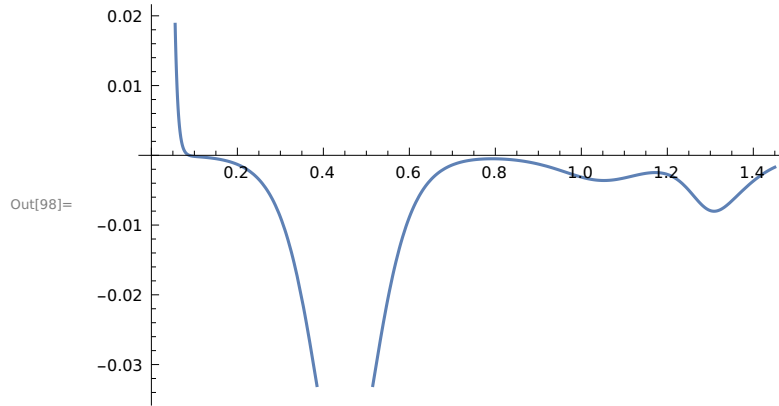
In[96]:= `Plot[Evaluate[dif2[x]], {x, 0, 1.45}, PlotRange -> {{0, 1.45}, {0, .05}}]`



In[97]:= `ddif2[x] /. x -> 1.33`

Out[97]= -0.0075543

In[98]:= `Plot[Evaluate[ddif2[x]], {x, 0, 1.45}(*, PlotRange -> {{0, 1.45}, {0, .3}}*)]`

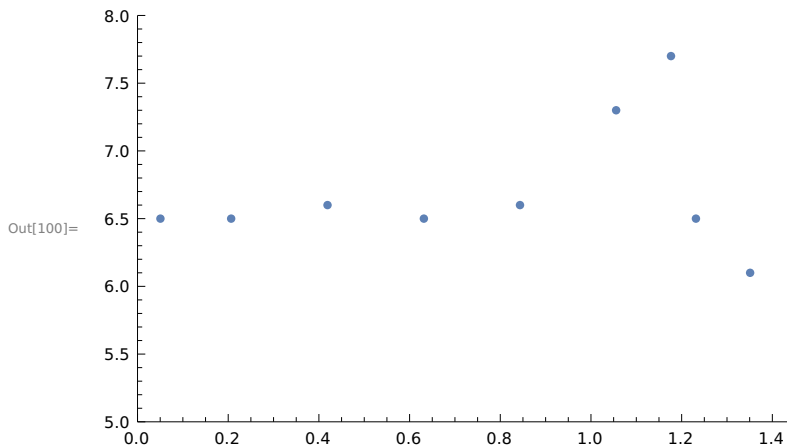


pH Fasted and Fed

The pH was measured for fasted and fed animals in-house (specific aim #2).

```
In[99]:= phfasttab = {{{(d0 + duo)/2}, 6.5}, {{(duo + jej1)/2}, 6.5}, {{(jej1 + jej2)/2}, 6.6},
  {{{(jej2 + jej3)/2}, 6.5}, {{(jej3 + jej4)/2}, 6.6}, {{(jej4 + jej5)/2}, 7.3},
  {{{(jej5 + ile)/2}, 7.7}, {{(ile + proxcol)/2}, 6.5}, {{(proxcol + distcol)/2}, 6.1}};
```

```
In[100]:= plot2 = ListPlot[phfasttab, PlotRange -> {{0, 1.45}, {5, 8}}]
```



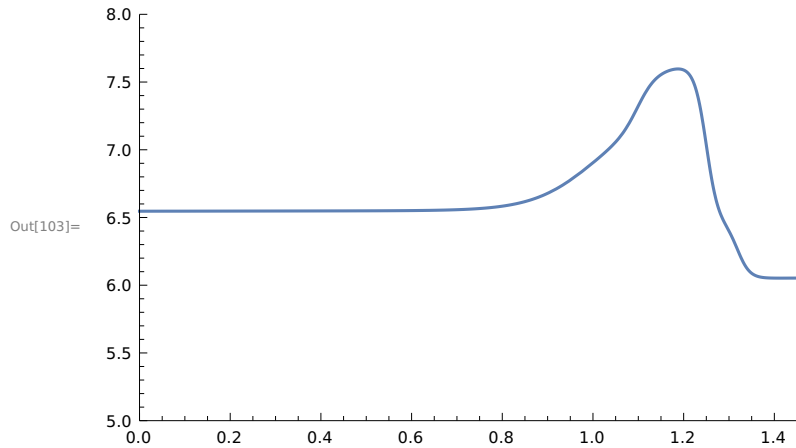
```
In[101]:= phfasttab[[9, 2]]
```

```
Out[101]= 6.1
```

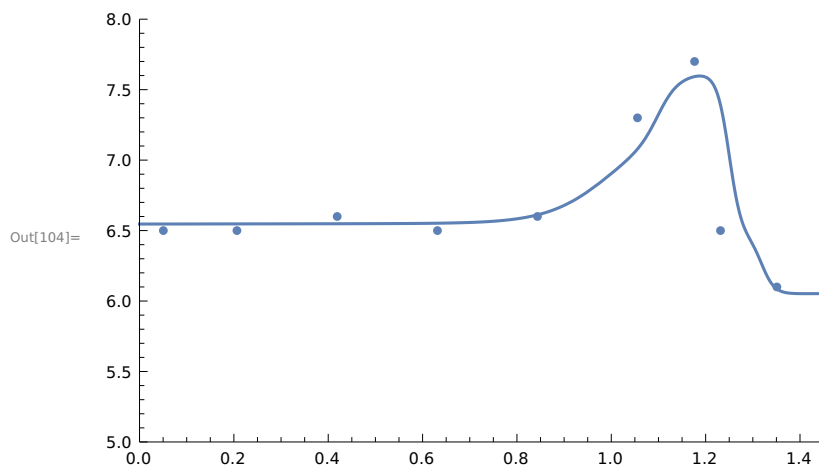
```
In[102]:= phfast[x] = phfasttab[[1, 2]] + (phfasttab[[5, 2]] - phfasttab[[1, 2]]) / (1 + e-2(x-jej3)) +
  (phfasttab[[6, 2]] - phfasttab[[5, 2]]) / (1 + e-15(x-1)) +
  (phfasttab[[7, 2]] - phfasttab[[6, 2]]) / (1 + e-50(x-1.1)) +
  (phfasttab[[8, 2]] - phfasttab[[7, 2]]) / (1 + e-75(x-1.25)) +
  (phfasttab[[9, 2]] - phfasttab[[8, 2]]) / (1 + e-75(x-1.32))
```

```
Out[102]= 6.5 - \frac{0.4}{1 + e^{-75 \cdot (-1.32 + x)}} - \frac{1.2}{1 + e^{-75 \cdot (-1.25 + x)}} + \frac{0.4}{1 + e^{-50 \cdot (-1.1 + x)}} + \frac{0.7}{1 + e^{-15 \cdot (-1 + x)}} + \frac{0.1}{1 + e^{-0.2 \cdot (-0.7375 + x)}}
```

```
In[103]:= plot1 = Plot[Evaluate[phfast[x], {x, 0, 1.45}], PlotRange -> {{0, 1.45}, {5, 8}}]
```

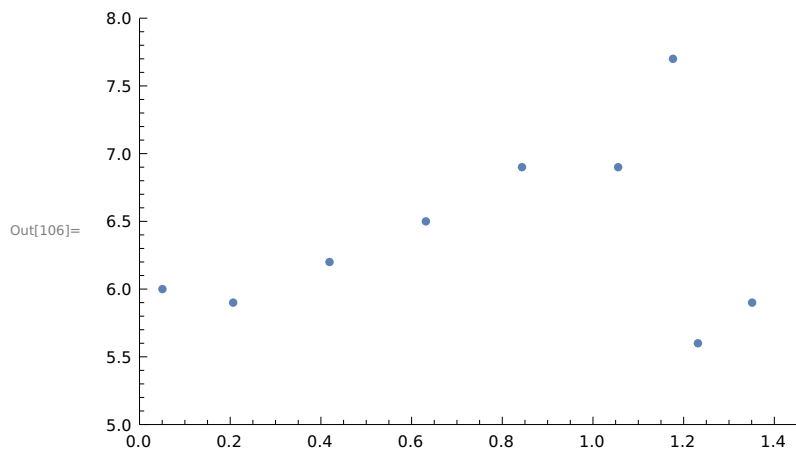


In[104]:= **Show[plot1, plot2]**



In[105]:= **phfedtab = {{{(d0 + duo)/2}, 6.0}, {{(duo + jej1)/2}, 5.9}, {{(jej1 + jej2)/2}, 6.2},
 {{{(jej2 + jej3)/2}, 6.5}, {{(jej3 + jej4)/2}, 6.9}, {{(jej4 + jej5)/2}, 6.9},
 {{{(jej5 + ile)/2}, 7.7}, {{(ile + proxcol)/2}, 5.6}, {{(proxcol + distcol)/2}, 5.9}};**

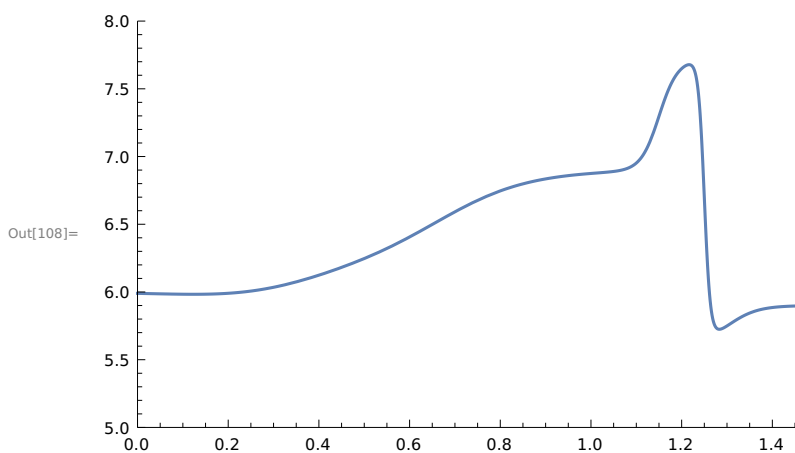
In[106]:= **plot2 = ListPlot[phfedtab, PlotRange -> {{0, 1.45}, {5, 8}}]**



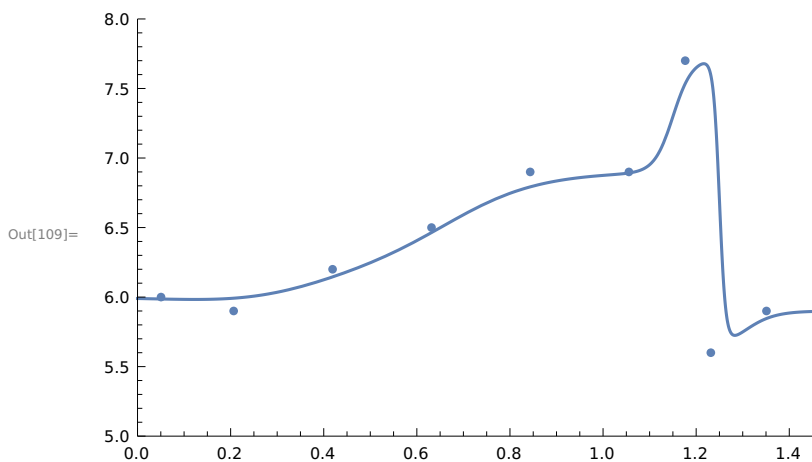
```
In[107]:= phfed[x] = phfedtab[[1, 2]] + (phfedtab[[2, 2]] - phfedtab[[1, 2]]) / (1 + e-10 (x-.15)) +
  (phfedtab[[3, 2]] - phfedtab[[2, 2]]) / (1 + e-10 (x-.37)) +
  (phfedtab[[5, 2]] - phfedtab[[3, 2]]) / (1 + e-10 (x-.67)) +
  (phfedtab[[7, 2]] - phfedtab[[6, 2]]) / (1 + e-50 (x-1.15)) +
  (phfedtab[[8, 2]] - phfedtab[[7, 2]]) / (1 + e-150 (x-1.25)) +
  (phfedtab[[9, 2]] - phfedtab[[8, 2]]) / (1 + e-30 (x-1.3))
```

```
Out[107]= 6. +  $\frac{0.3}{1 + e^{-30 \cdot (-1.3+x)}} - \frac{2.1}{1 + e^{-150 \cdot (-1.25+x)}} +$ 
 $\frac{0.8}{1 + e^{-50 \cdot (-1.15+x)}} + \frac{0.7}{1 + e^{-10 \cdot (-0.67+x)}} + \frac{0.3}{1 + e^{-10 \cdot (-0.37+x)}} - \frac{0.1}{1 + e^{-10 \cdot (-0.15+x)}}$ 
```

```
In[108]:= plot1 = Plot[Evaluate[phfed[x], {x, 0, 1.45}], PlotRange -> {{0, 1.45}, {5, 8}}]
```



```
In[109]:= Show[plot1, plot2]
```



Papp(x) with the point/slope method (i.e. far away from pKa on the linear pH logPapp curve)

```
In[110]:= (*ma=-4.05; mb=3.38;*)
```

```
In[111]:= (*papp[x]=10^(acidflag ma+acidflag mb)(ph[x]-ph0)+Log[10, papp0]*)
```

```
In[112]:= (*Plot[Evaluate[papp[x]], {x, 0, 10}]*)
```

Papp(x) with the modified FN method (i.e. including the non-linear part of the pH logPapp curve)-
assuming fasted conditions

Permeability v pH slope profiles do not correspond to the neutral fraction (which would give a slope of 10 in the linear pH range),
but have an average slope of 4.1 ± 2.1 for acids (ma) and 3.9 ± 2.4 for bases (mb)

```
In[113]:= ma ;
mb ;
```

```
In[115]:= fn[x] = 1 / (1 + acidflag (10 ^ (ma / 10 (phfast[x] - pkaa))) + baseflag (10 ^ (mb / 10 (pkab - phfast[x])))
1
```

```
Out[115]= 
$$\frac{1}{1. + 1. \times 10^{0.1 \times \left(1.4 - \frac{0.4}{1 + e^{-75(-1.32 \times x)}} - \frac{1.2}{1 + e^{-75(-1.25 \times x)}} + \frac{0.4}{1 + e^{-50(-1.1 \times x)}} + \frac{0.7}{1 + e^{-15(-1 \times x)}} + \frac{0.1}{1 + e^{-0.2(-0.7375 \times x)}}\right)}$$

```

```
In[116]:= fn0 = 1 / (1 + acidflag (10 ^ (ma / 10 (ph0 - pkaa))) + baseflag (10 ^ (mb / 10 (pkab - ph0))))
```

```
Out[116]= 0.370611
```

```
In[117]:= p = papp0 / fn0
```

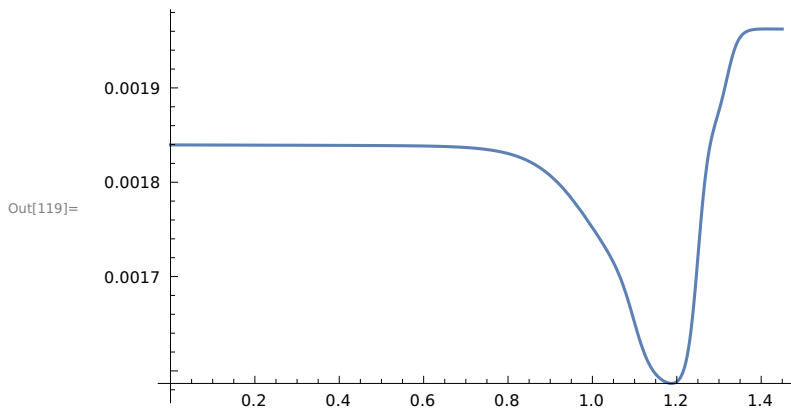
```
Out[117]= 0.00440612
```

```
In[118]:= papp[x] = p fn[x]
```

```
Out[118]= 
$$\frac{0.00440612}{1. + 1. \times 10^{0.1 \times \left(1.4 - \frac{0.4}{1 + e^{-75(-1.32 \times x)}} - \frac{1.2}{1 + e^{-75(-1.25 \times x)}} + \frac{0.4}{1 + e^{-50(-1.1 \times x)}} + \frac{0.7}{1 + e^{-15(-1 \times x)}} + \frac{0.1}{1 + e^{-0.2(-0.7375 \times x)}}\right)}$$

```

```
In[119]:= Plot[Evaluate [papp[x]], {x, 0, 1.45}]
```



Radial diffusion rate constant

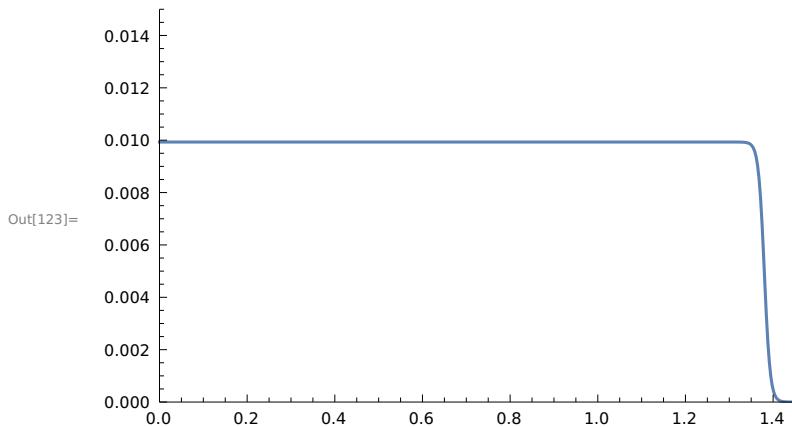
effective diffusion rate in 1 dimension m/hr, accounting for 8x increase due to mixing.

```
In[120]:= ClearAll [difr1]
```

```
In[121]:= difrad = 0.01;
```

```
In[122]:= difr1[x] = 0.5 difrad (1 - (1 - 0.014) Tanh[2. (x - 5.)]) × 0.5 × (1 - Tanh[75 (x - 1.38)]);
```

In[123]:= **Plot[Evaluate[diffr1[x]], {x, 0, 10}, PlotRange → {{0, 1.45}, {0, 0.015}}]**



In[124]:= **Evaluate[diffr1[x] /. x → {1.0, 1.45}]**

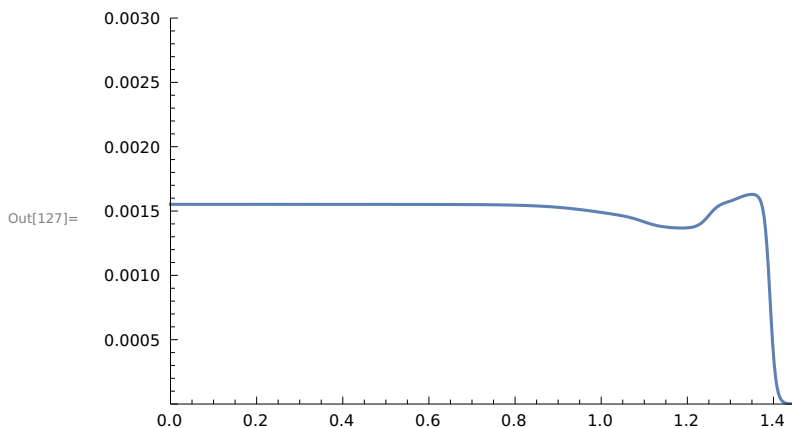
Out[124]= {0.00993, 2.73429×10^{-7} }

In[125]:= **papp[x] /. x → {1, 1.45}**

Out[125]= {0.00175197, 0.00196237}

In[126]:= **papp2[x] = diffr1[x] * papp[x] / (diffr1[x] + papp[x]);**

In[127]:= **Plot[Evaluate[papp2[x]], {x, 0, 10}, PlotRange → {{0, 1.45}, {0, 0.003}}]**



Drug Parameters

Partition coefficient based on 0.7 uL lipid per 1 mg microsomal protein

In[128]:= **Kp = ((1 - fumics) / fumics) * (1 / 0.0007)**

Out[128]= 176.565

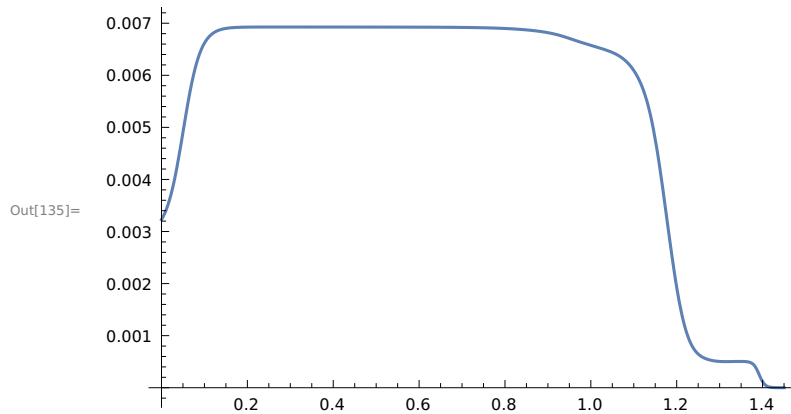
In[129]:= **cli[x] = 4 papp[x] * sa[x];**

In[130]:= **clo[x] = cli[x] / Kp;**

In[131]:= **cli2[x] = 4 papp2[x] * sa[x];**

```
In[132]:= c1o2[x] = c1i2[x]/Kp;
          c1i3[x] = 4 papp[x] 100 sa[x];
          c1o3[x] = c1i3[x]/Kp;
```

```
In[135]:= Plot[Evaluate[c1i2[x], {x, 0, 1.45}]]
```



```
In[136]:= c1i2[x] /. x -> 1.45
```

Out[136]= 8.44249×10^{-8}

Solution Pulse in stomach w lag

Velocity leaving stomach (m/hr)

```
In[137]:= vel0 = vel[x] /. x -> 0;
```

```
In[138]:= volcor = vol0 / (π r1 ^ 2 pl1 vel0)
```

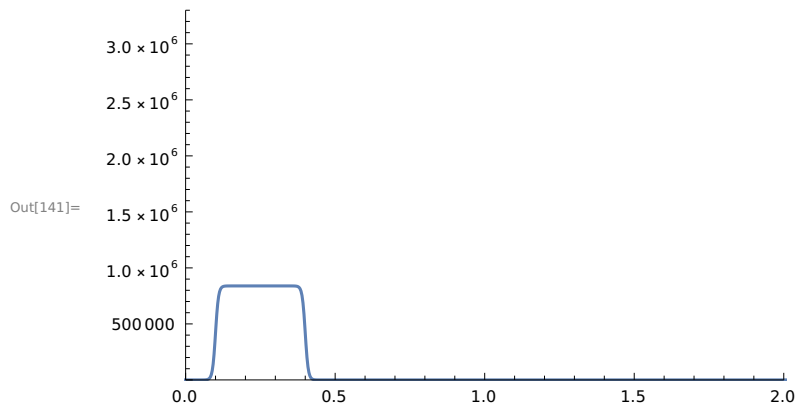
Out[138]= 0.279684

Use a smoothed pulse input function

```
In[139]:= upulse1[t] = 0.5 (Tanh[100. (t - lag)] - Tanh[100. (t - (pl1 + lag))]);
```

```
In[140]:= pulse1[t] = C0 volcor upulse1[t];
```

```
In[141]:= Plot[Evaluate[pulse1[t]], {t, 0, 10}, PlotRange -> {{0, 2}, {0, 1.1 dose1 / vol0}}
```



```
In[142]:= NIntegrate[pulse1[t] vel0 xa1, {t, 0, 1.0}]
```

Out[142]= 3.

In[143]:= **c10 = Evaluate[pulse1[t] /. t -> 0]**

Out[143]= 0.00172941

Solid Dose with Dissolution

Plug length time in m/(m/hr)

volume of the solid

In[144]:= **volAs = dose1 / rho**

Out[144]= 2.25564×10^{-9}

Calculate particle volume

In[145]:= **vpart = 4 π psize ^3 / 3**

Out[145]= 3.26116×10^{-13}

In[146]:= **(3 vpart / (1000 \times 4))^(1/3)**

Out[146]= 6.25381×10^{-6}

Calculate particle number

In[147]:= **pt = volAs / vpart**

Out[147]= 6916.68

Solubility in mg/m³

In[148]:= **sol = sol1;**

Dissolution in the stomach

Liquid volume of the stomach dose

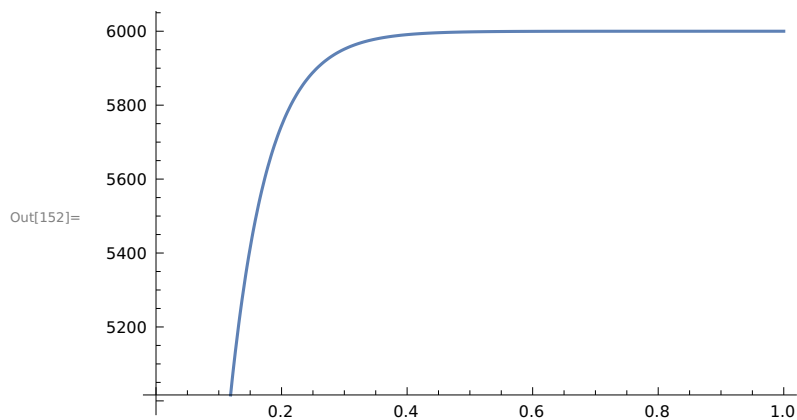
In[149]:= **cslim = (dose1 / vol0) 0.00001**

Out[149]= 30.

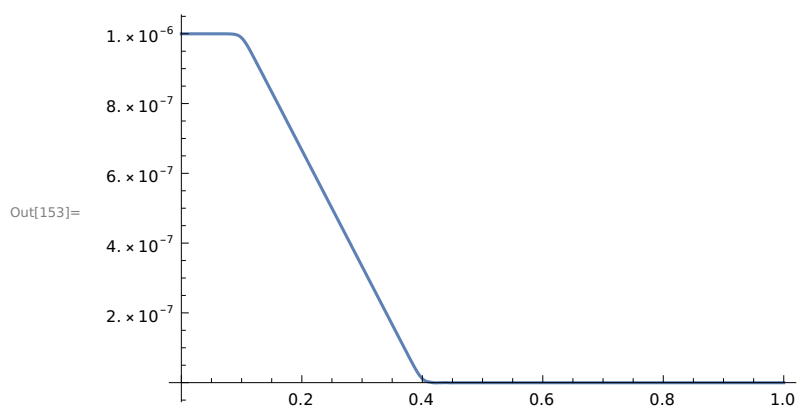
```
In[150]:= Clear[models1, tmax]
```

```
In[151]:= models1 = NDSolve[{
  Cps'[t] == 0,
  vol'[t] == -(upulse1[t]/pl1) vol0,
  Css'[t] == deldis[t] 0.5 * (1 + (Tanh[50. (Css[t] - cslim)])) *
    (-8 Cps[t] Pi difc Re[(3 Css[t]/(4 Pi rho Cps[t]))^(1/3)] (sol2 - Cds[t])),
  Cds'[t] == deldis[t] 0.5 * (1 + (Tanh[50. (Css[t] - cslim)])) *
    (8 Cps[t] Pi difc Re[(3 Css[t]/(4 Pi rho Cps[t]))^(1/3)] (sol2 - Cds[t])),
  deldis'[t] == 0.,
  Cps[0] == pt/vol0,
  vol[0] == vol0,
  Css[0] == dose1/vol0,
  Cds[0] == 0,
  deldis[0] == 0, WhenEvent[t == 0.01, deldis[t] -> 1.]},
  {Cps, vol, Css, Cds}, {t, 0, 24}, MaxSteps -> 1000000, PrecisionGoal -> 13][[1]];
```

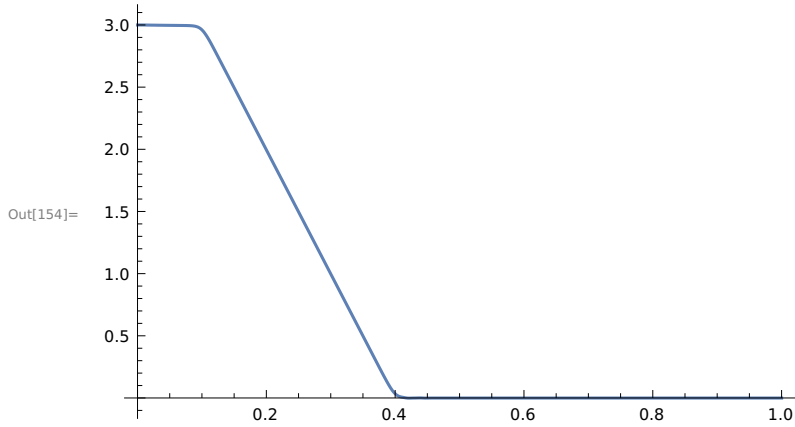
```
In[152]:= Plot[Cds[t] /. models1, {t, 0, 1}]
```



```
In[153]:= Plot[vol[t] /. models1, {t, 0, 1}]
```

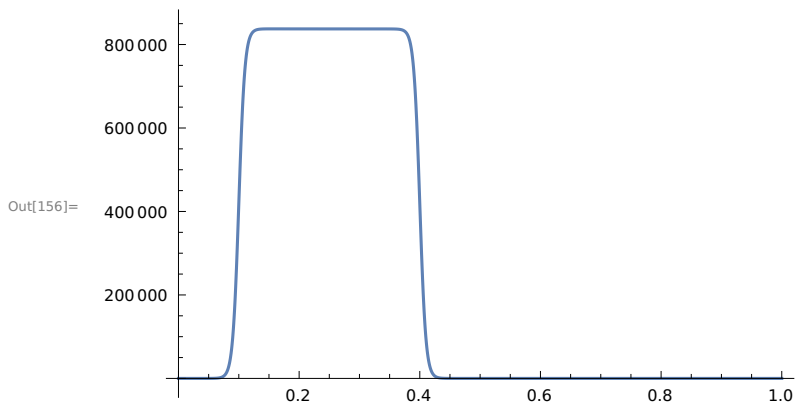


```
In[154]:= Plot[Css[t] * vol[t] /. models1, {t, 0, 1}]
```



In[155]:= **pulsess1[t] = upulse1[t] volcor Css[t] /. models1 ;**

In[156]:= **Plot[Evaluate [pulsess1[t]], {t, 0, 1}]**



In[157]:= **cs0 = Evaluate [(pulsess1[t]) /. t -> 0]**

Out[157]= **0.00172941**

In[158]:= **intpulsess1 = NIntegrate [pulsess1[t] vel1 xa1, {t, 0, 20.0}]**

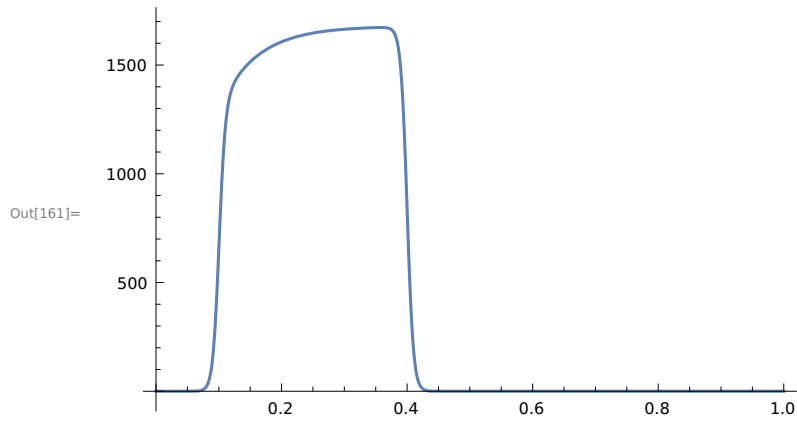
Out[158]= **2.99427**

In[159]:= **xa1**

Out[159]= **4.96643×10^{-6}**

In[160]:= **pulseds1[t] = upulse1[t] volcor Cds[t] /. models1 ;**

In[161]:= **Plot[Evaluate[pulseds1[t]], {t, 0, 1}]**



In[162]:= **c0 = Evaluate[pulseds1[t] /. t -> 0]**

Out[162]= 0.

In[163]:= **intpulseds1 = NIntegrate[pulseds1[t] vel1 xa1, {t, 0, 20.0}]**

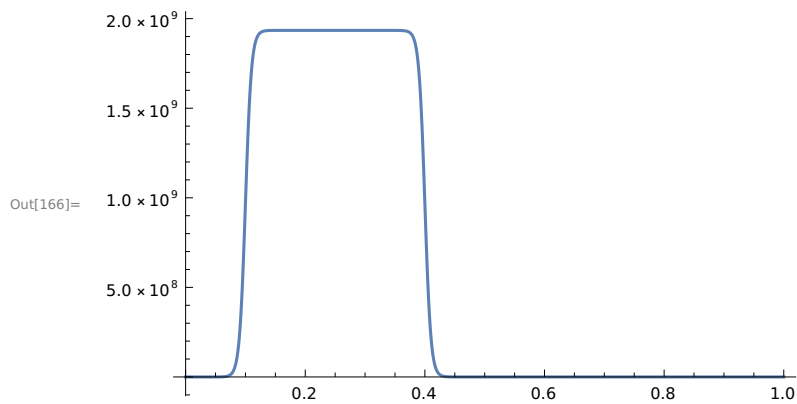
Out[163]= 0.00572913

In[164]:= **intpulsess1 + intpulseds1**

Out[164]= 3.

In[165]:= **pulsep1[t] = (upulse1[t] volcor Cps[t] /. models1);**

In[166]:= **Plot[Evaluate[pulsep1[t]], {t, 0, 1}]**



In[167]:= **intpulsep1 = NIntegrate[pulsep1[t] vel1 xa1, {t, 0, 20.0}]**

Out[167]= 6916.68

In[168]:= **cp0 = Evaluate[(pulsep1[t]) /. t -> 0]**

Out[168]= 3.98726

In[169]:= **(*cp0=0.05;*)**

```
In[170]:= coordx = Join[0. + Range[0, 60]/400, 0.15 + Range[1, 250]/1000,
  0.40 + Range[1, 200]/1000, 0.6 + Range[1, 45.0]/300.0, 0.75 + Range[1, 700]/1000];
```

```
In[171]:= Length[coordx]
```

```
Out[171]= 1256
```

PDEs Solution Dose

```
In[172]:= soln = NDSolve[{
  D[Cp1[t, x], t] == dif2[x] * D[Cp1[t, x], {x, 2}] + (-vel2[x] + ddif2[x] + dif2[x] * dxa[x] / xa[x]) *
    D[Cp1[t, x], x] + Cp1[t, x] * (-dvel[x] - (dxa[x] / xa[x]) * vel2[x]),
  D[Cs1[t, x], t] == dif2[x] * D[Cs1[t, x], {x, 2}] + (-vel2[x] + ddif2[x] + dif2[x] * dxa[x] / xa[x]) *
    D[Cs1[t, x], x] + Cs1[t, x] * (-dvel[x] - (dxa[x] / xa[x]) * vel2[x]) -
    (0.5 * (1 + (Tanh[3.0 (Cs1[t, x] - cslim)))) + 0.5 * (1 + (Tanh[-75. (sol - C1[t, x])))) *
    (8 Cp1[t, x] Pi difc Re[(3 Cs1[t, x]) / (4 Pi rho Cp1[t, x])^(1/3)] (sol - C1[t, x])),
  D[C1[t, x], t] == dif2[x] * D[C1[t, x], {x, 2}] + (-vel2[x] + ddif2[x] + dif2[x] * dxa[x] / xa[x]) *
    D[C1[t, x], x] + C1[t, x] * (-dvel[x] - (dxa[x] / xa[x]) * vel2[x]) +
    (0.5 * (1 + (Tanh[3.0 (Cs1[t, x] - cslim)))) + 0.5 * (1 + (Tanh[-75. (sol - C1[t, x])))) *
    (8 Cp1[t, x] Pi difc Re[(3 Cs1[t, x]) / (4 Pi rho Cp1[t, x])^(1/3)] (sol - C1[t, x])) -
    cli2[x] * C1[t, x] / xa[x] + clo2[x] * C2[t, x] / xa[x],
  D[C2[t, x], t] == cli2[x] * C1[t, x] / xamem[x] - (clo[x] + clo2[x]) * C2[t, x] / xamem[x] +
    cli[x] * C3[t, x] / xamem[x],
  D[C3[t, x], t] == clo[x] * C2[t, x] / xacell[x] - cli[x] * C3[t, x] / xacell[x] -
    cli3[x] * C3[t, x] / xacell[x] + clo3[x] * C4[t, x] / xacell[x] - (cli[x] / 2) * C3[t, x] / xacell[x],
  D[C4[t, x], t] == -clo3[x] * C4[t, x] / xalip[x] + cli3[x] * C3[t, x] / xalip[x],
  {Cp1[t, 0] == pulsep1[t], Cp1[0, x] == cp0, Cp1[t, 1.45] == 0, Cs1[t, 0] == pulsess1[t],
    Cs1[0, x] == 0, Cs1[t, 1.45] == 0, C1[t, 0] == pulsed1[t], C1[0, x] == c10,
    C1[t, 1.45] == 0, C2[0, x] == 0, C2[t, 0] == 0, C2[t, 1.45] == 0, C3[0, x] == 0,
    C3[t, 0] == 0, C3[t, 1.45] == 0, C4[t, 0] == 0, C4[0, x] == 0, C4[t, 1.45] == 0},
  {Cp1, Cs1, C1, C2, C3, C4}, {t, 0, 24}, {x, 0, 1.45}, (*MaxStepSize -> 0.005, *)
  (*Method -> {"FiniteElement", "MeshOptions" -> {MaxCellMeasure -> 0.0005}}*)
  Method -> {"PDEDiscretization" -> {"MethodOfLines",
    (*"DiscretizedMonitorVariables" -> True, *) "SpatialDiscretization" ->
    {"TensorProductGrid", "Coordinates" -> {coordx}, "DifferenceOrder" -> 2}}}]
```

```

Out[172]= {{Cp1 → InterpolatingFunction [  Domain : {{0., 24.}, {0., 1.45}} Output : scalar ],
          This object cannot be used as input.

Cs1 → InterpolatingFunction [  Domain : {{0., 24.}, {0., 1.45}} Output : scalar ],
          This object cannot be used as input.

C1 → InterpolatingFunction [  Domain : {{0., 24.}, {0., 1.45}} Output : scalar ],
          This object cannot be used as input.

C2 → InterpolatingFunction [  Domain : {{0., 24.}, {0., 1.45}} Output : scalar ],
          This object cannot be used as input.

C3 → InterpolatingFunction [  Domain : {{0., 24.}, {0., 1.45}} Output : scalar ],
          This object cannot be used as input.

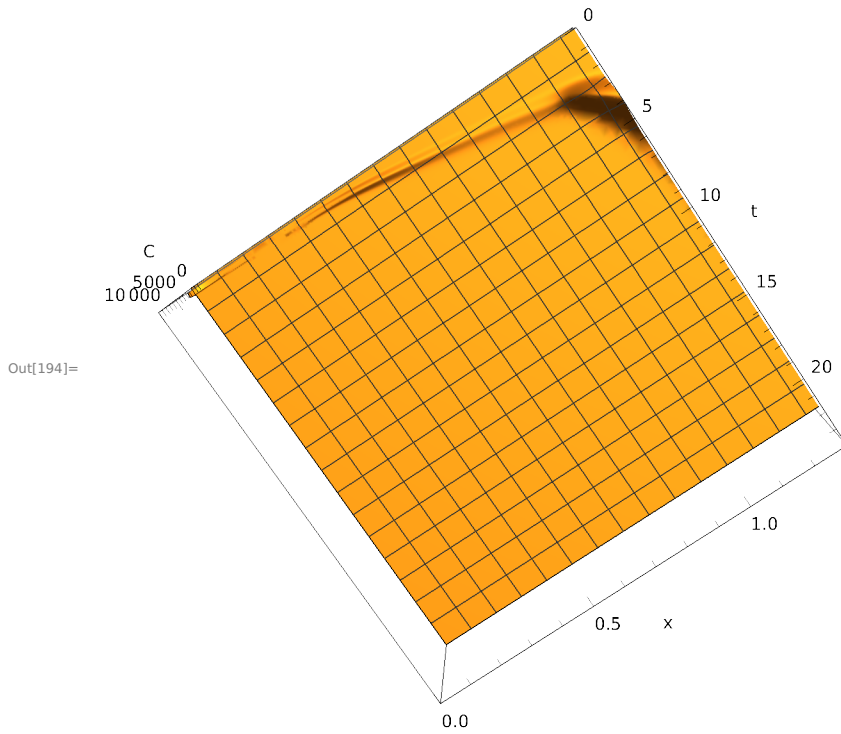
C4 → InterpolatingFunction [  Domain : {{0., 24.}, {0., 1.45}} Output : scalar ] ]}
          This object cannot be used as input.

```

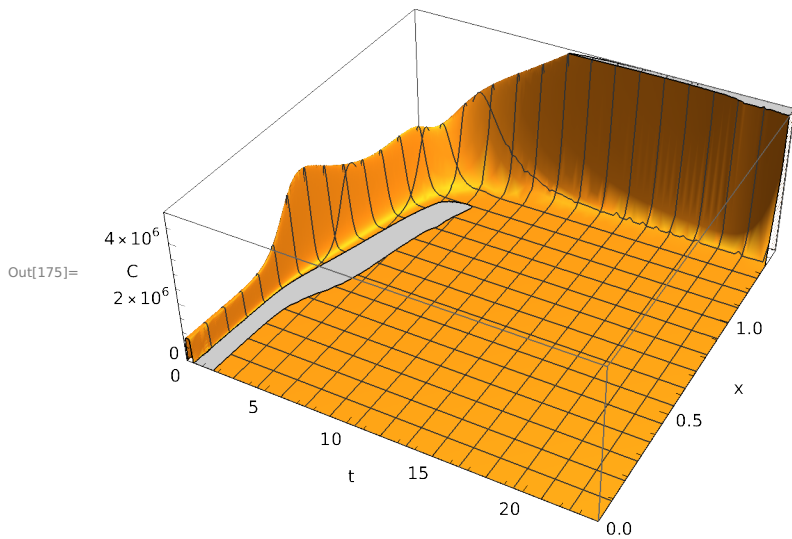
```
In[173]:= C1[0.2, .0] /. soln
```

```
Out[173]= {1606.67}
```

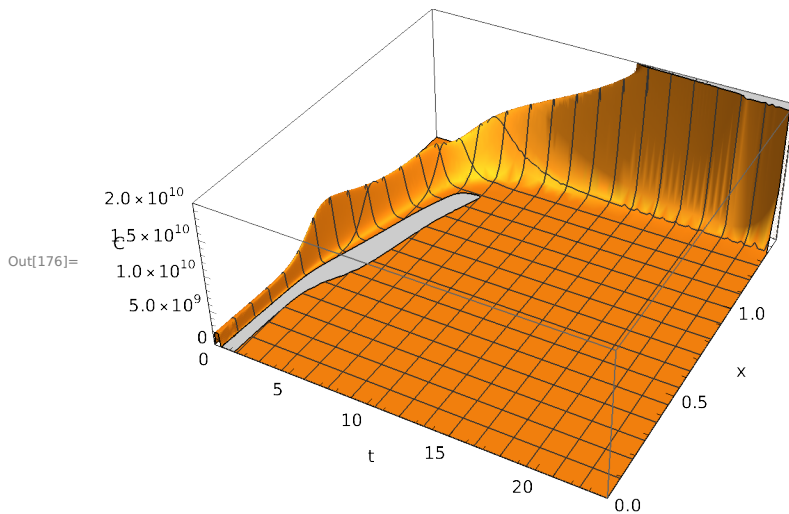
```
In[194]:= plot1 = Plot3D[C1[t, x] /. soln, {t, 0, 24},
  {x, 0, 1.45}, PlotRange → {{0, 24}, {0, 1.3}, {-2000, 10 000}},
  AxesLabel → {"t", "x", "C"}, MaxRecursion → 7]
```



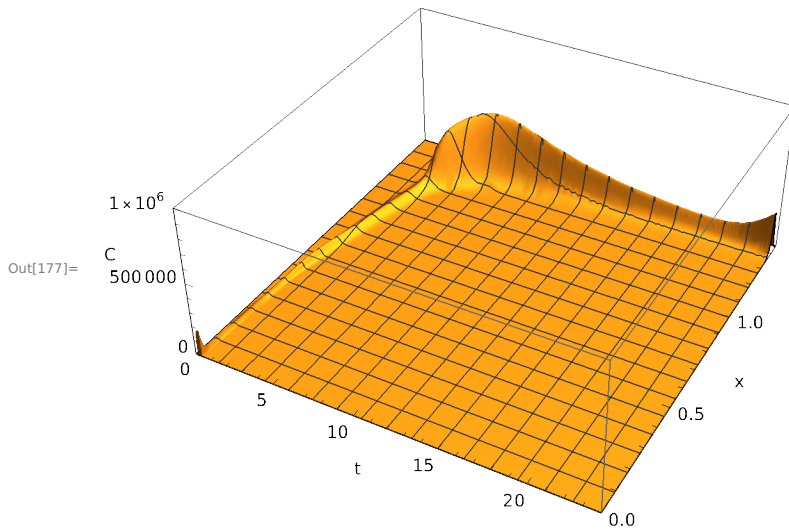
```
In[175]:= plot2 = Plot3D[Csoln[t, x] /. soln, {t, 0, 24},
  {x, 0, 1.45}, PlotRange -> {{0, 24}, {0, 1.45}, {-60, 5 000 000}},
  AxesLabel -> {"t", "x", "C"}, MaxRecursion -> 7]
```



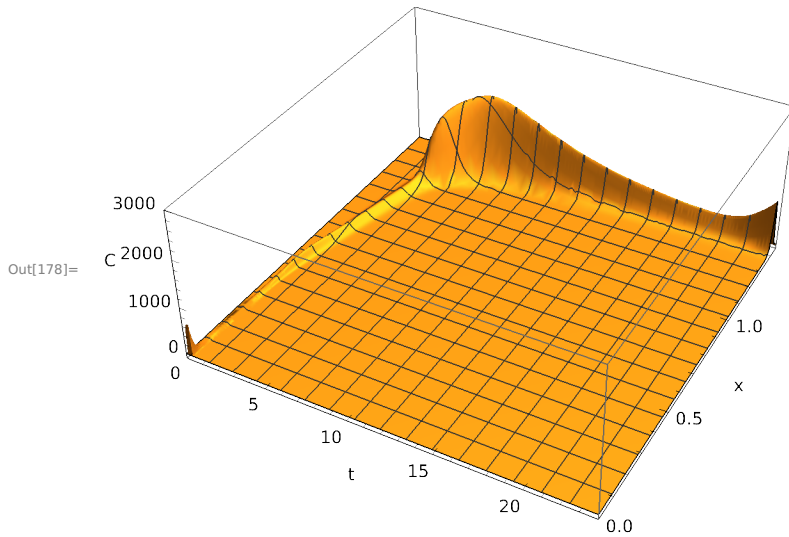
```
In[176]:= plot3 = Plot3D[Cp1[t, x] /. soln, {t, 0, 24}, {x, 0, 1.45},
  PlotRange -> {{0, 24}, {0, 1.45}, {-200 000, 20 000 000 000}},
  AxesLabel -> {"t", "x", "C"}, MaxRecursion -> 7]
```



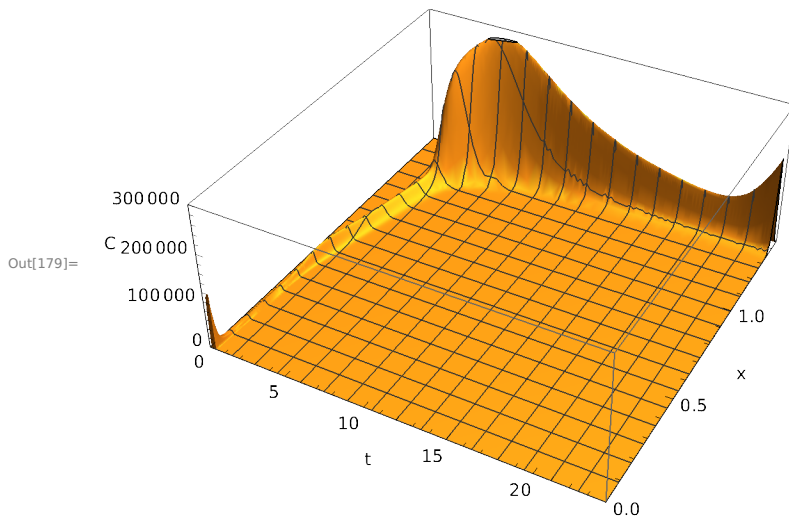
```
In[177]:= plot4 = Plot3D[C2[t, x] /. soln, {t, 0, 24},
  {x, 0, 1.45}, PlotRange -> {{0, 24}, {0, 1.45}, {-1000, 1 000 000}},
  AxesLabel -> {"t", "x", "C"}, MaxRecursion -> 7]
```



```
In[178]:= plot5 = Plot3D[C3[t, x] /. soln, {t, 0, 24},
  {x, 0, 1.45}, PlotRange -> {{0, 24}, {0, 1.45}, {-100, 3000}},
  AxesLabel -> {"t", "x", "C"}, MaxRecursion -> 7]
```



```
In[179]:= plot6 = Plot3D[C4[t, x] /. soln, {t, 0, 24},
  {x, 0, 1.45}, PlotRange -> {{0, 24}, {0, 1.45}, {-100, 300 000}},
  AxesLabel -> {"t", "x", "C"}, MaxRecursion -> 7]
```



```
In[180]:= amtout = NIntegrate[((cli[x]/2) * C3[t, x]) /. soln[[1]], {t, 0, 24},
  {x, 0, 1.45}, AccuracyGoal -> 7, Method -> "AdaptiveQuasiMonteCarlo "]
```

Out[180]= 0.626129

```
In[181]:= residC1 = NIntegrate[(C1[24, x] * xa[x]) /. soln[[1]],
  {x, 0, 1.45}, AccuracyGoal -> 7, Method -> "AdaptiveQuasiMonteCarlo "]
```

Out[181]= 0.00379996

```
In[182]:= residCs1 = NIntegrate[(Cs1[24, x] * xa[x]) /. soln[[1]],
  {x, 0, 1.45}, AccuracyGoal -> 7, Method -> "AdaptiveQuasiMonteCarlo "]
```

Out[182]= 321 894.

```

In[183]:= residC2 = NIntegrate [(C2[24, x] × xamem[x]) /. soln[[1]],
    {x, 0, 1.45}, AccuracyGoal → 7, Method → "AdaptiveQuasiMonteCarlo "]
Out[183]:= 2.2503 × 10-6

In[184]:= residC3 = NIntegrate [(C3[24, x] × xacell[x]) /. soln[[1]],
    {x, 0, 1.45}, AccuracyGoal → 7, Method → "AdaptiveQuasiMonteCarlo "]
Out[184]:= 7.28332 × 10-6

In[185]:= residC4 = NIntegrate [(C4[24, x] × xalip[x]) /. soln[[1]],
    {x, 0, 1.45}, AccuracyGoal → 7, Method → "AdaptiveQuasiMonteCarlo "]
Out[185]:= 0.0000964463

In[186]:= total = amtout + residC1 + residCs1 + residC2 + residC3 + residC4
Out[186]:= 321 895.

In[187]:= facalc = amtout / total
Out[187]:= 1.94514 × 10-6

In[188]:= total / dose1
Out[188]:= 107 298.

```

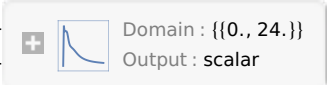
```

In[189]:= (*ClearAll [c42]*)

In[190]:= ClearAll [c5]
    C4 is dA/Dt in mg/hr

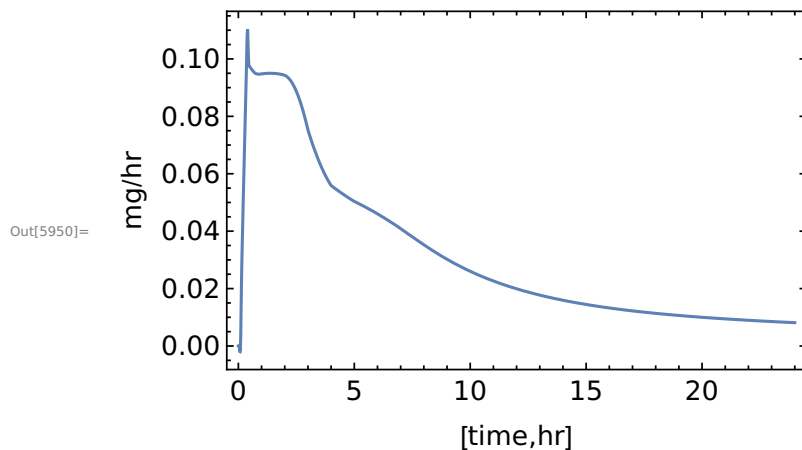
In[191]:= c5[t_] = NIntegrate [((cli[x]/2) × C3[t, x]) /. soln[[1]],
    {x, 0, 1.45}, AccuracyGoal → 7, Method → "AdaptiveQuasiMonteCarlo "]
Out[191]:= NIntegrate [  $\frac{1}{2}$  cli[x] × C3[t, x] /. soln[[1]], {x, 0, 1.45},
    AccuracyGoal → 7, Method → AdaptiveQuasiMonteCarlo ]

In[192]:= c5t1 = Table[{t, If[c5[t] < 0, 0, c5[t]]}, {t, 0, 2, 0.05}];
In[193]:= c5t2 = Table[{t, If[c5[t] < 0, 0, c5[t]]}, {t, 3, 24, 1.}];
Out[193]:= $Aborted

In[5946]:= c5t3 = Table[{t, 0}, {t, 25., 200., 10.0}];
In[5947]:= c5t = Join[c5t1, c5t2(*,c5t3*)];
In[5948]:= (*c5t=Table[{t,c5[t]},{t,0,24,0.05}];*)
In[5949]:= c5fun = Interpolation [c5t, InterpolationOrder → 2]
Out[5949]:= InterpolatingFunction [  ]

```

```
In[5950]:= plot6 = Plot[Evaluate[c5fun[t]], {t, 0, 24},
  PlotRange -> {{0, 1.45}, {0, 1.2 Max[Table[c5t1[[i, 2]], {i, 1, 100}]]}},
  (*Epilog->{PointSize[Medium],Point[c4t]},*)Frame -> True,
  FrameStyle -> Directive[Black, 14, Thickness[0.003]],
  LabelStyle -> (FontFamily -> "Arial"), FrameLabel -> {"[time,hr]", "mg/hr"}
```



```
In[5951]:= Integrate[c5fun[t], {t, 0, 24}]
```

```
Out[5951]= 0.758702
```

Apply to drug PK model for an IV dose.

```
In[5952]:= ClearAll[modelpkiv1, modelpkiv2, modelpko1, modelIV, fitiv, dataIV]
```

data in hr, Ug/mL - in house collection (n=3); dose - 4 mg/kg for a 300 g rat.

```
In[5953]:= dataIV = {{0.093, 11.878}, {0.267, 7.38}, {0.511, 4.06}, {1., 2.21}, {2.011, 1.26},
  {4., .515}, {6.017, 0.239}, {8.03, .130}, {10., 0.071}, {12., 0.0313}, {24, .0075}}
```

```
Out[5953]= {{0.093, 11.878}, {0.267, 7.38}, {0.511, 4.06}, {1., 2.21}, {2.011, 1.26},
  {4., 0.515}, {6.017, 0.239}, {8.03, 0.13}, {10., 0.071}, {12., 0.0313}, {24, 0.0075}}
```

```
In[5954]:= nt = Length[dataIV]
```

```
Out[5954]= 11
```

```
In[5955]:= colort = {Red, Blue, Orange, Green, Purple, Cyan, Brown};
```

```
In[5956]:= k10init = 0.39;
```

```
k12init = 2.9;
```

```
k21init = 0.97;
```

```
Vlinit = 70.;
```

```
In[5960]:= doseiv = 1000 dose2 (*in ug*)
```

```
Out[5960]= 1200.
```

```

In[5961]:= modelIV[k12_?NumericQ, k21_?NumericQ,
  k10_?NumericQ, V1_?NumericQ, te_?NumericQ] :=
(modeliv[k12, k21, k10, V1, te] =
  (Xc[te]/V1)/. First[NDSolve[{Xc'[t] == -(k12 + k10) Xc[t] + k21 Xp1[t],
    Xp1'[t] == k12 Xc[t] - k21 Xp1[t],
    Xc[0] == doseiv,
    Xp1[0] == 0},
  {Xc, Xp1}, {t, 0, 35}, MaxSteps -> 10 000, PrecisionGoal -> ∞]])

In[5962]:= fitiv = NonlinearModelFit[dataIV, modelIV[k12, k21, k10, V1, te],
  {{k12, k12init}, {k21, k21init}, {k10, k10init}, {V1, V1init}}, {te},
  PrecisionGoal -> ∞, MaxIterations -> 10 000, Weights -> (1/#2 &)]

Out[5962]= $Aborted

In[212]:= fitiv["ParameterTable "]

```

	Estimate	Standard Error	t-Statistic	P-Value
k12	1.65591	0.0956263	17.3165	5.26468×10^{-7}
k21	0.961097	0.0540464	17.7828	4.38715×10^{-7}
k10	1.52208	0.0426382	35.6975	3.51483×10^{-9}
V1	75.498	1.92375	39.2452	1.81611×10^{-9}

```

Out[212]=
In[213]:= fitiv["RSquared "]
Out[213]= 0.999052

In[214]:= fitiv["AICc "]
Out[214]= -20.428

In[215]:= TableForm[fitiv["CorrelationMatrix "]]
Out[215]/TableForm=

```

1.	0.549991	0.429617	-0.715717
0.549991	1.	0.10455	-0.231894
0.429617	0.10455	1.	-0.774881
-0.715717	-0.231894	-0.774881	1.

```

In[216]:= k12 = fitiv["BestFitParameters "][[1, 2]];
In[217]:= k21 = fitiv["BestFitParameters "][[2, 2]];
In[218]:= (*k13=fitiv["BestFitParameters "][[3, 2];*)
In[219]:= (*k31=fitiv["BestFitParameters "][[4, 2];*)
In[220]:= k10 = fitiv["BestFitParameters "][[3, 2]];
In[221]:= V1 = fitiv["BestFitParameters "][[4, 2]];
In[222]:= fitiv["FitResiduals "]

```

```
Out[222]= {-0.0367778 , 0.0969108 , -0.0957838 , 0.0706174 , 0.0203711 ,
          -0.052227 , -0.0191882 , 0.0122945 , 0.0164312 , 0.00629608 , 0.00726859 }
```

```
In[223]:= fitiv["PredictedResponse "]
```

```
Out[223]= {11.9148 , 7.28309 , 4.15578 , 2.13938 , 1.23963 , 0.567227 ,
          0.258188 , 0.117706 , 0.0545688 , 0.0250039 , 0.000231414 }
```

```
In[224]:= ClearAll[modelpkiv2];
```

```
modelpkiv2 = First[NDSolve[{Xc'[t] == -(k12 + k10) Xc[t] + k21 Xp1[t],
                          Xp1'[t] == k12 Xc[t] - k21 Xp1[t],
                          Xc[0] == doseiv ,
                          Xp1[0] == 0},
                      {Xc, Xp1}, {t, 0, 35}, MaxSteps -> 10000, PrecisionGoal -> ∞];
```

```
In[226]:= CL = k10 V1
```

```
Out[226]= 114.914
```

```
In[227]:= (*Vss=V1(k12+k21)/k21*)
```

```
In[228]:= beta = 1 / 2 ((k12 + k21 + k10) - ((k12 + k21 + k10)^2 - 4 k21 k10)^0.5)
```

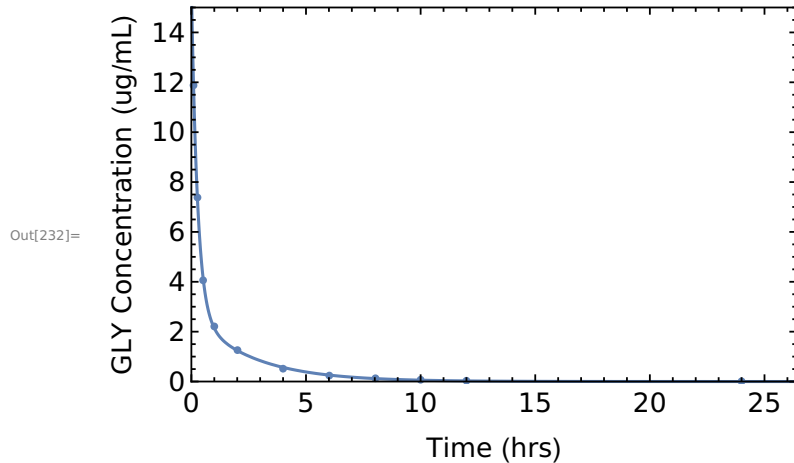
```
Out[228]= 0.390215
```

```
In[229]:= (*thalfbeta=0.693/beta*)
```

```
In[230]:= plot1 = Plot[(Xc[t]/V1) /. modelpkiv2, {t, 0, 1.1 dataIV[[nt, 1]]},
  PlotRange -> {{0, 1.1 dataIV[[nt, 1]], {0, 15}}, Frame -> True,
  FrameStyle -> Directive[Black, 14, Thickness[0.003]], LabelStyle ->
  (FontFamily -> "Arial"), FrameLabel -> {"Time (hrs)", "GLY Concentration (ug/mL)"}];
```

```
In[231]:= plot2 = ListPlot[dataIV, PlotRange -> {{0, 24}, {0, 15.}}];
```

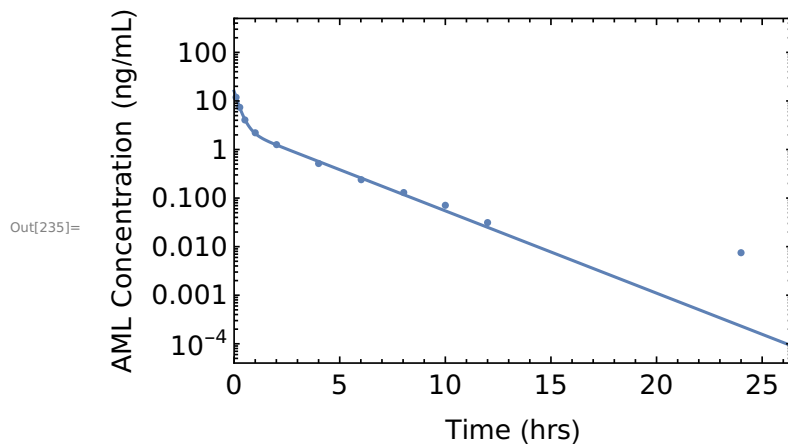
```
In[232]:= Show[plot1, plot2]
```



```
In[233]:= plot3 = LogPlot[(Xc[t]/V1) /. modelpkiv2, {t, 0, 1.1 dataIV[[nt, 1]]},
  PlotRange -> {{0, 1.1 dataIV[[nt, 1]], {0, 500}}, Frame -> True,
  FrameStyle -> Directive[Black, 14, Thickness[0.003]], LabelStyle ->
  (FontFamily -> "Arial"), FrameLabel -> {"Time (hrs)", "AML Concentration (ng/mL)"}];
```

```
In[234]:= plot4 = ListLogPlot[dataIV];
```

```
In[235]:= Show[plot3, plot4]
```



Oral PK inputs (10mg/kg dose-fasted 2hr-PS 42.7um), and in ug/ml and hr.

```
In[236]:= dataP0 = {{0.167, .0401}, {0.5, .0338}, {1., .0402},
  {1.5, .0501}, {2.5, 0.0633}, {4., .0649}, {6., 0.0684}, {8., .0654},
  {10., .0743}, {12., 0.0691}, {16., 0.0523}, {20., 0.0405}, {24., 0.0444}}
```

```
Out[236]:= {{0.167, 0.0401}, {0.5, 0.0338}, {1., 0.0402}, {1.5, 0.0501},
  {2.5, 0.0633}, {4., 0.0649}, {6., 0.0684}, {8., 0.0654}, {10., 0.0743},
  {12., 0.0691}, {16., 0.0523}, {20., 0.0405}, {24., 0.0444}}
```

```
In[237]:= nt = Length[dataP0]
```

```
Out[237]= 13
```

```
In[238]:= (*dataP0=Table[{dataP0[[i,1]],dataP0[[i,2]]1000.},{i,1,nt}]*
```

```
F=Fa*Fg*Fh
```

```
from Mason 1979
```

```
In[239]:= fgfh = f / facalc
```


```
Out[239]= 0.126847
```


```
In[240]:= (*If[fgfh>1., fgfh=1.]*)
```

Drug VD in mL

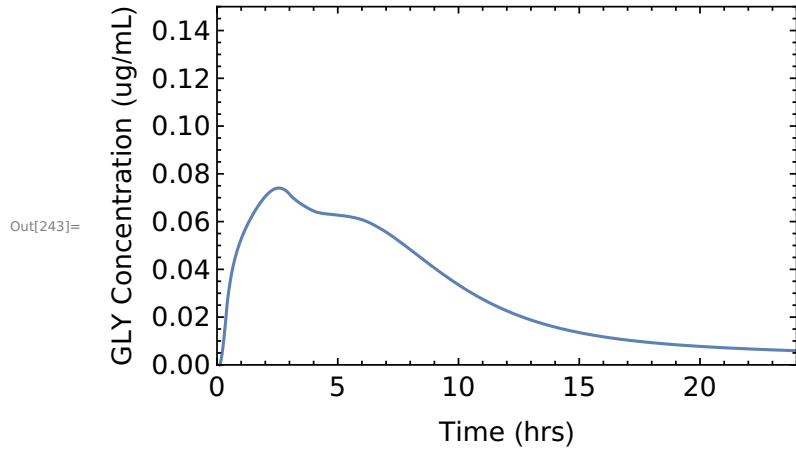
```
In[241]:= ClearAll[modelpk01];
```

```
modelpk01 = First[NDSolve[{Xc'[t] == 1000 fgfh c5fun[t] - (k12 + k10) Xc[t] + k21 Xp1[t],
  Xp1'[t] == k12 Xc[t] - k21 Xp1[t],
  Xc[0] == 0,
  Xp1[0] == 0},
  {Xc, Xp1}, {t, 0, 35}, MaxSteps -> 100000, PrecisionGoal -> ∞]]
```

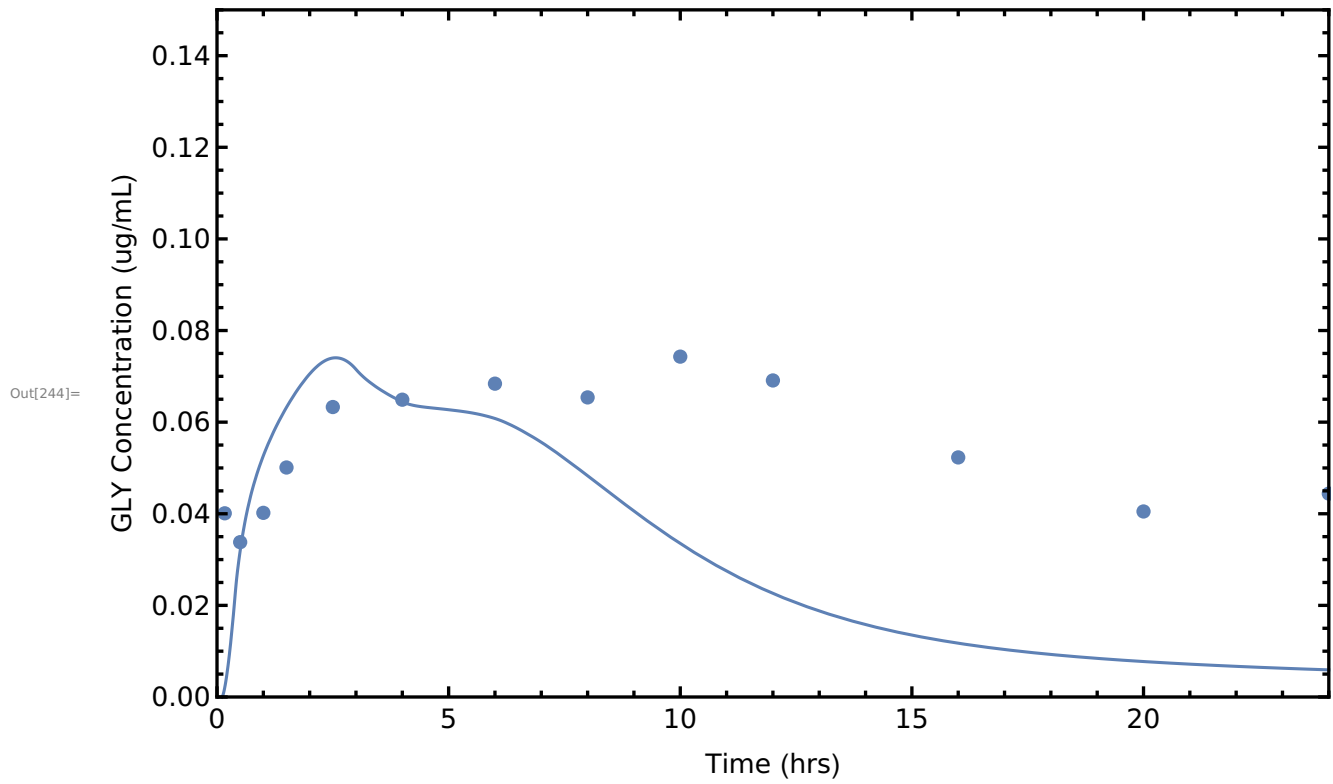
```
Out[242]= {Xc -> InterpolatingFunction [  Domain : {{0., 35.}}
  Output : scalar ],
```

```
Xp1 -> InterpolatingFunction [  Domain : {{0., 35.}}
  Output : scalar ] }
```

```
In[243]:= plotpk1 = Plot[(Xc[t]/V1) /. modelpk01, {t, 0, 24}, PlotRange -> {{0, 24}, {0, .15}},
  Frame -> True, FrameStyle -> Directive[Black, 14, Thickness[0.003]],
  LabelStyle -> (FontFamily -> "Arial"),
  FrameLabel -> {"Time (hrs)", "GLY Concentration (ug/mL)"}]
```



In[244]:= Show[plotpk1 , ListPlot [dataP0]]



```
In[245]:= ClearAll[dataP02, interpP0, plotintP0, aucon];
```

```
In[246]:= npo = Length[dataP0]
```

```
Out[246]= 13
```

```
In[247]:= auciv = NIntegrate[(Xc[t]/V1) /. modelpkiv2, {t, 0, 24}]
```

```
Out[247]= 10.442
```

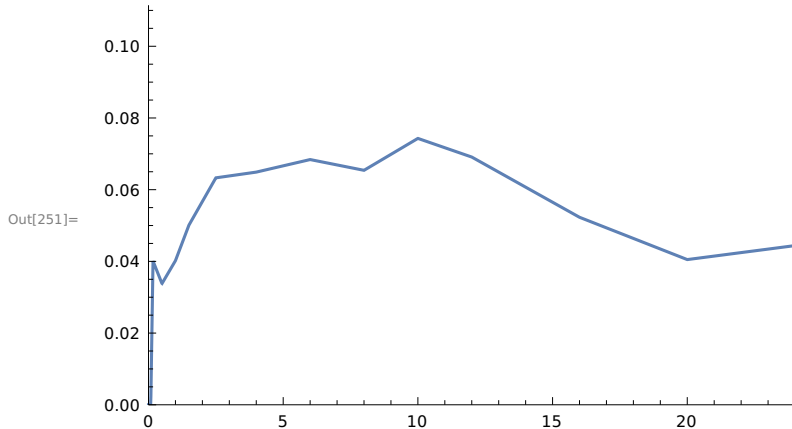
```
In[248]:= dataP02 = Join[{{0, 0}, {Min[0.1, dataP0[[1, 1]]/2], 0}}, dataP0];
```

```
In[249]:= ymax = Max[Flatten[dataP0][[2 ;; 2 npo ;; 2]]]
```

```
Out[249]= 0.0743
```

```
In[250]:= interpP0 = Interpolation[dataP02, InterpolationOrder -> 1, Method -> "Spline"];
```

```
In[251]:= plotintP0 = Plot[Evaluate[interpP0[t]],
  {t, 0, 1.2 dataP0[[npo, 1]]}, PlotRange -> {{0, dataP0[[npo, 1]], {0, 1.5 ymax}}]
```



```
In[252]:= aucintP0n = NIntegrate[interpP0[t], {t, 0, dataP0[[npo, 1]]}]
```

```
Out[252]= 1.3563
```

```
In[253]:= aucon = NIntegrate[Xc[t]/V1 /. modelpko1, {t, 0, dataP0[[npo, 1]]}]
```

```
Out[253]= 0.732966
```

```
In[254]:= overlap = NIntegrate[
  Min[interpP0[t], (aucintP0n / aucon) (Xc[t]/V1) /. modelpko1], {t, 0, dataP0[[npo, 1]]}]
```

```
Out[254]= 0.947134
```

```
In[255]:= (aucintP0n / aucon);
```

```
In[256]:= overlap / aucintP0n
```

```
Out[256]= 0.69832
```

```

In[257]:= plotnormsimP0 = Plot[Evaluate[(aucintP0n / aucon) ((Xc[t] / V1) /. modelpko1)],
  {t, 0, 1.5}, PlotRange -> {{0, 1.5}, {0, 1.5 Max[dataP02]}}, PlotStyle -> Red];

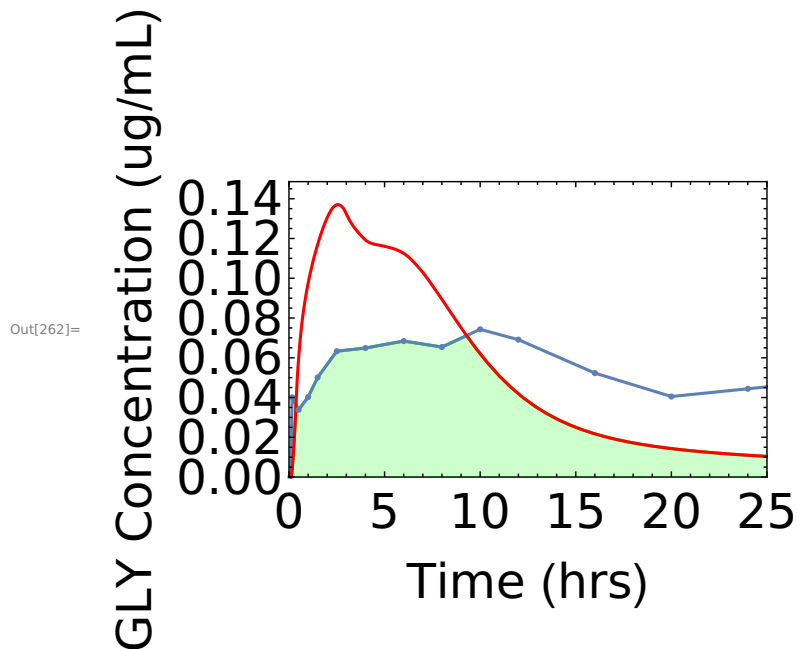
In[258]:= plotoverlap = Plot[Min[interpP0[t], (aucintP0n / aucon) ((Xc[t] / V1) /. modelpko1)], {t, 0, 24},
  PlotRange -> {{0, 1.5}, {0, 1.5 ymax}}, PlotStyle -> Green, Filling -> Axis,
  Frame -> True, FrameStyle -> Directive[Black, 14, Thickness[0.003]],
  LabelStyle -> (FontFamily -> "Arial"),
  FrameLabel -> {"Time (hrs)", "GLY Concentration (ng/mL)"}];

In[259]:= Show[plotoverlap, plotintP0, plotnormsimP0, ListPlot[dataP0]];

In[260]:= plotoverlap3 = Plot[Min[interpP0[t], (aucintP0n / aucon) ((Xc[t] / V1) /. modelpko1)],
  {t, 0, 30}, PlotRange -> {{0, 25}, {0, 2 ymax}}, PlotStyle -> Green, Filling -> Axis,
  Frame -> True, FrameStyle -> Directive[Black, 25, Thickness[0.003]],
  LabelStyle -> (FontFamily -> "Arial"),
  FrameLabel -> {"Time (hrs)", "GLY Concentration (ug/mL)"}];

plotnormsimP03 = Plot[Evaluate[(aucintP0n / aucon) ((Xc[t] / V1) /. modelpko1)],
  {t, 0, 30}, PlotRange -> {{0, 25}, {0, 1.5 Max[dataP02]}}, PlotStyle -> Red];
Show[plotoverlap3, plotintP0, plotnormsimP03, ListPlot[dataP0]]

```



Calculate experimental oral AUC by extending the oral data to infinity (assume 1st order terminal elimination).

```

In[263]:= auctailo = dataP02[[npo + 1, 2]] / beta;

In[264]:= aucpo = aucintP0n + auctailo;

In[265]:= fcalc = aucpo dose2 / (auciv dose1)

Out[265]= 0.0559315

```

Calculate Cmax and Tmax, exp and pred

```
In[266]:= ClearAll[cmax, intt];  
In[267]:= intt = Table[{i, interpP0[i]}, {i, 0, dataP02[[npo + 1, 1]], 0.1}];  
In[268]:= itt2 = Flatten[intt];  
In[269]:= cmax = Max[itt2[[2 ;; Length[itt2] - 1 ;; 2]];  
In[270]:= tmax = Flatten[Position[intt, cmax]][[1]] / 10 - 0.1;  
In[271]:= predt = Table[{i, Evaluate[(aucintP0n / aucon) ((Xc[i] / V1) /. modelpko1)}],  
  {i, 0, dataP02[[npo + 1, 1]], 0.1}];  
In[272]:= predt2 = Flatten[predt];  
In[273]:= cmaxpred = Max[predt2[[2 ;; Length[predt2] - 1 ;; 2]]  
Out[273]= 0.136983  
In[274]:= tmaxpred = Flatten[Position[predt, cmaxpred]][[1]] / 10 - 0.1  
Out[274]= 2.6
```
